Downloaded from orbit.dtu.dk on: Apr 28, 2024

DTU Library

Climatic Reliability of Electronics: Early Prediction and Control of Contamination and humidity effects

Verdingovas, Vadimas

Publication date:
2015

Document Version
Publisher's PDF, also known as Version of record

Link back to DTU Orbit

Citation (APA):
Verdingovas, V. (2015). *Climatic Reliability of Electronics: Early Prediction and Control of Contamination and humidity effects*. Technical University of Denmark.

General rights
Copyright and moral rights for the publications made accessible in the public portal are retained by the authors and/or other copyright owners and it is a condition of accessing publications that users recognise and abide by the legal requirements associated with these rights.

- Users may download and print one copy of any publication from the public portal for the purpose of private study or research.
- You may not further distribute the material or use it for any profit-making activity or commercial gain
- You may freely distribute the URL identifying the publication in the public portal

If you believe that this document breaches copyright please contact us providing details, and we will remove access to the work immediately and investigate your claim.

Climatic Reliability of Electronics:

Early Prediction and Control of Contamination and humidity effects

PhD Thesis

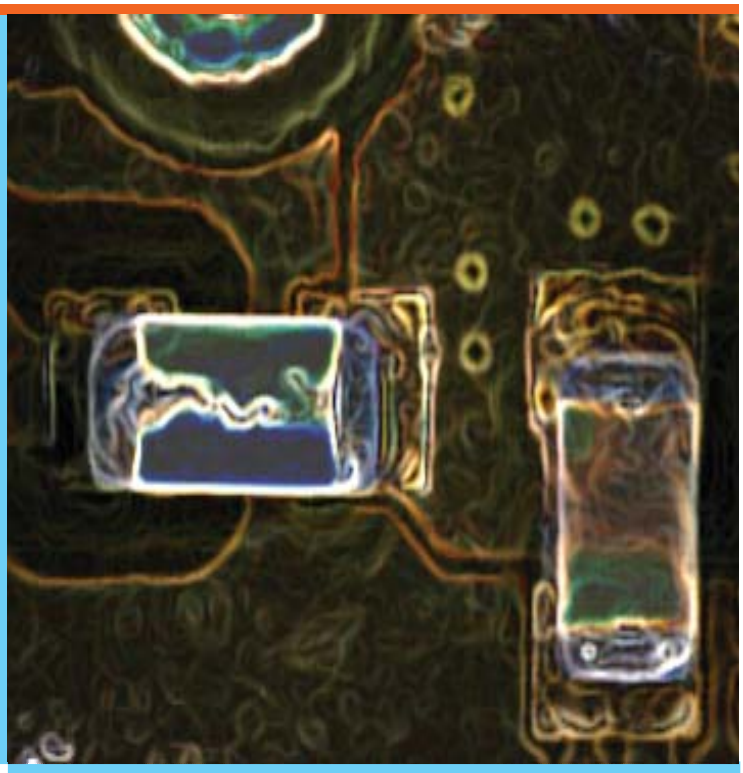

Vadimas Verdingovas
March 2015

DTU Mechanical Engineering
Department of Mechanical Engineering

Technical University of Denmark

CLIMATIC RELIABILITY OF ELECTRONICS:

EARLY PREDICTION AND CONTROL OF CONTAMINATION AND HUMIDITY EFFECTS

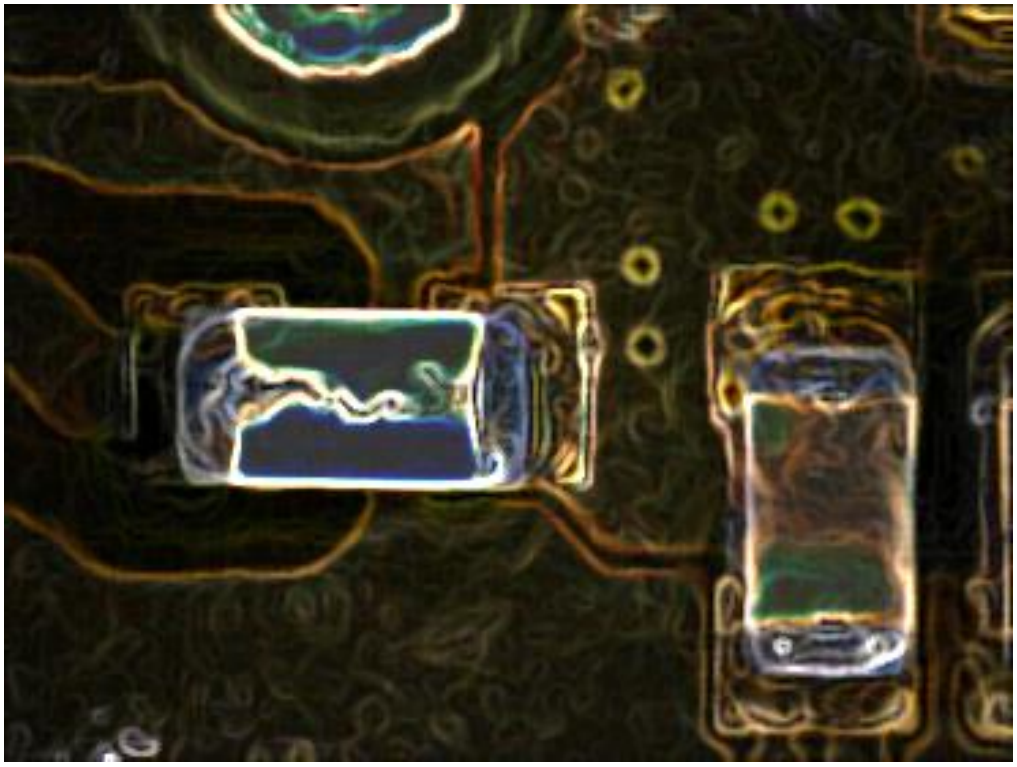

PhD thesis by
Vadimas Verdingovas

DTU Mechanical Engineering
Department of Mechanical Engineering

Celcorr

CLIMATIC RELIABILITY OF ELECTRONICS:
EARLY PREDICTION AND CONTROL OF CONTAMINATION AND HUMIDITY EFFECTS

PhD thesis
by
Vadimas Verdingovas

March 2015

Section of Materials and Surface Engineering
Department of Mechanical Engineering
Technical University of Denmark (DTU)
DK-2800, Kgs. Lyngby

PREFACE

This thesis is submitted in candidacy for a PhD degree from the Technical University of Denmark. The work has been carried out at the Department of Mechanical Engineering, Section of Materials and Surface Engineering, under supervision of Professor Rajan Ambat and Senior Researcher Morten Stendahl Jellesen. As a part of the PhD project, an investigation of Au-Al wire bonds corrosion in iodine environments was conducted at the Bosch GmbH, Automotive Electronics in Reutlingen, Germany, where the work was carried out under supervision of Senior Expert for Corrosion and Chemistry of Materials Lutz Müller. The duration of PhD programme was November 2011 – March 2015.

This PhD project is a part of the CreCon (Consortium for Climatically Reliable Electronics) industrial consortium under Centre for Electronic Corrosion (www.celcorr.com).

ACKNOWLEDGMENTS

First of all, I would like to greatly acknowledge my supervisors Rajan Ambat and Morten Stendahl Jellesen, for the guidance, continuous support, and invaluable advice throughout the study. I express my appreciation to my supervisors for their dedication to the project, the time spent for fruitful discussions, and the given freedom to explore and apply different approaches for achieving the set goals.

Celcorr/CreCon member companies Danfoss A/S, Grundfos A/S, Vestas Wind Systems A/S, and Eltek are acknowledged for the funding and overall support of the PhD program. Special thanks to Annemette Riis, Jens Peter Krog, John B. Jacobsen, Kirsten Stentoft-Hansen, Dorthe Johansen, Niels Martin Henriksen, Øystein Larsen, Willy Høydal for all the fruitful discussions and advice in connection with the PhD studies. I am thankful for the knowledge and resource contributions to the project.

The external research at Robert Bosch GmbH was an invaluable experience as part of the PhD studies. I express my gratitude to Lutz Müller, for his supervision, enthusiasm, and his helpfulness. I am grateful for his sincerity and for sharing professional insight into corrosion and materials. I would also like to express my thankfulness to "AE/ESI5 Engineering Sensors Inertial Application Components" group and all the people from "Automotive Electronics" who have supported me with various questions related to production, wire bonding, and testing.

I am also indebted to my colleagues from the research group, and the section of Materials and Surface Engineering. Special thanks to Hélène Conseil, Kamila Piotrowska, Salil Joshy, and Shruti Borgaonkar for their help, and contributions to the project. I also express my thankfulness to Daniel Minzari for the given advice related to experimental setups and techniques, as well as for the discussions of the results.

Finally yet importantly, I would like to thank my family and my friends for their invaluable support and encouragement during my study.

ABSTRACT

This PhD project is motivated by the demand for the deeper understanding of the effects of humidity and contamination on corrosion related issues and overall reliability of electronic devices. The information available today is limited and incoherent, thus the directions for the research subtopics were to a significant extent guided by the climatic reliability issues the electronic companies are currently facing. The research in this thesis is focused on the synergistic effects of process related contamination, humidity, potential bias, and PCBA design related aspects, while various tests methods suitable for electrical measurements are attempted and compared with standardized test methods. The focus is also placed on the methods for corrosion prediction on a PCBA layout with the aim of profiling corrosion prone regions or simulating the possible humidity effects on a circuit design assuming parasitic circuit due to water layer formation on the PCBA surface.

The chapters 2-5 review the factors influencing the climatic reliability of electronics namely humidity interaction with materials and ionic contamination on the PCBA surface, common types and sources of ionic contamination in electronics, the test methods and techniques, and failure mechanisms related to climate and contamination. Chapter 6 summarizes the materials and experimental methods employed in this thesis. The results of various investigations are presented as individual research papers as published or in the draft form intended for publication in international journals. Prior to the appended papers, chapter 7 provides a short summary of appended papers with important results and discussion.

The results are summarized in 8 papers, presented in chapters 8-15. Papers 1-3 investigate the interaction between ionic contaminants i.e. NaCl, flux residues, WOAs and humidity, and their effects on leakage current, corrosion and electrochemical migration. Paper 4 compares the two types of ionic contamination i.e. NaCl and flux residue in terms of their impact on leakage currents and probability for electrochemical migration, while Paper 5 is focused on the electrochemical migration of tin under pulsed voltage. Paper 6 contains a corrosion study of Au-Al wire bonds and Au-Al intermetallics in iodine environments. Paper 7 presents a novel method developed for profiling of tin corrosion on the PCBA surface. Paper 8 focuses on analysing the feasibility of corrosion prediction by circuit simulation using the combined empirical information from above works assuming parasitic circuit formation. Finally, chapter 16 provides an overall discussion, conclusions, and suggestions for future work.

Overall, the investigations clearly showed the importance of deliquescence RH of ionic contaminants for the degradation of surface insulation resistance and electrochemical migration. This is related to the increase of water layer thickness as a medium for ion transport. Under thin water layers, the concentration of ionic contaminant, bias voltage, and local pH formation are the factors influencing the formation of tin dendrites. Investigation of electrochemical migration under pulsed voltage has shown that the reduction of duty cycle prolongs the time to failure. Under these test conditions, the precipitation of tin hydroxides is more favourable, and fewer metal ions get to reduce at the cathode. Corrosion study of Au-Al wire bonds in iodine environments has shown that the Al metallization and Al-rich intermetallic phases are most susceptible to corrosion. The failure mechanism involves oxidation of Al via formation of Al iodides and consequent formation of Al oxides and/or hydroxides. The method developed for tin corrosion profiling using tin ion indicator gel provides a clear indication of tin corrosion and tin ions movements on the PCBA surface, giving valuable information for corrosion prediction or failure analysis.

RESUME

Dette ph.d.-projekt er motiveret af behovet for en dybere forståelse for effekten af fugt og kontaminering på korrosion og den overordnede pålidelighed af elektronik. Forskningen har i betydelig grad været drevet af de klimatiske pålideligheds spørgsmål, elektroniske virksomheder i øjeblikket står over for. I dag er tilgængelig viden på området begrænset. Arbejdet i denne afhandling fokuserer på synergieffekter mellem procesrelateret forurening, fugtighed, elektrisk spænding og printdesign ved hjælp af både nye samt standardiserede testmetoder. Fokus er også på udvikling af metoder til forudsigelse af korrosion i elektronik med det formål at påvise, hvor de korrosionsfølsomme områder findessamt at simulere de mulige effekter af høj luftfugtighed under brug af elektriske krebsløb, eksempelvis hvordan der kan dannes lækstrømme på grund af en dannet vandfilm på overfladen af et printkort.

Kapitlerne 2-5 giver et overblik over hvilke faktorer, der påvirker den klimatiske pålidelighed af elektronik såsom vekselvirkningen mellem fugtighed på printkortet og kontaminering af overfladen, almindelige typer og kilder til kontaminering, testmetoder og teknikker samt fejlmekanismer relateret til fugt og kontaminering. Kapitel 6 opsummerer anvendte eksperimentelle metoder. Resultater af undersøgelserne i denne afhandling præsenteres som individuelle artikler, publiceret eller i udkast til offentliggørelse i internationale tidsskrifter. Kapitel 7 indeholder en kort oversigt over vedhæftede artikler med vigtige resultater og diskussion.

Resultaterne er sammenfattet i 8 artikler præsenteret i kapitel 8-15. Artiklerne 1-3 undersøger samspillet mellem kontaminering med natriumklorid, flusrester, svage organiske syrer og fugtighed, og disses indvirkning på lækstrøm, korrosion og elektrokemisk migration. Artikel 4 sammenligner de to typer af forurening; natriumklorid og flusrester i form af deres indvirkning på lækstrømme og risikoen for elektrokemisk migration, mens artikel 5 er fokuseret på elektrokemisk migration af tin under pulserende spænding. Artikel 6 indeholder en undersøgelse af korrosion af Au-Al sammenføjninger og Au-Al intermetalliske forbindelser udsat for iod-holdigt miljø. Artikel 7 præsenterer en nyskabende fremgangsmåde udviklet til at påvise tin korrosion på overfladen af et printkort. Artikel 8 fokuserer på at analysere mulighederne for forudsigelse af korrosion i et elektrisk kredsløb ved at kombinere den indsamlede empiriske information under antagelse af lækstrømsdannelse. Kapitel 16 giver en samlet diskussion, konklusion og forslag til fremtidigt arbejde.

Samlet set påviste undersøgelserne betydningen af fugt og opløselighed af kontaminering ved bestemmelse af lækstrømme og elektrokemisk migration. Dette hænger sammen med vandfilmens lagtykkelse. For tynde vandlag er koncentrationen af ioner, elektrisk spænding og lokal pH væsentlige faktorer, der påvirker dannelsen af tin dendritter. Undersøgelse af elektrokemisk migration under pulserende spænding har vist, at en reducering af tidsintervallerne med påtrykt spænding forlænger den samlede tid, før der opstår migration. Ved kortere tid med påtrykt spænding er udfældning af tin hydroxider mere favorabel og færre metalioner reduceres ved katoden. Undersøgelse af Au-Al sammenføjninger eksponeret for jodholdigt miljø på gasform har vist, at aluminium-metallisering og intermetalliske faser rige på aluminium er mest modtagelige for korrosion. Nedbrydningsmekanismen involverer oxidation af aluminium ved dannelse af aluminium-jodid forbindelser og derpå følgende dannelse af aluminium oxider og/eller hydroxider. En metode er udviklet til profilering af tin korrosion ved hjælp af en tin-ion-indikator gel, der giver en klar indikation af tin korrosion, og dermed er et værdifuldt værktøj til forudsigelse af korrosion eller fejlanalyse af elektronik.

LIST OF ABBREVIATIONS

AC	Alternating Current
ATR	Attenuated Total Reflectance
ASHRAE	American Society of Heating, Refrigerating, and Air-Conditioning Engineers
BET	Brunauer-Emmett-Teller
BGA	Ball Grid Array
CAF	Conductive Anodic Filament
DC	Direct Current
DIC	Differential Interference Contrast
ECM	Electrochemical Migration
EDS	Energy-Dispersive X-ray Spectroscopy
ESEM	Environmental Scanning Electron Microscope
FT-IR	Fourier Transform Infrared Spectroscopy
GDOES	Glow Discharge Optical Emission Spectroscopy
HASL	Hot Air Solder Leveling
IMP	Intermetallic Phase
IPC	Association Connecting Electronics Industries
LC	Leakage Current
OCP	Open Circuit Potential
OSP	Organic Solder Protective (coating)
PCB	Printed Circuit Board
PCBA	Printed Circuit Board Assembly
RH	Relative Humidity
ROSE	Resistivity of Solvent Extract
SEC	Solvent Extract Conductivity
SEM	Scanning Electron Microscope
SIR	Surface Insulation Resistance
SMC	Surface Mount Component
TTF	Time to failure (time when the dendrite formation was detected)
VOC	Volatile Organic Compound
WOA	Weak Organic Acid
ZRA	Zero Resistance Ammetry

LIST OF PUBLICATIONS

LIST OF APPENDED PAPERS

1. **V. Verdingovas**, M. S. Jellesen, and R. Ambat, "Impact of NaCl contamination and climatic conditions on the reliability of printed circuit board assemblies," *IEEE Trans. Device Mater. Reliab.*, vol. 14, no. 1, pp. 42–51, 2014.

2. **V. Verdingovas**, M. S. Jellesen, and R. Ambat, "Solder flux residues and humidity-related failures in electronics: relative effects of weak organic acid used in no-clean flux systems," *J. Electron. Mater.,* vol. 14, no. 4, pp. 1116–1127, 2015.

3. **V. Verdingovas**, M. S. Jellesen, and R. Ambat, "Relative effect of solder flux chemistry on the humidity related failures in electronics," *Solder. Surf. Mt. Technol*, vol. 27, no. 4, pp 146-156, 2015.

4. **V. Verdingovas**, M. S. Jellesen, and R. Ambat, "Influence of sodium chloride and weak organic acids (flux residues) on electrochemical migration of tin on surface mount chip components," *Corros. Eng. Sci. Technol.*, vol. 48, no. 6, pp. 426–435, 2013.

5. **V. Verdingovas**, M. S. Jellesen, and R. Ambat, "Effect of pulsed voltage on electrochemical migration of tin in electronics," *J. Mater. Sci. Mater. Electron.*, vol 26, no. 10, pp. 7997-8007, 2015.

6. **V. Verdingovas**, L. Müller, M. S. Jellesen, F. B. Grumsen, and R. Ambat, "Effect of iodine on the corrosion of Au-Al wire bonds," *Corros Sci.*, vol. 97, pp. 161-171, 2015.

7. **V. Verdingovas**, M. S. Jellesen, and R. Ambat, "Colorimetric visualization of tin corrosion: A method for early stage corrosion detection on printed circuit boards," draft to be submitted to *Microelectron. Reliab.*, 2015.

8. **V. Verdingovas**, M. S. Jellesen, S. Joshy, and R. Ambat, "Analysis of surface insulation resistance related failures in electronics by circuit simulation," draft to be submitted to *Circuit World.*, 2015.

CONFERENCE PROCEEDINGS/ORAL PRESENTATIONS

1. **V. Verdingovas**, M. S. Jellesen, and R. Ambat, "Electrochemical migration in electronics: effect of contamination and bias conditions," *Proceedings of EUROCORR 2014*, Pisa, Italy, 2014.

2. M. S. Jellesen, **V. Verdingovas**, H. Conseil, K. Piotrowska, and R. Ambat, "Corrosion in electronics: Overview of failures and countermeasures," *Proceedings of EUROCORR 2014*, Pisa, Italy, 2014.

3. R. Ambat, M. S. Jellesen, **V. Verdingovas**, K. Piotrowska, H. Conseil, "Perspectives on the climatic reliability of electronic devices," *Proceedings of EUROCORR 2014*, Pisa, Italy, 2014.

4. H. Conseil, M. S. Jellesen, **V. Verdingovas**, and R. Ambat, "Decomposition studies of no-clean solder flux systems in connection with corrosion reliability of electronics**,"** *Proceedings of EUROCORR 2013*, Estoril, Portugal, 2013.

5. **V. Verdingovas**, M. S. Jellesen, R. Rizzo, H. Conseil, and R. Ambat, "Impact of hygroscopicity and composition of solder flux residue on the reliability of PCBA under corrosive conditions," *Proceedings of EUROCORR 2013*, Estoril, Portugal, 2013.

6. **V. Verdingovas**, M. S. Jellesen, and R. Ambat, "Electrochemical investigation on climatic reliability of electronic devices," Danish Metallurgical Society DMS PhD symposium 2013, Kgs. Lyngby, Denmark, 2013.

7. **V. Verdingovas**, M. S. Jellesen, and R. Ambat, "Effect of ionic contamination on climatic reliability of printed circuit board assemblies," *Proceedings of EUROCORR 2012*, Istanbul, Turkey, 2012.

8. M. S. Jellesen, M. Dutta, **V. Verdingovas**, and R. Ambat, "Process related contaminations causing climatic reliability issues," *Proceedings of IMAPS 2012*, Helsingør, Denmark, 2012.

9. M. S. Jellesen, P. Westermann, **V. Verdingovas**, P. Holm, and R. Ambat, "Relation between PCBA cleanliness and Climatic Reliability," *Proceedings of EUROCORR 2011*, Stockholm, Sweden, 2011.

OTHER ELECTRONICS RELIABILITY RELATED PUBLICATIONS

1. S. Pralgauskaitė, V. Palenskis, J. Matukas, B. Šaulys, V. Kornijčuk, and **V. Verdingovas**, "Analysis of mode-hopping effect in Fabry–Pérot multiple-quantum well laser diodes via low frequency noise investigation," *Solid. State. Electron.*, vol. 79, pp. 104–110, Jan. 2013.

TABLE OF CONTENTS

List of appended papers VI
Conference proceedings/oral presentations VII
Other electronics reliability related publications VII

INTRODUCTION

1. Introduction 1
   1.1 Background 1
   1.2 Challenges in predicting climatic reliability of electronics 2
   1.3 Aim of the current project 4
   1.4 Overview of the thesis 5

LITERATURE REVIEW

2. Factors influencing climatic reliability 7
   2.1 Humidity 7
      2.1.1 Water absorption by the PCBA 7
      2.1.2 Water adsorption by the hygroscopic contaminants on the PCBA 8
      2.1.3 Water adsorption to the surface of the PCBA 11
   2.2 Contamination 12
      2.2.1 Activators in the flux (flux residues) 12
      2.2.2 User environment related contamination 15
3. Humidity and contamination related failures 17
   3.1 Leakage current/SIR 17
   3.2 Electrochemical migration 17
   3.3 Conductive anodic filament formation 19
   3.4 Creep corrosion 20
   3.5 Corrosion of wire bonds in microelectronics 20
4. Testing of climate and contamination effects 21
   4.1 SIR testing 21
   4.2 Bono test 22
   4.3 Electrochemical impedance spectroscopy 23
5. Overview of literature and current work 25

References 27

MATERIALS AND METHODS

6. Materials and methods 33

6.1 Electrochemical migration setup for single components 33
6.2 Test printed circuit board 33
6.3 Climatic chamber 34
6.4 Quartz crystal microbalance 34
6.5 Electrical/electrochemical characterisation 34
6.6 Other material characterisation techniques 35
6.6.1 Optical microscopy 35
6.6.2 Electron microscopy and energy-dispersive X-ray spectroscopy 35
6.6.3 Fourier transform infrared microscopy 35
6.6.4 Glow discharged optical emission spectroscopy 36
6.6.5 X-ray diffraction 36
6.6.6 Thermal imaging camera 36
6.6.7 Wire bond shear testing 36
6.7 Tin corrosion identification using a tin ion indicator 36
6.8 Samples for corrosion studies of Au-Al interconnections 36

SUMMARY OF PAPERS

7. Summary of papers 37

APPENDED PAPERS

8. Impact of NaCl contamination and climatic conditions on the reliability of printed circuit board assemblies 47
9. Solder flux residues and humidity related failures in electronics: relative effects of weak organic acid used in no-clean flux systems 65
10. Relative effect of solder flux chemistry on the humidity related failures in electronics 83
11. Influence of sodium chloride and weak organic acids (flux residues) on electrochemical migration of tin on surface mount chip components 99
12. Effect of pulsed voltage on electrochemical migration of tin in electronics 115
13. Effect of iodine on the corrosion of Au-Al wire bonds 129
14. Colorimetric visualization of tin corrosion: a method for early stage corrosion detection on printed circuit boards 149
15. Analysis of surface insulation resistance related failures in electronics by circuit simulation 165

OVERALL DISCUSSION AND CONCLUSIONS

16. Overall discussion and conclusions 181
16.1 Overall conclusions 183
16.2 Suggestions for future work 185

1. INTRODUCTION

1.1 BACKGROUND

Today electronic devices and components worldwide experience climatic reliability issues resulting in premature fault and intermittent or permanent failures. Humidity related functionality issues and corrosion compromise durability and reliability of the devices resulting in large economic losses due to exact finding and replacement of failed parts as well as loss of credibility for the electronics producer. Often a faulty signal or erroneous function by an electronic device is linked to the water layer formation on the surface of the printed circuit board assembly (PCBA) due to humidity exposure and the related electrochemical process initiated by water layer acting as a conduction medium. The problem is compounded today due to a number of factors specific to electronic devices such as miniaturisation, high level of integration, and multi-material usage on the PCBA. Above factors together with the applied potential bias when the device is working and contamination introduced during the manufacturing process synergistically with humidity can result in a number of failure modes. Today electronic devices and control systems are part of almost all installations meaning that climatic exposure conditions of electronics vary from clean room to severe offshore conditions. Corrosion failure modes under humidity exposure conditions include: (i) leak current failures due to surface insulation reduction, (ii) electrochemical migration, (iii) galvanic corrosion due to micro-galvanic cell formation, (iv) creep corrosion, and corrosion caused by gaseous environment together with humidity. Among them, the leak current and electrochemical migration failures are more important due to the risk of intermittent electrical functionality issues causing premature device breakdown.

It is difficult to find a single solution for improving the climatic reliability of PCBA. A number of measures can be suggested from the PCBA design point of view to cleanliness of the manufacturing process [1], barrier protection by conformal coating [2], and device/enclosure design [3], [4]. In this respect, for an early prediction of humidity effects, it is important to understand the sensitivity of a particular circuit design to external climate conditions. The knowledge on circuit sensitivity provide means for the manufacturer to take remedial action at an early stage based on the design or optimising the protection needed for particular climate conditions. Such predictability analysis requires: (i) possibility of proof-testing PCBA design for any climatic interaction, (ii) predictability of surface insulation problems and possible corrosion mechanisms as a function of climate conditions, and (iii) tools based on empirical modelling to predict the lifetime expectancy of the device using accelerated testing and acceleration factors.

A comprehensive understanding of the synergetic effect of influencing factors such as material, contamination, temperature/humidity, and a bias voltage is needed for developing prediction capabilities based on the electrical properties of the water layer forming on the PCBA surface. Understanding and predictability of the electrical properties of the possible water layer formation would enable electronic industries to pinpoint corrosion hot spots on PCBAs as well as improve failure analysis by easily locating the corrosion prone areas based on climatic aspects and the data on the material, corrosion, thermal, and electrochemical factors.

1.2 CHALLENGES IN PREDICTING CLIMATIC RELIABILITY OF ELECTRONICS

Corrosion related failure mechanisms accelerate with increase of RH and temperature, however, the prediction of climate conditions for outdoor electronics is challenging due to the following reasons: i) changes in the temperature and humidity with the diurnal and seasonal cycles, and ii) dependency on the enclosure design, and local humidity and temperature effects on the PCBA surface. The temperature profile inside the device is important in relation to the dew point temperature, and it is dependent on the circuitry and operational conditions of the device. Figure 1.1 shows an example of temperature profile on a PCBA surface during power on and off conditions. For example, the varying temperature of the PCBA in a tight enclosure would cause variations in the local RH on the surface; thereby, dew formation for a short time interval as device starts is more likely (Figure 1.2).

High humidity is a threat for the reliability of electronic devices; therefore, the designs of the device as well as the climate control strategies are based on minimising the risk of local condensation occurrence and minimizing the time of exposure to high humidity conditions. On the other hand, if the ambient RH is too low, it can cause electrostatic charge build-up between the components of the printed circuit boards. However, this problem becomes relevant at RH below 30 %, and has less relevance to the scope of this current work.

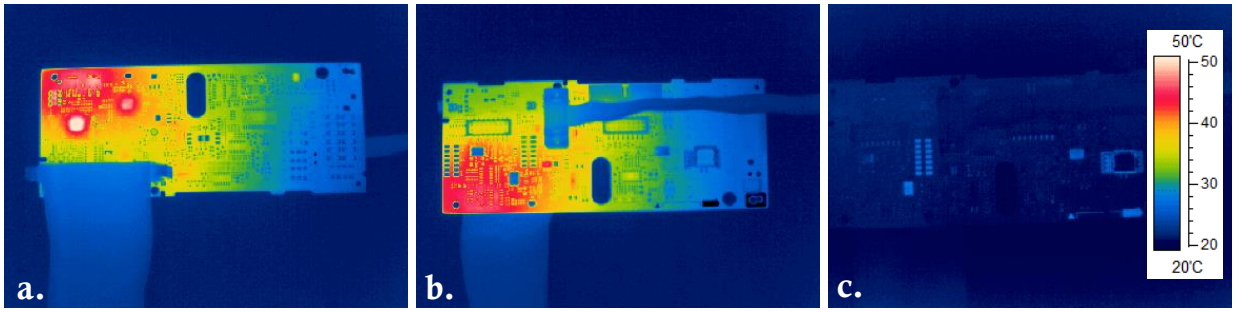

Figure 1.1: Temperature profile of PCBA: a.-b. side A and side B during ON condition, c. side B during OFF condition

The probability of failure in the electronic device increases with RH and it is significantly high when the conditions for water condensation are reached. The thickness of water layer is first dependent on the ambient RH, and condensation on a clean surface occurs at RH close to 100%. However, the amount of water adsorbed to the surface can be altered by the surface morphology i.e. microvoids or holes, and/or by the hygroscopic contaminants on the surface. A certain level of ionic contamination is always present on the PCBA and, dependent on the type and amount of contamination, it poses a threat to the functionality and overall reliability of electronics, in relation to the humidity conditions.

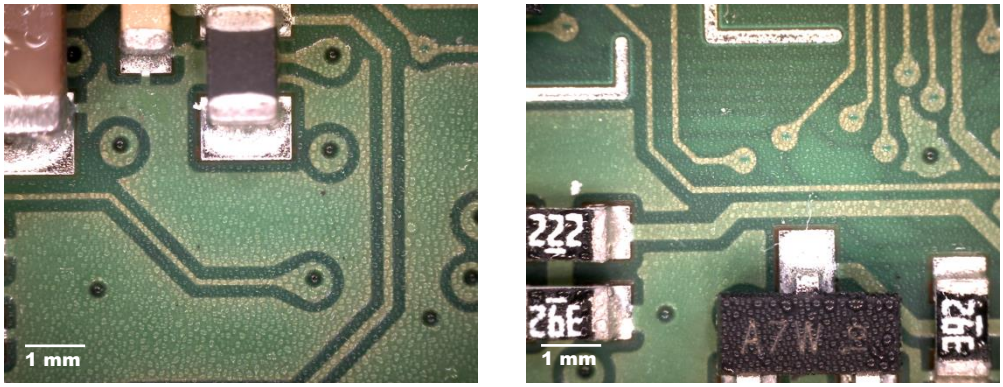

Figure 1.2: Water condensation on a device PCBA created by temperature difference between the surface and ambient

The hygroscopic contaminants on the PCBA surface are characterised by the deliquescence RH (also referred to as critical RH), which indicates the RH for the transition from solid to a solution. The transition is typically identified from the sorption isotherms. The thickness of water layer for the saturation of the contamination in the water layer forming on the surface is determined by the solubility of a contaminant in water. The dissolved ionic contamination dissociates in water, thereby increasing the ionic conductivity, which influences the rate of corrosion. An additional factor for consideration is the local pH of the solution close to the electrodes (oppositely biased conductors on the PCBA surface connected by the water layer) due to dissociation (electrolysis) of water producing hydrogen ions (acidification) at the positive electrode and hydroxyl ions (alkalisation) at the negative electrode. The rate of electrolysis of water is a function of the voltage; however, as the ionic contamination present on the PCBA surface dissolves into the water layer, it will also contribute to the pH conditions throughout the water film. As the stability of metals such as tin on the PCBA surface and tin ions in solution depends on the pH conditions, it is an important factor in relation to the failure mechanisms such as electrochemical migration.

The voltage conditions e.g. DC, AC or pulse, in combination with the architecture of the PCBA for example pitch sizes, metals and alloys, material properties like dielectric permittivity and water permeability will alter the response of the entire system to the effect of contamination and humidity thereby influencing the climatic reliability of electronics. An overview of the factors influencing the surface insulation resistance (SIR) related failures including electrochemical migration (ECM) and corrosion is summarised in Figure 1.3.

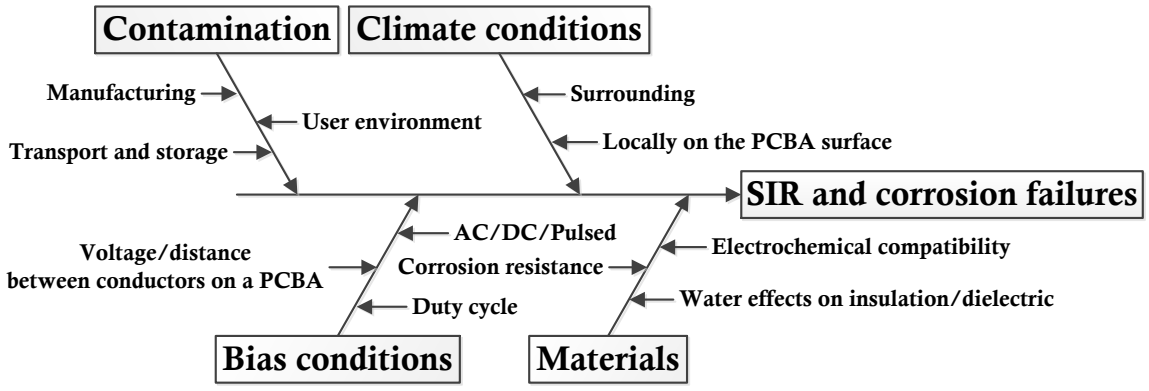

Figure 1.3: Important influencing factors related to corrosion, electrochemical migration and SIR failures on a PCBA

As the improvement of climatic reliability of electronics requires an accounting of the synergetic effects of several factors, it is important to understand the effect of various factors individually and in combinations on the onset of humidity related issues. Using such understanding, the electrical properties of the water layer can be reasonably predicted if PCBA and climatic parameters are known. This will allow one to develop design guidelines and logical methods similar to the circuit analysis carried out for electrical aspects. Therefore, it is important to improve the understanding of the effect of various factors such as contamination, humidity, and bias voltage on the electrical functionality of the PCBAs due to the reduction in SIR and corrosion related failure modes such as electrochemical migration. This also includes the analysis and prediction of the electrical functionality issues caused by the climatic exposure using the empirical relationships deduced from the experimental data.

1.3 AIM OF THE CURRENT PROJECT

This PhD project aims to develop reliability prediction capabilities using empirical relationships combining the climatic and corrosion data related to various climatic conditions and device parameters. The parameters for investigation include hygroscopic nature of PCBA contaminants, the influence of humidity, temperature, and bias characteristics on leak current and corrosion on the PCBA surface. As an overall aim of the project is to gain the knowledge on how to improve the robustness of electronics in harsh climate conditions, the important aspect here is the identification of corrosion prone areas and components under humidity exposure conditions. The extent of corrosion on a PCBA is a direct measure of SIR and related leakage current issues. However, in practice, due to low extent of corrosion and masking effects of tin hydroxides and flux residues, the identification of the sites for high leakage currents is not an easy task. Finding a method for identifying such critical areas on the PCBA is also a part of this project.

Main investigations in the current project include:

i. Corrosiveness of active (ionic) components in the flux and its influence on SIR in relation to humidity conditions.
ii. Comparison between various types of contamination such as NaCl and flux residue on humidity adsorption, absorption, and corrosion.
iii. Effect of hygroscopic contaminant and temperature variation on the water layer formation and leakage currents.
iv. Effect of bias voltage condition such as DC and pulse voltage on electrochemical migration of tin.
v. Corrosion profiling of PCBA surface using tin indicator gel concept as means to trace tin corrosion products and its trails as the paths for possible leak currents.
vi. Analysis and simulation of humidity related effects on PCBA designs using empirical data from testing.
vii. Investigations related to iodine corrosion of bond pad materials in integrated circuits.

1.4 OVERVIEW OF THE THESIS

The table below shows a bird view diagram of the thesis with a brief overview of various investigations presented as appended papers published or as manuscripts suitable for publication in scientific journals.

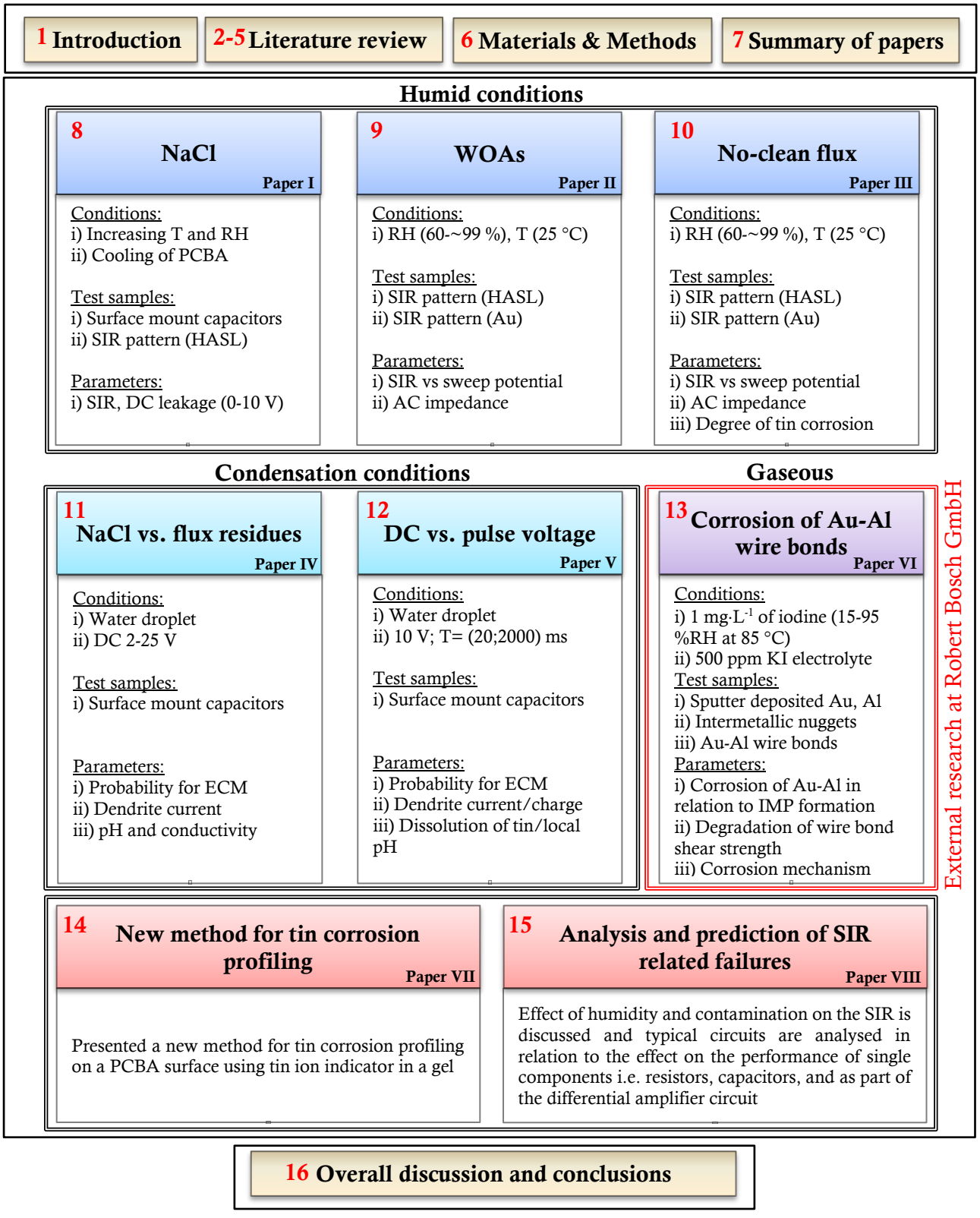

2. FACTORS INFLUENCING CLIMATIC RELIABILITY

2.1 HUMIDITY

Humidity interaction with the surface of the PCBA is one of the key factors determining the water layer formation and subsequent effect on leak current and corrosion. There are a number of aspects related to humidity interaction with the printed circuits boards, and the most relevant are reviewed in this chapter.

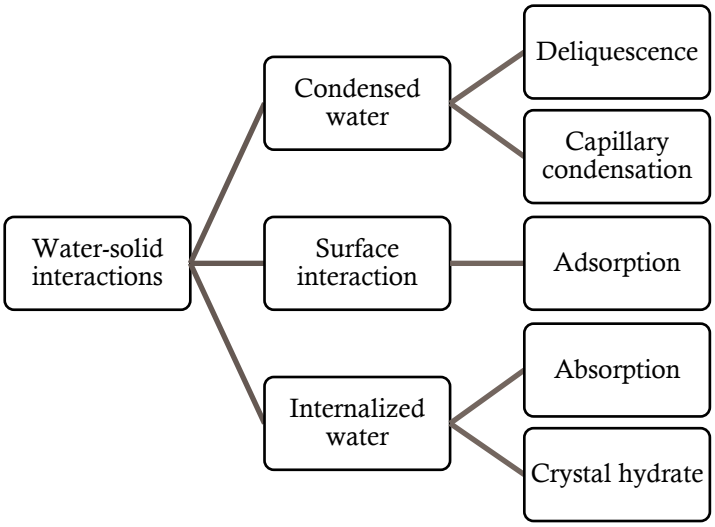

Figure 2.1: Types of water-solid interactions [5]

The solid-water interactions can be categorised in surface interactions, condensed water interactions, and water internalised into the solid (Figure 2.1). Further, 5 types of water-solid interaction can be distinguished [5]: i) adsorption, ii) deliquescence, iii) capillary condensation, iv) absorption, and v) formation of crystal hydrate. All these interactions are relevant for electronic assembly due to the material, architecture, and surface contamination. On the surface of the PCBA, most important aspects are the adsorption, deliquescence, and capillary condensation. Ingress of water via absorption alters the bulk material properties of PCB laminate or component and in that way causes internal degradation of the device e.g. due to conductive anodic filament formation (section 3.3).

2.1.1 WATER ABSORPTION BY THE PCBA

Firstly, the moisture ingress into PCB laminate can cause hygroscopic swelling [6] and induce delamination within multilayer PCB [7]–[9]. The moisture ingress prior to soldering e.g. during storage can cause delamination at the later stage of manufacturing e.g. reflow soldering of the surface mount components (SMCs) [10]–[12]. Secondly, if an electronic device is exposed to high humidity during service life, water absorption can affect the thermal properties of PCB materials [13], and the dielectric property of the laminate resulting in an increase of interfacial leakage [14], and an increase of the capacitance within the multi-layered PCBA [15]. The capacitance change of PCB laminates and the moisture content in the laminates follows a linear relationship [16] and therefore reported to be useful for evaluating the moisture content [17]. Relatively high adsorption to the surface and permeation through the FR-4 laminate is dependent on the morphology of the

laminate as shown in Figure 2.2. The FR-4 laminate typically shows a porous structure with the possibility of high water uptake due to capillary effects. During the assembly process, the circuitry is protected from interacting with the solder by applying a solder mask, thereby covering most of the laminate surface. Although solder mask acts as an insulator of known dielectric property between components and traces and protects holes and traces from collecting contaminants [18]; it does not protect the laminate against the moisture ingress, and typically has higher diffusion coefficient compared to FR-4 laminates.

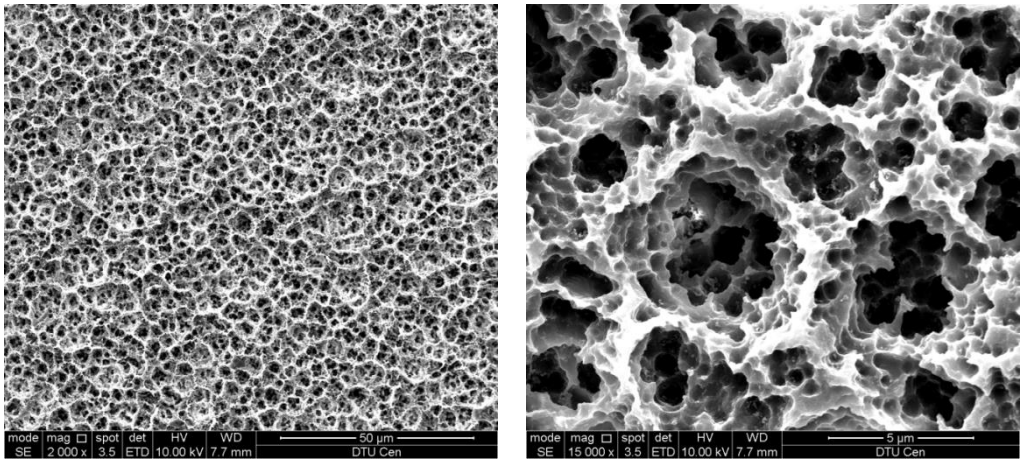

Figure 2.2: Surface morphology of a FR-4 laminate

The changes of electrical properties due to moisture ingress into PCB laminate can compromise functional parameters of the electronic device. Therefore, both short term and long term effect of humidity and temperature conditions have to be thoroughly evaluated in order to design robust electronics.

2.1.2 WATER ADSORPTION BY THE HYGROSCOPIC CONTAMINANTS ON THE PCBA

Water adsorption by the water soluble ionic residues and contaminants on the surface of the PCBA influences the surface insulation resistance (SIR). The number of adsorbed molecular layers of water increases with the RH, and when the ambient RH reaches a certain threshold value, hygroscopic substance deliquescence and forms a solution [19]. Deliquescence can be defined as a phase transformation of the solid to a saturated solution, which is triggered at a well-defined relative humidity that depends upon the properties of the solid and the temperature [20]–[22]. At the deliquescence RH, the aqueous solution is the thermodynamically favoured phase, while below this RH, the crystalline solid surrounded by gaseous water is present.

The schematic of the deliquescence process of particles of ionic residues on a typical surface and its effect on SIR is shown in Figure 2.3. When the ambient RH is below the deliquescence RH, water interacts with the hygroscopic particle through the mechanism of adsorption. For example, NaCl below deliquescence RH adsorbs 2-3 monolayers of water and bulk dissolution is not seen [23]. As the bulk dissolution of ionic residues does not occur at the RH below deliquescence, the SIR on the PCBA remains high.

Upon increasing the relative humidity, more water vapour is adsorbed at the surface, and when the RH exceeds critical RH of the solid, a thin film of a saturated solution of the solid develops on the particle. The colligative effect and high solubility of the solid causes a substantial reduction in the water vapour pressure of the saturated aqueous solution compared to the vapour pressure of pure water. Due to this effect water condense at a lower relative humidity value when ionic residues are present on the surface [24]. The chemical potential of pure liquid water in equilibrium with water vapour can be expressed [5]:

$$\mu = \mu_0 + RT \ln p_0 \quad (1)$$

where μ_0 is the standard chemical potential, R is the gas constant, T is the temperature in degree Kelvin, and p_0 is the vapour pressure. At a constant temperature, the saturated aqueous solution of ionic residues has a vapour pressure p_s, which is less than p_0, and a chemical potential μ_s, the difference in chemical potential between water in the solution and pure water can be expressed as:

$$\mu_s - \mu = RT \ln \left(\frac{p_s}{p_0}\right) \quad (2)$$

Water in the film of a saturated solution will have a lower thermodynamic activity relative to pure water and therefore act as a driving force for condensation of water when the vapour pressure exceeds p_s, or equivalently when the RH of the surroundings exceeds the critical. Water vapour condensing into the film raises the vapour pressure of the film similar to the surrounding water vapour pressure. However, continued dissolution of the ionic residues will result in keeping vapour pressure level to critical RH until all of the contaminant dissolves. Equilibration with the atmosphere is reached when complete dissolution and some degree of solution dilution have reached [25]. Increased dissolution of the ionic contaminants will contribute more to the faradaic current due to electrochemical corrosion process between two electrodes causing a reduction in SIR values. A significant reduction of the SIR will be observed when the complete dissolution of the contaminant takes place.

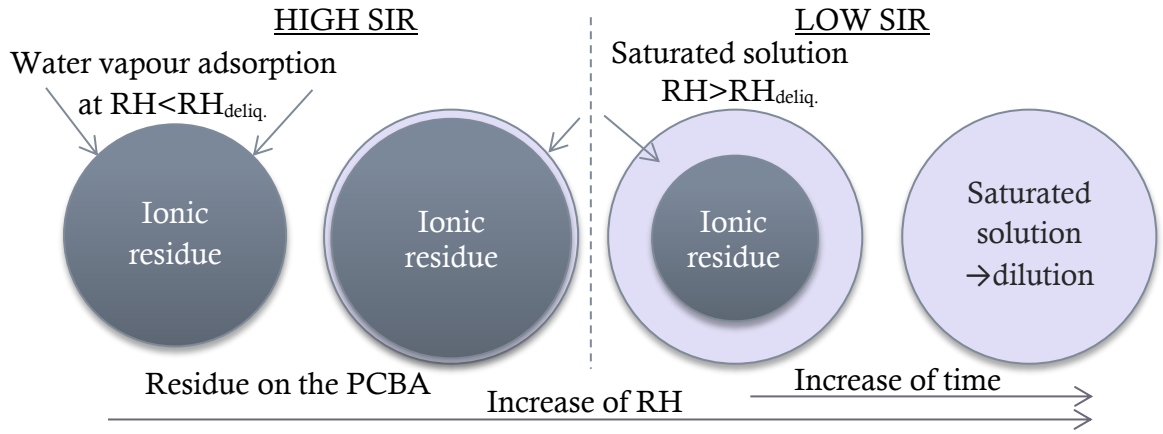

Figure 2.3: Schematic of deliquescence process in relation to the effect on SIR (adapted from [5][25])

From the climactic reliability point of view, the level of RH when deliquescence of ionic contaminant occurs is an important parameter, as it determines the limits for the RH when electronics will experience a significant reduction in SIR values. Table 2.1 provides a summary of the deliquescence RH for most commonly found contaminants on the PCBA. A clear correlation

between the deliquescence RH and solubility of the ionic contaminants can be seen. The contaminants with higher solubility in water show lower deliquescence RH. The deliquescence RH also varies with temperature as the solubility is a function of temperature. For most organic compounds, solubility typically increases with an increase in temperature which will lead to a decrease in deliquescence RH. The thermodynamics of temperature effects on deliquescence in detail can be found elsewhere [21], [22], [26].

Table 2.1: Deliquescence relative humidity of common contaminants on the PCBAs

Common contaminant	**Deliquescence RH (%)**	**Solubility in water (g/kg H_2O)** [29]
Activators in the flux systems		
Adipic	99.6[a]; ≥99[c]	$15_{15°C}$
Succinic	98[a]; >94[b]; 98.8[b*]; ≥98[c]	$83.5_{25°C}$
Glutaric	84[a]; 83.5-85[b]; 88.0-88.5[b*]; 89-99[c]; 85±5[d]	$1400_{25°C}$
DL-malic	86[a]; 78[e];	$1440_{26°C}$
Oxalic	97.3[b*]	$95.2_{20°C}$
Maleic	83±5[g]	$789_{25°C}$
Malonic	65.2[b*]	$736_{20°C}$
Citric	79[e]	$1440_{20°C}$
Suberic	No deliquescence <90%RH[h]	$2.43_{25°C}$
Palmitic	-	$0.007_{20°C}$
Abietic	-	
Hygroscopic salts		
NaCl	76[a]; 75-76[f]	$359_{25°C}$
NaF	97[a]	$43.34_{25°C}$
NaBr	84[a] ; 45[i], 58[i]	$945_{25°C}$
KCl	84[a]; 83.3[i], 91[i]	$355_{25°C}$
$MgCl_2$	44[a]	$560_{25°C}$
$CaCl_2$	29[a]; 32.3[i]	$812_{25°C}$
Other		
Polyethylene glycol 400 (PEG 400)**	0[a]	

[a] – calculated [30]; [b] – single particle levitation using an electrodynamic balance at 25 °C [31]; [b*] – saturated solution at 25 °C [31]; [c] – predicted by UNIFAC [32]; [d] – by using tandem differential mobility analyser system (TDMA) [33]; [e] – [34]; [f] – [35]; [g] – single particle levitation using an electrodynamic balance [36], and [h] – [37]; [i] – from the references provided by S. T. Martin [19]; **critical RH of PEG is strongly dependent on the molecular weight [38]

The deliquescence RH of a mixture of two or more contaminants will, in general, be lower than of any of the individual components [5], [27], [28]. This is due to the fact that the addition of a second highly water soluble component will dilute the amount of water in the system with a corresponding decrease in the relative vapour pressure, as predicted by Raoult's law.

A prediction on the extent of deliquescence lowering can be done using Ross equation, which states that the deliquescence point of a mixture is dependent on the individual critical RH values. Therefore, the effect can be approximated by the product of the water activities of a saturated solution of each component:

$$a_w = (a_w^0)_1 + (a_w^0)_2 + (a_w^0)_3 \ldots \quad (3)$$

where a_w^o is water activity of the saturated solution, for solution 1, 2, 3 etc. The Ross equation can be rewritten in terms of critical RH, using the assumption that a_w^o is approximately equal to $RH_c/100$ by ignoring kinetic effects [5]:

$$\frac{RH_{c_comb}}{100} = \frac{RH_{c_1}}{100} + \frac{RH_{c_2}}{100} + \frac{RH_{c_3}}{100} \cdots \quad (4)$$

Ross equation provides a reasonable prediction of deliquescence lowering for binary systems [5], [28], however, the prediction capability decreases with the increase of number of solid ingredients. At first, this is related to the contributions of solute-solute interactions to a_w, while for the measurements of critical RH the likelihood that all compounds are in physical contact decreases with increase of number of ingredients.

2.1.3 WATER ADSORPTION TO THE SURFACE OF THE PCBA

The SIR on the printed circuit board is influenced by the number of water molecules adsorbed to the surface, and it can be defined as:

$$SIR = (\sigma t)^{-1} \quad (5)$$

where σ is the bulk conductivity and t is the film thickness. The number of ions increases with the amount of water adsorbed, but unless the surface is completely covered with the water molecules, the molecules are rather strongly bound to the surface by interaction with the solid. After the completion of the first layer, the water molecules become mobile, and consequently, not only the number of ions but also their average mobility will increase with the amount of adsorbed water [39]. The ion mobility and the charge carrier density both are unknown functions of water film thickness and influences the conductivity of the water layer and thus the SIR. However, it can be assumed that the SIR is mainly determined by the layer thickness of water adsorbed to the surface [40].

Brunauer-Emmett-Teller (BET) type equation, which was first derived from Langmuir theory by Brunauer, Emmett, and Teller in 1938 [41] for multilayer physical adsorption of the gas molecules on a solid can be effectively used for describing moisture adsorption from the atmosphere to the surface of the PCBA [40], [42], [43]:

$$\frac{x}{m(1-x)} = \frac{1}{m_0 c} + \frac{c-1}{m_0 c} x \quad (6)$$

where $x = p/p_0$ is the ratio of equilibrium and saturation pressure, m is the ratio of the weight of adsorbed water to the weight of the dry specimen, m_0 is the ratio of the weight of adsorbed monolayer to the weight of the dry specimen, and c is the BET constant. The BET type equation is useful for describing water vapour adsorption at low water activities, however, it shows a deviation for higher activities ($a_w > 0.5$) [44], [45]. Water activity is described as the ratio of vapour pressure in the substance and the vapour pressure of pure water at the same temperature. Alternatively, the models more effectively characterising the water adsorption for higher water activities can be found in the following references [46]–[48].

Adsorption isotherm for fiberglass reinforced epoxy [49] indicated that a significant increase of moisture adsorption occurs at RH greater than 80%. The adsorption isotherms obtained on Teflon and on the quartz [39] indicated that the surface of Teflon has a weak attraction for water molecules, and the conductivity increases exponentially with the number of adsorbed water

layers, whereas for quartz, the attraction is strong, thus the conductivity only commences to increase exponentially after the completion of first water layers. Therefore, the base materials of the PCBA, together with the surface morphology, as described for laminates in section 2.1.1, will have an influence on the water adsorption to the surface, and thus on measured SIR values.

2.2 CONTAMINATION

Ionic contamination on the printed circuit boards can be categorised as related to manufacturing processes or originating from the user environment as shown in Figure 2.4. Examples of process related contamination are arising from polymer additives, chemicals from etching, plating, and soldering processes. Service related contamination is strongly dependent on the place of exposure, however, it is mostly comprised of hygroscopic aerosols and dust particles consisting of a number of ionic substances. Among the manufacturing process related contamination often found on the PCBA, the residues resulting from the soldering processes can be considered as the most common cause of SIR and corrosion related issues on the PCBA.

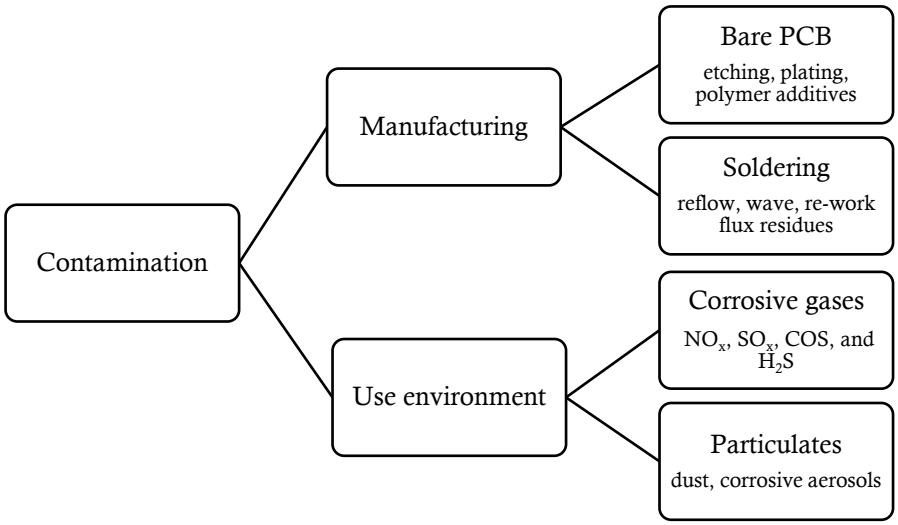

Figure 2.4: A generalised view of contamination on PCBA arising from manufacturing process and service life

2.2.1 ACTIVATORS IN THE FLUX (FLUX RESIDUES)

The components on the printed circuit boards are joined by the automated soldering processes such as wave or reflow soldering process. Selective soldering process is employed when only a part of the PCBA or components need to be soldered. The soldering process involves the use of a solder flux with a chemistry designed to remove the metal oxides natively present on the surfaces to be soldered. Solder flux also will remove any contamination which can act as a barrier between the pure metal and the solder, and increase the wettability of the PCBA surface for molten solder. The wave soldering process involves the use of liquid fluxes, which are sprayed or applied locally (selective wave soldering process). In the case of reflow soldering process, the flux is incorporated into the paste as a mixture with the powdered solder. Regardless of the soldering process, a certain amount of flux residues will be remaining on the finished PCBAs, thereby compromising the corrosion reliability of electronics [1]. The alternative method for joining the components

avoiding the use of flux is by using conductive adhesives, however, this method is not as common [50]–[52].

The formulation of the flux for reflow and wave soldering and the appearance of the flux residue on the soldered PCBA is different, although both flux residue types contain organic acids or/and halogens as activators. The activator which appears as a part of flux residue on the PCBA is known to cause a reduction of SIR and associated corrosion issues if exposed to humid conditions. The requirements for soldering fluxes and SIR testing are addressed in the following standards: IPC J-STD-004B [53], and IPC-9201 [54].

In current work, attention is drawn to the wave soldering fluxes, as in general, the amount of active components in the flux residue directly exposed to the ambient environment is higher compared to reflow soldering [55]. Although, it is known that for the reflow residue, the active acids can be released over time, especially at elevated temperature and humidity conditions [56].

Wave soldering fluxes are comprised of a solvent, which is either water or volatile organic compound (VOC) such as alcohol, or a mixture of both. The solid content in the flux refers to the activator and the film-former. The film-former carries the activators in the flux and acts as a protective layer for further oxidation of the metal surface after evaporation of the solvent. The film-former also to an extent encapsulates the activator thereby shielding it from the exposure to humidity; however, it is more effective for the reflow solder residues. An example of flux residues resulting from the selective wave soldering is shown in Figure 2.5. The white residues in the picture are comprised of weak organic acid (activator) and resin (film-former).

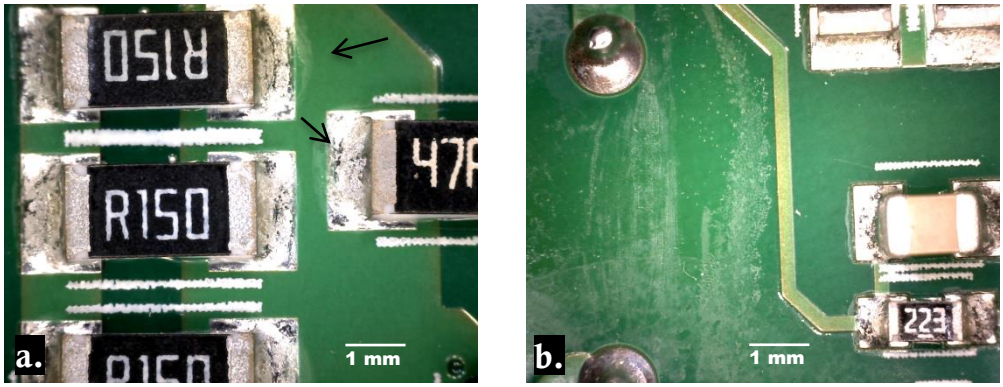

Figure 2.5: An example no-clean flux residues on a PCBA surface: a. reflow and b. selective wave soldering

According to IPC J-STD-004B [53], flux systems can be divided into four groups: i) rosin (RO), ii) resin (RE), iii) organic (OR), and iv) inorganic (IN). Further, fluxes are ranked based on their activity. Non-activated or activated fluxes refers to whether chemicals have been added to increase activity [57]. Generally, pure rosin flux is said to be non-activated, while other resin-based flux is activated. Activated flux can be further categorised based on its activity, and these categories can be sub-divided into 0 or 1 indicating whether it contains halide or not [53], [57]:

L – Low, or no flux or flux residue activity (<0.05% (0) and <0.5% (1))
M – Moderate flux or flux residue activity (<0.05% (0) and (0.5-2)% (1))
H – High flux or flux residue activity (<0.05 (0) and >2% (1))

The fluxes can also be categorised as washable or no-clean. The advantage of no-clean flux is that the residue, which is typically composed of resin and weak organic acid (WOA), decomposes and

volatizes during soldering. Therefore, the remaining residue is aimed to be benign and do not require post-soldering cleaning process. No-clean fluxes can be formulated with various levels of resin, which are generally referred to as solids. Typically, high solid content flux does not require the use of inert environment for soldering, however, it will leave excessive residues on the board, while the low solids flux (<5 wt.%) will leave barely visible residue and thus is commonly assumed to have a low influence on corrosion. However, visual observations not always match with the actual corrosivity of the residues. From the corrosion point of view, the most important component in the flux is the ionic activator namely the WOAs or halogens. The WOAs typically used in soldering fluxes are known to be hygroscopic [29] and characterised by different acidity and decomposition temperatures. A summary of the physical/chemical properties of commonly used WOAs is provided in Table 2.2.

Table 2.2: Summary of selected physical and chemical properties of WOAs found in no-clean solder flux [29]

Acid	Molecular formula	Molecular weight (g/mol)	pK_{a1}	pK_{a2}	Solubility (g/1000 g H_2O)	Melting point (°C)	Boiling point (°C)
Adipic	$HO_2C(CH_2)_4CO_2H$ 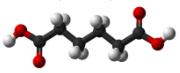	146.14	$4.41_{18°C}$	$5.41_{18°C}$	$15_{15°C}$	151.5	337.5
Succinic	$HO_2C(CH_2)_2CO_2H$ 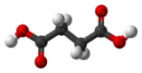	118.09	$4.21_{25°C}$	$5.64_{25°C}$	$83.5_{25°C}$	185	234
Glutaric	$HO_2C(CH_2)_3CO_2H$ 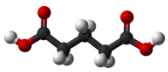	132.12	$4.32_{18°C}$	$5.42_{25°C}$	$1400_{25°C}$	97.9	273
DL-malic	$HO_2CCH(OH)CH_2CO_2H$ 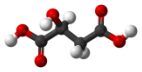	134.09	$3.40_{25°C}$	$5.11_{25°C}$	$1440_{26°C}$	132	
Palmitic	$H_3C(CH_2)_{14}CO_2H$ 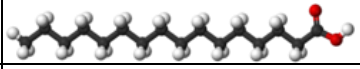	256.42	4.78	-	$0.007_{20°C}$	62.5	351
Suberic	$HO_2C(CH_2)_6CO_2H$ 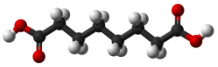	174.19	$4.52_{25°C}$		$2.43_{25°C}$	142.3	345.5
Maleic	$HO_2C(CH)_2CO_2H$ 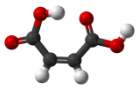	116.07	$1.92_{25°C}$	$6.23_{25°C}$	$789_{25°C}$	143.5	
Abietic	$C_{20}H_{30}O_2$ 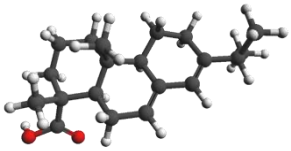	302.45	4.64		-	173.5	250

The extent of WOAs dissociation and ionisation determines the strength of the acid and the conductivity of water film formed on a PCBA surface. Higher ionic conductivity can be expected for the WOAs with higher dissociation rate, which is described as the ratio of the concentrations of the dissociated ions and the undissociated molecules. The negative of the logarithm of the acid dissociation constant denoted as pK_a for the 1st and 2nd dissociation constants is provided in Table

2.2. It is important to note that the pK_a values provide dissociation in water, whereas in the case of WOAs present as residue on the surface of PCBA, the accessibility of water for the acids to be dissolved is a function of RH. The RH level for the complete dissolution of WOA is determined by the hygroscopic property of WOA i.e. deliquescence RH. The deliquescence RH of WOAs is also related to the solubility of WOAs. The acids with high solubility would saturate in a tiny droplet of water, whereas low solubility acid would require a higher amount of water to be adsorbed to the surface, and will be dissolved at higher RH (more information in section 2.1.2).

The temperature effect on the WOAs has an importance, as the residues of no-clean flux are supposed to degrade and volatilize during exposure to soldering temperature, and the remaining residue of no-clean flux is aimed to be benign. This was shown on the di-carboxylic acids namely adipic and succinic acids at wave soldering temperatures [58], [59]. The melting and boiling temperatures provided in Table 2.2 indicate the variation in the response of different WOAs to the temperature rise during the soldering process. It is also important to note that as the temperature increases the reaction rate of the WOAs with the metal surface also increase. The properties of the formed acid-metal complexes and acid anhydrides can differ from that of the WOA itself. For example, in the study of characterising the weak organic acids used in low solids fluxes [60], different behaviour of adipic-acid-copper complexes was observed. The formation of dendrites was observed for the green crystalline residue which was proposed to be soluble in water i.e. the copper adipate complex. Whereas formation of chelated copper adipate, complex not soluble in water, resulted in no dendrites and relatively high SIR values on a standard SIR test pattern with copper finish [60]. The temperature has also an effect on the removal of copper oxide. The rate of copper oxide removal was greater for adipic acid compared to maleic at 180 °C; however, the effect was reversed at 140 °C, as suggested, likely due to relatively low decomposition temperature for maleic acid and reformation of copper oxides [61].

2.2.2 USER ENVIRONMENT RELATED CONTAMINATION

User environment related contamination can be divided into particulate contaminants and corrosive gases. The corrosive gasses can be readily present in the atmosphere, or they can be formed in the surrounding of electronics during life in service e.g. degassing from the polymer packaging. The exposure to corrosive gasses like NO_x, SO_x, COS, and H_2S, or highly reactive halogens, can cause corrosion and failures in conductors, solder joints, interconnects and electrical contacts. It may also affect the SIR under humid conditions and cause formation of dendrites i.e. silver sulphide dendrites due to the presence of sulphur gases [62].

The particulate contamination (dust) present in the atmosphere includes: sulphate, chloride, nitrate, formate, acetate, ammonium etc. [63]–[65]. Deposition of corrosive aerosols on the PCBAs alone usually will not affect the electrical functionality of the device especially if electronics is operating under controlled humidity. Therefore, the corrosive particles can accumulate on a circuit board over the years and create bridges of agglomerated particles between adjacent conductors [66], which are so-called dust dendrites. It is more commonly seen for electronic assemblies that are cooled by forced air circulation, as shown in Figure 2.6. The detailed discussion on the design aspects of electronics devices with respect to the effect of dust can be found elsewhere [67], [68]. The deposition of particles at certain locations on the PCBA is also enhanced by the electrostatic forces between the components [66].

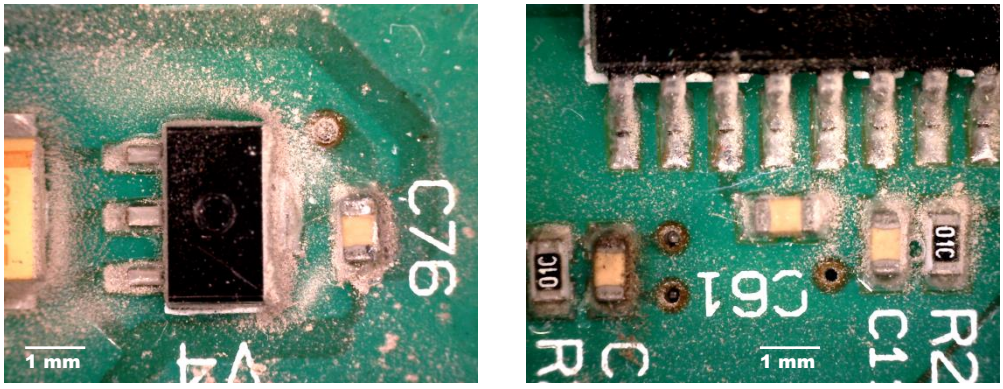

Figure 2.6: An example of dust deposited on a PCBA cooled by forced air circulation

Particulate contamination can be divided into coarse (> 1 μm diameter) and fine particles (< 1 μm diameter). According to ISO 14644-1:1999, the 9 classes of environments for cleanrooms are described based on the quantity and size of the particles from 0.1 μm to 5 μm. The corrosivity of air is commonly determined by the method described in ISA-71.04 (ISA 1985). When a copper coupon is exposed to the environment for one month, and the thickness and chemistry of the corrosion product are analysed using coulometric reduction to classify the environments. Environments are classified at one of four severity levels starting from G1 as mild with 300 Å/month to GX as harsh with >2000 Å /month.

Failure modes by dust particles as listed by ASHRAE [69] are following: i) mechanical e.g. obstruction of cooling airflow, interference with moving parts, abrasion, optical interference, interconnect interference, or deformation of surfaces, ii) chemical e.g. dust settled on the printed circuit boards can lead to component corrosion and/or to the electrical short circuiting of closely spaced features, and iii) electrical e.g. impedance changes and electronic circuit conductor bridging.

The probability of the chemical and/or electrical failure on the PCBA contaminated with dust increases significantly when the RH locally on the PCBA increases above a critical RH, when deliquescence of corrosive particles occurs. The classification of the dust and prediction of their effect on the electrical performance on the devices is difficult due to complex nature of dust particles. However, the particulate contamination can be characterised by its quantity and its corrosivity. In turn, the corrosivity of the dust can be estimated by determining the deliquescence RH. Dust with high deliquescence RH is generally more benign, while the dust with low deliquescence RH is generally more corrosive [69]. Low deliquescence RH of dust also shows that it contains more water soluble ionic substances. The deliquescence of some common aerosol contaminants can be found in Table 2.1 in section 2.1.2.

In general, the most important parameter determining the impact of dust on the electrical effects on PCBA is the RH [3]. The degradation of impedance measured on the SIR patterns pre-contaminated with natural dust particles [70] indicated the importance of deliquescence of the dust particles in relation to the reduction of impedance. The effect of hygroscopic particle depositions on the electrical functioning of electronics was demonstrated at television sets, which were selected to represent typical electronic devices in the office buildings, such as computers [66]. Failures of circuit boards due to hygroscopic dust have been reported [71], [72].

3. HUMIDITY AND CONTAMINATION RELATED FAILURES

3.1 LEAKAGE CURRENT/SIR

The SIR related failures are directly linked to the humidity and ionic contamination present on the PCBAs, as described previously. In general, on a relatively clean PCBA operating under normal humidity conditions (~70 %RH), the leakage currents are below nA level and seldom create any problems for the functioning of electronic circuitry. The levels of leak current may exceed nA level if condensation on the clean surface occurs, and a significant increase of leakage currents can be detected if ionic contamination deliquescence on the surface of a PCBA. The corrosion of metallic parts under bias voltage will further increase the leakage currents, thus likelihood for failure. Due to the fact that the SIR related failures can occur without leaving visible traces of corrosion on the PCBA, the identification of such failures is hardly possible, and during failure analysis, they are commonly attributed to 'no-fault found' category [73], [74].

The impact of process related contamination and climate is commonly ascertained by the SIR measurements (more details on the test method can be found in section 4.1), and the most common cause of leakage currents and corrosion on the PCBAs is the flux residue [75]–[81]. To prevent the corrosion of PCBAs under severe conditions, the common practice is to apply a conformal coating. However, applying the conformal coatings on a PCBA with high amounts of no-clean flux residues in a long term can cause delamination of the coating. Both hygroscopic effects and hydrolytic processes impair the adhesion of the coatings and the protection they typically provide. High leakage currents can be observed at the interface, where hygroscopic contaminants will absorb the water permeated through the coating [2], [55], [82]–[84].

A reduction of surface insulation resistance was also reported to affect the radio frequency performance [85], [86]. Ionic contamination such as flux residues changes the capacitance of the trough-connection contact areas, which primarily affects the signal integrity of high-density integrated and high-frequency circuits. A reduction of SIR and subsequent corrosion finally leading to dendritic growth (see section 3.2) have been reported between solder balls under a ball grid array (BGA) [80]. As a solution of SIR related issues arising due to no-clean flux residues, the cleaning process for electronic assemblies can be addressed [87], [88]. However, cleaning process has its own challenges related to the component compatibility with the cleaning process, removal of the cleaning agents and the contamination after cleaning process, and the possibility for cleaning agents to influence corrosion resistance of metals and alloys on the PCBA [1].

3.2 ELECTROCHEMICAL MIGRATION

The phenomenon of metal migration (electrochemical migration) was first observed in the late 1940s and early 1950s [89]. First large scale problems related to electrochemical migration were silver migration in post office equipment where contact springs were silver-plated in an attempt to reduce contact resistance. The phenomenon of electrochemical migration is still relevant today. In fact, it can be named as one of the main threats to the reliability of electronics operating under humid and condensing environments. The impact on the functioning of an electronic device is due to a significant reduction of SIR, which occurs at the event of short circuiting of adjacent

conductors on the PCBA when dendrite forms. An example of electrochemical migration and tin dendrites is shown in Figure 3.1.

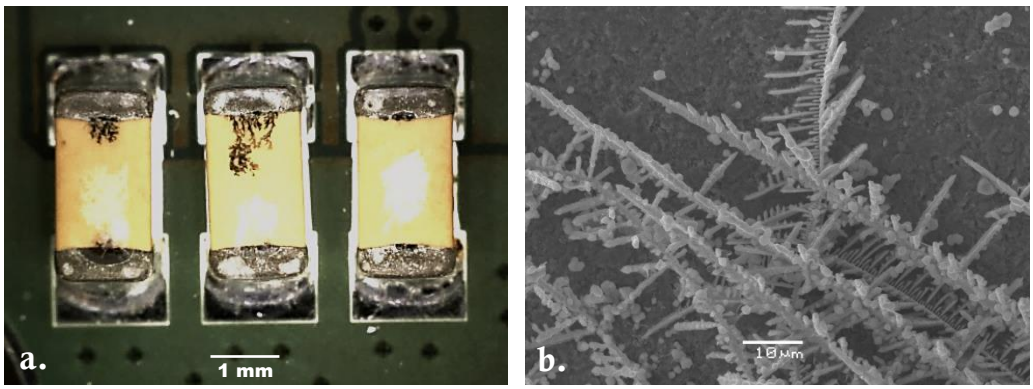

Figure 3.1: An example of ECM on a PCBA: a. overall view on the PCBA and b. SEM image of tin dendrites

The electrochemical migration can be viewed as a three-step process:

i) Electrodissolution: oxidation of metal which usually occurs at the anode (positive electrode), but may also occur at the cathode (negative electrode) for some amphoteric metals such as aluminium.
ii) Ion transport: transport of ionic metal species is driven by the electric field, also diffusion, and/or convection.
iii) Electrodeposition: reduction of ionic metal species at the dendrite nucleation site at the cathode.

There are three conditions to be fulfilled for electrochemical migration to occur: i) presence of water layer supporting ion transport, ii) electrical bias, which acts to dissolution of metal, ion transport, and consequent reduction, and iii) pH conditions favourable for metal ion transport and reduction at the cathode. The electrical bias [90], [91] and the distance between the electrodes [92], [93] influence the time to electrochemical migration. The amount of contamination under water droplet condition influences the dissolution rate of metal ions [94]–[96], while under humid conditions, it affects the adsorption and absorption of water from the atmosphere thereby increasing the water layer thickness and allowing metal ion transport.

A number of investigations were performed to rank common metal alloys on PCBAs for electrochemical migration susceptibility [90], [97], [98]. A correlation between the solubility of metal ion hydroxides in water with the time to dendrite formation was reported [90], [97]–[99]. Among the common materials on a PCBA, Sn^{2+} hydroxides are least soluble in water, thus suggesting the highest amount of hydroxide precipitation and longest time to failure, whereas, Ag^{+} are highly soluble in water, and thus are characterised by relatively short time to dendrite formation. The reason for this behaviour is connected to the availability of ions for migration in the solution, which is higher for more soluble compounds.

The tests for electrochemical migration susceptibility can be performed under water droplet condition [90], [94], [95], [97], [98], [100], thin electrolyte layers [101], [102], or at elevated humidity/temperature conditions [77], [103], [104]. The tests are typically performed under DC voltage, and only a limited number of investigations were performed under AC [105]–[108], or pulse voltage [109].

3.3 CONDUCTIVE ANODIC FILAMENT FORMATION

Conductive anodic filament (CAF) formation is an electrochemically induced failure mode in which conductive copper-containing salt grows from the anode to the cathode along the epoxy/glass interface. This failure mode was first reported in 1970s [49], [110], [111]. The failure was generated during testing of laminate materials for telecommunication and computer industry using accelerated test conditions (temperature, humidity, and bias voltage). Presently, the means to assess the propensity for CAF growth are described in IPC-TM-650 method 2.6.25.

Formation of CAF can be defined as two-step process [49]:

i) Degradation of the epoxy/glass interface: creation of a path for migration of the copper-conductive filament
ii) Electrochemical reaction: water absorption of the PCB laminate provides aqueous medium for electrochemical reactions on Cu conductors

During CAF formation, the electrolysis of water generates a pH gradient between the anode and cathode, and due to the pH drop at the anode, the Cu corrosion products become soluble. These soluble products will move through the weak opening in the laminate from the anode to the cathode due to the pH and concentration gradient [112], [113]. A substantial reduction in insulation resistance will be observed between the conductors at the event of conductive filament growing from the anode reaches the cathode. In contrast with dendrite formation during electrochemical migration, the CAF occurs at the interior of the PCB, and the filaments are composed of conductive salts, rather than metal ions reduced to metal. Further, the conductive salt filaments are growing from the anode towards the cathode.

The formation of CAF can occur for different conductor configurations in the PCB i.e. hole-to-hole, hole-to-trace (≈trace-to-hole), or trace-to-trace [113] (Figure 3.2 a.). The propensity for CAF formation for various conductor configurations will be determined by the distance between the anode and the cathode, and the properties of glass epoxy laminate and the orientation of the fibres within the matrix [114], [115]. The formation CAF is influenced by humidity, temperature, and bias voltage [116]. Further, the manufacturing process related contaminants i.e. residues from plating baths [117], or flux residues [116], [118] will influence CAF formation.

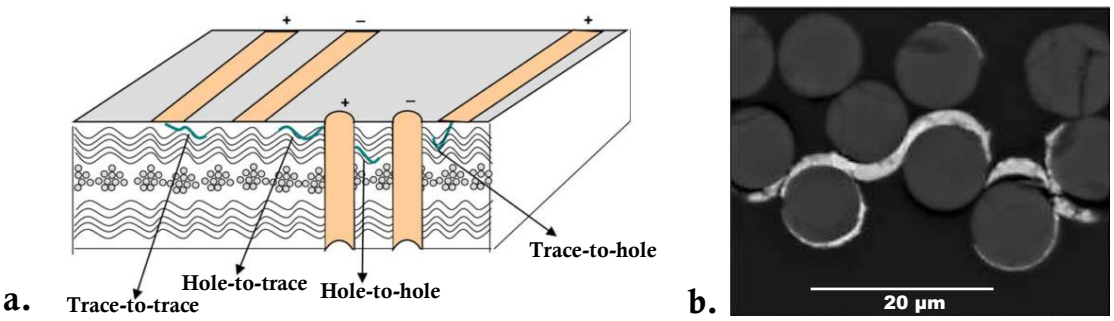

Figure 3.2 CAF formation: a. an illustration of CAF formation paths [113], b SEM image of CAF [117]

3.4 CREEP CORROSION

The corrosion of silver and copper metallisation on the printed circuit boards in presence of corrosive gasses can result in creep of solid corrosion product, mostly sulphides and chlorides of copper or silver, over a surface without the influence of an electric field. This type of corrosion on the PCBAs is commonly referred to as creep corrosion. The creep of corrosion product over a surface reduces the SIR and may lead to short circuiting of neighbouring features on the PCBA. Creep corrosion is accelerated by humidity, temperature, and the corrosive gasses [119]–[121]. The examples of creep corrosion of silver and copper are shown in Figure 3.3.

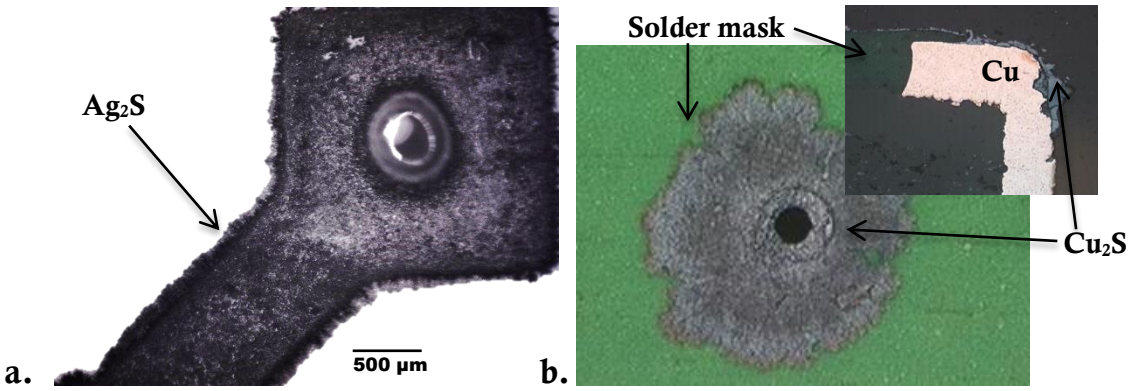

Figure 3.3 Examples of creep corrosion: a. Ag corrosion in H_2S environment, b. Cu corrosion (OSP surface finish) [122]

3.5 CORROSION OF WIRE BONDS IN MICROELECTRONICS

Wire bonding is a key technology in electrical interconnections between integrated circuits and the external circuitry of microelectronics. Different combinations of wire and bond pad materials can be used [123], however, Au, Al, Cu, and Ag are most commonly used metals. There are various aspects for consideration when selecting the materials for interconnects, that are described in detail elsewhere [123]. However, from the corrosion reliability point of view, a combination of dissimilar metals is more prone to failure, as due to galvanic corrosion. Acceleration factor for the wire bond failures, in that case, becomes the RH, temperature, contamination and corrosive gasses.

The degradation of wire bond strength due to halides is a well-known problem in microelectronics. Halogens can also corrode wire bonds, thereby reducing the strength of the bonds or eventually causing ball lifts. The commonly reported corrosion issues related to halogens can be generally attributed to chlorine [124]–[126], bromine [124]–[128], or fluorine [129]. The source of halogens in microelectronic devices is typically the polymeric mould-compounds used for the encapsulation of the integrated circuits or the halide surface contaminations on the dies prior to moulding. Degassing from the relatively stable halogenated compound tetrabromobisphenol-A, which is used as flame retardant in mould-compounds [130] and laminated printed circuit boards [131] also reported to corrode Au-Al wire bonds [124] [132].

4. TESTING OF CLIMATE AND CONTAMINATION EFFECTS

Climatic testing is used evaluate the performance of particular components of a PCBA or an entire electronic device in severe environments that involve high humidity and elevated temperatures. The aim of climatic testing is to gain a better understanding of the effects of climate changes on electronic components such as failures due to the parameter shifts i.e. due to SIR reduction and corrosion. An overview of test methods commonly used to evaluate the impact of particular climate and contamination conditions on the functioning of electronics is shown in Figure 4.1.

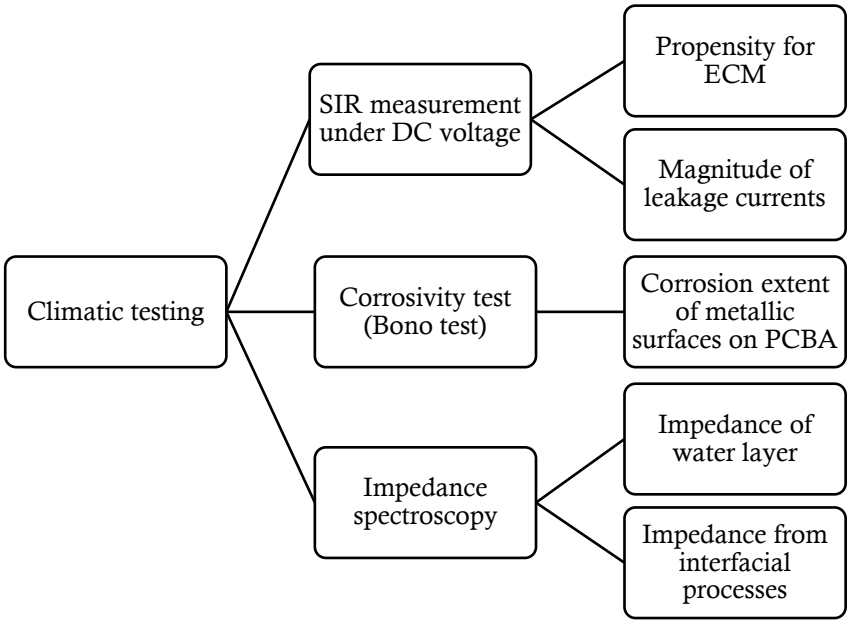

Figure 4.1: Various methods applied in climatic testing of electronics

4.1 SIR TESTING

Surface insulation resistance (SIR) measurement is the most common test method for process quality control. The SIR specifications and methodology were adopted in early 1970's when solder fluxes were almost entirely rosin based [133]. The purpose of the SIR testing is primarily to understand the impact of flux residues/contamination on the electrical performance of a device, specifically the conductive and corrosive nature of contaminants. The data obtained during SIR measurements provide a combined result of the leakage current and corrosion. The SIR testing can also be used to evaluate deterioration of SIR comb material under desired environmental conditions. Typically, the SIR testing is performed under constant RH and temperature conditions under DC voltage. The test conditions from various relevant standards are provided in Table 4.1.

Table 4.1: Overview of SIR and electrochemical migration tests

Standard	Environment	Bias voltage (V)	Test voltage (V)	Test duration (hours)	Pass-Fail criteria
IPC-TM-650 2.6.3.3	85°C/85%RH	45-50	-100	168	<100 MOhm
IPC-TM-650 2.6.14.1	40°C/93%RH, 65°C/88%RH, 85°C/85%RH	10	45-100	500	Dendrites
J-STD-004B (IPC-TM-650 2.6.3.7)	40°C/90%RH	5	5	>72	<100 MOhm Dendrites, corrosion
GR-78-CORE	65°C/85%RH	10	45-100	500	Dendrites
IEC 61189-5	40°C/93%RH	5	5	72	

The current between the comb pattern electrodes during the test is converted into SIR values. The measure of SIR gives the resistivity of the surface in ohms per square (normalised area). The geometry of test coupons i.e. width of the conductive lines, and the spacing in-between, and the number of squares varies with the test board. Copper surface finish is most common; however, SIR patterns may also have solder finish i.e. hot air solder leveling (HASL), or any other metallisation relevant to PCBA designs. Most commonly used standardised test boards are the following: IPC-B-24 (surface insulation resistance), IPC-B-25(A) (multipurpose test board), IPC-B-36 (cleaning alternatives) and IPC-B-52 (cleanliness and residue evaluation).

The drawback of SIR measurements is the nonlinear dependence on the geometry of the test pattern and applied voltage used to obtain the SIR data. The SIR values tend to be higher for higher voltages. Also, under low humidity the measured SIR values tend to be higher due to depletion of the ions across the electrodes, whereas when condensation occurs (due to variation in ambient conditions, or because of the deliquescence of highly soluble contaminants on the surface), the SIR decreases significantly due to corrosion and narrowing of the gap between the electrodes.

4.2 BONO TEST

The Bono test was presented as the test method to assess the corrosivity of the soldering fluxes in the late 1980's [134]. The concept was originally described by W. Rubin and B. M. Allen [135], and it was an improvement of then used specification QQS 571D (relevant standards are IPC J-STD-006 and ASTM B32) and Japanese JIS-Z-2519 test method employing polarization of copper wires. The improved method was a semi-quantitative corrosion test using a range of fine copper wires of varying diameter treated with heated soldering flux and exposed to a bias voltage. The time required for the wires to break was indexed as corrosivity. In contrast, the Bono test assesses the extent of corrosion by the change of resistance with respect to time.

The test board used for Bono test measurements is characterised by a set of significantly lower anode electrodes in parallel to thick cathode electrodes as indicated in Figure 4.2. The width of the anode electrodes is ~10 μm, the distance between anode and cathode was reduced from 2 mm in the original design [134] to 120 μm in the recent studies [136], [137]. The length of anode electrodes was changed accordingly from ~75 mm to 145 mm.

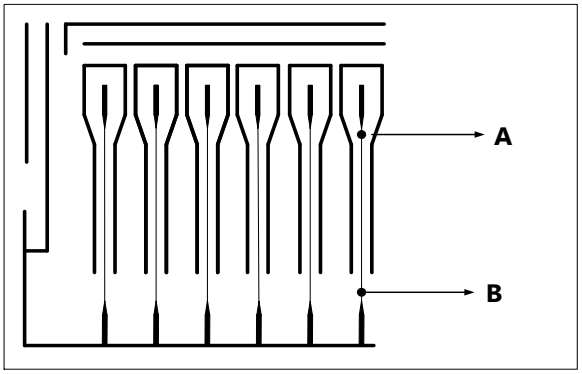

Figure 4.2: An example of the test pattern for resistance measurement (resistance reduction due to corrosion between A and B)

The tests are performed under desired humidity/temperature conditions. Prior to climatic exposure the test patterns are treated with soldering flux, or soldering paste, and exposed to soldering temperature profiles. Thereafter, the test patterns are exposed to accelerated humidity/temperature conditions under desired test voltage and the electrical resistance of anode tracks is measured. When corrosion occurs, the cross-sectional area of the anode tracks decreases, thereby the resistance of the track increases. The extent of corrosion is given by the 'corrosion factor', $\mathrm{CF}(t)$ derived from:

$$\mathrm{CF}(t) = \frac{R(t)-R(0)}{R(0)} \cdot 100\% \qquad (7)$$

where $R(t)$ is the electrical resistance of the anode electrode at a time t.

Bono test was effectively used to characterise corrosion effect of WOAs namely: abietic, succinic, glutaric, adipic, and malic, under humid conditions [137]. The advantage of Bono test over conventional SIR measurements was shown in the study of solder paste residue corrosivity assessment [136]. The comparison of test methods for characterising soldering fluxes and their interactions with substrates and metallisation including Bono test is also reported [138].

In contrast to SIR measurements, Bono test method directly represents the effect of corrosion. The effects from corrosion product or dendrite formation do not alter the experimental results. However, this test does not provide a direct link to the implications of corrosion on the functionality of PCBAs e.g. caused by leakage currents.

4.3 ELECTROCHEMICAL IMPEDANCE SPECTROSCOPY

Electrochemical impedance spectroscopy is an effective technique for characterising humidity and contamination effects in electronics. It has been used for studying moisture uptake by the glass-epoxy laminates [139], the conduction mechanisms on the surface of the printed circuit boards precontaminated with the flux [105], [140]–[143], studying the effect of hygroscopic dust particulates [70], and other ionic contaminants [144]. This technique can be used for electrical and electrochemical characterisation of the samples with various geometries. Dependent on the sample, and on the parameters of interest, several electrode configurations can be used, and the most common are depicted in Figure 4.3.

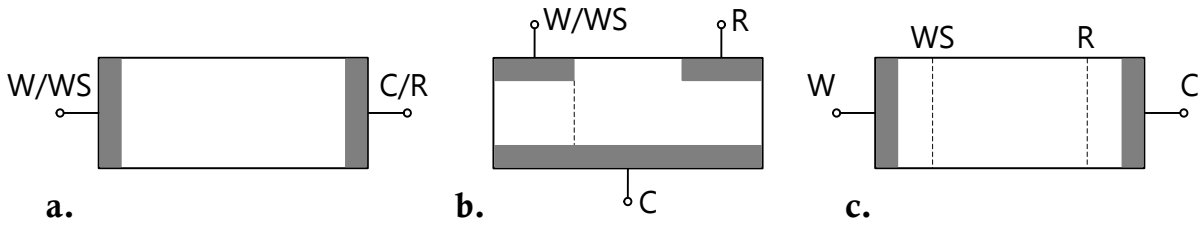

Figure 4.3: Electrode configurations for electrochemical impedance measurements: a. two-electrode, b. three-electrode, and d. four-electrode. (W-working, WS-working sense, C-counter, and R-reference)

A two-electrode configuration is the simplest and can be easily adapted for the measurements of impedance due to ionic contamination on the surface of the PCBAs. The contact is made to two opposite external surfaces, and the same set of electrodes serves to both, supply current to the sample and measure the voltage drop across the sample. The disadvantage of this configuration is the errors, the significance of which is important to evaluate when using this configuration. The impedance measurement with two probe configuration contains the parasitic capacitance (stray capacitance between the leads), the resistance of the connections made to the sample, and the inductance of the leads. For the measurements of the impedance change on the surface of the PCBA, the resistance of the contacts made to the samples can be neglected as it is much lower than the surface resistance of the board. The inductance of the leads may limit the impedance measurements at high frequencies i.e. above 100 kHz. Whereas the stray capacitance can be evaluated by measurement without the sample connected, and subtracting that value from the measurement conducted on the sample. There will be a limitation for using two-electrode configuration for measurements on the samples with low capacitance values.

Three-electrode configuration is most common for typical electrochemical applications and most suitable to study of electrochemical reactions occurring at the electrode-electrolyte interface. The measured current is that which flows from the counter electrodes to the working electrode, while the potential is measured between the reference electrode and the working electrode. If modified, the three electrode configuration can also be used for the bulk conductivity measurements i.e. PCB laminate or the coatings used in electronics. For that purpose, the guarding of the current measuring electrode is required, so that the surface current flow paths are interrupted, and the current passing through the bulk of specimen is recorded.

In the four-electrode configuration, the current supplying electrodes are separated from the voltage measuring electrodes. The impedance is calculated using current flowing through the specimen and the voltage across the set of inner voltage probes. The electrode impedances are excluded from the impendence measurements since the voltage measuring electrodes do not draw the current and are placed inside the current supplying electrodes. This configuration is typical for the electrolyte solution conductivity measurements. Similarly, it can be used for the surface conductivity measurements.

Impedance measurements on the PCBAs with different contamination levels as a function of humidity provide information on the water interaction with the test sample via resistivity of the water layer, charge transfer resistance, and double layer capacitance. The latter two are indicative of the electrochemical processes at the water-metal interface. The advantage of impedance measurement is that the small amplitude AC signal has minimal effect on the nature of electrodes and gives an indication of the surface conductivity in a wide range of RH and temperature

(including condensing conditions). However, the direct effect of such conditions on actual PCBAs (high humidity, or condensation) naturally leading to corrosion and/or electrochemical migration is not given, and requires testing at higher voltages, either DC or AC. For this purpose, the impedance of the system can be studied with small amplitude perturbation voltage, while the sample is biased continuously under DC voltage.

5. OVERVIEW OF LITERATURE AND CURRENT WORK

This chapter gives an overview of the investigations carried out in the current PhD thesis put into perspective with the literature summarized in chapters 2, 3, and 4.

The impact of contamination on the reliability of electronics is commonly assessed by SIR measurements. The effects of ionic contamination can also be characterized by impedance spectroscopy or corrosiveness measurements using Bono test as described in chapter 4. These tests are typically performed under constant temperature and humidity conditions, however, temperature cycling can also be used in order to increase the stress or create transient conditions for water condensation on the PCBA surface. The aim of the studies presented in papers 1, 2 and 3 (chapters 8-10) was to investigate the effect of contaminants, in particular, WOAs, solder flux, and NaCl, on the surface resistivity, corrosion, and electrochemical migration. The test conditions were optimised for the differentiation of corrosiveness of contaminants in respect to various humidity conditions. The solubility of the contaminants, and related deliquescence RH levels were shown to have a significant influence on corrosion reliability of printed circuit boards.

Literature available on electrochemical migration in electronics is extensive (section 3.2). The electrochemical migration susceptibility of various alloys was studied under water droplet conditions, thin layers of electrolyte, and humid conditions. Further, the investigations were performed on various samples such comb patterns, simplified two electrode systems, or directly on the surface mount components. The mechanism of electrochemical migration was explained in detail. The focus of the current investigation in paper 4 (chapter 11) was placed on the probability for electrochemical migration dependence on concentration and voltage. The aim was to show the differences between the two types of contaminant: NaCl and flux residue, and the importance when ranking the contaminants in terms of solution conductivity, leakage current, and the probability of electrochemical migration.

The effect of pulse voltage on electrochemical migration is not well understood yet; however, there are applications where a pulse voltage is used and the effect of pulse width and duty cycle needs to be investigated. This was also the aim of the investigations carried out in paper 5 (chapter 12), where the influence of pulse width and duty cycle was shown on the time to dendrite formation, and the related ratio of the metal ions reduced at the cathode and precipitated as tin hydroxides.

Au-Al interconnects are commonly used in microelectronics. The corrosion of Au-Al wire bonds have been studied in a wide range of environmental conditions, and the results are available in literature. The paper 6 (chapter 13) contains a study of Au-Al wire bond corrosion in iodine environment. The current work was motivated by the lack of information available on the corrosion in iodine environment and the fact that iodine degassing from the polyamide in the surrounding environment was reported as a current issue resulting in corrosion and deboning of

wire bonds. The emphasis was placed on the corrosion of Au-Al intermetallics in gaseous iodine (readily present due to degassing), and aqueous potassium iodide solutions (iodide attack of the wire bonds when condensation occurs).

The identification of SIR related failures in electronics is difficult, and the possibility of detection strongly depends on the extent of corrosion. Because the corrosion attack is often low, and the appearance of tin hydroxides due to corrosion is similar to the flux residues, the humidity related failures are commonly assigned to the 'no-fault found' category. The threshold conditions for failure in respect to RH level and contamination are dependent on the sensitivity of the circuit to the reduction of SIR. The identification of such failures occurring under thin electrolyte layers, resulting in tiny amounts of corrosion products would provide the capability for identification of corrosion prone areas during device level testing. This could be used for studying various aspects in relation to corrosion and climatic reliability i.e. PCBA layout, soldering process and related contamination, enclosure design etc. The new approach for identification of such failures on the PCBAs was developed during the current PhD project. The developed test method is based on the use of tin ion indicator in a gel (Paper 7, chapter 14).

The prediction of climate and contamination effects on the functioning of a circuitry and the overall reliability of electronic devices is important and highly useful if this can be carried out at the circuit design stage. Using such methods possible effects of climate can be assessed and needed design changes to the PCBAs and device can be made wherever possible. Paper 8 in chapter 15 describes how the empirical SIR and other electrochemical data can be used for simulating the climatic effects on performance of electronic components and electrical circuits. The paper also discusses certain approaches for improving reliability based on such analysis.

REFERENCES

[1] B. Kanegsberg and E. Kanegsberg, *Handbook for Critical Cleaning. Applications, processes, and controls*, 2nd ed. CRC Press, 2011, p. 524.

[2] K. Seeling and T. O'Neill, "Conformal Coating over No-Clean Flux," *SMT Surf. Mt. Technol. Mag.*, vol. 29, no. 4, pp. 52–58, 2014.

[3] M. Tencer and J. S. Moss, "Humidity Management of Outdoor Electronic Equipment: Methods, Pitfalls, and Recommendations," *IEEE Trans. Components Packag. Technol.*, vol. 25, no. 1, pp. 66–72, Mar. 2002.

[4] J. B. Jacobsen, J. P. Krog, A. H. Holm, L. Rimestad, and A. Riis, "Climate-Protective Packaging: Using basic physics to solve climatic challenges for electronics in demanding applications," *IEEE Ind. Electron. Mag.*, vol. 8, no. 3, pp. 51–59, 2014.

[5] L. J. Mauer and L. S. Taylor, "Water-solids interactions: deliquescence," *Annu. Rev. Food Sci. Technol.*, vol. 1, pp. 41–63, Jan. 2010.

[6] X. J. Fan, S. W. R. Lee, and Q. Han, "Experimental investigations and model study of moisture behaviors in polymeric materials," *Microelectron. Reliab.*, vol. 49, no. 8, pp. 861–871, 2009.

[7] E. H. Wong, S. W. Koh, K. H. Lee, and R. Rajoo, "Comprehensive treatment of moisture induced failure - Recent advances," *IEEE Trans. Electron. Packag. Manuf.*, vol. 25, no. 3, pp. 223–230, 2002.

[8] H. Frémont, W. Horaud, and K. Weide-Zaage, "Measurements and FE-simulations of moisture distribution in FR4 based printed circuit boards," in *7th International Conference on Thermal, Mechanical and Multiphysics Simulation and Experiments in Micro-Electronics and Micro-Systems*, 2006, pp. 1–6.

[9] F. Xuejun, Z. Jiang, and A. Chandra, "Package structural integrity analysis considering moisture," in *2008 58th Electronic Components and Technology Conference*, 2008, pp. 1054–1066.

[10] M. Lai, J. Botsis, J. Cugnoni, and D. Coric, "An experimental-numerical study of moisture absorption in an epoxy," *Compos. Part A Appl. Sci. Manuf.*, vol. 43, no. 7, pp. 1053–1060, 2012.

[11] "IPC-1601 Printed Board Handling and Storage Guidelines," Bannockburn, IL, 2010.

[12] "IPC/JEDEC J-STD-020D.1 Moisture/Reflow Sensitivity Classification for Nonhermetic Solid Statate Surface Mount Devices." 2008.

[13] L. Ma, B. Sood, and M. Pecht, "Effect of Moisture on Thermal Properties of Halogen-Free and Halogenated Printed-Circuit-Board Laminates," *IEEE Trans. Device Mater. Reliab.*, vol. 11, no. 1, pp. 66–75, Mar. 2011.

[14] A. Bradwell, "Importance of preventing moisture ingress to polymeric insulators," *IEE Proc. B Electr. Power Appl.*, vol. 131, no. 6, pp. 245–251, 1984.

[15] H. Frémont, J. Kludt, M. Wade, K. Weide-zaage, and I. Bord-majek, "Qualification procedure for moisture in embedded capacitors," *Microelectron. Reliab.*, vol. 54, no. 9–10, pp. 2013–2016, 2014.

[16] M. G. Pecht, H. Ardebili, A. A. Shukla, J. K. Hagge, and D. Jennings, "Moisture ingress into organic laminates," *IEEE Trans. Components Packag. Technol.*, vol. 22, no. 1, pp. 104–110, Mar. 1999.

[17] O. Thomas, M. Wickham, and C. Hunt, "Obtaining the moisture content of printed circuit boards from capacitance measurements," *Circuit World*, vol. 38, no. 2, pp. 68–74, May 2012.

[18] "IPC-HDBK-840 Solder Mask Handbook," Bannockburn, IL, 2006.

[19] S. T. Martin, "Phase transitions of aqueous atmospheric particles," *Chem. Rev.*, vol. 100, no. 617, pp. 3403–3453, 2000.

[20] G. Zografi, "Water-solid state interactions in pharmaceutical systems," *Top. Pharm. Sci. 1993*, pp. 405 – 419, 1994.

[21] A. S. Wexler and J. H. Seinfeld, "Second-generation inorganic aerosol model," *Atmos. Environ. Part A. Gen. Top.*, vol. 25, no. 12, pp. 2731–2748, 1991.

[22] I. N. Tang and H. R. Munkelwitz, "Aerosol phase transformation and growth in the atmosphere," *Journal of Applied Meteorology*, vol. 33. pp. 791–796, 1994.

[23] M. C. Foster and G. E. Ewing, "Adsorption of water on the NaCl(001) surface. II. An infrared study at ambient temperatures," *J. Chem. Phys.*, vol. 112, no. 15, pp. 6817–6826, 2000.

[24] G. Zografi, "States of water associated with solids," *Drug Dev. Ind. Pharm.*, vol. 14, no. 14, pp. 1905–1926, 1988.

[25] L. Van Campen, G. L. Amidon, and G. Zografi, "Moisture sorption kinetics for water-soluble substances. I: Theoretical considerations of heat transport control," *J. Pharm. Sci.*, vol. 72, pp. 1381–1388, 1983.

[26] C. F. Braban, M. F. Carroll, S. a. Styler, and J. P. D. Abbatt, "Phase transitions of malonic and oxalic acid aerosols," *J. Phys. Chem. A*, vol. 107, no. 34, pp. 6594–6602, 2003.

[27] A. K. Salameh and L. S. Taylor, "Deliquescence in binary mixtures," *Pharm. Res.*, vol. 22, no. 2, pp. 318–324, 2005.
[28] A. K. Salameh, L. J. Mauer, and L. S. Taylor, "Deliquescence lowering in food ingredient mixtures," *J. Food Sci.*, vol. 71, no. 1, pp. E10–E16, 2006.
[29] W. M. Haynes and D. R. Lide, *CRC Handbook of chemistry and physics*, 94th Editi. CRC Press, 2013, p. 2668.
[30] K. M. Adams, J. E. Anderson, and Y. B. Graves, "Ionograph Sensitivity to Chemical Residues from 'No Clean' Soldering Fluxes: Comparison of Solvent Extract Conductivity and Surface Conductivity," *Circuit World*, vol. 20, no. 2, pp. 41–44, 1994.
[31] C. Peng, M. N. Chan, and C. K. Chan, "The hygroscopic properties of dicarboxylic and multifunctional acids: measurements and UNIFAC predictions.," *Environ. Sci. Technol.*, vol. 35, no. 22, pp. 4495–501, Nov. 2001.
[32] P. Saxena and L. M. Hildemann, "Water absorption by organics: survey of laboratory evidence and evaluation of UNIFAC for estimating water activity," *Environ. Sci. Technol.*, vol. 31, no. 11, pp. 3318–3324, Nov. 1997.
[33] C. Cruz and S. Pandis, "Deliquescence and hygroscopic growth of mixed inorganic-organic atmospheric aerosol," *Environ. Sci. Technol.*, vol. 34, no. 20, pp. 4313–4319, 2000.
[34] A. Apelblat, M. Dov, J. Wisniak, and J. Zabicky, "The vapour pressure of water over saturated aqueous solutions of malic, tartaric, and citric acids, at temperatures from 288 K to 323 K," *J. Chem. Thermodyn.*, vol. 27, no. 1, pp. 35–41, Jan. 1995.
[35] I. N. Tang, H. R. Munkelwitz, and J. G. Davis, "Aerosol growth studies — IV. Phase transformation of mixed salt aerosols in a moist atmosphere," *J. Aerosol Sci.*, vol. 9, no. 6, pp. 505–511, 1978.
[36] L. Treuel, S. Schulze, T. Leisner, and R. Zellner, "Deliquescence behaviour of single levitated ternary salt/carboxylic acid/water microdroplets," *Faraday Discuss.*, vol. 137, pp. 265–278, 2008.
[37] N. C. Man, S. M. Kreidenweis, and C. K. Chan, "Measurements of the hygroscopic and deliquescence properties of organic compounds of different solubilities in water and their relationship with cloud condensation nuclei activities," *Environ. Sci. Technol.*, vol. 42, no. 10, pp. 3602–3608, 2008.
[38] J. A. Braid, R. Olayo-Valles, C. Rinaldi, and L. S. Taylor, "Effect of molecular weight, temperature, and additives on the moisture sorption properties of polyethylene glycol," *J. Pharm. Sci.*, vol. 99, no. 1, pp. 154–168, 2010.
[39] Y. Awakuni and J. H. Calderwood, "Water vapour adsorption and surface conductivity in solids," *J. Phys. D. Appl. Phys.*, vol. 5, no. 5, pp. 1038–1045, 1972.
[40] F. N. Fuss, C. T. Hartwig, and J. M. Morabito, "Corrosion of solder-coated TiPdAu thin film conductors in a moist chlorine atmosphere," *Thin Solid Films*, vol. 43, pp. 189–213, 1977.
[41] S. Brunauer, P. H. Emmett, and E. Teller, "Adsorption of Gases in Multimolecular Layers," *J. Am. Chem. Soc.*, vol. 60, no. 1, pp. 309–319, 1938.
[42] P. Dumoulin, J.-P. Seurin, and P. Marce, "Metal migrations outside the package during accelerated life tests," *IEEE Trans. Components, Hybrids, Manuf. Technol.*, vol. CHMT-5, no. 4, pp. 479–486, 1982.
[43] G. DiGiacomo, "Metal Migration (Ag, Cu, Pb) in Encapsulated Modules and Time-to-Fail Model as a Function of the Environment and Package Properties," in *20th International Reliability Physics Symposium*, 1982, pp. 27–33.
[44] A. D. McLaren and J. W. Rowen, "Sorption of Water Vapor by Proteins and Polymers: A Review," *J. Polym. Sci.*, vol. VII, no. 2, pp. 289–324, 1951.
[45] J. A. Barrie, "Water in polymers," in *Diffusion in polymers*, T. Crank and G. S. Park, Eds. Academic Press, 1968, pp. 259–313.
[46] C. Maggana and P. Pissis, "Water sorption and diffusion studies in an epoxy resin system," *J. Polym. Sci. Part B Polym. Phys.*, vol. 37, no. 11, pp. 1165–1182, 1999.
[47] E. O. Timmermann, J. Chirife, and H. a. Iglesias, "Water sorption isotherms of foods and foodstuffs: BET or GAB parameters?," *J. Food Eng.*, vol. 48, no. 1, pp. 19–31, 2001.
[48] J. Blahovec and S. Yanniotis, "'Gab' generalised equation as a basis for sorption spectral analysis," *Czech J. Food Sci.*, vol. 28, no. 5, pp. 345–354, 2010.
[49] D. J. Lando, J. P. Mitchell, and T. L. Welsher, "Conductive Anodic Filaments in Reinforced Polymeric Dielectrics: Formation and Prevention," in *17th International Reliability Physics Symposium*, 1979, pp. 51–63.
[50] Y. Li and C. P. Wong, "Recent advances of conductive adhesives as a lead-free alternative in electronic packaging: Materials, processing, reliability and applications," *Mater. Sci. Eng. R Reports*, vol. 51, no. 1–3, pp. 1–35, 2006.

[51] Y. Fu, J. Liu, and M. Willander, "Conductive Adhesives," in *Lead-free Electronics*, 2006, pp. 437–505.
[52] Y. Li, D. Lu, and C. P. Wong, *Electrical Conductive Adhesives with Nanotechnologies*. Boston, MA: Springer US, 2010, p. 437.
[53] "IPC J-STD-004B Requirements for Soldering Fluxes," Bannockburn, IL, 2008.
[54] "IPC-9201 Surface Insulation Resistance Handbook," Northbrook, IL, 1996.
[55] H. Conseil, M. Stendahl Jellesen, and R. Ambat, "Contamination profile on typical printed circuit board assemblies vs soldering process," *Solder. Surf. Mt. Technol.*, vol. 26, no. 4, pp. 194–202, Aug. 2014.
[56] M. S. Jellesen, M. Dutta, V. Verdingovas, and R. Ambat, "Detection of acid release from reflow solder flux residues using localized test methods," in *Eurocorr 2012*, 2012, pp. 1–10.
[57] M. Judd and K. Brindley, "Flux," in *Soldering in electronics assembly*, Newnes, 1999, pp. 89–108.
[58] K. Tellefsen and K. Stromgrem, "The Disappearance of Dicarboxylic Acid No-Clean Flux Activators with Time and Temperature," in *IPC PRINTED CIRCUITS EXPO*, 1996, pp. S9–5.
[59] K. S. Hansen, M. S. Jellesen, P. Moller, P. J. S. Westermann, and R. Ambat, "Effect of Solder Flux Residues on Corrosion of Electronics," in *Annual reliability and maintainability symposium*, 2009, pp. 503–509.
[60] B. A. Smith and L. J. Turbini, "Characterizing the weak organic acids used in low solids fluxes," *J. Electron. Mater.*, vol. 28, no. 11, pp. 1299–1306, Nov. 1999.
[61] G. Qu, S. S. S. Vegunta, K. Mai, C. J. Weinman, T. Ghosh, W. Wu, and J. C. Flake, "Copper Oxide Removal Activity in Nonaqueous Carboxylic Acid Solutions," *J. Electrochem. Soc.*, vol. 160, no. 4, pp. E49–E53, 2013.
[62] D. Minzari, M. S. Jellesen, P. Møller, and R. Ambat, "Morphological study of silver corrosion in highly aggressive sulfur environments," *Eng. Fail. Anal.*, vol. 18, no. 8, pp. 2126–2136, Dec. 2011.
[63] P.-E. Tegehall, "Impact of Humidity and Contamination on Surface Insulation Resistance and Electrochemical Migration," in *The ELFNET Book on Failure Mechanisms, Testing Methods, and Quality Issues of Lead-Free Solder Interconnects*, Springer, 2011, pp. 227–253.
[64] M. G. Perrone, B. R. Larsen, L. Ferrero, G. Sangiorgi, G. De Gennaro, R. Udisti, R. Zangrando, a. Gambaro, and E. Bolzacchini, "Sources of high PM2.5 concentrations in Milan, Northern Italy: Molecular marker data and CMB modelling," *Sci. Total Environ.*, vol. 414, pp. 343–355, 2012.
[65] J. D. Sinclair, L. A. Psota-Kelty, C. J. Weschler, and H. C. Shields, "Measurement and modeling of airbone concentrations and indoor surface accumulation rates of ionic substances at Neenah, Wisconsin," *Atmos. Environ. Part A. Gen. Top.*, vol. 24, no. 3, pp. 627–638, 1990.
[66] A. Litvak, A. J. Gadgil, and W. J. Fisk, "Hygroscopic fine mode particle deposition on electronic circuits and resulting degradation of circuit performance: An experimental study," *Indoor Air*, vol. 10, no. 1, pp. 47–56, 2000.
[67] M. Tencer, "Deposition of aerosol ('hygroscopic dust') on electronics - Mechanism and risk," *Microelectron. Reliab.*, vol. 48, pp. 584–593, 2008.
[68] David Lohbeck, "Design for dust," *Test Meas. World*, vol. 28, no. 3, pp. 47–52, 2008.
[69] ASHRAE, "2011 Gaseous and Particulate Contamination Guidelines For Data Centers," *Am. Soc. Heating, Refrig. Air-Conditioning Eng.*, pp. 1–22, 2011.
[70] B. Song, M. H. Azarian, and M. G. Pecht, "Effect of Temperature and Relative Humidity on the Impedance Degradation of Dust-Contaminated Electronics," *J. Electrochem. Soc.*, vol. 160, no. 3, pp. C97–C105, Jan. 2013.
[71] R. P. Frankenthal, D. J. Siconolfi, and J. D. Sinclair, "Accelerated Life Testing of Electronic Devices by Atmospheric Particles: Why and How," *J. Electrochem. Soc.*, vol. 140, no. 11, pp. 3129–3134, 1993.
[72] D. W. Cooper, "Particulate Contamination and Microelectronics Manufacturing: An Introduction," *Aerosol Sci. Technol.*, vol. 5, no. January 2015, pp. 287–299, 1986.
[73] D. A. Thomas, K. Avers, and M. Pecht, "The 'trouble not identified' phenomenon in automotive electronics," *Microelectron. Reliab.*, vol. 42, no. 4–5, pp. 641–651, 2002.
[74] H. Qi, S. Ganesan, and M. Pecht, "No-fault-found and intermittent failures in electronic products," *Microelectron. Reliab.*, vol. 48, pp. 663–674, 2008.
[75] J. E. Sohn, U. Ray, V. Heideman, B. Schubert, J. E. Anderson, K. M. Adams, and G. Becka, "How clean is clean: effect of no-clean flux residues and environmental testing conditions on surface insulation resistance," in *Proceedings of Surface Mount International*, 1994.
[76] D. X. Xu, D. Bin Wang, and Y. P. Lei, "Study of VOC-Free, No-Clean Flux for Lead-Free Soldering in Electronic Packaging," *Adv. Mater. Res.*, vol. 154–155, pp. 1012–1018, 2010.

[77] S. Zhan, M. H. Azarian, and M. Pecht, "Reliability of Printed Circuit Boards Processed Using No-Clean Flux Technology in Temperature – Humidity – Bias Conditions," *IEEE Trans. Device Mater. Reliab.*, vol. 8, no. 2, pp. 426–434, 2008.
[78] R. Rörgren, P. Tegehall, and P. Carlsson, "Reliability of BGA Packages in an Automotive Environment," *J. Surf. Mt. Technol.*, vol. 11, no. 2, pp. 35–44, 1998.
[79] D. Pauls, "Residues in printed wiring boards and assemblies," *Circuit World*, vol. 27, no. 1, pp. 32–41, 2000.
[80] R. Michalkiewicz, "Addressing flux corrosion and reliability concerns early," *SMT Surf. Mt. Technol. Mag.*, vol. 28, no. 1, pp. 20–29, 2014.
[81] M. S. Jellesen, D. Minzari, U. Rathinavelu, P. Møller, and R. Ambat, "Corrosion failure due to flux residues in an electronic add-on device," *Eng. Fail. Anal.*, vol. 17, no. 6, pp. 1263–1272, Sep. 2010.
[82] P.-E. Tegehall and B. D. Dunn, "Influence of flux residues and conformal coatings on the surface resistance properties of spacecraft circuit boards," *ESA J.*, vol. 16, no. 3, pp. 255–273, 1992.
[83] C. Hunt, A. Mensah, A. Buxton, and R. Holman, "Determining conformal coating protection," *Solder. Surf. Mt. Technol.*, vol. 18, pp. 38–47, 2006.
[84] U. Rathinavelu, M. S. Jellesen, P. Moller, and R. Ambat, "Effect of No-Clean Flux Residues on the Performance of Acrylic Conformal Coating in Aggressive Environments," *IEEE Trans. Components, Packag. Manuf. Technol.*, vol. 2, no. 4, pp. 719–728, 2012.
[85] D. Geiger and D. Shangguan, "Investigation of the effect of solder flux residues on RF signal integrity using real circuits," *Solder. Surf. Mt. Technol.*, vol. 17, no. 4, pp. 27–32, 2005.
[86] M. Duffy, L. Floyd, P. Mccloskey, C. Ó. Mathúna, K. Tellefsen, M. Liberatore, and A. Sreeram, "RF Characterisation of No-clean Solder Flux Residues," *Proc. SPIE - Int. Soc. Opt. Eng.*, vol. 4587, pp. 138–143, 2001.
[87] "IPC-CH-65B Guidelines for Cleaning of Printe Boards and Assemblies," Northbrook, IL, 2011.
[88] W. Harald, "Preventing contamination-caused assembly failure," *Circuits Assem.*, vol. 20, no. 6, pp. 42–43, 2009.
[89] J. Cavasin, "Silver migration problem," *Mach. Des.*, vol. 42, no. 14, 1970.
[90] D. Q. Yu, W. Jillek, and E. Schmitt, "Electrochemical migration of Sn-Pb and lead free solder alloys under distilled water," *J. Mater. Sci. Mater. Electron.*, vol. 17, no. 3, pp. 219–227, Mar. 2006.
[91] S.-B. Lee, M.-S. Jung, H.-Y. Lee, T. Kang, and Y.-C. Joo, "Effect of bias voltage on the electrochemical migration behaviors of Sn and Pb," *IEEE Trans. Device Mater. Reliab.*, vol. 9, no. 3, pp. 483–488, 2009.
[92] B. Noh, J. Yoon, W. Hong, and S. Jung, "Evaluation of electrochemical migration on flexible printed circuit boards with different surface finishes," *J. Electron. Mater.*, vol. 38, no. 6, pp. 902–907, 2009.
[93] B. Noh, J. Lee, and S. Jung, "Effect of surface finish material on printed circuit board for electrochemical migration," *Microelectron. Reliab.*, vol. 48, pp. 652–656, 2008.
[94] D. Minzari, M. S. Jellesen, P. Møller, and R. Ambat, "On the electrochemical migration mechanism of tin in electronics," *Corros. Sci.*, vol. 53, no. 10, pp. 3366–3379, Oct. 2011.
[95] D. Minzari, M. S. Jellesen, P. Møller, P. Wahlberg, and R. Ambat, "Electrochemical Migration on Electronic Chip Resistors in Chloride Environments," *IEEE Trans. Device Mater. Reliab.*, vol. 9, no. 3, pp. 392–402, 2009.
[96] S. Canumalla, K. Ludwig, R. Pedigo, and T. Fitzgerald, "A study on ranking of commercial fluxes for electrochemical migration (ECM) propensity for Cu, Sn and Ag surface finishes," in *56th Electronic Components & Technology Conference*, 2006, pp. 625–632.
[97] G. Harsányi and G. Inzelt, "Comparing migratory resistive short formation abilities of conductor systems applied in advanced interconnection systems," *Microelectron. Reliab.*, vol. 41, no. 2, pp. 229–237, Feb. 2001.
[98] B. Medgyes, B. Illés, and G. Harsányi, "Electrochemical migration behaviour of Cu, Sn, Ag and Sn63/Pb37," *J. Mater. Sci. Mater. Electron.*, vol. 23, no. 2, pp. 551–556, Jun. 2011.
[99] J. J. Steppan, J. A. Roth, and L. C. Hall, "A review of corrosion failure mechanisms during accelerated tests Electrolytic metal migration," *J. Electrochem. Soc.*, vol. 134, no. 1, pp. 175–190, 1987.
[100] D. Minzari, F. B. Grumsen, M. S. Jellesen, P. Møller, and R. Ambat, "Electrochemical migration of tin in electronics and microstructure of the dendrites," *Corros. Sci.*, vol. 53, no. 5, pp. 1659–1669, May 2011.
[101] X. Zhong, G. Zhang, Y. Qiu, Z. Chen, W. Zou, and X. Guo, "In situ study the dependence of electrochemical migration of tin on chloride," *Electrochem. commun.*, vol. 27, pp. 63–68, Feb. 2013.
[102] X. Zhong, G. Zhang, Y. Qiu, Z. Chen, and X. Guo, "Electrochemical migration of tin in thin electrolyte layer containing chloride ions," *Corros. Sci.*, vol. 74, pp. 71–82, Sep. 2013.

[103] C. Xie, X. Tang, J. Chen, B. Song, J. Jin, and H. Zhang, "Reliability Analysis and Accelerated Statistical Model of CNC PCB for Electrochemical Migration," *IEEE Trans. Device Mater. Reliab.*, vol. 14, no. 1, pp. 90–98, Mar. 2014.
[104] X. He, M. Azarian, and M. Pecht, "Evaluation of Electrochemical Migration on Printed Circuit Boards with Lead-Free and Tin-Lead Solder," *J. Electron. Mater.*, vol. 40, no. 9, pp. 1921–1936, Jun. 2011.
[105] L. C. Zou and C. Hunt, "Characterization of the Conduction Mechanisms in Adsorbed Electrolyte Layers on Electronic Boards Using AC Impedance," *J. Electrochem. Soc.*, vol. 156, no. 1, pp. C8–C15, 2009.
[106] S. W. Chaikin, J. J. Janney, F. M. Church, and C. W. McClelland, "Silver Migration and Printed Wiring," *Ind. Eng. Chem.*, vol. 51, no. 3, pp. 299–304, Mar. 1959.
[107] J. Kim, M. Park, D. Nam, and H. Kwon, "Electrochemical Migration Behavior of a Fine-Pitch IC Substrate by Alternating Current," *J. Nanosci. Nanotechnol.*, vol. 14, no. 11, pp. 8258–8263, Nov. 2014.
[108] O. Short, "Silver Migration in Electric Circuits," *Tele-Tech Electron. Ind.*, no. February, pp. 64–65 and 110–113, 1956.
[109] X. Zhong, X. Guo, Y. Qiu, Z. Chen, and G. Zhang, "In Situ Study the Electrochemical Migration of Tin under Unipolar Square Wave Electric Field," *J. Electrochem. Soc.*, vol. 160, no. 11, pp. 495–500, 2013.
[110] P. J. Boddy, R. H. Delaney, J. N. Lahti, E. F. Landry, and R. C. Restrick, "Accelerated Life Testing of Flexible Printed Circuits," in *14th International Reliability Physics Symposium*, 1976, pp. 108–117.
[111] J. N. Lahti, R. H. Delaney, and J. N. Hines, "The Characteristic Wearout Process in Epoxy-Glass Printed Circuits for High Density Electronic Packaging," in *17th International Reliability Physics Symposium*, 1979, pp. 39–43.
[112] B. Rudra and D. Jennings, "Failure-mechanism models for conductive-filament formation," *IEEE Trans. Reliab.*, vol. 43, no. 3, pp. 354–360, 1994.
[113] A. Caputo, L. J. Turbini, and D. D. Perovic, "Conductive anodic filament formation part II: Electrochemical reactions leading to CAF," *J. Electron. Mater.*, vol. 39, no. 1, pp. 92–96, 2010.
[114] K. Karavakis and S. Bertling, "Conductive anodic filament (CAF): the threat to miniaturization of the electronics industry," *Circuitree Mag.*, 2004.
[115] A. Caputo, L. J. Turbini, and D. D. Perovic, "Design limitations related to conductive anodic filament formation in a micro-world," *Microsyst. Technol.*, vol. 15, pp. 39–44, 2009.
[116] W. J. Ready and L. J. Turbini, "The effect of flux chemistry, applied voltage, conductor spacing, and temperature on conductive anodic filament formation," *Journal of Electronic Materials*, vol. 31, no. 11. pp. 1208–1224, 2002.
[117] L. C. Zou and C. Hunt, "A new approach to investigate conductive anodic filament (CAF) formation," *Solder. Surf. Mt. Technol.*, vol. 27, no. 1, pp. 22–30, 2015.
[118] A. Caputo, L. J. Turbini, and D. D. Perovic, "Characterization and electrochemical mechanism for bromide-containing conductive anodic filament (CAF) failure," *J. Electron. Mater.*, vol. 40, no. 9, pp. 1884–1894, 2011.
[119] W. Wang, A. Choubey, M. H. Azarian, and M. Pecht, "An Assessment of Immersion Silver Surface Finish for Lead-Free Electronics," *J. Electron. Mater.*, vol. 38, no. 6, pp. 815–827, Apr. 2009.
[120] P. Zhao, M. G. Pecht, S. Kang, and S. Park, "Assessment of Ni/Pd/Au-Pd and Ni/Pd/Au-Ag preplated leadframe packages subject to electrochemical migration and mixed flowing gas tests," *IEEE Trans. Components Packag. Technol.*, vol. 29, no. 4, pp. 818–826, 2006.
[121] W. S. Chao, W. H. Wang, T. C. Luo, T. C. Huang, M. C. Liao, and T. H. Wei, "The comparison on the corrosion resistance of different kinds of PCB surface finishing: OSP, LF HASL and ENIG," in *Proceedings of Technical Papers - International Microsystems, Packaging, Assembly, and Circuits Technology Conference, IMPACT*, 2012, pp. 159–162.
[122] R. Schueller, "Creep Corrosion on Lead-Free Printed Circuit Boards in High Sulfur Environments," in *SMTA International Proceedings*, 2007.
[123] G. Harman, *Wire bonding in microelectronics*, 3rd ed. McGraw Hill Professional, 2010, p. 426.
[124] M. Khan, H. Fatemi, J. Romero, and E. Delenia, "Effect of high thermal stability mold material on the gold-aluminum bond reliability in epoxy encapsulated VLSI devices," in *Reliability Physics Symposium*, 1988, pp. 40–49.
[125] R. Gale, "Epoxy degradation induced Au-Al intermetallic void formation in plastic encapsulated MOS memories," *Reliab. Phys. Symp.*, pp. 37–47, 1984.
[126] R. Lum and L. Feinstein, "Investigation of the Molecular Processes Controlling Corrosion Failure Mechanisms in Plastic Encapsulated Semiconductor Devices," *Microelectron. Reliab.*, vol. 21, no. 1, pp. 15–31, 1981.

[127] S. S. Ahmad, R. C. Blish, T. J. Corbett, J. I. King, and C. G. Shirley, "Effect of Bromine in Molding Compounds on Gold - Aluminum Bonds," *IEEE Trans. Components, Hybrids, Manuf. Technol.*, vol. 9, no. 4, pp. 379–385, 1986.
[128] Y. Jianhai, B. Shengxiang, M. Lili, and L. Dechun, "Failure analysis of halide of epoxy molding compound used for electronic packing," in *2009 International Conference on Electronic Packaging Technology and High Density Packaging*, 2009, pp. 759–762.
[129] R. Ritchie and D. Andrews, "CF4/O2 Plasma Accelerated Aluminum Metallization Corrosion in Plastic Encapsulated ICs in the Presence of Contaminated Die Attach Epoxies," in *Reliability Physics Symposium*, 1981, pp. 88–92.
[130] H. F. M. M. Khan, "Gold-aluminum bond failure induced by halogenated additives in epoxy molding compounds," in *1986 International Symposium on Microelectronics*, 1986, pp. 420–427.
[131] G. Grause, M. Furusawa, A. Okuwaki, and T. Yoshioka, "Pyrolysis of tetrabromobisphenol-A containing paper laminated printed circuit boards.," *Chemosphere*, vol. 71, no. 5, pp. 872–8, Mar. 2008.
[132] K. N. Ritz, W. T. Stacy, and E. K. Broadbent, "The Microstructure of Ball Bond Corrosion Failures," in *Reliability Physics Symposium*, 1987, pp. 28–33.
[133] H. Chan, "Surface insulation resistance methodology for today's manufacturing technology," *IEEE Trans. Components, Packag. Manuf. Technol. C*, vol. 19, no. 4, pp. 300–306, 1996.
[134] D. Bono, "The assessment of the corrosivity of soldering flux residues using printed copper circuit board tracks," *Solder. Surf. Mt. Technol.*, vol. 1, no. 2, pp. 22–29, 1989.
[135] W. Rubin and B. M. Allen, "The chemistry and behaviour of fluxes," *Trans. Inst. Met. Finish.*, vol. 50, no. 3, pp. 133 – 137, 1972.
[136] C. Puechagut, A. Laügt, E. Guéné, and R. Anisko, "Solder Paste Residue Corrosivity Assessment : Bono Test," in *IPC APEX EXPO Technical Conference 2010*, 2010, vol. 2, pp. 1336–1364.
[137] Y. Zhou, L. J. Turbini, D. Ramjattan, B. Christian, and M. Pritzker, "Characterizing Corrosion Effects of Weak Organic Acids Using a Modified Bono Test," *J. Electron. Mater.*, vol. 42, no. 12, pp. 3609–3619, Aug. 2013.
[138] L. J. Turbini, "Comparison of methods for characterising soldering fluxes and their interactions with substrates and metallisation," *Circuit World*, vol. 23, no. 1, 1996.
[139] K. M. Takahashi, "Conduction Paths and Mechanisms in FR-4 Epoxy/Glass Composite Printed Wiring Boards," *J. Electrochem. Soc.*, vol. 138, no. 6, p. 1587, 1991.
[140] J. R. White, "Conduction mechanisms in contaminant layers on printed circuit boards," *IBM J. Res. Dev.*, vol. 37, no. 2, pp. 243–248, 1993.
[141] J. C. Galvan, J. M. Bastidas, and S. Feliu, "A Study of Corrosive Effect of Soldering Fluxes on Printed Circuit Boards," *Weld. J.*, vol. 75, no. 11, pp. 366–371, 1996.
[142] J. Guy and M. Fredrickson, "Analyzing Residues Using AC Impedance Techniques," in *NEPCON WEST*, 1997, vol. 3, pp. 1270–1279.
[143] N. M. Amin and A. M. Seitz, "Evaluation of Solder Flux/Substrate Interfaces Using Impedance Spectroscopy," in *NEPCON WEST*, 1999, vol. 2, no. 845–853, pp. 845–853.
[144] M. M. Madani, R. R. Kodnani, and R. D. Granata, "Electrochemical impedance spectroscopic study of encapsulated triple tracks test (TTT) circuits," *IEEE Trans. Reliab.*, vol. 46, no. 1, pp. 45–51, 55, Mar. 1997.
[145] G. Sauerbrey, "The Use of Quartz Oscillators for Weighing Thin Layers and for Microweighing," *Z. Phys.*, vol. 155, pp. 206–222, 1959.

6. MATERIALS AND METHODS

This section provides an overall summary of materials, components, test boards and the experimental methods employed for various investigations presented in the appended papers. More detailed discussion on specific "materials and experimental methods" connected to each investigation can be found in the appended papers.

6.1 ELECTROCHEMICAL MIGRATION SETUP FOR SINGLE COMPONENTS

Investigations with single surface mount components (SMCs) were carried out using an in-house built cell setup shown in Figure 6.1. Investigations include leakage current measurements under elevated humidity/temperature conditions and the propensity for electrochemical migration under water droplet conditions. The setup consists of a sample holder having two small adjustable stainless steel probes, which act as connectors to each end of the surface mount component under test. A single component is fixed between the probes and the spring loading on the metal probes ensures proper electrical contact.

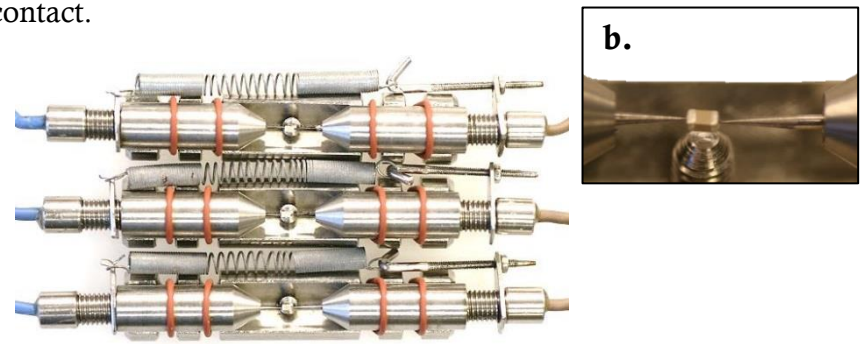

Figure 6.1: a. Setup for testing of single SMCs and b. magnified view of a SMC mounted in the setup

6.2 TEST PRINTED CIRCUIT BOARD

The PCBA level testing was carried out using an in-house built test PCBA. The FR-4 laminate of the test board complies with specifications of IPC-4101/21 and has the dimensions of 168 × 112.4 mm, and thickness of 1.6 mm (Figure 6.2).

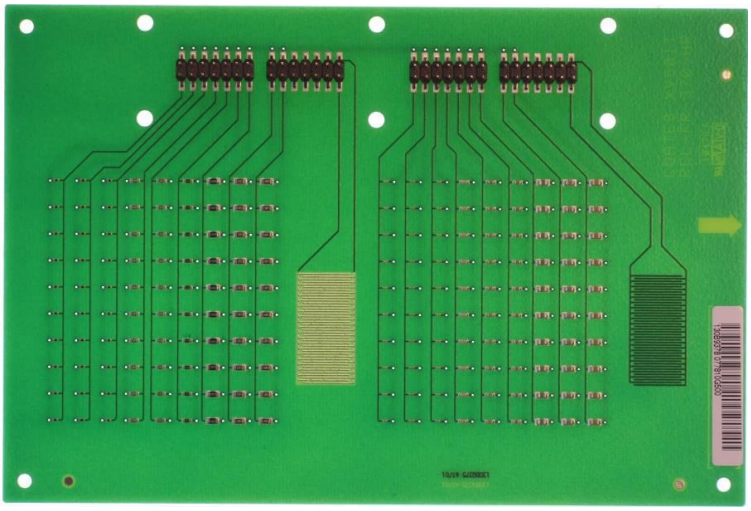

Figure 6.2: Test printed circuit board

The test PCBA consisted of known surface mount components such as chip capacitors and chip resistors, all reflow soldered in rows of 10 components, connected in parallel, and two SIR comb patterns. The SIR comb patterns used for the experiments had a hot air solder leveled (HASL) finish, with two available solder alloys: i) SAC, and ii) SN100C. The SIR patterns with SAC solder finish were used for the investigations reported in papers 1, 2, 3 (chapters 8-10), while the results reported in papers 7 and 8 (chapters 14-15) were obtained on SIR pattern with SN100C surface finish. The dimensions of the SIR pattern were 13 × 25 mm; the width of conductor lines and the spacing between them was 0.3 mm. The geometry of SIR patterns yields the nominal square count of 1476. For comparison, the standard IPC-B-36 and IPC-B-24 comb patterns have 3538 and 1020 squares [54].

A set of experiments for characterisation of water layer formation on the printed circuit boards using AC impedance measurements was performed on a simple FR-4 board with two parallel conductor lines. For this pattern, the width was 0.66 mm with a length of 5.8 mm, and the distance between the lines was 1.3 mm. The resulting nominal square count of the test coupon was ~4.5. The surface finish of the conducting line was electroplated gold (6.5 ± 1 μm) with an intermediate layer of nickel (9 ± 1 μm).

6.3 CLIMATIC CHAMBER

An "Espec PL-3KPH" climatic chamber was used for all the testing using PCBAs under various humidity and temperature conditions. The operational range for temperature and humidity conditions is -40 °C to +100 °C and 20 %RH to 98 %RH. The accuracy of temperature and humidity control in the climatic chamber is ±0.3 °C and ±2.5 %RH, as specified by the manufacturer.

6.4 QUARTZ CRYSTAL MICROBALANCE

A "QCM200" quartz crystal microbalance (QCM) from SRS Inc. with a 5 MHz AT-cut gold contact quartz crystal was used for *in situ* measurement of water adsorption and absorption by weak organic acids and flux residues. The quantitative relationship between the change in frequency of the piezoelectric crystal and a change in mass of the piezoelectric crystal due to surface changes [145] enabled estimation of the adsorbed water layer thickness, and the deliquescence RH of contamination on the crystal.

6.5 ELECTRICAL/ELECTROCHEMICAL CHARACTERISATION

A "BioLogic model VSP" multichannel workstation from Bio-Logic Instruments was the main instrument used for electrical measurements. The workstation has 20 V compliance voltage with adjustable range (upper limits at -20 V and +20) and a 760 pA current resolution. The unit has a built-in electrochemical impedance analyser with frequency range from 10 μHz to 1 MHz. The measurement techniques used for electrical/electrochemical characterisation in the current work are summarised in Table 6.1.

Table 6.1: Summary of electrochemical techniques

Aim	Method	Samples
Characterisation of the water layer formation and consequent charge transfer mechanism on the test board	AC impedance in the frequency range from 10 mHz to 100 kHz with signal amplitude of 50 mV	PCB with two oppositely facing Au electroplated electrodes
SIR measurements under various humidity/temperature conditions	DC measurements at 5 V or 10 V (Chronoamperometry at fixed potential)	SIR pattern on the test PCBA
Corrosion of SIR pattern and the resulting leakage current as a function of RH	Potentiodynamic leakage current measurement (adapted from the Corrosimetry method in "EC-LAB")	SIR pattern on the test PCBA
Electrochemical migration on surface mount components under water droplet condition with applied DC voltage	DC measurements at 5 V or 10 V (Chronoamperometry at fixed potential)	Surface mount components
Electrochemical migration on surface mount components under water droplet condition with applied pulse voltage	Current measurements were obtained with zero resistance ammetry (ZRA) technique[a]	Surface mount components
Corrosion of Au-Al intermetallics in aqueous electrolyte solution	Potentiodynamic polarisation and open circuit potential measurements[b]	Au-Al intermetallic nuggets and sputter deposited layers

[a] – "Tektronix AFG 3021B" arbitrary function regenerator was used to apply the voltage on the components

[b] – Measurements were performed with "Gamry PCI4/300" potentiostat at Robert Bosch GmbH

6.6 OTHER MATERIAL CHARACTERISATION TECHNIQUES

6.6.1 OPTICAL MICROSCOPY

Several optical microscopes were used in the current work to image the surfaces before and after testing: i) "Leica MZ 12$_5$" stereo microscope equipped with "Leica DFC450 C" digital camera, ii) "Olympus GX41" metallurgical microscope, and iii) "Carl Zeiss Axioskop 2 MAT" with several imaging modes i.e. differential interference contrast (DIC), dark field, and bright field. The *in situ* observation of the surface of the component during humidity testing was performed using an "AD7013MZT Dino-Lite" digital microscope.

6.6.2 ELECTRON MICROSCOPY AND ENERGY-DISPERSIVE X-RAY SPECTROSCOPY

Most of the SEM analysis in the current PhD thesis was performed using a "FEI Quanta 200" field-emission environmental scanning electron microscope (ESEM-FEG) with the capability of energy-dispersive X-ray analysis (Oxford Instruments 80 mm^2 X-Max silicon drift detector, MnK_α resolution at 124 eV). A "JEOL JSM 5900" scanning electron microscope was used for the imaging of tin dendrites on the surface mount components.

6.6.3 FOURIER TRANSFORM INFRARED MICROSCOPY

A "Nicolet iN10 MX" infrared imaging microscope was used for identification of activators (WOAs) present in the solder flux. The measurements were performed in the attenuated total reflectance (ATR) mode on the residue after solvent evaporation.

6.6.4 GLOW DISCHARGED OPTICAL EMISSION SPECTROSCOPY

"Horiba Jobin Yvon GD-Profiler 2" glow discharge optical emission spectrometer was used for the depth profiling of multi-layer coatings used for the investigations related to the corrosion of Au-Al wire bond connections. The aim was to understand the intermetallic phase formation between the layers due to diffusion during heat treatment.

6.6.5 X-RAY DIFFRACTION

X-ray diffraction (XRD) technique was used for the identification of Au-Al intermetallic phases formed during heat treatment of the samples used for corrosion studies in iodine environments. The measurements were carried out on a "Bruker D8" equipped with a parallel beam (Göbel mirror) and a secondary side divergence assembly in 1D, and an MRI temperature controlled dome stage.

6.6.6 THERMAL IMAGING CAMERA

Thermal imaging camera "Trotec IC080LV" was used for imaging the temperature distribution on the test PCBA under cooling conditions, and on the device PCBA due to power dissipation from the components under working conditions.

6.6.7 WIRE BOND SHEAR TESTING

The Au-Al wire bond shear testing was performed with "Dage series 4000" multi-function bond tester with the ball shear cartridge BS250 (maximum shear force of 250 g), and a flat chisel shape shearing tool (062-006).

6.7 TIN CORROSION IDENTIFICATION USING A TIN ION INDICATOR

A colorimetric reagent dissolved in water and mixed with agar gel was used for identification of tin corrosion on the PCBAs. The preparation of the gel and indicator was as follows: i) agar gel (type A7921, Sigma-Aldrich) was added into the Millipore water with conductivity of 18.2 MOhm·cm at 25 °C at concentrations of 1-10 $g \cdot L^{-1}$, ii) the water containing agar gel was heated to a temperature above 80 °C for homogeneity of solution, and iii) tin ion indicator was added into the solution, while solution was being stirred. The prepared gel solution was applied by spraying onto the entire printed circuit board, or by applying locally on the areas of interest by using a pipette. The indicator in the gel reveals the tin ions and tin hydroxides formed during corrosion of tin solder pads, solder joints, and component terminals. Reaction with the tin indicator changes the colour of the gel from light yellow to blue, and the intensity of the colour represents the extent of corrosion.

6.8 SAMPLES FOR CORROSION STUDIES OF AU-AL INTERCONNECTIONS

Three sets of samples were used for corrosion studies of Au-Al interconnections due to iodine, namely: i) Au-Al wire bonds on the integrated circuits, ii) Au-Al intermetallic nuggets prepared by remelting Au and Al under argon atmosphere, and iii) Sputter deposited layers of Au on Al on Si wafer. The sputter deposited layers were heat treated for the formation of Au-Al intermetallics at 175 °C.

7. SUMMARY OF PAPERS

7.1 IMPACT OF NACL CONTAMINATION AND CLIMATIC CONDITIONS ON THE RELIABILITY OF PRINTED CIRCUIT BOARD ASSEMBLIES

Objectives:

Investigate the effect of NaCl contamination on the leakage current and probability for electrochemical migration with regard to varying climate conditions (varying temperature and humidity, and establishing temperature differential between PCBA and ambient).

Findings:

A marginal increase of leakage current in the nA range was observed on surface mount capacitors exposed to elevated humidity conditions from 60 % to 98 % at a constant temperature of 25 °C, and an almost two orders of magnitude increase in current from 10 nA to 1 µA in the case of temperature change (implying an increase of water content in the air) from 15 °C at 98 % RH to 65 °C at 98 % RH. This is equivalent to a reduction of SIR below 100 MOhm, which is commonly used as failure criterion in climatic testing. The increase of leakage currents was primarily attributed to the increase of water layer thickness on the surface of the PCBA. The water layer thickness on the PCBA is a function of: (i) relative humidity, (ii) increase of absolute humidity during increase of temperature at constant RH, (iii) increase of RH locally on the PCBA by establishing temperature differential between PCBA and ambient, or (iv) the amount of hygroscopic contaminant. It was found, that the prolonged exposure to near condensing conditions causes corrosion of anode terminals of surface mount components. As a result of depletion of tin oxide film, the growth of whiskers and hillocks was observed on the anode terminals of surface mount components.

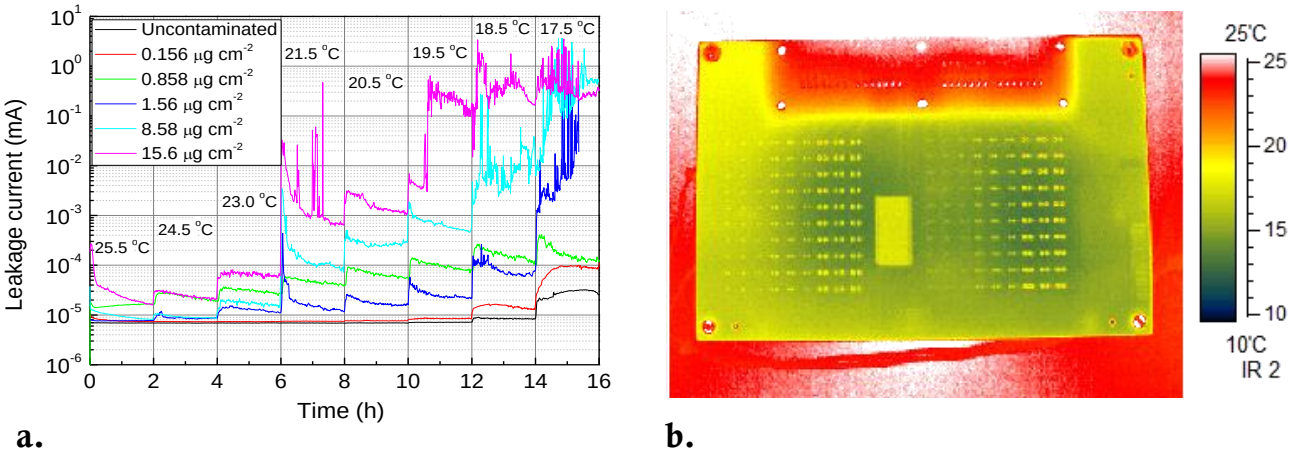

Figure 7.1: a. Leakage current as a function of NaCl contamination and temperature of the PCBA (ambient is kept at 25 °C and 60 %RH), and b. Infrared image of PCBA cooled from ambient of 25 °C

7.2 SOLDER FLUX RESIDUES AND HUMIDITY-RELATED FAILURES IN ELECTRONICS: RELATIVE EFFECTS OF WEAK ORGANIC ACID USED IN NO-CLEAN FLUX SYSTEMS

Objectives:

Investigate the effect of WOAs namely: adipic, succinic, glutaric, DL-malic, and palmitic on the water adsorption, resistivity of water layer formed, and consequent SIR reduction and corrosion as a function of relative humidity at 25 °C.

Findings:

The SIR testing of WOAs (activators in the flux systems) as a function of relative humidity was shown to be an effective method for differentiation of ionic contamination in regards to their hygroscopic properties, and for identification of deliquescence RH. The electrochemical testing of WOAs used in flux systems showed a clear correlation between the hygroscopic property and the magnitude of leakage current. An abrupt increase in the leakage current followed by electrochemical migration was observed at RH close to the deliquescence point of some of the more active acids. Heating of the test boards with flux residue to a soldering temperature of 220 °C to 245 °C for 45 s has reduced the leakage currents for all five WOAs. The effect of heating was more pronounced for glutaric and DL-malic acids. The difference in leak current behaviour is attributed to the high solubility of the acids. Highly soluble acids on the printed circuit boards would form a saturated solution (high ionic conductivity) in a thin layer of water, also would adsorb more water and at lower levels of RH, compared to that of low soluble weak organic acids (adipic, succinic, and palmitic acids). Overall, the results show that the climatic behaviour of the WOAs used in no-clean fluxes can be very different, and a similar variation can be expected for no-clean flux systems containing those WOAs as activators. The results suggest that the type of WOAs in the flux systems has a significant importance when electronics is likely to experience operation under humid conditions.

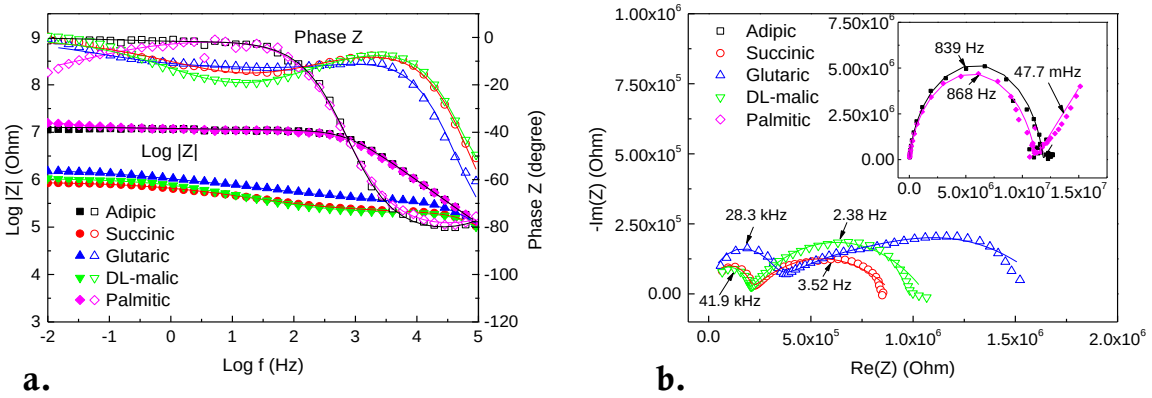

Figure 7.2: Impedance data for test PCB contaminated with 100 µg·cm^{-2} of WOAs at ~99 % RH/25 °C: a. Bode plots and b. Nyquist plots

7.3 RELATIVE EFFECT OF SOLDER FLUX CHEMISTRY ON THE HUMIDITY RELATED FAILURES IN ELECTRONICS

Objectives:

Investigate the influence of no-clean flux chemistry with various weak organic acids (WOAs) as activators on the corrosion reliability of electronics with emphasis on the hygroscopic nature of the residue.

Findings:

The results showed that the solder flux residues are characterised by different threshold RH, above which a sudden increase in leakage current by 2-4 orders of magnitude was observed, while a significant reduction of surface resistance was observed in the impedance measurements. The results are primarily attributed to the WOAs in the flux system, and especially their hygroscopic property. Although the film-former of the flux may influence the adsorption and absorption of water, as it was observed from the measurements with quartz crystal microbalance, the hygroscopic property of the activator (WOA) is a dominating factor determining leakage current on the PCBAs. The corrosiveness of the flux systems, determined by the tin ion indicator gel applied on the SIR patterns after climatic testing matched very well the results of SIR testing. The observation suggests the possibility of use of tin ion indicator gel for profiling corrosion on the boards as a complementary method during climatic testing.

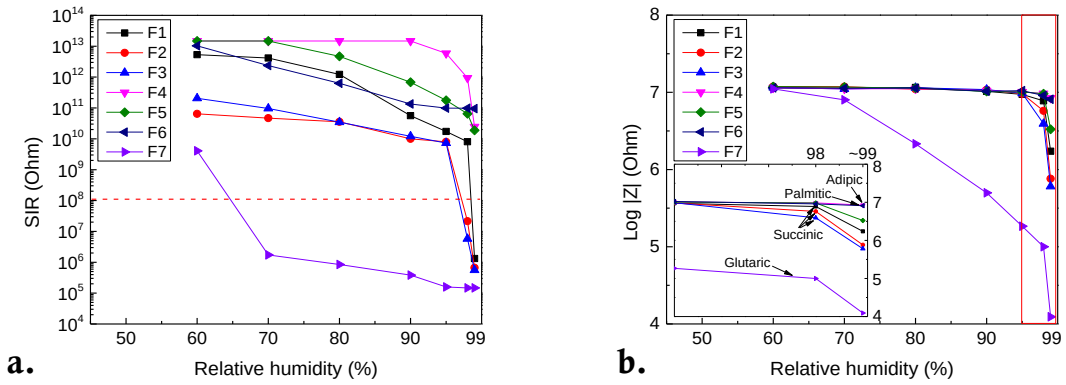

Figure 7.3: Summary of a. SIR from leakage current measurements at 10 V DC, and b. Impedance at $f \approx 1$ kHz

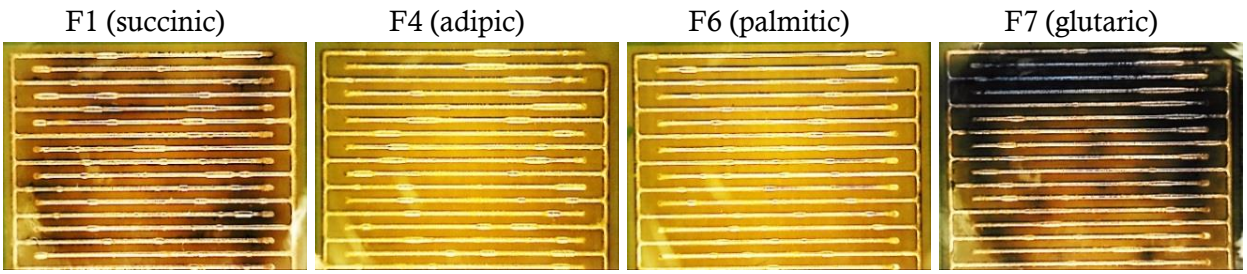

Figure 7.4: Optical micrographs of SIR patterns after climatic testing (corrosion of tin is indicated by blue coloration, while clear yellow colour indicates no corrosion of the SIR pattern)

7.4 INFLUENCE OF SODIUM CHLORIDE AND WEAK ORGANIC ACIDS (FLUX RESIDUES) ON ELECTROCHEMICAL MIGRATION OF TIN ON SURFACE MOUNT CHIP COMPONENTS

Objectives:

Compare the effect of NaCl and flux residues (adipic acid based) on the electrochemical migration of tin on the surface mount components under water droplet condition, and show the importance of measurement method for quantifying the amount of ionic contamination on the PCBAs, i.e. leakage current under DC voltage (comparable to SIR testing) and ionic conductivity measurement, commonly known as resistivity of solvent extract (ROSE) or solvent extract conductivity (SEC).

Findings:

The results indicated the differences arising from the comparison of two types of ionic contamination on the PCBAs. When comparing the two types of contamination in terms of electrolyte conductivity, equivalent amounts can vary and are dependent on whether the ionic conductivity measurement was performed under AC signal with varying frequency, as it is commonly assessed with conductivity meter in ROSE testing, or under DC voltage, which is more close to the conditions of SIR testing. Equivalent concentration found from DC measurements include polarisation effects on the electrodes, thus the amount equivalent to 1.56 µg·cm^{-2} of NaCl in terms of conductivity is higher, compared to the amount found from the AC method. The ECM testing under water droplet condition showed that the flux residue at high concentration hinders the formation of tin dendrites, or tin hydroxide precipitation, although a severe corrosion of the terminals of the surface mount capacitors was observed. The testing of ECM probability as a function of NaCl concentration and bias voltage indicated an initial increase of probability with maximum followed by a slow decrease with the increase of voltage and concentration of NaCl.

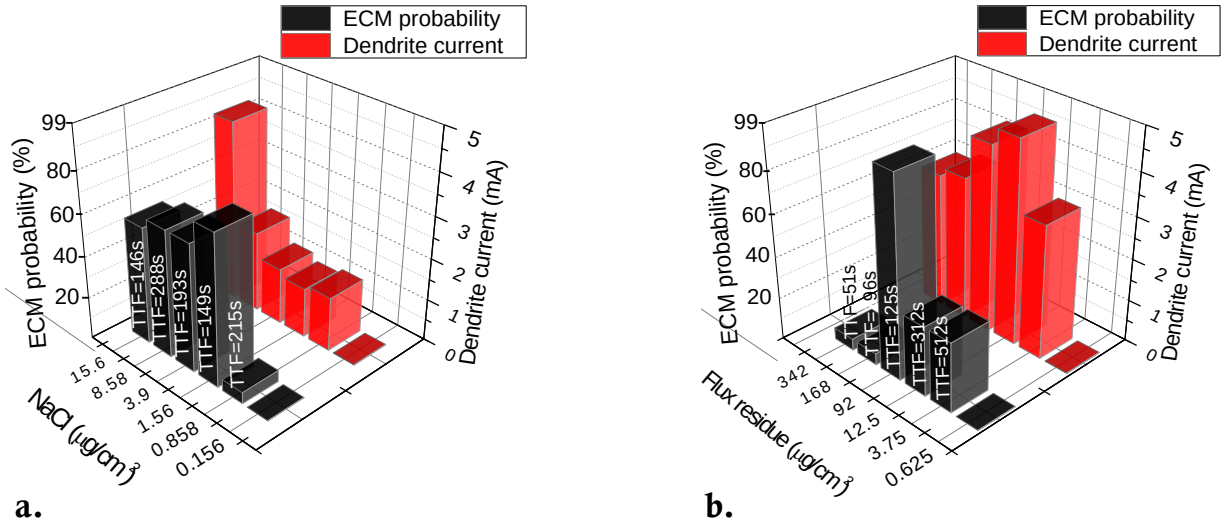

Figure 7.5: ECM probability and dendrite current as a function of concentration: a. NaCl and b. flux residue

7.5 EFFECT OF PULSED VOLTAGE ON ELECTROCHEMICAL MIGRATION OF TIN IN ELECTRONICS

Objectives:

Investigate the effect of pulsed voltage (duty cycle and pulse width) on the electrochemical migration of tin on surface mount chip capacitors under water droplet condition.

Findings:

The increase of duty cycle reduces the time to dendrite formation, and to an extent the rate of dendrite formation. The result is primarily attributed to the number of tin ions being dissolved from the positively biased electrode, which in this work was visualised by a tin ion indicator. The reduction of time to dendrite formation and the increase of dendrite current were observed with increasing NaCl concentration from 1.56 µg·cm^{-2} to 15.6 µg·cm^{-2}. The comparable amount of tin ions was dissolved from the anode after equivalent ON times for various duty cycles; however, the formation of tin dendrites was less efficient with duty cycles of 0.2 (t_{ON} = 50 ms, t_{OFF} = 200 ms) and 0.33 (t_{ON} = 100 ms, t_{OFF} = 200 ms). It resulted in a slight increase of time to failure (TTF) and reduction of charge transferred between the electrodes. The significantly larger amounts of tin hydroxides observed for the duty cycle of 0.2 indicated that this condition is least favourable for ECM. The results suggest that the use of pulse voltage with lower duty cycles could improve the time to failure due to dendrite formation on the PCBA operating under conditions when short-term events of condensation are likely to occur.

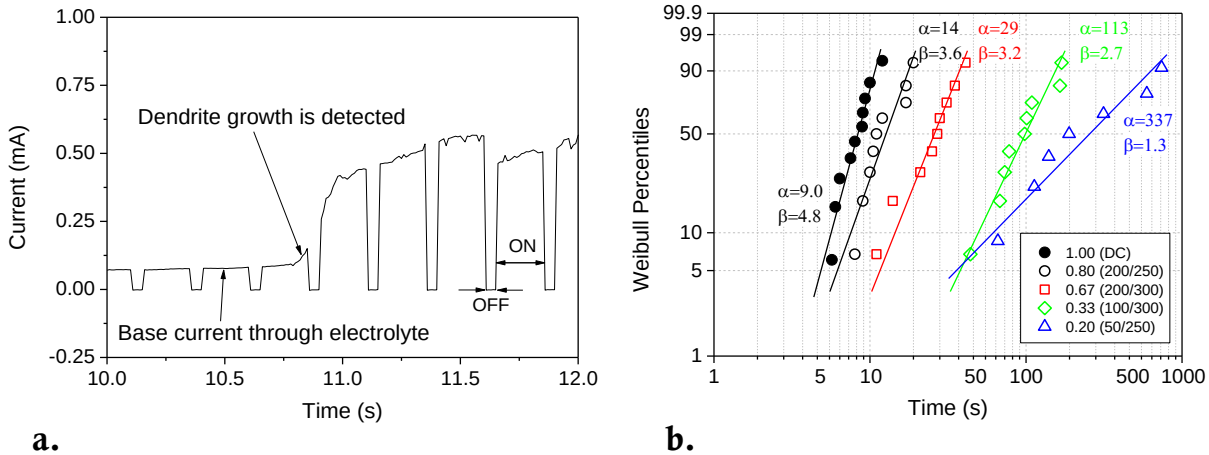

Figure 7.6: a.: Current measurement on the component under pulsed voltage (t_{ON} = 200 ms, t_{OFF} = 50 ms), droplet with equivalent NaCl concentration of 1.56 µg·cm^{-2}, and b. Weibull percentiles of time to dendrite detection for varying duty cycle at 1.56 µg·cm^{-2}

7.6 EFFECT OF IODINE ON THE CORROSION OF AU-AL WIRE BONDS

Objectives:
Investigate the corrosion of Au-Al wire bond interconnects due to iodine in gaseous and aqueous environments with emphasis on the role of Au-Al intermetallics on corrosion.

Findings:
Electrochemical testing in aqueous potassium iodide solution showed that an increase of Al in the intermetallic phase reduces the corrosion potential and increases the corrosion current density of intermetallics. The increase of RH in the iodine containing environment significantly increases the corrosion of Al, Au, and Au-Al intermetallics. Corrosion of intermetallics at the Au-Al bond pad interface has resulted in the reduction of wire bond shear strength with the increase of RH and iodine concentration. The failures of Au-Al wire bonds in iodine environment are mainly attributed to the corrosion and oxidation of Al via formation of Al iodides and consequent formation of Al oxides and/or hydroxides. Al metallisation and Al rich intermetallic phases were found to be most susceptible to corrosion. The chemical reactions describing corrosion mechanism and consequent degradation of the wire bonds were suggested.

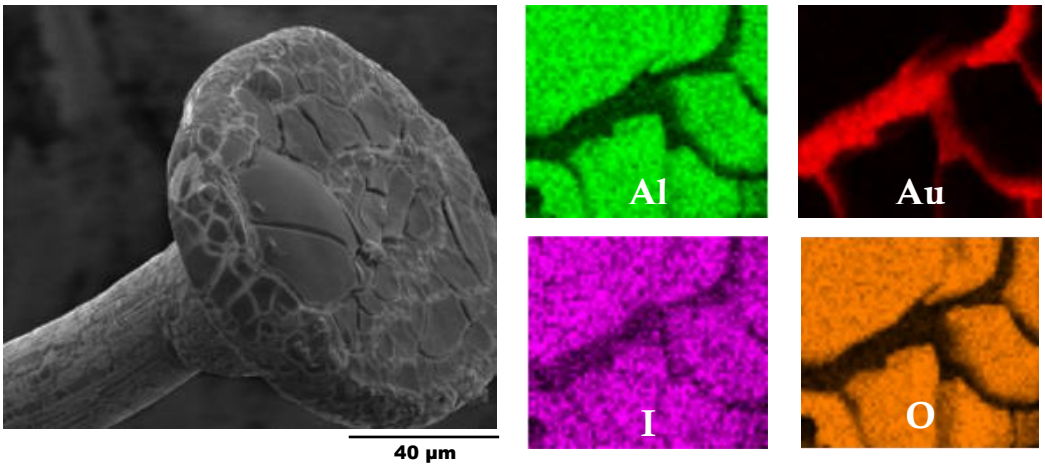

Figure 7.7: SEM EDS mapping of the wire bond after ball lift off (after 24 h exposure to 1 mg·L^{-1} of iodine at 85°C/85%RH)

7.7 COLORIMETRIC VISUALIZATION OF TIN CORROSION: A METHOD FOR EARLY STAGE CORROSION DETECTION ON PRINTED CIRCUIT BOARDS

Objectives:
Illustrate the application of colorimetric tin ion indicator gel as a method for mapping tin corrosion and movement of tin ions on the printed circuit boards due to water layer formation and bias.

Findings:
A new method was developed for the identification and mapping of tin corrosion on PCBAs. The motivation for identification of tin corrosion in its early stage was due to that fact that the information could be used for understanding the possible effects of humidity and leak current paths following the trails of tin ions and corrosion products under electric field. As the failures under humid conditions are likely to occur under thin layers of water and the resulting extent of corrosion is hardly detectable, analysis of such failures by conventional microscopy methods is very difficult. On the other hand, this paper shows that the use of colorimetric reagent for tin corrosion detection enables to obtain a picture of the corrosion profile, thus to identify areas of high leakage currents over the entire surface area of the printed circuit board. The method can be used in combination with accelerated humidity testing to identify corrosion prone areas on the actual device PCBAs. It can also be used for *ex situ* analysis of the test boards, as complementary technique to the SIR testing, as it provides an overall picture of the corrosion due to effect of various parameters. Application of tin ion indicator gel on the PCBAs returned from the field can be used as part of failure analysis, to locate the corrosion sites and understand the cause of failure.

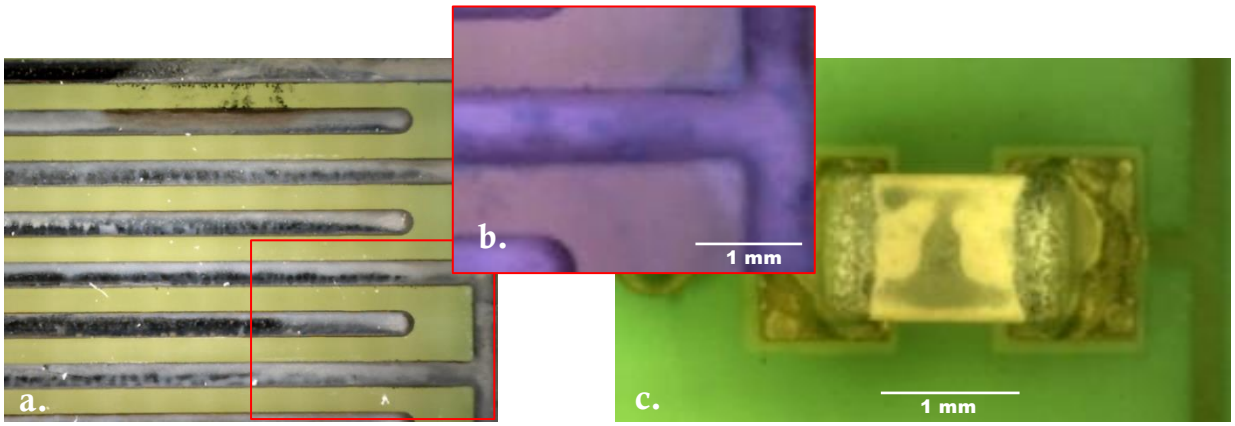

Figure 7.8: Corrosion of tin revealed by tin ion indicator: a. Initial appearance of corroded SIR pattern contaminated with DL-malic acid, b. Corrosion nearby electrodes revealed by tin ion indicator, and c. Corrosion of surface mount capacitor contaminated succinic acid and exposed to humid conditions

7.8 ANALYSIS OF SURFACE INSULATION RESISTANCE RELATED FAILURES IN ELECTRONICS BY CIRCUIT SIMULATION

Objectives:

Simulate effects of humidity and contamination on the electrical functionality of the components like resistors and capacitors, and other simple circuits using empirical data on the electrical properties of water layer. The analysis is based on the parasitic circuit effects owing to the formation of water layer as an electrical conduction medium.

Findings:

This paper discusses the effect of surface insulation resistance decrease due to humidity and contamination, and its possible effects on the functioning of electronic devices. When analysing the electronic circuits, the components are selected with the tolerances according to their sensitivity in the circuits. However, the circuit design engineer should also be aware of possible additional deviation of functional parameters due to humidity in the user environment, and the contamination either from manufacturing or in service life. The aim of the paper is to show the possibility of analysing humidity and contamination effects by circuit simulation using empirical SIR data.

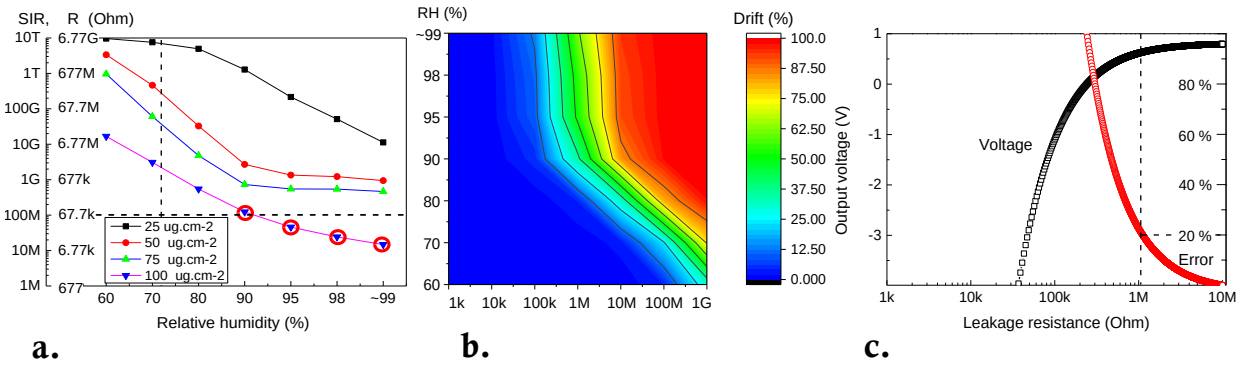

Figure 7.9: a. SIR degradation as a function of RH and for various levels of glutaric acids, b. Drift from the nominal value of resistors dependency on the RH for 100 μg·cm^{-2}, and c. Output voltage of differential amplifier dependency on the leakage resistance over resistor R8, which is indicated in Figure 7.10

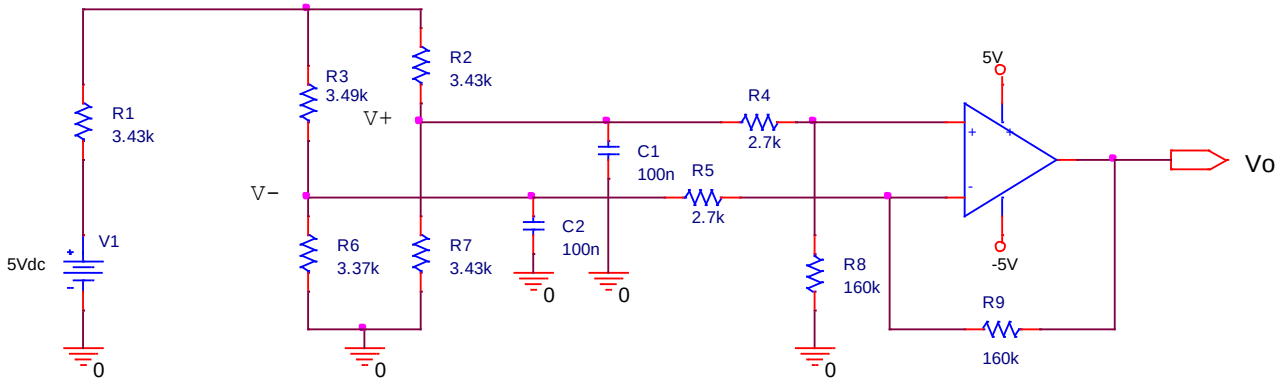

Figure 7.10: Diagram of differential amplifier based measurement circuit

APPENDED PAPERS

8. IMPACT OF NACL CONTAMINATION AND CLIMATIC CONDITIONS ON THE RELIABILITY OF PRINTED CIRCUIT BOARD ASSEMBLIES

Vadimas Verdingovas, Morten Stendahl Jellesen, and Rajan Ambat

Abstract—The effect of climatic conditions and ionic contamination on the reliability of printed circuit board assembly has been investigated in terms of leakage current (LC) and electrochemical migration susceptibility. The change of LC as a function of relative humidity (RH) and temperature was measured using single components (size 0805) and surface insulation resistance comb patterns precontaminated with sodium chloride at levels adjacent to levels used in the IPC J-STD-001 standard. The potential bias of 5–10 V was applied during experiments, and the climatic conditions were in the range 60%–98% RH and 15 °C–65 °C. The variation of RH at the surface of the test specimens was imposed by: i) increasing the RH of the surrounding air and ii) reducing the temperature of the printed circuit boards using a cooling stage, while maintaining a constant climatic condition in the chamber. A considerable increase in LC was observed at sodium chloride concentrations above 1.56 $\mu g \cdot cm^{-2}$, as the RH on the surface was close to the critical RH for sodium chloride. Prolonged exposure to conditions close to condensation resulted in the formation of tin whiskers and hillocks growing from the component electrodes due to corrosion of the electrodes freeing the whisker growth.

Keywords—Ionic contamination, Leakage current (LC), Corrosion, Reliability

I. INTRODUCTION

The climatic reliability of electronics is an important issue due to the complex electronic circuitry developed in recent years, the increased requirements for long term reliability, and increasingly harsh operating environments [1]–[3]. In addition, with the ever-increasing use of high frequency in high-density interconnected assemblies, increasing package component densities and decreasing component clearances, the issue of presence of high humidity and temperature variations, and the effects of contamination have become important considerations [4]–[6].

The design of electronics and the nature of the operating environment are both critical because corrosion failures in the integrated circuits and components on printed circuit boards can occur at extremely low levels of moisture and contamination [7]. The presence of ionic contamination on the surface of printed circuit boards assemblies (PCBAs) acts as corrosion accelerating factor. Most ionic residues are hygroscopic and therefore cause water adsorption to the surface. Once the temperature and humidity is such that critical relative humidity (RH) or deliquescent point of ionic residue is reached, the propensity of increased leakage currents (LCs) and under certain conditions growth of conductive metal filaments, known as electrochemical migration (ECM), is observed [8]–[13]. The electrochemical process that occurs on metals covered by a thin film of electrolyte is often primarily responsible for the damage of electrical and electronic components, which can lead to premature failures [1], [14].

V. Verdingovas, M. S. Jellesen, and R. Ambat, "Impact of NaCl contamination and climatic conditions on the reliability of printed circuit board assemblies," *IEEE Trans. Device Mater. Reliab.*, vol. 14, no. 1, pp. 42–51, 2014.

The origin of contamination on the printed circuit boards can usually be attributed to either manufacturing processes, or to the operating environment. The latter is difficult to predict due to the widespread application of electronics; however, it can be controlled to a significant extent by proper encapsulation. The key factor for long term reliability therefore becomes cleanliness levels obtained during the PCB manufacturing and assembling processes. Commonly found contaminants on the printed circuit boards are the weak organic acids from the flux residues, and chloride, fluoride, bromide, phosphate, sulphate resulting from other processes [5], [15]–[18]. The residues and contamination from the manufacturing processes and incorrect handling are factors that can initiate corrosion and ECM [19]. In the case of conformal coated electronics, the residues from the soldering process are able to reduce the adhesion of the coating and promote the water uptake, leading to the formation of ion conduction paths and thus reducing the surface insulation resistance (SIR) [20]–[22].

The nature of the surface contamination influences moisture adsorption from the atmosphere, and the surface conductivity of the electrolyte layer thus formed [7], [12]. Moisture condensation on the PCBAs depends on a number of factors, including RH, the temperature difference between the surface and surrounding air, the surface roughness and porosity, and finally the presence of hygroscopic contaminants [23], [24]. The chance for condensation can be enhanced if electronics is operating under conditions when variations in temperature are likely to occur. The RH on a surface of the PCBA increases with the bulk environment, and it is increased further if the temperature of the PCBA remains lower than that of the bulk environment. Similar conditions are often simulated by cycling temperature/humidity in a climatic chamber during testing [25]–[29].

This paper discusses the effect of NaCl tested over a range of RH and temperature on the LC measured on single components and at the PCBA level, which in an actual application leads to intermittent faults and premature failures. In order to understand the effect of humidity and contamination on the chip components, which are often susceptible to corrosion and ECM due to their bi-polar nature and small size, the direct LC measurements under various climatic and contamination conditions were performed. Experiments were carried out at the single component level on size 0805 ceramic chip capacitors, and as part of the test PCBA on size 0805 ceramic chip capacitors, size 0805 chip resistors, and an SIR comb pattern.

II. MATERIALS AND METHODS

ELECTRONIC COMPONENTS AND TEST PCBA

A surface mount multilayer ceramic chip capacitor with 0805 housing size, 10 nF capacitance and 50 V voltage rating (Yageo, Phycomp) was used for the investigation. The average distance between terminals of the capacitor was 1 mm. The electrode terminals of the chip capacitor were made of pure tin [30].

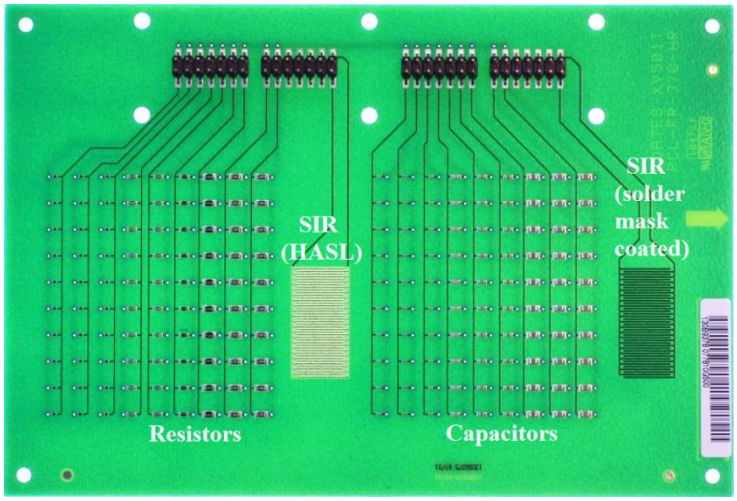

Figure 8.1: Test PCBA used for climatic testing showing various components

The PCBA level testing was carried out on a board made in accordance to IPC-4101/21 from FR4 substrate, with the dimensions 168 × 112.4 mm and a thickness of 1.6 mm (Figure 8.1). The test PCBA consisted of known surface mount components such as chip capacitors and chip resistors, all reflow soldered in rows of 10 components (connected in parallel), and two SIR comb patterns (solder mask coated SIR is on the board to use as reference, but was not used in the present work). The SIR comb pattern used for experiments had a hot air solder levelled (HASL) finish (Sn/Ag/Cu solder alloy) with dimensions of 13 × 25 mm, and pitch and spacing size of 0.3 mm. The overlapping area was 10.8 mm in height and there was 41 set of common overlap giving 442.8 mm as the total length of the opposing faces. The ratio of the total length of the opposing faces and the spacing of all segments yields the nominal square count, which is 1476 for this SIR. For reference, the standard IPC-B-36 and IPC-B-24 comb patterns have 3538 and 1020 squares. The sensitivity of an SIR pattern increases with increasing number of squares.

LC MEASUREMENTS AT THE SINGLE COMPONENT LEVEL

LC measurements at the single component level were conducted using a set-up that was built in-house (Figure 8.2), described elsewhere [30], [31]. The setup consists of a sample holder having two small adjustable probes, which act as connectors to each end of the surface mount component under test. A single component is fixed between the metal probes which being spring-loaded onto the sample to ensure good electrical contact.

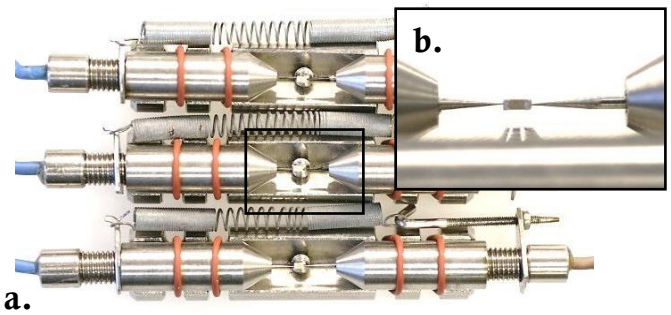

Figure 8.2: View of single component electrochemical migration setup: a. whole set up with three chip capacitors mount for testing, and b. magnified view of one chip capacitor

The chip components were precontaminated prior to the experiment with known levels of NaCl by placing a micro droplet of aqueous NaCl solution and allowing the droplet to evaporate. The volume of the droplet applied, and thereby the concentration of NaCl, was confined to the surface area of the component, leading to a fixed level of contamination per surface area. The concentrations of NaCl selected were below and above the limit of 1.56 of $\mu g \cdot cm^{-2}$, which is referred to in the IPC J-STD-001 standard as a maximum allowable level of ionic contamination on the PCBA after the manufacturing process. A relationship of 1 µL of solution over 1 mm^2 area was used, which relates $g \cdot L^{-1}$ to $\mu g \cdot cm^{-2}$ with a ratio of 1:100. A chip capacitor with dimensions 2 × 1.25 × 0.8 mm was used, and a droplet of 2.5 µL was applied to its upper surface prior to experiments. The LC from each component was measured using a "BioLogic VSP" multichannel potentiostat, Bio-Logic Instruments, France.

PCBA LEVEL TESTING USING COOLING STAGE

The temperature differential that is likely to be experienced in service due to diurnal changes or on/off cycles was simulated by controlling the temperature of the test PCBA by placing it on an aluminium block with embedded Peltier elements (cooling stage). The heat generated by operating the Peltier elements was dissipated by passing coolant through the stage at a controlled temperature. The voltage on the Peltier elements was applied using a programmable DC power source (EA-PSI 6032-06 32 V/6 A). The temperature of the PCBA mount on the aluminium block was measured with two platinum resistance temperature detectors (PT1000 class A) connected in a 2-wire circuit. A DaqLink data logger "Fourier Systems DBSA720" was used to log the temperature/voltage readings on a surface throughout the experiment. Figure 8.3 shows the cooling effect on the PCBAs measured with an infrared imaging camera when 3 V DC was applied to the Peltier elements.

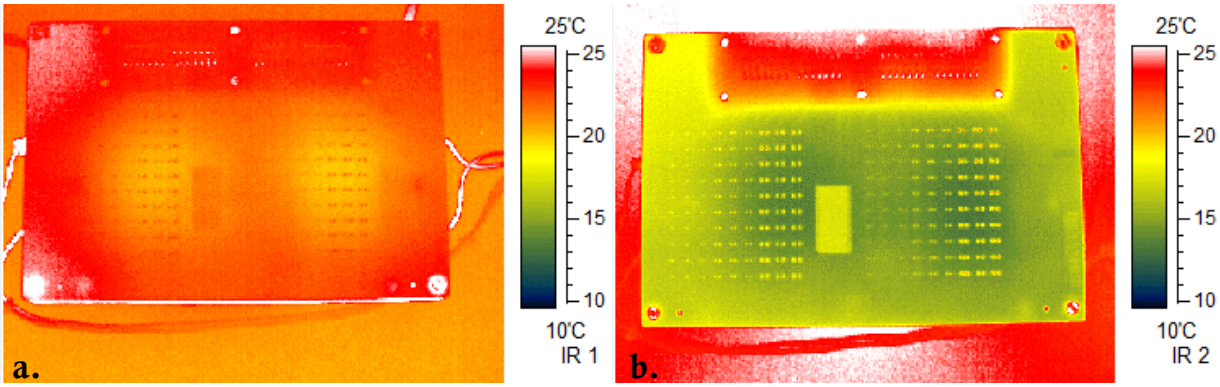

Figure 8.3: Cooling effect on aluminium block with embedded Peltier elements: a. PCBA on aluminium block without cooling and b. 3 V DC is applied on Peltier elements reducing temperature of PCBA to approximately 17 °C

The cooling studies on a test PCBA using the Peltier stage were performed inside the climatic chamber at 25 °C and 60 %RH, which made it possible to use a video microscope for *in situ* monitoring of the effect of temperature change on water layer formation and related corrosion processes.

CLIMATIC CONDITIONS FOR TESTING

"Espec PL-3KPH" climatic chamber was used for the study of temperature and humidity effects at the single component and PCBA level. The uncertainty associated with temperature and RH fluctuations in the climatic chamber is ±0.3 °C / ±2.5 %RH.

Single Component Level: The LC between the terminals of size 0805 10 nF multilayer ceramic capacitors mounted in the single component ECM setup and biased at 5 V DC was measured as a function of temperature elevated from 15 °C to 65 °C at constant RH of 98%, and as a function of RH elevated from 60% to 98% at a constant temperature of 25 °C. The elevation of RH and temperature was performed in steps of 10% and 10 °C, with step duration of 5 h.

Test PCBA level: The climatic conditions inside the chamber were kept constant at 25 °C and 60% RH. The water vapour density on the surface of the test PCBA was controlled by reducing the temperature of the PCBA. The temperature was reduced in steps of 1 °C–1.5 °C with a step duration of 2 hours, until a visible water layer on a surface of the PCBA was formed. The LC during these tests was measured on size 0805 100 nF capacitors, size 0805 1 MΩ resistors, and SIR comb pattern biased at 5 V DC and precontaminated with NaCl at different levels.
Additionally, an experiment with duration of 20 days and conditions close to condensation was performed. The temperature measured on the surface of the PCBAs was between 21.5°C and 22 °C, while the temperature of surrounding air was kept at 25 °C and 60% RH. The temperature difference between PCBA and surrounding air enabled to establish ~75%–80% RH [32] locally on the surface of the PCBA, which is close to the critical RH for NaCl [33].

III. RESULTS

LC UNDER NONCONDENSING AND SHORT-TERM CONDENSING CONDITION

Figure 8.4 represents the effect of RH and contamination on the LC between the terminals of single ceramic chip capacitors biased at 5 V DC at increasing humidity levels. Curves 1, 2, 3 represent results from 3 components tested at a time.

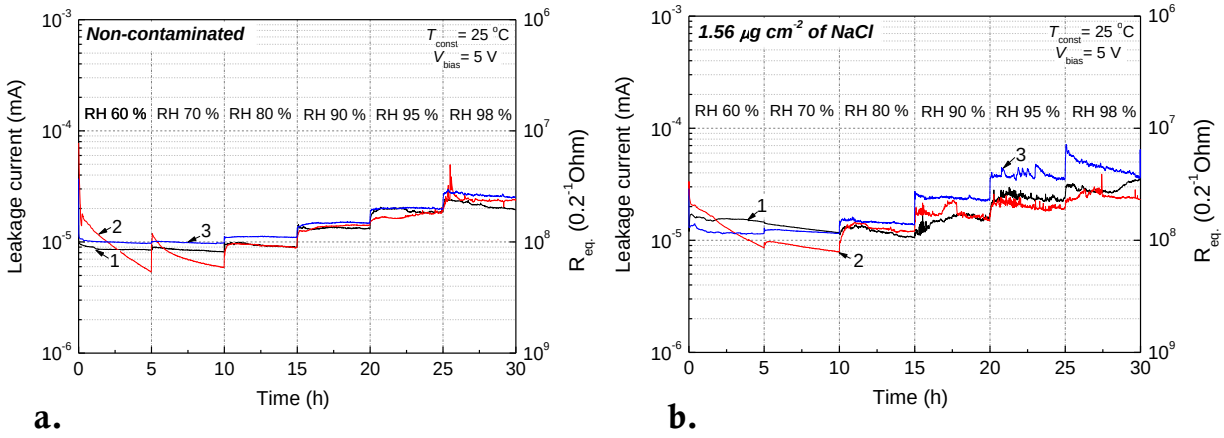

Figure 8.4: Effect of RH on the LC measured on size 0805 capacitors: a. non-contaminated and b. precontaminated at 1.56 µg·cm^{-2} of NaCl (1, 2, 3 represents 3 capacitors tested at a time)

Under RH levels of 60% and 70% the difference in LC measured on non-contaminated and NaCl contaminated samples was negligible, while at higher RH levels, an increase in LC with increase

in RH became apparent, and the difference between non-contaminated samples and NaCl contaminated samples was more pronounced. The LC curve for NaCl contaminated samples showed intermittent fluctuations that did not occur with the non-contaminated samples, while no ECM was observed with optical microscope.

Figure 8.5 shows the effect of temperature at a constant RH of 98% (implying an increase of water vapour content of the air with the temperature) on LC between the terminals of a single chip capacitor. The increase of LC with increase in temperature and water vapour content of the air for both uncontaminated and precontaminated samples was significantly higher with an increase of two orders of magnitude over a temperature shift of 50 °C from 15 °C to 65 °C. On average, no major difference in LC level was observed between contaminated and non-contaminated samples. The highest level of current observed was in the range of 1 µA.

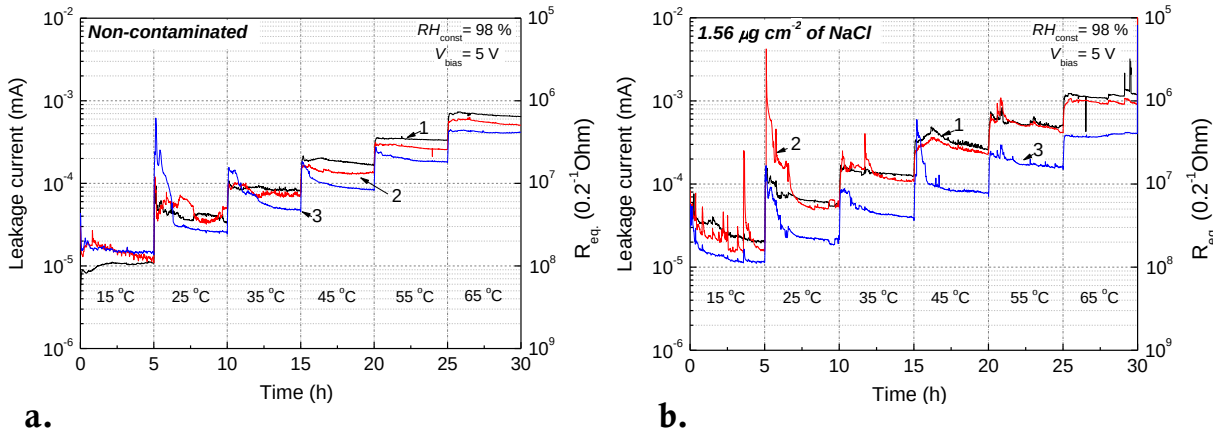

Figure 8.5: Effect of temperature implying an increase of water vapour content in the air on the LC measured on size 0805 capacitors: a. non-contaminated and b. pre-contaminated at 1.56 µg·cm^{-2} of NaCl (1, 2, 3 represents three capacitors tested at a time)

The initial peaks in the current curve during the temperature shift (Figure 8.5) are attributed to the temporary increase in RH on the surface of the ceramic chip capacitor, since the amount of water vapour in the air increases with the temperature. At the transition of the temperature cycles, the same level of RH was maintained by increasing the actual amount of water vapour, and thus, the peak appears before the conditions are stabilized in the climatic chamber.

The effect of contamination level on the LC between the terminals of ceramic chip capacitor as a function of RH and temperature is summarized in Figure 8.6. The current values plotted in these graphs represent the mean current values measured on three capacitors (the standard deviation is shown on each curve). The LC curves showed an increase in current with increased humidity, temperature, and contamination level. Almost 3 times the increase in LC level was found between zero contaminated samples to the sample precontaminated with 15.6 µg·cm^{-2} of NaCl. However, none of the samples exhibited ECM even at 65 °C/98% RH within the time of exposure to these conditions, as was confirmed by inspection with optical microscope.

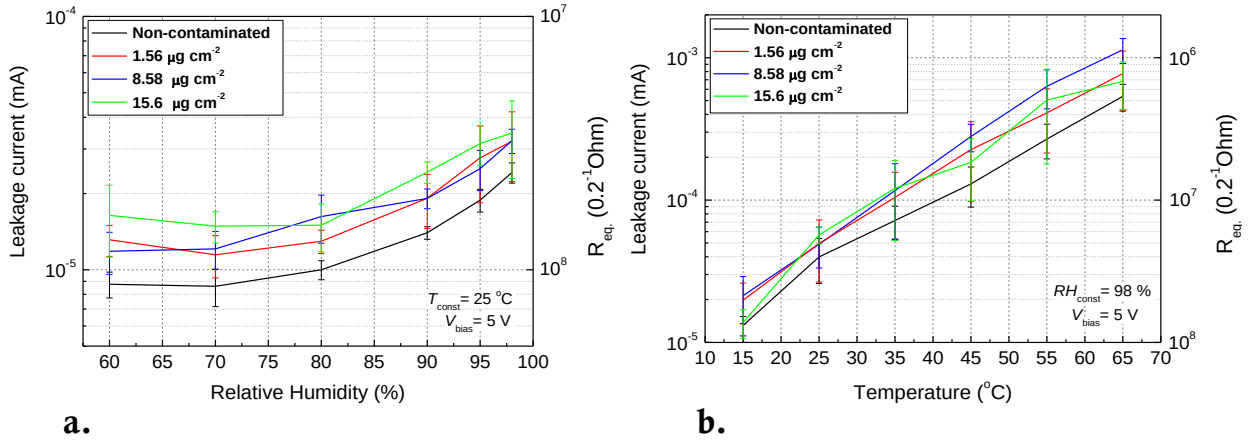

Figure 8.6: Effect of contamination level on the LC as a function of: a. RH at constant temperature and b. effect of temperature at constant RH

A marginal increase in LC with a magnitude of 20-30 nA was observed with an increase of RH from 60% to 98% at 25 °C (Figure 8.6 a.), but an increase of almost two orders of magnitude was observed for temperature change from 15 °C to 65 °C at 98% RH. The observed behaviour is attributed to the change of water vapour content of the air with the change of temperature and RH. In the latter case, the water vapour content of the air underwent a change from 12.5 g·m^{-3} to 155.2 g·m^{-3}, while an increase or RH from 60% to 98% at 25 °C caused a much lower change form 13.7 g·m^{-3} to 22.4 g·m^{-3} (Figure 8.6 b.). However, no significant differences were observed between the various contamination levels.

LC UNDER CONDENSING CONDITION

Figure 8.7 shows typical photographs taken *in situ* showing the water film formation on capacitors as the temperature of the PCBA is reduced compared to the ambient temperature in the climatic chamber. Temperature inside the climatic chamber was kept at 25 °C, while the RH was maintained at 60%. No visible water film formation was observed until the temperature had dropped below 19 °C, while the temperature drop to 17 °C caused condensation and thick water layer formation. The decrease of temperature of the PCBA from 25 °C at 60% RH down to 19 °C and 17 °C would cause, respectively, ~90% RH and ~100% RH locally on the surface of the PCBA.

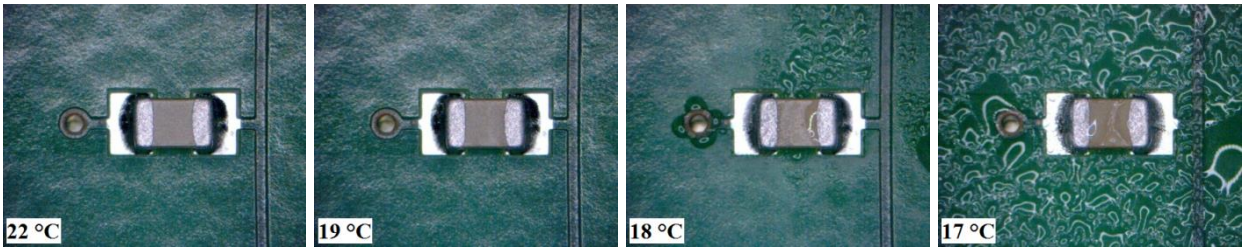

Figure 8.7: Temperature effect on condensation on size 0805 100 nF chip capacitors pre-contaminated with 8.58 µg·cm^{-2} of NaCl

Figure 8.8 shows the corresponding LC from three different sets of components from the test PCBA namely: i) size 0805 resistors, ii) size 0805 capacitors, and iii) SIR comb pattern. The LC obtained on the capacitors and resistors was measured on 10 components connected in parallel.

The temperatures indicated in the graphs are the average values of temperatures obtained with two resistance temperature detectors fixed on the test PCBAs. The expected error of temperature reading is ~1 °C.

The LC measurements at NaCl concentrations higher than 1.56 µg·cm^{-2} shown in Figure 8.8 indicate significant build-up of water layer thickness at 21.5 °C on the surface of components and SIR patterns, though it was not apparent in the captured images (Figure 8.7). Further decrease in temperature on the PCBA increased the thickness of the water layer, until it reached full condensation with a temperature drop to ~18 °C (Figure 8.7). Overall, an increase of measured current amplitude with the level of condensation was observed.

The LC curves for chip resistors (Figure 8.8 a.) showed current increase only when the temperature dropped to ~19 °C, while chip capacitors showed a current increase earlier at ~21 °C, as for the SIR patterns. The reading of LC through the resistors during the first 3 steps of experiment could be lost due to the base current through the resistors, which was subtracted from the measured current in the Figure 8.8 (a). Despite of this fact, when the deliquescent point of NaCl is achieved, the LC increases by 2–3 orders of magnitude and made it possible to identify the condensation.

Temperature measurements showed no difference between the resistor and capacitor area. Maximum current levels achieved for resistors and capacitors under full condensation conditions were similar, while the SIR patterns showed higher current levels due to the higher surface area of the component.

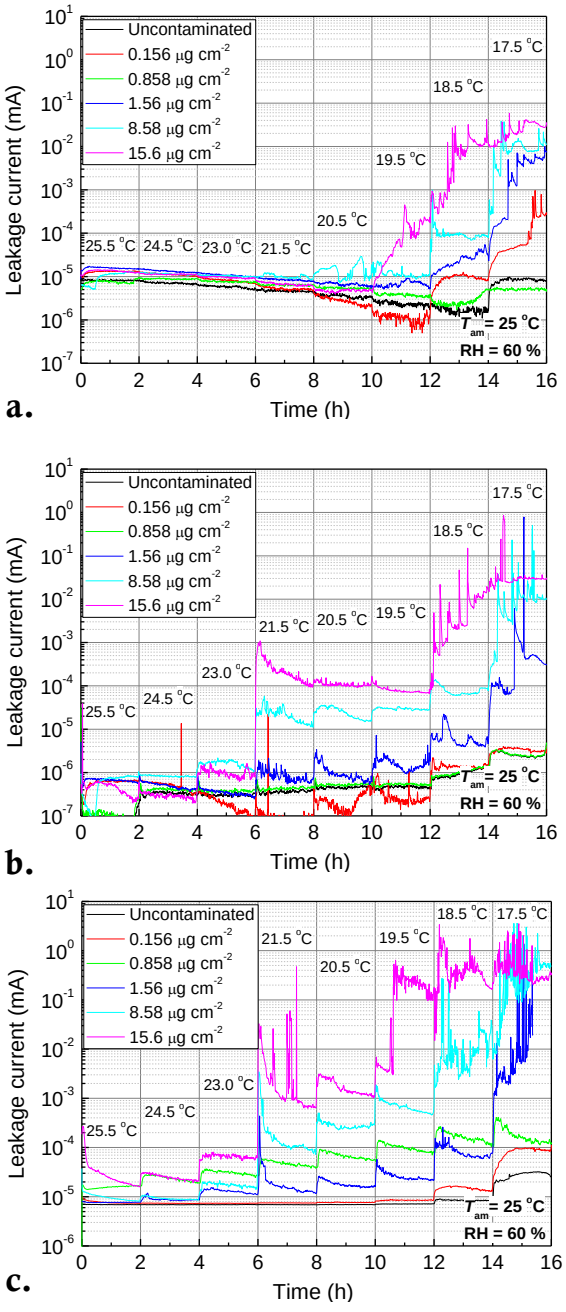

Figure 8.8: Effect of contamination and temperature difference on LC measured on test PCBA components biased at 5 V DC: a. size 0805 1MΩ resistors, b. size 0805 100 nF capacitors, and c. open SIR comb pattern

For the non-contaminated components, the increase of measured current was negligible, while very little increase was observed at close to dew-point temperature. The increase in LC at 0.156 µg·cm^{-2} occurred at the same steps as under the non-contaminated condition, but with a slightly higher magnitude. It was observed that an increase in NaCl concentrations caused not only an increase in current magnitude but also decreased the time (representing temperature)

when it occurred. For the non-contaminated samples, the increase of current was observed at the very last step, when the temperature was around 17.5 °C, while with increase in contamination a smaller temperature difference was enough to reach the dew-point, namely ~18.5 °C for 0.156 μg·cm^{-2} and ~19.5 °C for 15.6 μg·cm^{-2} contaminated specimens.

LONG-TERM EXPERIMENT UNDER NEAR TO CONDENSING CONDITIONS

A long term experiment under close to condensation condition was performed on the test PCBA in order to verify the likelihood of ECM as a function of time. For this purpose, the 0805 100 nF ceramic chip capacitors on the test PCBA were used for the analysis. Three samples with different contamination levels were tested during the experiment. The test was performed with the non-contaminated capacitors and the capacitors precontaminated with 1.56 μg·cm^{-2} and 15.6 μg·cm^{-2} of NaCl. In order to be able to perform three simultaneous experiments, the entire rows of the capacitors were cut off from three test PCBAs and fixed on the aluminium block with embedded Peltier elements.

The near condensation condition was established by keeping the atmosphere in the climatic chamber at 25 °C and 60% RH, while reducing the temperature of the PCBAs to around 21.5 °C. As a result, around 75%–80% RH was established locally on the surface of the PCBA. Previous experiments have shown that these conditions increase the water vapour density on a surface, and thereby form a water layer sufficient to cause a noticeable increase in the LC, while the humidity level was also above the critical RH level for NaCl contamination.

The experiment lasted for 20 days, and the environmental conditions were kept constant throughout (Figure 8.9). The LC values during the first 10 days represent a potential bias of 5 V DC, while in the time period from 10 to 20 days, the potential bias was increased to 10 V DC. It was done in order to create ECM, as it was not observed within reasonable time at 5 V DC.

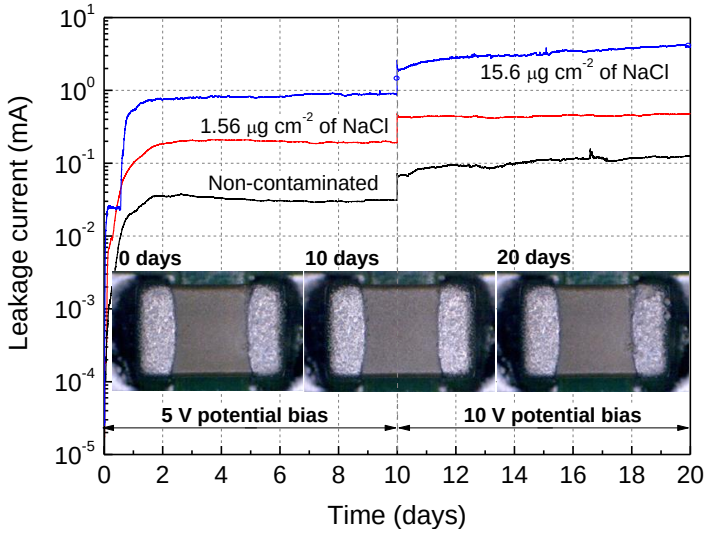

Figure 8.9: LC measured on 10 ceramic chip capacitors connected in parallel; corrosion of the terminals of capacitor pre-contaminated with 15.6 μg·cm^{-2} of NaCl (anode-right, cathode-left) is shown on the micrographs taken throughout the experiment

The magnitude of the measured LC was proportional to the level of contamination on the components. The non-contaminated capacitors showed the lowest current values in the range of

0.03 mA at 5 V DC and 0.1 mA at 10 V DC. The capacitors precontaminated with 1.56 μg·cm^{-2} showed 0.2 mA at 5 V and 0.45 mA at 10 V, while 15.6 μg·cm^{-2} of NaCl showed 0.8 mA and 3.5 mA current at 5 V and 10 V, respectively. An overall look at the LC curves shows that the LC increased over the first day, but stabilized further until the end of the experiment with an increase of LC values with increase in contamination level.

The measurements of LC and visual inspection of the components with stereo microscope after the completion of the test showed that none of the components exhibited dendrite growth during the experiment; however, severe corrosion was seen on the anode terminals of capacitors (micrographs in Figure 8.9).

A close-up view of the corroded terminal is shown in Figure 8.10 and is characterized by severe corrosion. The formation of hillocks (another close-up view is shown in Figure 8.11) similar to tin whiskers was also observed on the anode terminal of the capacitor with increased time of exposure.

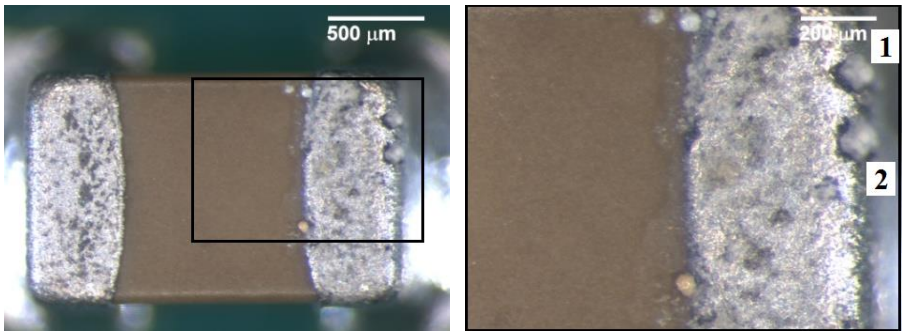

Figure 8.10: Close-up of anode terminal of capacitor precontaminated with 15.6 μg·cm^{-2} of NaCl after 20 days experiment

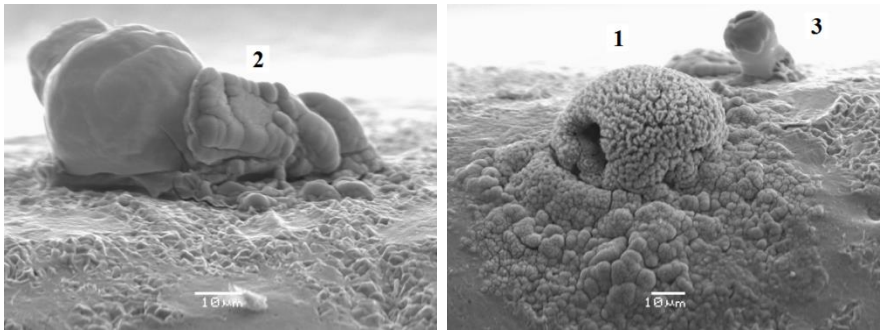

Figure 8.11: Tin hillocks formed on the surface of anode terminal of capacitor precontaminated with 15.6 μg·cm^{-2} of NaCl. Numbers 1, 2 and 3 can be, respectively found in Figure 8.10 and Figure 8.12

The images in Figure 8.10 and Figure 8.11 show that several hillocks were formed on one terminal of capacitor (positive terminal during experiments, anode). However, a detailed analysis of the captured images revealed that the growth of whiskers also appeared on the terminal of a capacitor (Figure 8.12). The whiskers grew from the anode terminal of the capacitor at different rates and after a certain period of time they broke. It was observed that the whiskers tended to form during the first 10 days of the experiment when the potential bias was 5 V. When the potential bias was increased to 10 V, more hillocks started to appear instead.

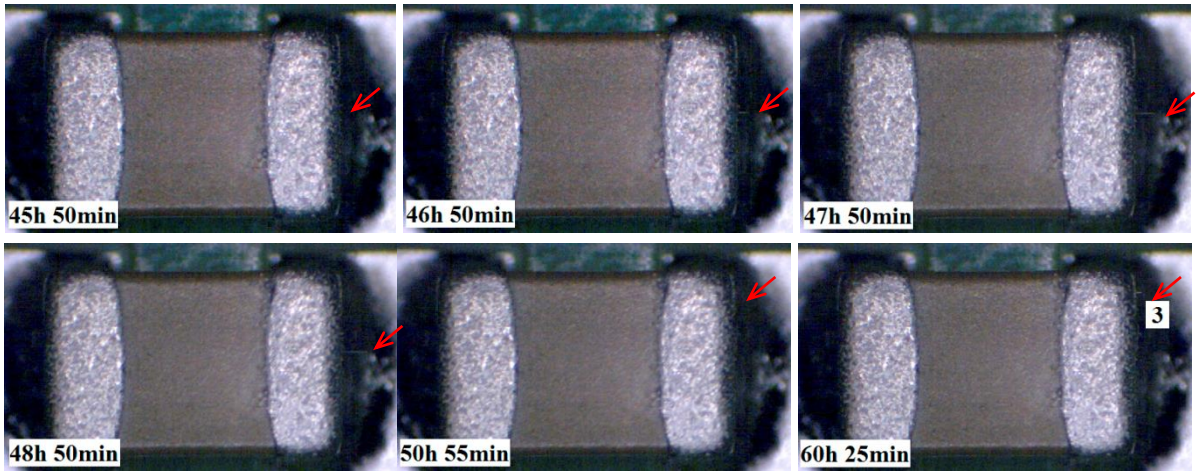

Figure 8.12: Tin whisker growth observed on the capacitor precontaminated with 15.6 μg·cm^{-2} of NaCl

A comparison between *in situ* images and SEM images indicated that the hillock, which is marked by number 3 in Figure 8.11, grew initially as a whisker (Figure 8.12 image taken at 60 h 25 min). However, due to external stresses, the whisker probably broke, and therefore, in the SEM images, it appears as a hillock. An optical microscope inspection of other samples indicated that the formation of short bumps was more usual – hillocks, rather than long tin whiskers.

IV. DISCUSSION

LC UNDER NONCONDENSING AND SHORT-TERM CONDENSING CONDITIONS

The increase in LC with increasing RH at 25 °C without any variation in temperature between the surface mount component or PCBA and ambient was found to be negligible (Figure 8.4 and Figure 8.6 a.) irrespective of the level of contamination. However, the increase of LC with high humidity and temperature (Figure 8.6 b.) reached 0.5 μA and showed a reduction of SIR on a single component to below 100 MΩ, which is referred in IPC J-STD-004A method 3.4.5.1 and IPC-9201 as constituting SIR failure. However, it is interesting to note that even with contamination and RH levels higher than the critical RH for NaCl, the increase in LC was minor when tested on single components biased at 5 V DC. The applied potential is an important factor, since an increase of electric field can magnify the effect of contamination, and increase the LC levels under high humidity conditions, or cause metal migration and dendritic growth under condensing conditions [17], [30].

The effect of ionic contamination and humidity levels are commonly evaluated by SIR testing with standardized comb patterns; however, similar testing on single chip components does not seem to have been reported, so a direct comparison of the results with previous data is not possible. However, the results obtained with SIR comb patterns under similar conditions can be compared with what has been reported in the literature. Previous investigations found that a decrease in SIR from approximately $2 \cdot 10^{12}$ Ω to $7 \cdot 10^{11}$ Ω with increasing RH from 65% to 85% at 65 °C is observed on a clean Au-Ni finish comb pattern with 0.64 mm pitch and 0.32 mm gap, and approximately 2800 squares, when biased at 5 V DC [34]. For a precontamination with adipic acid, which is an acid commonly used in soldering flux systems, at concentrations close to the cleanliness level specified by IPC J-STD-001 standard, an approximate decrease of SIR from

$1 \cdot 10^{11}$ Ω to $1 \cdot 10^{10}$ Ω has been reported [34]. Similar results were obtained on the standard IPC-B-24 copper comb patterns biased at 40 V DC and 50 V DC and exposed to varying environmental conditions (35 °C/90% RH; 65 °C/85% RH; 85 °C/85% RH) [29], [35]. The results obtained on the surface mount components in the present work indicated a marginal change in LC which can be attributed to the change of SIR on the components. The variation of SIR within the same order of magnitude from $4 \cdot 10^8$ Ω to $1 \cdot 10^8$ Ω was measured in the case of RH increase from 60% to 98% at 25 °C (Figure 8.6 a.), and a change of almost two orders of magnitude from $3 \cdot 10^8$ Ω to $6 \cdot 10^6$ Ω when temperature was increased (and also absolute water content) from 15 °C at 98 % RH to 65 °C at 98 % RH (Figure 8.6 b.).

The increase in LC with the temperature (Figure 8.5 and Figure 8.6 b.) is caused by several factors. First of all, the increase of temperature increases the amount of water vapour the air can hold. As a result, the increase of temperature leads to an increase of water vapour density on the surface of capacitors, reducing the SIR. In addition, the ion mobility, and therefore the migration rate, also increases with temperature. As a result, the charge transfer through the bridging media is accelerated, and this results in an increase in the LC with temperature.

It is known that an increase of temperature from 35 °C/90% RH to 85 °C/85% RH can reduce SIR by two orders of magnitude and thereby increase LC, if measured on the non-contaminated IPC-B-24 copper comb patterns at 40 V DC [29]. In the case of an Au-Ni finish comb pattern biased at 5 V DC, an increase of temperature from 50 °C/85% RH to 85 °C/85% RH increased the LC by nearly two orders of magnitude for non-contaminated components and those precontaminated with adipic acid at the level close to what is specified in the relevant IPC standard (which is thereby comparable to the NaCl concentrations used in this work) [34]. The results obtained on single chip capacitors are reasonably consistent with the results obtainable with SIR patterns, indicating a change in SIR of the same order of magnitude as has been reported in the literature.

Overall, the results obtained for single components with contamination levels, RH, and temperature showed that without a difference in temperature between the component and its surroundings, the resulting LC is significantly low with 5 V DC bias. At 98% RH and 25 °C it was below 50 nA, which can be attributed to the SIR higher than 100 MΩ, and it was reduced down to 10 MΩ when the temperature was increased up to 65 °C, implying an increase in water vapour in the air to maintain 98% RH. Although a further increase can be expected with an increase in potential bias, the results indicate that it is the temperature differential between the PCBA surface and its surroundings that magnifies the effects.

EFFECT OF CONDENSING AND NEAR TO CONDENSING CONDITIONS

LC curves obtained under the condensing conditions (Figure 8.8) showed the importance of a temperature difference between the surface of the PCBA and surrounding synergetic with contamination in the water layer. The surface temperature of the device needed to be closer to the dew point of the environment or the deliquescent point of the salt/contamination, and that the deliquescent point was generally a higher temperature than the dew point. With increased contamination on a surface, the temperature difference needed to form a sufficiently thick water layer to support measurable LC was reduced by 2 °C–3 °C.

The LC curve obtained on the non-contaminated samples shown in Figure 8.8 indicated that a temperature of 17.5 °C was needed to measure an increase in LC, which can be attributed to the build-up of water layer on a surface. According to the Mollier diagram [32], that temperature difference is very close to saturate the vapour density at the surface and lead to condensation. The introduction of NaCl contamination on the surface even at small concentration (0.858 μg·cm^{-2}) led to an increase in LC at RH levels around 90 % (T ≈ 18.5 °C). A further increase in contamination level up to 15.6 μg·cm^{-2} shifted the increase in current to RH values ~75%–85% (T ≈ 21.5-19.5 °C). The difference in the current for different contamination levels was of the same order of magnitude under noncondensing conditions; however, when the condensation occurred, the difference between non-contaminated samples and 15.6 μg·cm^{-2} of NaCl was as much as 2–3 orders of magnitude. This is highly significant from the point of view of the application of electronic devices, as it indicates that the temperature differential that leads to a significant level of water layer formation on the surface can be reduced due to the presence of ionic contamination [36], [37]. Further, when the water layer thickness became significantly higher, LC values showed a significant increase with increased levels of contamination that did not occur under humidity conditions without temperature variance.

It should be noted that the chip resistors were less prone to water layer formation compared to the chip capacitors. This indicates the importance of surface features in forming the water layer with each decrease in temperature and increase in contamination. No temperature difference was observed between resistors and capacitors. This might also be due to the dissipation of low levels of generated heat; therefore it is below the sensitivity of the temperature measurements. Another factor is the low wettability glass passivation layer on the resistors [17]. On the other hand, the ceramic layer on the capacitors assisted water layer formation due to its micro scale surface roughness. However, further work is needed to establish the exact reason for the difference in behaviour.

Long term experiments at near condensation condition (Figure 8.9) also showed a result similar to condensation conditions exhibiting an increase in LC with each increase in contamination. Since the temperature of the PCBA was kept at 21.5 °C, which is equivalent to producing 70%–80% RH close to the PCBA surface, it is significant in relation to the NaCl contamination as the humidity exceeds the critical RH, which is close to 75% [38], [39]. Above the critical RH, the NaCl deliquesces, forming a liquid brine – the brine will increase in volume as the temperature decreases/RH increases, leading to the formation of a continuous layer if there is sufficient contamination present. The results showed that unlike when NaCl is present on the surface of the component without a temperature difference with the surroundings, slight temperature cycling around critical humidity levels can cause thicker water layer formation and increased LCs.

The formation of hillocks found on the anode terminal of a chip capacitor (Figure 8.10 and Figure 8.11) is due to release of surface stress due to corrosion of top layer, which leads to the growth of hillocks similar to whiskers [40]. Tin whisker growth is a common phenomenon for tin coatings [41]–[45]. The whisker growth is started by compressive stress in the tin layer. Without the surface oxide layer, the internal compressive stress inside the tin layer relieves uniformly throughout the surface, and no whiskers appear in that area. However, when there are weak spots in the oxide layer, the internal compressive stress inside the bulk of the material can be relieved

by driving the tin material out of the opening and thereby causing whisker growth [44]. Analysis of *in situ* video of the capacitor showed that the hillocks started to form when the bias potential was increased from 5 V to 10 V. Visual inspection of the components after the experiment revealed that hillocks were formed on the capacitor when it was precontaminated with 1.56 μg·cm^{-2} of NaCl too, but to a lesser extent and smaller in size. The hillocks appeared on the anode terminal in most of the cases. This appearance indicates that corrosion of the anode terminal and depletion of the oxide layer created defects and weak spots on the surface, and thereby promoted the formation of hillocks or whiskers at these spots [46]–[48]. SEM/EDS analysis of the hillocks showed their composition to be pure tin.

The experiments showed the importance of temperature variation for the LC, and its effect on the reliability of PCBAs. Temperature variation on a PCBA can occur due to diurnal temperature variations, turn on/off cycles etc. [49]–[51], and it can be greatly accelerated if the components with high thermal capacity and conductivity are present on the PCBA or are in contact with it. The level of contamination plays a significant role in determining the differential temperature needed for condensing conditions on the PCBA [36], [37]. This shows the importance of controlling process related contamination levels so that the risk for later water formation can be significantly reduced.

V. CONCLUSIONS

1. A marginal increase in LC in the nA range was observed on surface mount capacitors exposed to elevated humidity condition from 60% to 98% at a constant temperature of 25 °C, and an almost two orders of magnitude increase in current from 10 nA to 1 μA in the case of temperature change (implying an increase of water content in the air) from 15 °C at 98% RH to 65 °C at 98% RH. This is equivalent to reduction of SIR below 100 MΩ, which is commonly used as failure criterion in climatic testing.
2. Effect of ionic contamination level was more pronounced with an increase of water vapour density on the surface of the PCBA due to differential temperature between PCBA and surroundings. Almost 2–3 orders of magnitude increase in LC was observed between non-contaminated samples and 15.6 μg·cm^{-2} of NaCl when a visible water layer formed on the chip component.
3. Presence of NaCl with deliquescent point greater than the dew point of the air caused formation of water layer on a surface at higher temperatures. For the non-contaminated samples, the condensation started at 17.5 °C (equivalent to 95% RH, at ambient 25 °C/60%RH), while NaCl even at concentration of 0.156 μg·cm^{-2} caused the same effect at lower RH, around 90%, and at 75%–85% RH when the level of contamination was further increased to 15.6 μg·cm^{-2}.
4. Chip resistors used in this work were found to be less prone to water layer formation compared to chip capacitors, although no temperature difference was found between resistors and capacitors.
5. *In situ* video showed formation of tin whiskers and hillocks from the anode terminal of the capacitor during testing under differential temperature conditions at potential bias from 5 V to 10 V. The growth of hillocks and whiskers was much more likely on the anode terminal of

a capacitor, indicating that corrosion of the anode terminal and depletion of the oxide film increased the formation of sites for whisker growth.

VI. ACKNOWLEDGMENT

The research reported here was conducted as part of the CELCORR/CreCon consortium (www.celcorr.com) and authors would like to acknowledge the funding and help received from the consortium partners.

VII. REFERENCES

[1] J. Henriksen, R. Hienonen, T. Imrell, C. Leygraf, and L. Sjögren, *Corrosion of electronics (A handbook based on experiences from nordic research project)*. Swedish Corrosion Institute, 1991, p. 86.

[2] H. Schweigart, "Humidity and pollution effects on electronic equipment," *CEEES Publ.*, 2001.

[3] J. D. Sinclair, L. A. Psota-Kelty, C. J. Weschler, and H. C. Shields, "Deposition of Airborne Sulfate, Nitrate, and Chloride Salts as It Relates to Corrosion of Electronics," *J. Electrochem. Soc.*, vol. 137, no. 4, pp. 1200–1206, 1990.

[4] B. Kanegsberg and E. Kanegsberg, *Handbook for Critical Cleaning. Applications, processes, and controls*, 2nd ed. CRC Press, 2011, p. 524.

[5] D. Pauls, "Residues in printed wiring boards and assemblies," *Circuit World*, vol. 27, no. 1, pp. 32–41, 2000.

[6] R. B. Comizzoli, C. A. Jankoski, G. A. Peins, L. A. Psota-Kelty, D. J. Siconolfi, and J. D. Sinclair, "Reliability of Electronics in Harsh Environments: Electrical Leakage and Corrosion Caused by Hygroscopic Pollutant Particles," *Corros. Reliab. Electron. Mater. Devices, Proc.*, vol. 99, no. 29, pp. 186–193, 1999.

[7] G. W. Warren, P. Wynblatt, and M. Zamanzadeh, "The Role of Electrochemical Migration and Moisture Adsorption on the Reliability of Metallized Ceramic Substrates," *J. Electron. Mater.*, vol. 18, no. 2, pp. 339–353, 1989.

[8] M. S. Jellesen, D. Minzari, U. Rathinavelu, P. Møller, and R. Ambat, "Corrosion failure due to flux residues in an electronic add-on device," *Eng. Fail. Anal.*, vol. 17, no. 6, pp. 1263–1272, Sep. 2010.

[9] S. Zhan, M. H. Azarian, and M. Pecht, "Reliability of Printed Circuit Boards Processed Using No-Clean Flux Technology in Temperature – Humidity – Bias Conditions," *IEEE Trans. Device Mater. Reliab.*, vol. 8, no. 2, pp. 426–434, 2008.

[10] C. Dominkovics and G. Harsányi, "Effects of Flux Residues on Surface Insulation Resistance and Electrochemical Migration," in *International Spring Seminar of Electronics Technology*, 2006, pp. 158–162.

[11] P.-E. Tegehall, "Impact of Humidity and Contamination on Surface Insulation Resistance and Electrochemical Migration," in *The ELFNET Book on Failure Mechanisms, Testing Methods, and Quality Issues of Lead-Free Solder Interconnects*, Springer, 2011, pp. 227–253.

[12] C. Schimpf, K. Feldmann, C. Matzner, and A. Steinke, "Failure of electronic devices due to condensation," *Microsyst. Technol.*, vol. 15, no. 1, pp. 123–127, Jun. 2009.

[13] V. Verdingovas, M. S. Jellesen, and R. Ambat, "Influence of sodium chloride and weak organic acids (flux residues) on electrochemical migration of tin on surface mount chip components," *Corros. Eng. Sci. Technol.*, vol. 48, no. 6, pp. 426–435, Sep. 2013.

[14] R. Hienonen and R. Lahtinen, "Corrosion and climatic effects in electronics," *Vtt Publ.*, 2007.

[15] Peter Biocca, "Flux chemistries and thermal profiling considerations in SMT assembly," in *National Electronic Packaging and Production Conference-Proceedings of the Technical Program (West and East)*, 1999, vol. 2, pp. 971–977.

[16] K. S. Hansen, M. S. Jellesen, P. Moller, P. J. S. Westermann, and R. Ambat, "Effect of Solder Flux Residues on Corrosion of Electronics," in *Annual reliability and maintainability symposium*, 2009, pp. 503–509.

[17] D. Minzari, M. S. Jellesen, P. Møller, P. Wahlberg, and R. Ambat, "Electrochemical Migration on Electronic Chip Resistors in Chloride Environments," *IEEE Trans. Device Mater. Reliab.*, vol. 9, no. 3, pp. 392–402, 2009.

[18] D. Pauls, C. Slach, and N. Devore, "Process Qualification Using the IPC-B-52 Standard Test Assembly," in *Printed Circuits Expo, Apex, and the Designers Summit 2006: Perfectly Cutting Edge*, 2006, pp. 1035–1073.

[19] D. Minzari, "Doctoral Thesis, 'Investigation of Electronic Corrosion Mechanisms,'" Technical University of Denmark, 2010.
[20] U. Rathinavelu, M. S. Jellesen, P. Moller, and R. Ambat, "Effect of No-Clean Flux Residues on the Performance of Acrylic Conformal Coating in Aggressive Environments," *IEEE Trans. Components, Packag. Manuf. Technol.*, vol. 2, no. 4, pp. 719–728, 2012.
[21] S. Zhan, M. H. Azarian, and M. G. Pecht, "Surface Insulation Resistance of Conformally Coated Printed Circuit Boards Processed With No-Clean Flux," *IEEE Trans. Electron. Packag. Manuf.*, vol. 29, no. 3, pp. 217–223, 2006.
[22] J. S. Osenbach and J. L. Zell, "Corrosion of thin film aluminum metallization: conformal coating materials," *IEEE Trans. Components, Hybrids, Manuf. Technol.*, vol. 16, no. 3, pp. 350–359, May 1993.
[23] M. Tencer and J. S. Moss, "Humidity Management of Outdoor Electronic Equipment: Methods, Pitfalls, and Recommendations," *IEEE Trans. Components Packag. Technol.*, vol. 25, no. 1, pp. 66–72, Mar. 2002.
[24] G. H. Findenegg and S. Herminghaus, "Wetting: statics and dynamics," *Curr. Opin. Colloid Interface Sci.*, vol. 2, no. 3, pp. 301–307.
[25] S. J. Krumbein, "Metallic Electromigration Phenomena," *IEEE Trans. Components, Hybrids, Manuf. Technol.*, vol. 11, no. 1, pp. 5–15, Mar. 1988.
[26] H. Cui, "Accelerated Temperature Cycle Test and Coffin-Manson Model for Electronic Packaging," in *Annual Reliability and Maintainability Symposium, 2005 Proceedings: The International Symposium on Product Quality and Integrity*, 2005, pp. 556–560.
[27] R. Rörgren, P. Tegehall, and P. Carlsson, "Reliability of BGA Packages in an Automotive Environment," *J. Surf. Mt. Technol.*, vol. 11, no. 2, pp. 35–44, 1998.
[28] M. J. Cushing, D. E. Mortin, T. J. Stadterman, and A. Malhotra, "Comparison of Electronics-Reliability Assessment Approaches," *IEEE Trans. Reliab.*, vol. 42, no. 4, pp. 542–546, 1993.
[29] J. E. Sohn and U. Ray, "Weak Organic Acids and Surface Insulation Resistance," *Circuit World*, vol. 21, no. 4, pp. 22–26, 1994.
[30] D. Minzari, M. S. Jellesen, P. Møller, and R. Ambat, "On the electrochemical migration mechanism of tin in electronics," *Corros. Sci.*, vol. 53, no. 10, pp. 3366–3379, Oct. 2011.
[31] D. Minzari, F. B. Grumsen, M. S. Jellesen, P. Møller, and R. Ambat, "Electrochemical migration of tin in electronics and microstructure of the dendrites," *Corros. Sci.*, vol. 53, no. 5, pp. 1659–1669, May 2011.
[32] T. F. Irvine and J. P. Hartnett, *Steam and air tables in SI units: Including data for other substances and a separate mollier chart for steam*. Hemisphere publishing, 1976, p. 127.
[33] W. M. Haynes and D. R. Lide, *CRC Handbook of chemistry and physics*, 94th Editi. CRC Press, 2013, p. 2668.
[34] C. Hunt and L. Zou, "The impact of temperature and humidity conditions on surface insulation resistance values for various fluxes," *Solder. Surf. Mt. Technol.*, vol. 11, no. 1, pp. 36–43, 1999.
[35] K. M. Adams, J. E. Anderson, and Y. B. Graves, "Ionograph Sensitivity to Chemical Residues from 'No Clean' Soldering Fluxes: Comparison of Solvent Extract Conductivity and Surface Conductivity," *Circuit World*, vol. 20, no. 2, pp. 41–44, 1994.
[36] F. Cirolia, C. Finan, and P. Coast, "The Effects of Airborne Contaminants on Electronic Power Supplies," in *Sixteenth Annual IEEE Applied Power Electronics Conference*, 2001, pp. 238–242.
[37] M. Tencer, "Conductive aqueous layer formation at the gel-substrate interface in equilibrium with 100% RH environment," *IEEE Trans. Components Packag. Technol.*, vol. 23, no. 4, pp. 693–699, 2000.
[38] L. Kräמer, U. Pöschl, and R. Niessner, "Microstructural rearrangement of sodium chloride condensation aerosol particles on interaction with water vapor," *J. Aerosol Sci.*, vol. 31, no. 6, pp. 673–685, 2000.
[39] E. Mikhailov, S. Vlasenko, D. Rose, and U. Pöschl, "Mass-based hygroscopicity parameter interaction model and measurement of atmospheric aerosol water uptake," *Atmos. Chem. Phys.*, vol. 13, no. 2, pp. 717–740, Jan. 2013.
[40] W. J. Boettinger, C. E. Johnson, L. A. Bendersky, K.-W. Moon, M. E. Williams, and G. R. Stafford, "Whisker and Hillock formation on Sn, Sn–Cu and Sn–Pb electrodeposits," *Acta Mater.*, vol. 53, no. 19, pp. 5033–5050, Nov. 2005.
[41] S. W. Liang, C. Chen, J. K. Han, L. Xu, K. N. Tu, and Y.-S. Lai, "Blocking hillock and whisker growth by intermetallic compound formation in Sn-0.7Cu flip chip solder joints under electromigration," *J. Appl. Phys.*, vol. 107, no. 9, p. 093715, 2010.

[42] M. N. Islam, Y. C. Chan, and M. O. Alam, "Effects of intermetallic compounds on properties of Sn-Cu lead-free soldered joints," in *International Conference on Asian Green Electronics - Design for Manufacturability and Reliability*, 2004, pp. 185–191.

[43] P. Su, J. Howell, and S. Chopin, "A Statistical Study of Sn Whisker Population and Growth During Elevated Temperature and Humidity Tests," *IEEE Trans. Electron. Packag. Manuf.*, vol. 29, no. 4, pp. 246–251, Oct. 2006.

[44] Y. Nakadaira, S. Jeong, J. Shim, J. Seo, S. Min, T. Cho, S. Kang, and S. Oh, "Growth of tin whiskers for lead-free plated leadframe packages in high humid environments and during thermal cycling," *Microelectron. Reliab.*, vol. 48, no. 1, pp. 83–104, Jan. 2008.

[45] J. W. Osenbach, R. L. Shook, B. T. Vaccaro, B. D. Potteiger, a. N. Amin, K. N. Hooghan, P. Suratkar, and P. Ruengsinsub, "Sn whiskers: material, design, processing, and post-plate reflow effects and development of an overall phenomenological theory," *IEEE Trans. Electron. Packag. Manuf.*, vol. 28, no. 1, pp. 36–62, Jan. 2005.

[46] J. Cheng, S. Chen, P. T. Vianco, and J. C. M. Li, "Quantitative analysis for hillocks grown from electroplated Sn film," *J. Appl. Phys.*, vol. 107, no. 7, p. 074902, 2010.

[47] K.-N. Tu, "Spontaneous Tin Whisker Growth: Mechanism and Prevention," in *Solder Joint Technology*, Springer Series in Materials Science, 2007, pp. 153–181.

[48] B. Illés, B. Horváth, and G. Harsányi, "Effect of strongly oxidizing environment on whisker growth form tin coating," *Surf. Coatings Technol.*, vol. 205, no. 7, pp. 2262–2266, Dec. 2010.

[49] C. E. Hoge, "Corrosion Criteria for Electronic Packaging : Part III- Corrosion by Package Family," *IEEE Trans. Components, Hybrids, Manuf. Technol.*, vol. 13, no. 4, pp. 1105–1109, 1990.

[50] G. F. Cerofolini and C. Rovere, "The role of water vapor in the corrosion of microelectronic circuits," *Thin Solid Films*, vol. 47, no. 2, pp. 83–94, 1977.

[51] L. J. Klein, M. Schappert, and H. F. Hamann, "Corrosion Risk Management in IT Facilities," in *2012 13th IEEE Intersociety Conference on Thermal and Thermomechanical Phenomena in Electronic Systems*, 2012, no. 914, pp. 353–357.

9. SOLDER FLUX RESIDUES AND HUMIDITY RELATED FAILURES IN ELECTRONICS: RELATIVE EFFECTS OF WEAK ORGANIC ACID USED IN NO-CLEAN FLUX SYSTEMS

Vadimas Verdingovas, Morten Stendahl Jellesen, and Rajan Ambat

Abstract—This paper presents the results of humidity testing of weak organic acids (WOAs), namely adipic, succinic, glutaric, DL-malic, and palmitic acids, which are commonly used as activators in no-clean solder fluxes. The study was performed under humidity conditions varying from 60% relative humidity (RH) to ~99 %RH at 25 °C. The following parameters were used for characterisation of WOAs: mass gain due to water adsorption and deliquescence of the WOA (by using quartz crystal microbalance), resistivity of water layer formed on the printed circuit board (by impedance spectroscopy) and leakage current measured using the surface insulation resistance pattern in the potential range from 0 V to 10 V. The combined results indicated the importance the WOA chemical structure for the water adsorption and therefore conductive water layer formation on the printed circuit board assembly (PCBA). A substantial increase of leakage currents and probability of electrochemical migration was observed at humidity levels above the RH corresponding to the deliquescence point of WOAs present as contaminants on the printed circuit boards. The results suggest that use of solder fluxes with WOAs having higher deliquescence point could improve the reliability of electronics operating under circumstances in which exposure to high humidity is likely to occur.

Keywords—Flux residue, Surface insulation resistance, Leakage current, Corrosion, Reliability of electronics, Impedance spectroscopy

I. INTRODUCTION

No-clean fluxes containing weak organic acids as activators are widely used for reflow, wave, and selective soldering process for manufacturing of printed circuit board assemblies (PCBAs). Usually, they are halide-free and provide the ability to activate the metal surface through low-molecular-weight dicarboxylic acids. The advantage of no-clean flux over conventional solder flux is that the residue, which is typically composed of resin and weak organic acid (WOA), volatizes and decomposes during soldering, hence the remaining residue is expected to be benign and does not require post-soldering cleaning process. The development of such fluxes was driven by the ban of chlorofluorocarbons (CFCs) [1], which were used in solvents for cleaning conventional rosin-based fluxes, and by attempts to increase soldering efficiency and to reduce costs related to soldering.

No-clean fluxes can be formulated with various levels of resin, generally referred to as solids. Typically, high-solid-content fluxes do not require use of an inert environment for soldering but will leave excessive residues on the board, while low-solids (<5 wt.%) fluxes seldom leave a

V. Verdingovas, M. S. Jellesen, and R. Ambat, "Solder flux residues and humidity-related failures in electronics: relative effects of weak organic acid used in no-clean flux systems," *J. Electron. Mater.,* vol. 14, no. 4, pp. 1116–1127, 2015.

residue visible to the naked eye visible and are expected to have low influence on corrosion. From the corrosion point of view, the most important component in the flux is the ionic activator, namely the WOAs. The WOAs typically used in soldering fluxes are known to be hygroscopic [2], thus the residues are able to adsorb moisture from the surroundings at lower humidity levels than are typical for moisture condensation on clean PCBs. As a result, the residues of WOAs can enhance leakage currents and cause other corrosion-related issues, e.g., affecting the integrity of electrical circuits through electrical shorts and open circuits, or electrochemical migration [3]–[5].

A commonly used technique for studying the effect of flux residues (WOAs) is measurement of surface insulation resistance (SIR), as described in IPC J-STD-004B standard. SIR testing is performed at 40°C/90%RH, for 168 h at 5 V DC or 25 $V \cdot mm^{-1}$. The purpose of the SIR testing is to understand the impact of flux residues on the electrical reliability of a device, specifically the conductive and corrosive nature of the residue. SIR measurement provides the resistivity of the residue in ohms per square (normalized area). Compared with SIR testing, the effect of corrosive acids from wave solder flux or reflow solder paste can be studied by resistance measurements on test coupons typically having narrower anodes and wider cathode electrodes [6]–[8]. In this case, the change of resistance of the anodes due to corrosion is measured and compared with the initial values. Another, not as commonly used, but very effective method for studying the conduction mechanisms on the surface of the printed circuit boards is the impedance spectroscopy [9]–[13]. The advantage of impedance spectroscopy over conventional SIR testing is that the low-amplitude alternating current (AC) signal used in the test itself does not alter the nature of the test patterns, and enables one to distinguish between the impedance of the water layer and impedance from interfacial electrochemical processes. However, this technique requires more advanced measurement instruments, and specific knowledge for data analysis.

It is known that some of the WOAs have a more detrimental effect in terms of SIR and corrosion than other acids when tested under a variety of temperature-humidity-bias conditions. A number of investigations have been reported on the effects of flux residues on leakage current and corrosion as a function of humidity, temperature, flux type, and its concentration [3], [10], [14]–[18]. The effect of WOAs and no-clean flux was tested under varying climate conditions: 40°C/93%RH, 60°C/93%RH, 35°C/90%RH, 65°C/85%RH, and 85°C/85%RH. Substantial differences in SIR among adipic, succinic, glutaric, and malic acid was observed, and it was found that SIR testing at higher temperature minimizes the differences in SIR [3]. Another study of processing temperature and accelerated aging conditions showed that the SIR behaviour of the WOAs is a temperature dependent, and as most appropriate condition for testing 40°C/93%RH is suggested [19].

The effects of WOA in the flux residue are commonly studied in terms of SIR, dendritic growth, and corrosion. The test is typically performed under a direct current (DC) voltage and constant climate conditions, however if the test is performed under RH levels below the critical relative humidity level of the ionic contamination, it will not necessarily reveal its potential danger, or the ranking of particular contaminants can change if tested under different climate conditions. Different from literature, the present work focuses on the effect of ionic contamination arising from WOAs in no-clean flux systems on the leakage current and SIR from the point of view of residue hygroscopicity. The hygroscopicity of WOAs characterizes their ability to take in moisture from the atmosphere by adsorption and absorption, therefore determining the amount that can be dissolved in the thin water layer to influence the conductivity of the water layer formed

on the surface of the PCBA. In this work, hygroscopicity of various WOAs (adipic, glutaric, succinic, DL-malic, and palmitic acids) is investigated using a quartz crystal microbalance to quantify the mass gain after contaminating the crystal surface with known amount of WOAs. Furthermore, the influence of WOAs on the impedance and leakage current through the water layer formed under exposure to humidity is studied using a test PCB setup. The range of humidity employed in the testing is 60% to ~99% at 25 °C.

II. MATERIALS AND METHODS

CLIMATIC CHAMBER

All humidity exposure experiments were performed in an "Espec PL-3KPH" climatic chamber. The fluctuation of temperature and humidity is ±0.3°C/±2.5%RH, in the range -40°C to +100°C/20°CRH to 98%RH. The highest RH used in the experiments was above the range for which fluctuations of temperature and humidity are specified. Thus, this test condition is further denoted as ~99%RH.

TEST BOARDS

Leakage current measurements were performed on the SIR pattern with hot air solder leveling (HASL) (Sn/Ag/Cu) finish, on the FR-4 test board in accordance with IPC-4101/21. The size and thickness of the board were 168 mm × 112.4 mm and 1.6 mm, respectively, and a detailed description of the test board can be found elsewhere [20]. The dimensions of SIR pattern used for leakage current measurements were 13 mm × 25 mm; the width of conductor lines and the spacing between them was 0.3 mm (Figure 9.1 a.). The nominal square count calculated for a SIR pattern of the current dimensions is 1476 [21].

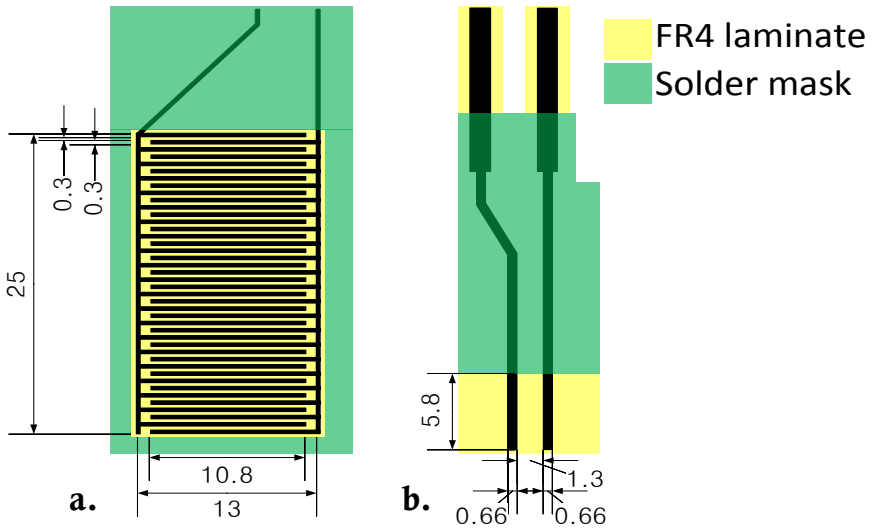

Figure 9.1: Test boards: a. SIR pattern and b. PCB with two electrodes used for impedance spectroscopy. The dimensions provided in the drawing are in millimetres (mm).

The test board for impedance measurements was a 1.6 mm FR-4 laminate with two opposing conduction lines having width of 0.66 mm, length of 5.8 mm, and separation of 1.3 mm (Figure 9.1 b.). The dimensions of the SIR pattern (area without solder mask) provide an approximate

nominal square count of 4.5. The base material of the conducting lines was copper (~35 μm), with an intermediate layer of nickel (9 ± 1 μm), and a top layer of gold (6.5 ± 1 μm).

Prior to application of WOAs, the test boards were cleaned with a mixture of isopropyl alcohol and deionized water and then rinsed in deionized water with resistivity of 18.2 MΩ·cm at 25°C. An ultrasonic bath was used for the cleaning of the test board for impedance measurement (Figure 9.1 b). The cleaned boards were precontaminated with the WOAs dissolved in isopropyl alcohol at concentration of 10 $g \cdot L^{-1}$. The volume of the droplet was confined to the surface area of the test coupons, resulting in 100 $\mu g \cdot cm^{-2}$ of the WOAs after solvent evaporation at room temperature. A set of precontaminated test boards was also exposed to temperature ramping from 220°C to 245°C for 45s to simulate the temperature profile likely to be experienced during the soldering process.

WEAK ORGANIC ACIDS

A summary of physical properties of WOAs commonly used in no-clean solder flux is shown in Table 1. The acids were selected after chemical composition analysis of a number of no-clean solder fluxes currently available on the market. One of the important parameters describing the WOAs is the dissociation rate, which is described as the ratio of the concentrations of dissociated ions and undissociated molecules. The negative of the logarithm of the acid dissociation constant (pK_a) for the first and second dissociation constants is given in Table 9.1. The larger the value of pK_a, the lesser the extent of dissociation and the lower the ionic conductivity in water.

Table 9.1: Selected properties of weak organic acids **[2]**

Acid	**Molecular formula**	**Molecular weight (g/mol)**	**pK_{a1}**	**pK_{a2}**	**Melting point (°C)**	**Boiling point (°C)**	**Solubility (g/1000 g H_2O)**
Adipic	$HO_2C(CH_2)_4CO_2H$	146.14	$4.41_{18°C}$	$5.41_{18°C}$	151.5	337.5	$15_{15°C}$
Succinic	$HO_2C(CH_2)_2CO_2H$	118.09	$4.21_{25°C}$	$5.64_{25°C}$	185	234	$83.5_{25°C}$
Glutaric	$HO_2C(CH_2)_3CO_2H$	132.12	$4.32_{18°C}$	$5.42_{25°C}$	97.9	273	$1400_{25°C}$
DL-malic	$HO_2CCH(OH)CH_2CO_2H$	134.09	$3.40_{25°C}$	$5.11_{25°C}$	132		$1440_{26°C}$
Palmitic	$H_3C(CH_2)_{14}CO_2H$	256.42	4.78	-	62.5	351	$0.007_{20°C}$

The residue of no-clean flux is supposed to degrade and evaporate during exposure to the soldering temperature, and the remaining residue of no-clean flux must be benign. Therefore, the melting and boiling temperatures are of importance, although due to the small amounts of WOAs resulting from no-clean fluxes, the residue volatilizes before it reaches boiling point. The solubility is another important factor regarding the thickness of the water layer formed under humidity exposure. The water layer thickness formed due to deliquescence of highly soluble WOA is higher when compared to the water layer formed by the less soluble WOA at equivalent weight amount.

HYGROSCOPIC PROPERTY OF THE WEAK ORGANIC ACIDS

A "QCM200" quartz crystal microbalance (QCM) from SRS Inc. with 5 MHz AT-cut gold contact quartz crystal was used for *in situ* measurement of water adsorption and absorption by the WOAs. The quantitative relationship between the change in frequency of the piezoelectric crystal and a change of mass caused by the mass loading on a piezoelectric crystal surface is given according to Sauerbrey equation [22]:

$$\Delta f = \left(\frac{-2 f_0^2}{\left(\mu_q \rho_q\right)^{1/2}} \right) \frac{\Delta m}{A} = -C_f \frac{\Delta m}{A} \quad (1)$$

where f_0 (Hz) is the resonant frequency of the crystal; μ_q (g·cm^{-1}·s^{-2}) is the shear modulus of quartz, ρ_q (g·cm^{-3}) is the density of quartz, A (cm^2) is the surface area of the electrode, and Δm (g) is the change in mass on the crystal. The sensitivity factor C_f for the crystal used in this work at room temperature was 56.6 Hz μg^{-1}·cm^2.

The hygroscopicity of WOAs was determined by putting a 1.4 μL droplet of acid dissolved in isopropyl alcohol at concentration of 1 g·L^1 on the active gold electrode of the crystal, letting solvent evaporate, and exposing the crystal to elevated humidity inside the climatic chamber. The relative humidity (RH) was ramped from 20 % to 98 % at 25°C during 8 h interval and elevated from 60 % to ~99 % at 25°C in steps of 10 %, 5 %, and 2 %. The increase of mass of the crystal was associated with water adsorption onto the surface and the residue initially applied onto the crystal. The abrupt change in mass and motional resistance of the crystal was attributed to the critical RH or deliquescence of WOA on the crystal.

ELECTROCHEMICAL MEASUREMENTS

Electrochemical measurements were performed with a "BioLogic VSP" multichannel workstation (Bio-Logic Instruments, France). The channels of the instrument were connected in two-electrode cell configuration.

LEAKAGE CURRENT MEASUREMENTS

The leakage current was measured on SIR patterns precontaminated with WOAs at concentration of 100 μg·cm^{-2} and exposed to elevated humidity inside the climatic chamber. The humidity was elevated from 60 %RH to ~99 %RH, while the temperature was kept constant at 25 °C throughout the experiment. After each step of humidity increase, the samples were left to equilibrate with the environment for 2 h, then potential sweep measurements were performed. The current was measured as a function of the applied potential, which was scanned from 0 V to 10 V at 2 mV·s^{-1} sweep rate. The measurements were performed at 60 %, 70 %, 80 %, 90 %, 95 %, and 98 %, at 25 °C.

AC IMPEDANCE

Impedance measurements were performed using an AC signal with amplitude of 50 mV (V_{rms}≈35.36 mV) in the frequency range from 10 mHz to 100 kHz. The average of five measurements per frequency was recorded. Impedance and phase angle measurements were generated at the open-circuit potential. Impedance spectroscopy measurements were performed simultaneously with the leakage current measurements under the same climatic conditions. Fitting of the impedance data to the equivalent circuits was done by using "ZSimpWin 3.21" electrochemical impedance modelling software.

III. RESULTS

HYGROSCOPICITY OF THE WEAK ORGANIC ACIDS

The RH level at which the WOA begins to adsorb moisture from the atmosphere is usually referred to as the critical RH and can also be designated as the deliquescence RH. The deliquescence RH was investigated by applying a droplet of WOAs dissolved in isopropyl alcohol on the active electrode of the piezoelectric quartz crystal and exposing it to the elevated humidity condition. The change of frequency and motional resistance of the crystal at series resonance as a function of time and relative humidity for adipic and glutaric acids is shown in Figure 9.2. The negative change of frequency is attributed to the gain of mass, while the positive change of motional resistance indicates the change of viscoelastic properties of the substance on the crystal. Typically, the motional resistance of the crystal at series resonance varies from about 10 Ohm to 40 Ohm for a dry crystal, to about 375 Ohm for a crystal in water. The critical RH for WOAs was determined from the change of frequency and resistance of the crystal.

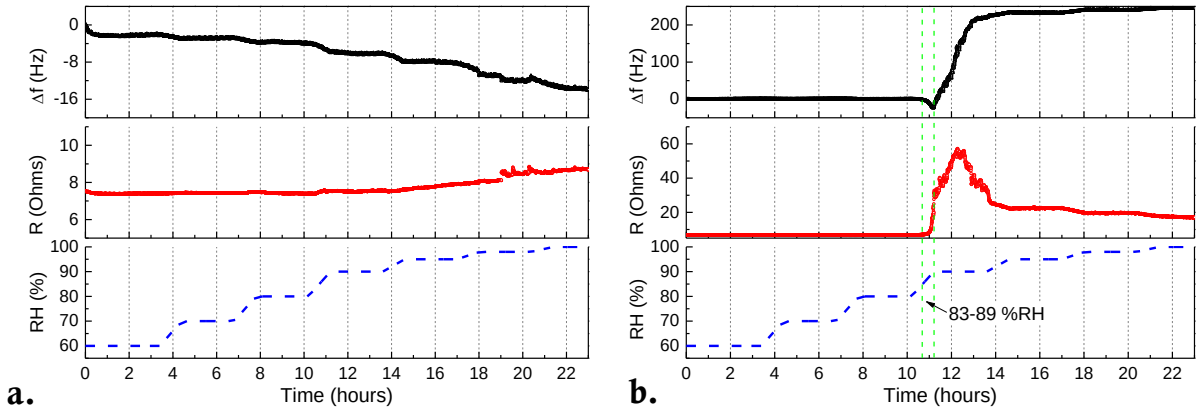

Figure 9.2: Representative graphs from QCM measurement: a. adipic and b. glutaric acids

In the case of adipic acid (Figure 9.2 a.), a steady decrease of frequency and increase of resistance with increasing RH were observed over the entire range of humidity tested, whereas for glutaric acid (Figure 9.2 b.) the frequency first abruptly decreased (startling from ~83%RH) followed by a steep increase (from ~87%RH). The resistance increased from 6.7 Ohm to 57.0 Ohm during this measurement. The abrupt change of the resonant frequency and the significant increase of the motional resistance indicate the change in the viscoelastic property of the substance on the crystal, attributable to deliquescence of the WOA. The range of RH for deliquescence of glutaric acid is indicated by green dashed line in Figure 9.2 b. The same procedure was carried out for all five WOAs, and a summary of the results is presented in Table 9.2. The first deliquescence RH column for the WOAs presents data reported in the literature, while the second column presents the deliquescence RH range observed with QCM in a number of tests performed under elevated RH conditions.

Table 9.2: Deliquescence relative humidity (DRH) of WOAs

Acid	$DRH_{literature}$ (%)	DRH_{QCM} (%)
Adipic	99.6[a]; ≥99[c]	>98
Succinic	98[a]; >94[b]; 98.8[b*]; ≥98[c]	>98
Glutaric	84[a]; 83.5-85[b]; 88.0-88.5[b*]; 89-99[c]; 85±5[d]	83-89
DL-malic	86[a]; 78[e]; no deliquescence[b]	75-84
Palmitic	-	-

[a] – Calculated [23]. [b] – Single-particle levitation using an electrodynamic balance at 25 °C [24]. [b*] – Saturated solution at 25 °C [24]. [c] – Predicted by UNIFAC [25]. [d] – By using tandem differential mobility analyser (TDMA) system [26] [e] – [27].

Before and after exposing the contaminated quartz crystal to humidity, pictures of residues on the quartz crystal were taken. The images of quartz crystal precontaminated with five WOAs before and after exposure to relative humidity from 20 % to 98 % are shown in Figure 9.3.

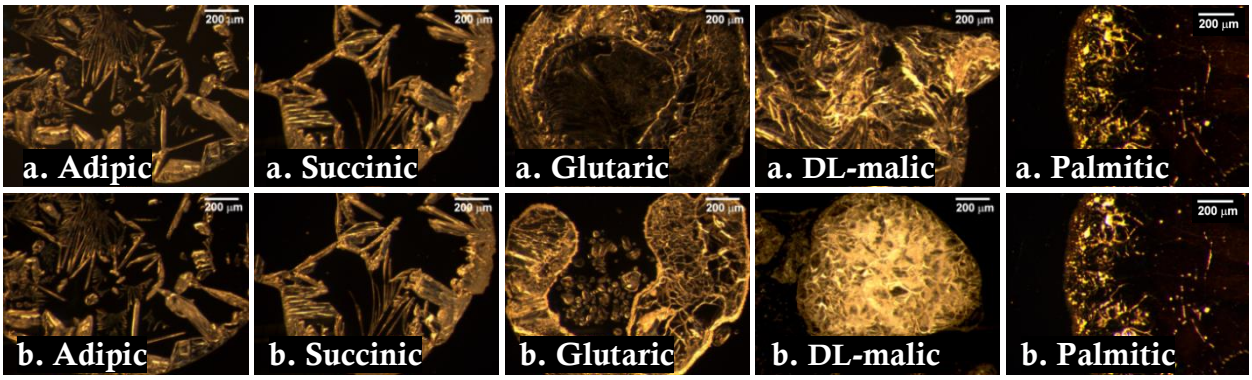

Figure 9.3: Appearance of WOA on a quartz crystal: a. before and b. after the exposure to 98 %RH at 25 °C

The unchanged appearance of adipic, succinic, and palmitic acids after exposure to 98 %RH at 25 °C indicates that humidity level was below the deliquescence RH values for these acids. Conversely, the appearance of recrystallized residue of glutaric and DL-malic acids shows that these acids were dissolved into the water during the experiment, indicting deliquescence RH values lower than 98 %RH at 25 °C.

LEAKAGE CURRENT MEASUREMENTS

The leakage current measured on the SIR pattern as a function of applied potential under RH levels from 60 % to ~99 % at 25 °C is shown in Figure 9.4. The left-side graphs in Figure 9.4 were obtained with WOA residue formed by evaporation from isopropyl alcohol solution at room temperature, while the graphs on the right side show the leakage current measured after contaminated SIR patterns were exposed from 220°C to 245°C for 45 s. The heating of the board was performed to simulate the possible effect of temperature experienced during the soldering process, since the principle of no-clean flux is based on decomposition and evaporation of the acid during soldering.

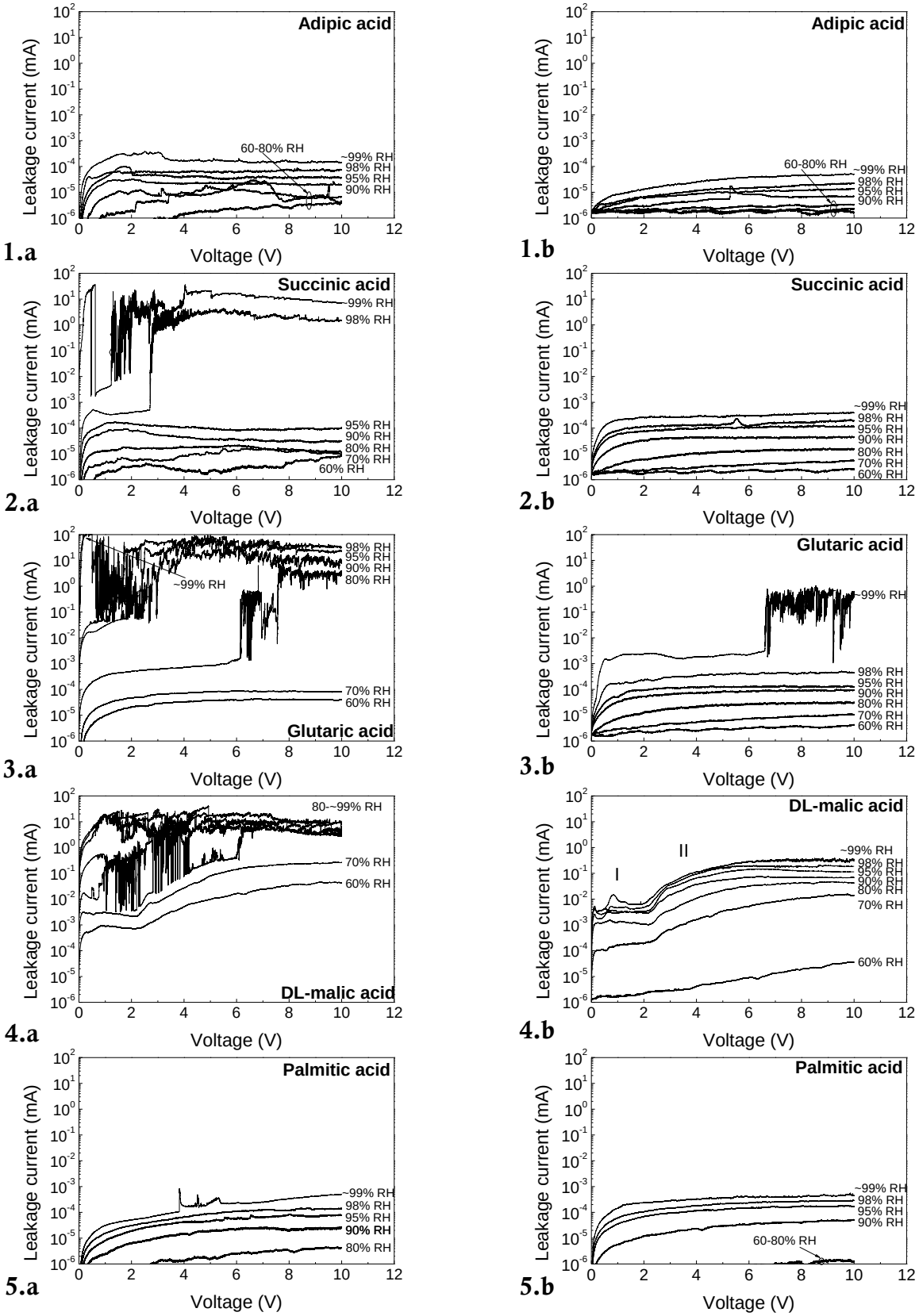

Figure 9.4: Leakage current measured on a SIR pattern precontaminated with: 1. adipic, 2. succinic, 3. glutaric, 4. DL-malic, and 5. palmitic acids at concentrations 100 µg·cm^{-2} at: a (left side) room temperature and b (right side) heated at 220°C to 245°C for 45 s

The magnitude of the leakage current represents the Faradaic current resulting from the corrosion rate of the SIR pattern, and it increases with increase of humidity. The current levels in the range of mA measured on the board under noncondensing conditions typically indicate short-circuiting due to the formation of tin dendrites and corrosion product bridging between oppositely biased electrodes of the SIR pattern. An overview of corroded SIR patterns is provided in Figure 9.5, with magnified views of corrosion features in Figure 9.6. For reference, the leakage current for an uncontaminated SIR pattern exposed to 98 %RH at 25 °C measured at 10 V DC is below 10 nA.

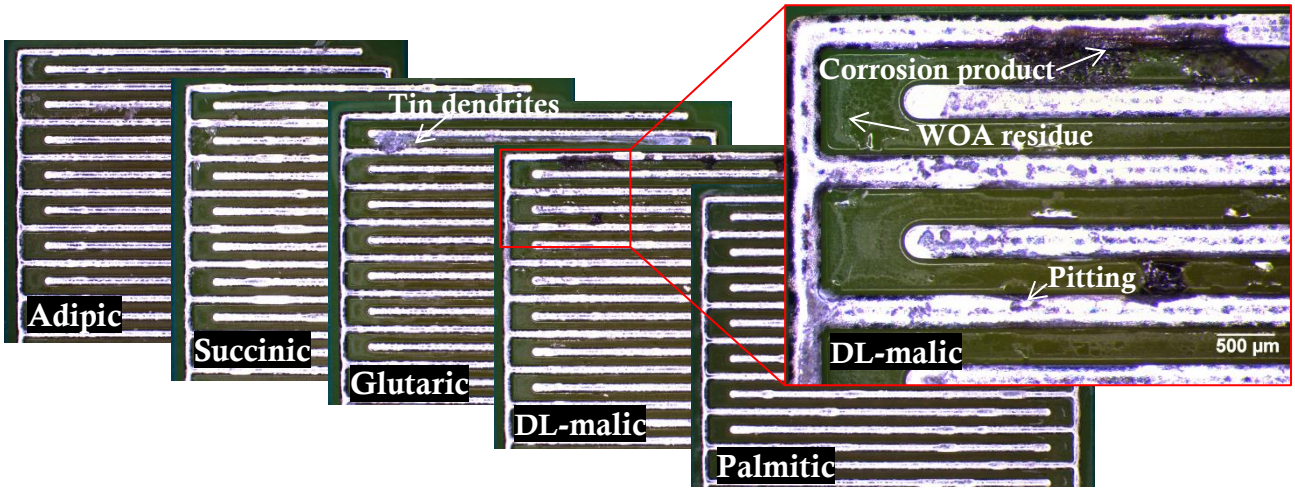

Figure 9.5: Overview of corroded SIR patterns showing important features (representative of leakage current measurements in Figure 9.4 a.

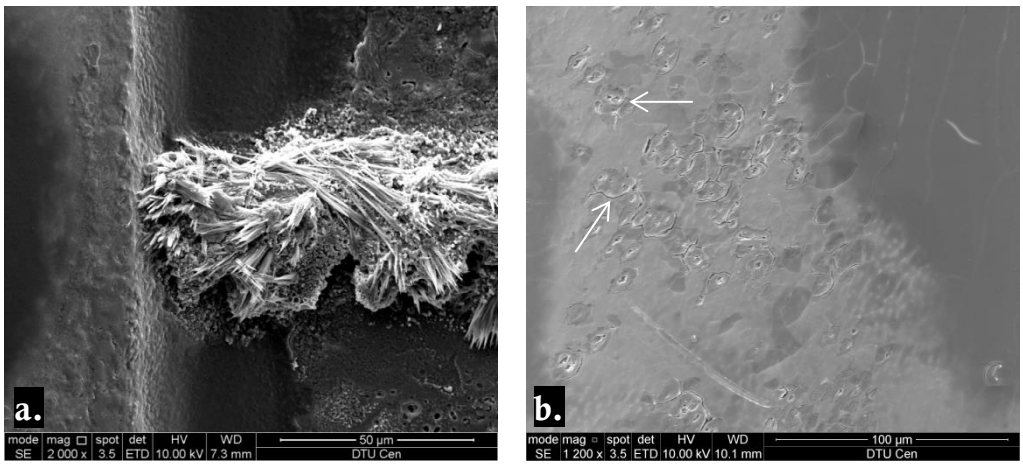

Figure 9.6: SEM images of corrosion features: a. bridging of anode and cathode electrodes of SIR pattern by dendrite formation due to electrochemical migration, and b. corrosion of anode electrode indicating pitting (related locations are indicated in Figure 9.5)

Optical observation after humidity testing indicated significant corrosion of SIR patterns precontaminated with DL-malic and glutaric acids, while a large amount of WOA residues was visible on all the patterns in Figure 9.5. Pitting of the tin was observed on some electrodes of the SIR pattern precontaminated with DL-malic acid (Figure 9.5 b.).Among all the acids, DL-malic acid was most aggressive, having the lowest critical RH value and highest dissolution in the water layer, and therefore resulting in the highest leakage currents. The leakage current for adipic and palmitic acids was below µA level even at the highest RH of ~99 % (Fig. 4). However, the leakage

current for SIR patterns precontaminated with succinic, glutaric, and DL-malic acids showed an increase of current up to the range of mA. It can be noted that the threshold RH for a rise of current for succinic, glutaric, and DL-malic acids is close to the deliquescence RH. The heating of the test PCB with the SIR pattern prior to the climatic testing reduced the amount of acid, which is reflected in the leakage current graph in Figure 9.4. In the case of DL-malic, dendrite bridging of the SIR pattern electrodes due to electrochemical migration was observed at 80 %RH, similar to glutaric acid. However, two steps (denoted as I and II) in the leakage current curve were observed for DL-malic (Figure 9.4).

IMPEDANCE MEASUREMENT

The electrochemical process initiates with the adsorption of a thin water layer from the humid atmosphere onto the surface of the PCBA and the formation of a conductive electrolyte which results from the dissociation of the WOAs. Figure 9.7 shows the effect of different WOAs on the impedance spectra measured on the printed circuit board as a function of RH at 25 °C.

The impedance data in Figure 9.7 were fit using two equivalent circuits. The bulk of the test board was characterized by $C_{FR\text{-}4}$ and $R_{FR\text{-}4}$ (Figure 9.8). The other parameters were assumed to characterize the contamination layer and associated conduction mechanism between the electrodes on the board. The resistance R_{Ω} characterizes the ohmic resistance of the contamination layer, Q_{DL} characterizes the double-layer capacitance at the contamination layer and electrode interface, and R_{CT} represents the charge-transfer resistance associated with Faradic reaction occurring at the interface. In the equivalent circuit (Figure 9.8 b), a constant-phase element Q, which represents the deviation from the capacitive behaviour, was used. The deviation depends upon n ($Q \approx \omega^n$); i) for n = 1, Q acts as a capacitance, ii) for n = 0.5, Q acts as a Warburg impedance, and iii) for n = 0, Q acts as a resistance. The element representing a Warburg impedance is denoted as Z_w in the equivalent circuit. More information about the physical meaning of the elements used to fit the impedance spectra can be found in the references [28], [29].

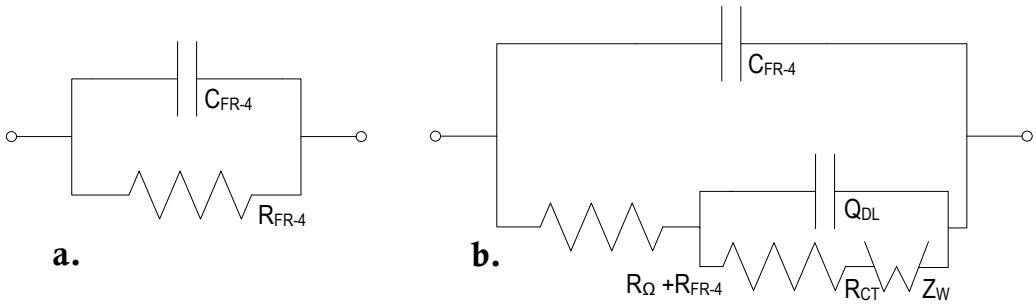

Figure 9.7: Equivalent circuits used for modelling of the impedance data: a. circuit characterizing the test board (RC), and b. circuit valid in presence of semi-infinite linear diffusion to the electrodes, especially at high RH (C(R(Q(RW)))) The element marked as $R_{\Omega}+R_{FR\text{-}4}$ is mainly representing the resistance of water layer forming on the surface, though a minor effect of resistance resulting from the bulk of PCB laminate is also included

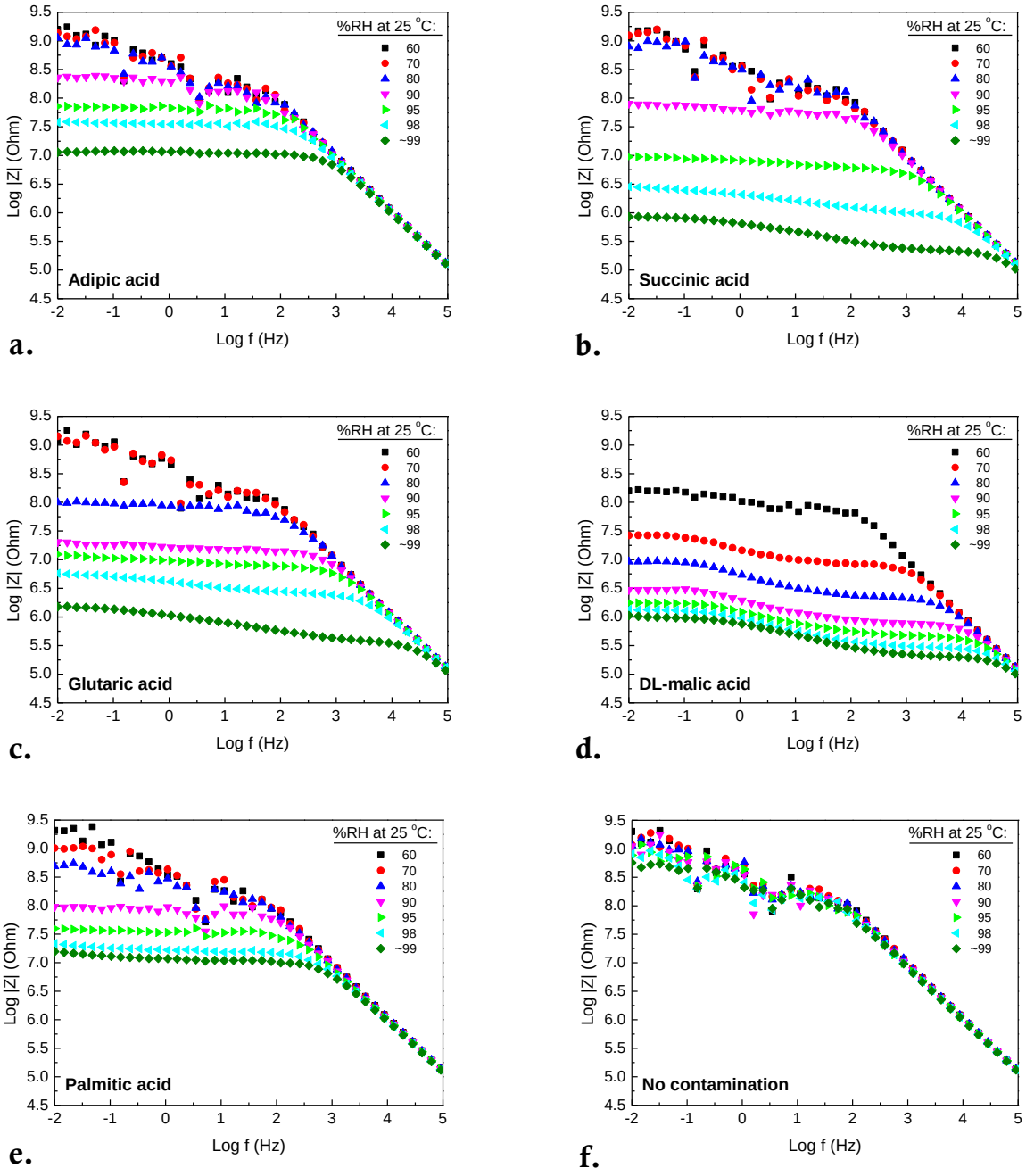

Figure 9.8: Bode plots obtained at different RH levels on the test board precontaminated with WOAs (100 µg·cm^{-2}): a. adipic, b. succinic, c. glutaric, d. DL-malic, e. palmitic and f. control sample with no contamination

The contamination layer resulting from the WOAs is a crystalline solid, and it can form a discontinuous layer between the electrodes, as shown in Figure 9.5. When water is adsorbed onto the surface, some of the acid dissolves and dissociates to form ionic conduction pathway, thereby reducing R_{Ω} and providing an alternative surface pathway for the bulk conduction through $R_{FR\text{-}4}$. In that case, the impedance is more effectively characterized by the model (C(R(Q(RW)))) rather than the model (RC) shown in Figure 9.8 a. The impedance measured on a clean test board at 60 %RH resulted in a capacitance of 1.37×10^{-11} F and resistance of 1.26×10^{9} Ohms, as calculated

from the (RC) equivalent circuit. The latter parameter values were used as a reference for fitting the impedance data using the equivalent circuits shown in Figure 9.8, although a slight increase of capacitance with increase of RH was expected [30]. The stray capacitance associated with the current experimental setup is 7.5×10^{-12} F, and it was included in the measurements.

For low RH, the dominant conduction pathway is through the glass-reinforced epoxy laminate and solder mask. As can be seen from the Bode plots in Figure 9.7, at the highest frequencies, only the capacitive behaviour of the test board is observable and it is independent of the nature of the contamination layer. The dependence of the impedance on the characteristics of the contamination is more pronounced at lower frequencies. At low humidity levels, the spectra follow the (RC) circuit, though with relatively high scatter of the data. The scatter is reduced for measurements above 80 %RH for glutaric acid and above 90 %RH for adipic, succinic, and palmitic acids. The increase of the RH from 60 % to 80 % for adipic and succinic acids is barely reflected in the impedance spectra. This shows that an increase of the RH in this range had only a minor effect on the SIR of the test board. Compared with glutaric acid, the same behaviour was observed at humidity levels from 60 % to 70 %, while DL-malic acid exhibited completely different behaviour compared with other acids. The decrease of impedance was clearly seen, starting from 60 % RH. This behaviour indicates a different humidity adsorption mechanism for DL-malic acid.

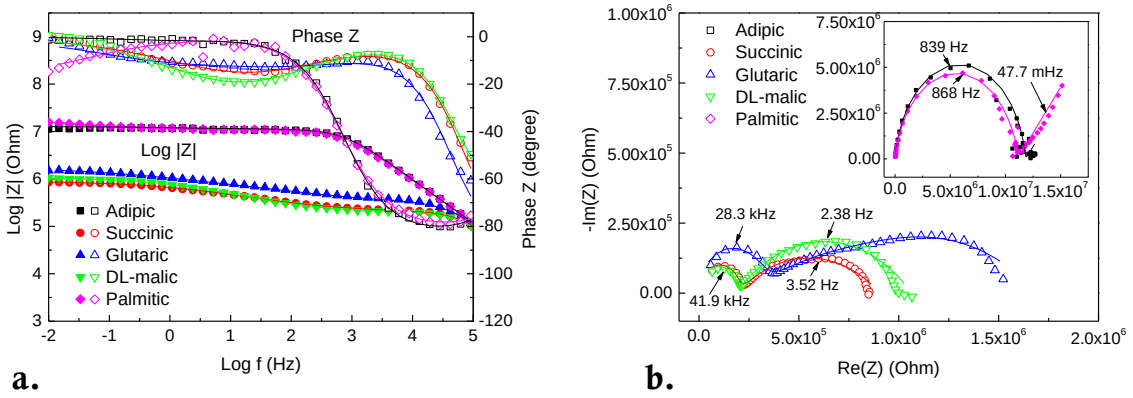

Figure 9.9: Impedance data for test PCB contaminated with 100 µg·cm^{-2} of WOAs at ~99 % RH/25 °C: a. Bode plots and b. Nyquist plots

A comparison between the impedance spectra obtained for WOAs at ~99%RH/25°C is shown in Figure 9.9. The data obtained from the fitting of the impedance spectra using the model shown in Figure 9.8 b. are presented in Table 9.3. Detailed information on the analysis of impedance data lies beyond the scope of this paper and can be found elsewhere [28], [29].

The capacitance $C_{FR\text{-}4}$ provided in Table 9.3 is a combined measure of the dielectric properties of the laminate and the contamination layer between the electrodes, measured under high RH. The resistance denoted as $R_{FR\text{-}4+\Omega}$ mainly represents the resistance of the water layer forming on the surface, though a negligible resistance through the bulk of the laminate is also included. A more adequate representation of the resistance under a DC voltage is the combined resistance of $R_{\Omega} + R_{FR\text{-}4}$ and R_{CT} as presented in the last column of Table 9.3. In this case, adipic and palmitic acids are characterized by higher resistances compared to succinic, glutaric and DL-malic acids. The Warburg admittance, which is the reciprocal of the impedance, represents the diffusion of ions from and to the electrodes. An increase of Warburg admittance for succinic, glutaric, and

DL-malic acids can be attributed to the increased water layer thickness on the PCB, as it enhances ion transport from and to the electrodes. The exponent of the constant-phase element denoted as Q_{DL} in Table 9.3 for succinic, glutaric, and DL-malic acids also suggests an electrical property similar to that of a Warburg element, while in the case of adipic and palmitic acids, constant-phase elements have properties more closely related to a capacitor. In the Nyquist plots for succinic, glutaric, and DL-malic acids in Figure 9.9 b two time constants indicating electrode reactions can be clearly seen, whereas in the cases of adipic and palmitic acids, the plots are similar to the (RC) circuit, while a 45° angle between the real and imaginary parts of the impedance at low frequencies indicates diffusion-controlled charge transfer at the electrode, being more evident for palmitic acid.

Table 9.3: Data from impedance spectra fitting

Acid	C_{FR-4} (F)	$R_{\Omega}+R_{FR-4}$* (Ohm)	Q_{DL} ($S \cdot sec^n$)	n (0<n<1)	R_{CT} (Ohm)	Warburg ($S \cdot sec^{0.5}$)	$R_{FR4+\Omega}$ + R_{CT} (Ohm)
Adipic	8.39E-12	8.81E4	3.99E-11	0.86	1.17E7	3.44E-6	1.18E+07
Succinic	1.30E-11	1.95E5	3.84E-7	0.43	7.11E5	2.64E4	9.06E+05
Glutaric	1.29E-11	2.71E5	3.75E-7	0.32	1.56E6	1.92E5	1.83E+06
DL-malic	1.32E-11	1.90E5	2.71E-7	0.51	8.73E5	3.41E5	1.06E+06
Palmitic	7.18E-12	5.91E4	5.54E-11	0.84	1.10E7	5.98E-7	1.11E+07

* Combined resistance of water layer forming on the surface (R_{Ω}) and resistance resulting from the laminate bulk between the electrodes (R_{FR-4}). The resistance of the laminate is much higher than the resistance of the water layer. Both components act as connected in parallel, thus the resistance of the bulk is negligible.

IV. DISCUSSION

HYGROSCOPICITY OF ACIDS AND WATER LAYER FORMATION

Comparing the solubility in water (Table 9.1) and the deliquescence point (Table 9.2), it can be noted that, the higher the solubility of the WOA in water, the lower its deliquescence point. From the solubility point of view, this implies that, on a PCBA surface, a WOA with lower solubility would require a thicker water layer to dissolve the same weight of acid. For example, if adipic, succinic, glutaric, and DL-malic acids are present at the levels typically found as residues after a no-clean wave soldering process (~10 $\mu g \cdot cm^{-2}$) [31], a water thickness of 6.7 µm, 1.2 µm, 0.071 µm, and 0.069 µm, respectively, would be required to dissolve the acids. As a result, the residue with the least soluble acid could easily saturate the water layer compared to the highly soluble acid and contribute less to the leakage currents.

Among the acids investigated, adipic, succinic, and glutaric acids differ only by the number methylene groups. Therefore, it can be expected similar behaviour of those WOAs under humid conditions. However, the deliquescence points for the acids are different, lying in the following order: adipic > succinic > glutaric. For glutaric acid, literature suggests mass transfer limitation, which delays complete deliquescence of the acid at the critical RH level, while this is not the case for adipic or succinic acid [24]. Different behaviour might be due to the length of the chain. With increased chain length, the carboxylic group can easily twist, reducing the steric interaction when in contact with water molecules. On the other hand, DL-malic acid is highly soluble in water and has the lowest RH for deliquescence. Results in the literature [24] show that, due to the chemical structure of malic acid, i.e., the presence of hydroxyl and carboxylic functional groups, neither crystallization nor deliquescence is observed, thus DL-malic acid adsorbs and desorbs water

continuously. Palmitic acid has a long hydrocarbon chain, which gives the molecule a nonpolar character, making it insoluble in water. Due to low adsorption of water, palmitic acid has different corrosive nature under humid conditions.

Overall, the following order of deliquescence point was observed for various WOAs: palmitic > adipic > succinic > glutaric > DL-malic acid. A number of findings in the literature [24]–[27], [32] comply with the results obtained by QCM in this work (Table 9.2). SIR testing of adipic, succinic, glutaric, and malic acids [3], showed a similar ranking of the acids to that observed from the leakage current and AC impedance measurements in this work.

ELECTRICAL EFFECTS UNDER HUMID CONDITIONS

The summary of leakage currents presented in Figure 9.10 is based on the leakage current values for various acids at 10 V in Figure 9.4. The upper boundary lines in the graph indicate the current due to WOAs applied on the SIR pattern at concentration of 100 μg·cm^{-2} at room temperature, while the lower lines represent the current corresponding to the residue after 45 s of exposure to temperatures from 220 °C to temperatures from 245 °C. As can be noticed, glutaric and DL-malic acids caused the highest leakage currents, and also the greatest reduction in the currents was observed for these acids after heat exposure for 45 s. The observation is attributed to the high solubility of these acids, thus a high amount of acid can be dissolved in a thin layer of water, or at lower RH. This results in very high currents when present at 100 μg·cm^{-2}; however, when exposed to heat, a high amount of acid volatilizes, thus resulting in a significant reduction of the current. In contrast, the heating appears to have less effect on low-solubility acids (adipic, succinic, and palmitic acids), but this is due to the lower currents they generated when present at 100 μg·cm^{-2}. Overall, the reduction of leakage current observed for all the acids is related to the volatilization and decomposition of the WOA. Similar findings are reported in literature [3], [19].

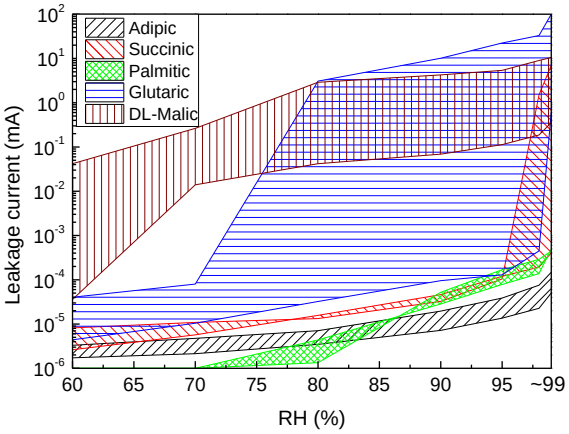

Figure 9.10: Summary graph showing comparison of leakage current for various acids as a function of humidity at 10 V bias. Upper and lower boundaries of each curve represent the leakage current corresponding to the contamination on the SIR after room-temperature evaporation and the board with contamination after 45 s of exposure to temperatures in the range from 220 °C to 245 °C

Among the acids investigated, adipic and palmitic acids were characterized by the lowest leakage currents in the measured humidity range, in agreement with the low deliquescence nature of these acids (Figure 9.4; Table 9.2). On the other hand, succinic and glutaric acids showed lower leakage

currents initially, but the current increased abruptly above the deliquescent point due to electrochemical migration.

DL-malic acid with two carboxylic and one hydroxyl group was found to generate the highest levels of leakage current (Figure 9.4 and Figure 9.10). The two steps are observed in the leakage current curves for DL-malic acid in Figure 9.4. This could be an indication of the contributions of hydroxyl and carboxylic functional groups to the conduction mechanism; however, this requires further investigation. The impedance spectra for DL-malic acid showed a great reduction in impedance at low frequencies with every step increase in RH, thus indicating an ability to conduct high leakage currents over a wide range of humidity.

In the case of palmitic acid, the minor though steady increase of leakage current (Figure 9.4) and a similar reduction of impedance at the lowest frequencies (Figure 9.9) when measured as a function of RH indicate a steady increase of surface conductivity. Also, the presence of diffusion-controlled charge transfer at the electrode/contamination layer interface was observed from the impedance measurements. The described phenomenon indicates a slow build-up of the water layer on top of the layer of palmitic acid. The diffusion-controlled charge transfer is assumed to be observed due to the long hydrocarbon chain and low water adsorption onto the surface.

Overall, the reduction of the ohmic resistance from the impedance measurements is in correlation with the increased leakage currents measured on the standard SIR pattern under varying humidity levels. The magnitude of the effects was related to the water adsorption and deliquescence of the WOAs. From the electrical testing, DL-malic acid appeared to be most aggressive, followed by glutaric acid. The test boards precontaminated with DL-malic and glutaric acids showed corrosion issues at humidity levels as low as 80 %RH at 25°C. In contrast, adipic and palmitic acids showed relatively low increases in leakage current across the entire tested range of humidity at 25 °C. For comparison, following order of increasing corrosion due to WOAs at equivalent molar concentrations was reported [8]: succinic < adipic < glutaric < DL-malic acids. In the same study [8], abietic acid, which is very low soluble in water like palmitic acid, showed the least corrosion under 40°C/93%RH, 60°C/93%RH, and 85°C/85%RH conditions, so the importance of the solubility and hygroscopicity of the residue for the corrosion on the PCBA can be addressed.

Presently, there are a variety of no-clean solder flux systems in the market. The composition of the solder flux varies from one system to another, although the classification of the flux according to IPC J-STD-004 does not specify the WOAs in the flux. However, the hygroscopic property of WOAs in the flux must be a factor for consideration when the reliability of electronic devices under humid conditions is of importance.

V. CONCLUSIONS

1. Electrochemical testing of adipic, succinic, glutaric, DL-malic, and palmitic acids used as part of no-clean flux systems showed a clear correlation between the hygroscopic property and leakage current magnitude. An abrupt increase of the leakage current, followed by electrochemical migration, was observed at RH close to the deliquescence point of the acids.
2. Climatic testing of the WOAs at equivalent wt.% concentrations provided the following ranking of the acids: palmitic, adipic, succinic, glutaric, and DL-malic. Palmitic acid is very low soluble in water and showed the least increase of leakage current, while for DL-malic acid

a continuous increase of current and a reduction of the water layer resistance was observed over the range of RH tested.

3. Palmitic acid showed diffusion-controlled charge transfer at the contamination layer/electrode interface. The presence of palmitic acid on the printed circuit board appeared to be least critical, since it does not dissolve in the water layer forming on the surface and the conduction mechanism in a thin water layer is slower than for the other acids tested in this work.
4. Heating of the test boards reduced the leakage currents on the SIR patterns precontaminated with all five WOAs. The heating effect was more pronounced for glutaric and DL-malic acids, which is attributed to the high solubility of the acids, as they can saturate at high concentration in a thin water layer compared to low-solubility acids (adipic, succinic, and palmitic acids).
5. Overall, the results show that the climatic behaviour of the WOAs used in no-clean fluxes can be very different, and a similar variation in the performance of the flux containing these WOAs can be expected. Therefore, it is important to take into account the composition of the flux when electronics are likely to experience operation under humid conditions.

VI. ACKNOWLEDGMENTS

The research reported here was conducted as part of the CELCORR/CreCon consortium (www.celcorr.com), and the authors would like to acknowledge the funding and help received from the consortium partners.

VII. REFERENCES

[1] *Montreal Protocol on Substances that Deplete the Ozone Layer*. United Nations Environment Programme, 1987.

[2] W. M. Haynes and D. R. Lide, *CRC Handbook of chemistry and physics*, 94th Editi. CRC Press, 2013, p. 2668.

[3] J. E. Sohn and U. Ray, "Weak Organic Acids and Surface Insulation Resistance," *Circuit World*, vol. 21, no. 4, pp. 22–26, 1994.

[4] M. S. Jellesen, D. Minzari, U. Rathinavelu, P. Møller, and R. Ambat, "Corrosion failure due to flux residues in an electronic add-on device," *Eng. Fail. Anal.*, vol. 17, no. 6, pp. 1263–1272, Sep. 2010.

[5] D. Geiger and D. Shangguan, "Investigation of the effect of solder flux residues on RF signal integrity using real circuits," *Solder. Surf. Mt. Technol.*, vol. 17, no. 4, pp. 27–32, 2005.

[6] L. J. Turbini, G. B. Freeman, M. H. Smith, J. D. Finney, R. D. Boswell, and J. F. Lane, "Characterising the Corrosion Properties of Flux Residues: Part 1: Test Method Development and Failure Mode Identification," *Solder. Surf. Mt. Technol.*, vol. 3, no. 2, pp. 24–31, 1991.

[7] C. Puechagut, A. Laügt, E. Guéné, and R. Anisko, "Solder Paste Residue Corrosivity Assessment : Bono Test," in *IPC APEX EXPO Technical Conference 2010*, 2010, vol. 2, pp. 1336–1364.

[8] Y. Zhou, L. J. Turbini, D. Ramjattan, B. Christian, and M. Pritzker, "Characterizing Corrosion Effects of Weak Organic Acids Using a Modified Bono Test," *J. Electron. Mater.*, vol. 42, no. 12, pp. 3609–3619, Aug. 2013.

[9] J. R. White, "Conduction mechanisms in contaminant layers on printed circuit boards," *IBM J. Res. Dev.*, vol. 37, no. 2, pp. 243–248, 1993.

[10] J. C. Galvan, J. M. Bastidas, and S. Feliu, "A Study of Corrosive Effect of Soldering Fluxes on Printed Circuit Boards," *Weld. J.*, vol. 75, no. 11, pp. 366–371, 1996.

[11] J. Guy and M. Fredrickson, "Analyzing Residues Using AC Impedance Techniques," in *NEPCON WEST*, 1997, vol. 3, pp. 1270–1279.

[12] N. M. Amin and A. M. Seitz, "Evaluation of Solder Flux/Substrate Interfaces Using Impedance Spectroscopy," in *NEPCON WEST*, 1999, vol. 2, no. 845–853, pp. 845–853.

[13] L. C. Zou and C. Hunt, "Characterization of the Conduction Mechanisms in Adsorbed Electrolyte Layers on Electronic Boards Using AC Impedance," *J. Electrochem. Soc.*, vol. 156, no. 1, pp. C8–C15, 2009.

[14] C. Hunt and L. Zou, "The impact of temperature and humidity conditions on surface insulation resistance values for various fluxes," *Solder. Surf. Mt. Technol.*, vol. 11, no. 1, pp. 36–43, 1999.

[15] S. Zhan, M. H. Azarian, and M. Pecht, "Reliability of Printed Circuit Boards Processed Using No-Clean Flux Technology in Temperature – Humidity – Bias Conditions," *IEEE Trans. Device Mater. Reliab.*, vol. 8, no. 2, pp. 426–434, 2008.

[16] K. G. Schmitt-Thomas and C. Schmidt, "The Influence of Flux Residues on the Quality of Electronic Assemblies," *Solder. Surf. Mt. Technol.*, vol. 3, no. 18, pp. 4–7, 1994.

[17] Peter Biocca, "Flux chemistries and thermal profiling considerations in SMT assembly," in *National Electronic Packaging and Production Conference-Proceedings of the Technical Program (West and East)*, 1999, vol. 2, pp. 971–977.

[18] K. S. Hansen, M. S. Jellesen, P. Moller, P. J. S. Westermann, and R. Ambat, "Effect of Solder Flux Residues on Corrosion of Electronics," in *Annual reliability and maintainability symposium*, 2009, pp. 503–509.

[19] B. A. Smith and L. J. Turbini, "Characterizing the weak organic acids used in low solids fluxes," *J. Electron. Mater.*, vol. 28, no. 11, pp. 1299–1306, Nov. 1999.

[20] V. Verdingovas, M. S. Jellesen, and R. Ambat, "Impact of NaCl Contamination and Climatic Conditions on the Reliability of Printed Circuit Board Assemblies," *IEEE Trans. Device Mater. Reliab.*, vol. 14, no. 1, pp. 42–51, 2014.

[21] IPC-9201, "Surface Insulation Resistance Handbook," Northbrook, 1996.

[22] G. Sauerbrey, "The Use of Quartz Oscillators for Weighing Thin Layers and for Microweighing," *Z. Phys.*, vol. 155, pp. 206–222, 1959.

[23] K. M. Adams, J. E. Anderson, and Y. B. Graves, "Ionograph Sensitivity to Chemical Residues from 'No Clean' Soldering Fluxes: Comparison of Solvent Extract Conductivity and Surface Conductivity," *Circuit World*, vol. 20, no. 2, pp. 41–44, 1994.

[24] C. Peng, M. N. Chan, and C. K. Chan, "The hygroscopic properties of dicarboxylic and multifunctional acids: measurements and UNIFAC predictions.," *Environ. Sci. Technol.*, vol. 35, no. 22, pp. 4495–501, Nov. 2001.

[25] P. Saxena and L. M. Hildemann, "Water absorption by organics: survey of laboratory evidence and evaluation of UNIFAC for estimating water activity," *Environ. Sci. Technol.*, vol. 31, no. 11, pp. 3318–3324, Nov. 1997.

[26] C. Cruz and S. Pandis, "Deliquescence and hygroscopic growth of mixed inorganic-organic atmospheric aerosol," *Environ. Sci. Technol.*, vol. 34, no. 20, pp. 4313–4319, 2000.

[27] A. Apelblat, M. Dov, J. Wisniak, and J. Zabicky, "The vapour pressure of water over saturated aqueous solutions of malic, tartaric, and citric acids, at temperatures from 288 K to 323 K," *J. Chem. Thermodyn.*, vol. 27, no. 1, pp. 35–41, Jan. 1995.

[28] M. E. Orazem and B. Tribollet, *Electrochemical impedance spectroscopy*. John Wiley & Sons Inc., 2008, p. 524.

[29] E. Barsukov and J. Ross Macdonald, *Impedance spectroscopy theory, experiment, and applications*. Wiley-Interscience, 2005, p. 595.

[30] O. Thomas, M. Wickham, and C. Hunt, "Obtaining the moisture content of printed circuit boards from capacitance measurements," *Circuit World*, vol. 38, no. 2, pp. 68–74, May 2012.

[31] H. Conseil, M. Stendahl Jellesen, and R. Ambat, "Contamination profile on typical printed circuit board assemblies vs soldering process," *Solder. Surf. Mt. Technol.*, vol. 26, no. 4, pp. 194–202, Aug. 2014.

[32] K. M. Adams, J. E. Anderson, and Y. B. Graves, "Ionograph Sensitivity to Chemical Residues from 'No Clean' Soldering Fluxes: Comparison of Solvent Extract Conductivity and Surface Conductivity," *Circuit World*, vol. 20, no. 2, pp. 41–44, 1994.

10. RELATIVE EFFECT OF SOLDER FLUX CHEMISTRY ON THE HUMIDITY RELATED FAILURES IN ELECTRONICS

Vadimas Verdingovas, Morten Stendahl Jellesen, and Rajan Ambat

Abstract—*Purpose* – This paper aims to investigate the effect of no-clean flux chemistry with various weak organic acids (WOAs) as activators on the corrosion reliability of electronics with emphasis on the hygroscopic nature of the residue. *Design/methodology/approach* – The hygroscopicity of flux residue was studied by quartz crystal microbalance, while corrosive effects were studied by leakage current and impedance measurements on standard test boards. The measurements were performed as a function of relative humidity (RH) in the range from 60 to ~99 %RH at 25 °C. The corrosiveness of solder flux systems was visualized by the *ex situ* analysis using a gel with tin ion indicator. *Findings* – The results showed that the solder flux residues are characterized by different threshold RH, above which a sudden increase in direct current leakage by 2–4 orders of magnitude and a significant reduction in surface resistance in the impedance measurements were observed. *Practical implications* – The findings are attributed to the deliquescence RH of the WOA(s) in the flux and chemistry of water-layer formed on the surface. The results show the importance of WOA type in relation to its solubility and deliquescence RH on the corrosion reliability of printed circuit boards under humid conditions. *Originality/value* – The classification of solder flux systems according to IPC J-STD-004 standard does not specify the WOAs in the flux; however, ranking of the flux systems based on the hygroscopic property of activators would be useful information when selecting no-clean flux systems for electronics with applications in humid conditions.

Keywords—Flux, Impedance, Corrosion, Reliability, Metal dissolution, Quality control, Flux chemistry, Leakage current, Reliability of electronics, Deliquescence

I. INTRODUCTION

No-clean solder flux is commonly used in the manufacturing of printed circuit board assemblies (PCBAs). Chemistry of solder flux is designed to activate the surface by removing metal oxides natively present on the surfaces to be soldered, therefore contain an activator. The no-clean fluxes usually contain less corrosive activators compared to washable flux systems. The weak organic acids (WOAs), which decompose and volatize at the higher temperatures during soldering process are commonly used as activators in no-clean fluxes. No-clean flux is not a zero-residue flux, and a certain amount of activator will be present on the electronic assembly after the soldering process. This is commonly called as flux residue, and it influence the corrosion reliability of electronics under humid conditions.

The studies of various aspects related to no-clean flux can be found in literature e.g. effect on surface insulation resistance (SIR) [1]–[3], propensity for electrochemical migration [4]–[6], or performance on conformal coatings [7]–[11]. The flux residue has been reported as a root cause of different issues on the PCBAs [10], [12]–[14]. The main issues linked to solder flux residue are

V. Verdingovas, M. S. Jellesen, and R. Ambat, "Relative effect of solder flux chemistry on the humidity related failures in electronics," *Solder. Surf. Mt. Technol*, vol. 27, no. 4, pp 146-156, 2015.

related to leakage currents or short circuiting due to electrochemical migration, however it can cause other problems i.e. increase in contact resistance and corrosion [15] or affect the radio frequency performance [16]–[18].

The corrosiveness of flux residue is mostly dependent upon the type of activator. As mostly WOAs are used as activators in no-clean fluxes, the physical and chemical properties of flux vary with the type of WOA. The importance of some chemical and physical properties of WOAs on SIR was highlighted [19]. The corrosive nature of the WOA and acid number of the flux determines the chemical activity of the flux system, while the hygroscopicity and solubility in water determines the climate conditions (humidity and temperature) when particular WOA will be dissolved into the water layer on the surface of electronic assembly. The latter process is primarily accountable for high leakage currents, and the prolongation of leak current could lead to electrochemical migration.

The effect of particular type of flux residue (WOA) on the performance of electronics depends also on the user environment. The WOA tested under varying humidity and temperature conditions show significant difference in the corrosiveness [20], and surface insulation resistance (SIR) measured with DC voltage [19], [21], [22] and AC voltage [22]. Typically, SIR tests [23], [24] are conducted under constant RH conditions, and do not provide a full picture of the hygroscopic property of contaminant. Whereas DC leakage [25] and AC impedance [26] measurements under elevated RH conditions allows determination of deliquescence and crystallization RH levels of contaminant. The determination of deliquescence RH from the increase of surface conductivity suggests the importance of deliquescence RH on the SIR and corrosion related issues in electronics.

The effect of WOAs on the surface insulation resistance obtained as a function of RH showed a clear variation in the SIR values, and the threshold RH for significant reduction in SIR values was shown to be in close correlation with the deliquescence RH of WOA [22]. However, this paper addresses the results from humidity exposure testing of a number of commercially available no-clean solder fluxes, containing various types of WOAs. The aim is to compare the SIR measured as a function of RH by DC and AC techniques with the water adsorption and absorption by the residue, the deliquescence RH of the acids in the flux, and overall effects on the corrosion of SIR pattern under bias conditions.

II. MATERIALS AND METHODS

TEST BOARDS

The leakage current measurements were performed on the SIR comb pattern with Sn/Ag/Cu hot air solder leveling (HASL) surface finish on FR-4 laminate (IPC-4101/21). Overall surface area of the SIR pattern was 13 × 25 mm. The width of conduction lines, and the distance between them was 0.3 mm. The geometry related nominal square count of SIR pattern was 1476 [27].

The test board for impedance measurements was a FR-4 laminate with two parallel conducting lines having width of 0.66 mm, length of 5.8 mm, and the distance between the lines 1.3 mm (approximate nominal square count is 4.5). The thickness of the board was 1.6 mm. The surface finish of the conducting lines was 6.5 ± 1 μm gold with an intermediate layer of nickel 9 ± 1 μm.

PREPARATION OF BOARDS PRIOR TO TESTING

Prior to application of the flux, the test boards were cleaned with a mixture of isopropyl alcohol and deionized water with resistivity of 18.2 MΩ·cm at 25 °C. The test boards were precontaminated with solder flux applied by using a micropipette. The volume of dispensed solution was fixed for all the fluxes, which is equal to 13 µl. Use of 13 µl of flux solution with approximate solid content of 2.5 (% w/w) provides ~100 µg·cm^{-2} of flux residue on the SIR pattern with 325 mm^2 area. One set of the boards consequently after application of the flux was exposed to 220-245°C for 45 seconds to simulate the effect of higher temperature likely to be experienced during the soldering process [28].

NO-CLEAN SOLDER FLUX

Table 10.1 contains summary of no-clean wave soldering fluxes used for the investigation. The fluxes were selected for varying type of weak organic acid, acid number, and solid content. The ranking of the flux according to IPC J-STD-004 standard can be also seen in the table. All the flux systems are alcohol based except F7, while the flux F1 contained minor levels of halides. The composition of the fluxes is not always provided by the manufacturer; and in the present work it characterized using FT-IR spectroscopy. This is a common technique used for characterizing flux residues on microelectronics assembly [9], [29], [30]. The constituent WOAs are shown in the Table 10.1, while the FT-IR spectra are presented in the results section.

Table 10.1: Summary of no-clean wave soldering fluxes

Flux	Solvent	IPC J-STD-004 Designation*	Acid number, mg KOH/g	Solid content, % wt/wt	Constituent WOA (FT-IR)
F1	VOC	ROL1	21.6	5.0	Succinic
F2	VOC	ORL0	17.5	2.2	Succinic
F3	VOC	ORL0	26	4.0	Succinic and adipic
F4	VOC	REL0	15.8	2.2	Adipic
F5	VOC	ORL0	14.7	2.0	Adipic
F6	VOC	ROL0	20.3	7.1	Palmitic
F7	Water	ORM0	36.85	4.0	Glutaric

*First two letters specify the film-former type: RO-rosin, RE-resin, OR-organic; third letter specifies the level of activator in the flux: L-low, M-medium; and the last number specifies halides content: 0-(<0.05 % wt/wt), 1-(>0.5%-2% wt/wt).

The acid number quantifies the amount of acid in the flux, and it is defined as the mass of KOH in milligrams that is required to neutralize 1 g of acid. The solid content of flux contains the weight of activator (typically WOAs) and film-former after evaporation of the solvent. The film-former can be either rosin (RO), resin (RE) or the organic (OR).

FOURIER TRANSFORM INFRARED SPECTROSCOPY

A "Nicolet iN10 MX" infrared imaging microscope was used for identification of activators (WOAs) in the flux. The FT-IR measurements were carried out on the residues after solvent evaporation at room temperature. The detailed description of the FT-IR analysis is beyond the scope of this paper, however more details can be found elsewhere[31], [32]. The WOAs in the flux were identified from the comparison of the absorption peaks for analytical grade WOAs with

the peaks in the measured spectra. The measurements were performed in the attenuated total reflectance (ATR) mode.

QUARTZ CRYSTAL MICROBALANCE MEASUREMENTS

"QCM200" quartz crystal microbalance (QCM) from with 5 MHz AT-cut gold contact quartz crystal was used for *in situ* measurement of water adsorption by the solder flux residue. A 1.4 μL droplet of the solder flux solution was applied on the contact surface of the crystal which was subsequently exposed to controlled humidity at 25 °C in the "Espec PL-3KPH" climatic chamber (±0.3 °C / ±2.5 %RH). The relative humidity during experiment was ramped from 60 % RH to ~99 %RH, at the rate of 1% RH per 5 min. The deliquescence RH for the flux residue was determined from the change of resonant frequency.

ELECTRICAL/ELECTROCHEMICAL MEASUREMENTS

Leakage current and impedance measurements were performed with "BioLogic VSP" multichannel workstation. The leakage current was measured as a function of applied potential, which was scanned from 0 V to 10 V at 2 $mV \cdot s^{-1}$ sweep rate. The humidity was elevated from 60 %RH to ~99 %RH, while the temperature was kept constant at 25 °C. After each step of humidity increase, the samples were left to equilibrate with environment for 2 hours, and thereafter the potential sweep measurements were performed.

Impedance measurements were performed in two-electrode configuration. The impedance was measured at the open-circuit potential with signal amplitude of 50 mV in the frequency range from 10 mHz to 100 kHz. The average of 5 measures per frequency was recorded. All the measurements were performed in "Espec PL-3KPH" climatic chamber at 60, 70, 80, 90, 95, 98, and ~99 %RH at 25 °C.

EX SITU TEST USING GEL WITH TIN ION INDICATOR

A gel containing tin ion indicator was used for visualization of tin corrosion on the SIR patterns after humidity exposure under bias conditions. The preparation of the gel is similar to the method described in patent [33], using high viscosity liquid for immobilization of the ions on the PCBA. The indicator used in this work is optimized for detection of post-corrosion products rather than claimed in the patent production residues or service life contaminants [33]. The indicator is sensitive to the tin ions and tin hydroxides corrosion products on the SIR electrode pattern. Gel in contact with tin compounds produce colour change from light yellow to blue. The intensity of the blue colour represents the extent of corrosion due to dissolution of tin.

III. RESULTS

ACTIVATORS IN THE FLUX SYSTEMS

The comparison of FT-IR spectra for the WOAs and the tested flux systems is provided in Figure 10.1. The characteristic absorption peaks at around 1680 cm^{-1} in the IR transmittance graphs (Figure 10.1) are attributed to the carbonyl C=O asymmetric stretching vibrations related to carboxylic group, which are present in the case of all the WOAs and investigated fluxes. The C-H stretching vibrations for CH_2 groups appear in the range of vibration frequencies from 2950 to 2880 cm^{-1}. As it can be seen from the IR spectra, the absorption of IR radiation in this region is significantly higher for the palmitic acid. This is due to a long chain of methylene CH_2 groups absorbing the IR radiation. The presence of methyl group CH_3 for this acid is also indicated in the same region.

The comparison of the absorption peaks in the so called fingerprint region (from about 1500 to 500 cm^{-1}) was used for identification of the acids in the flux. The difference between the chemical structures of adipic and succinic acid is two methylene (CH_2) groups. The appearance of shifted peaks attributed to the bending modes of C-H bond group is used to distinguish between the two carboxylic acids. Succinic acid is identified by the appearance of absorption peak at 1320 cm^{-1}, whereas for the adipic acid this peak is shifted to the region of 1280 cm^{-1}. The merging of those two characteristic peaks seen in the spectrum for the flux F3 indicates the presence of both adipic and succinic acids.

In the fingerprint region it is possible to assign C-O stretching vibrations (around 1200 cm^{-1}) and O-H bending modes (around 1550 cm^{-1} and 950-910 cm^{-1}), both attributed to the carboxylic group. The spectra of fluxes F6 and F7 match closely with the spectra for palmitic and glutaric acid provided in the graph.

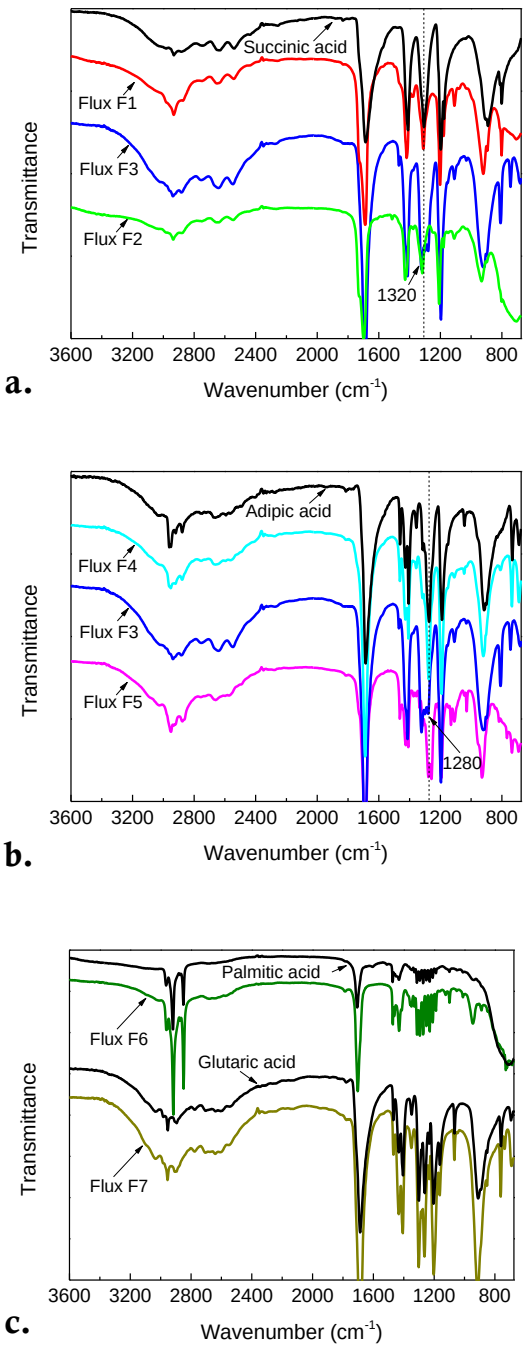

Figure 10.1: FT-IR spectra for the solder fluxes and pure WOA: a. succinic (F1, F2, F3), b. adipic (F3, F4, F5), c. palmitic (F6) and glutaric (F7)

WATER ADSORPTION BY THE FLUX RESIDUE

The isotherms of water adsorption and absorption by flux residue are presented in Figure 10.2. The results are presented as change of mass calculated using the Sauerbrey equation [34]. It represents the interaction of water from the air by the residue on the quartz crystal. The residue on the crystal contains WOA(s) and film-former as indicated in Table 10.1. Activators in the flux are water soluble, thus interact with water molecules in the air, whereas film-former is low soluble, and is more likely to act as a protective barrier for the water to access the highly soluble activator incorporated into the film-former.

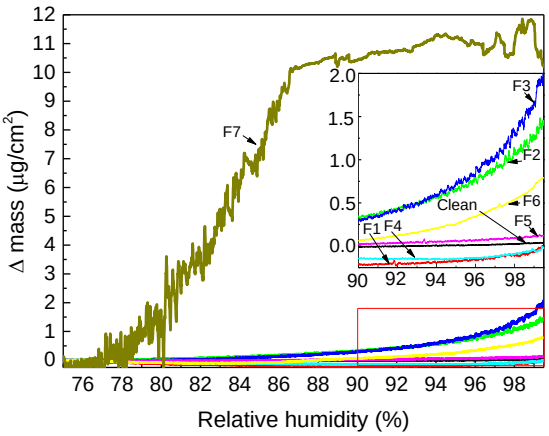

Figure 10.2: Results from QCM measurement presented as relative change of mass on the crystal calculated from Sauerbrey equation [22]

The two extremes can be noted in Figure 10.2 namely the adsorption of water by the clean surface with negligible gain of mass and glutaric acid with significant adsorption from 77 % RH. The plateau of measured change of mass from 86 % RH indicates saturation of water layer on the surface of the quartz crystal precontaminated with glutaric acid.

The succinic acid containing fluxes F2 and F3 in Figure 10.2 adsorb more water compared to the flux systems containing adipic or palmitic acids. A slight increase of mass could also be seen for the succinic acid flux F1 at RH above 98 %. In the case of adipic acid fluxes F4 and F5, a relatively low adsorption was observed, though with a marginal increase at RH above 99 % for the flux F4. For the palmitic acid flux F6, a steady gain of mass with increase of RH was observed, indicating steady build-up of the water layer on the crystal with flux residue.

IMPEDANCE AND LEAKAGE CURRENT MEASUREMENTS

The impedance spectra and leakage current measurements obtained for a number of solder fluxes under different humidity levels are presented in Figure 10.3. The first column (a.F1 – a.F7) represents the change of impedance spectra with increase in RH levels. At high frequencies the capacitive behaviour of the glass–reinforced epoxy laminate is dominant and independent of the nature of the residue. The impedance at low frequencies characterises the surface resistance between the conductors. At low humidity levels the conduction pathways on the surface are limited (high surface resistance), therefore relatively high scattering of impedance data at lower frequencies is observed. However, as the RH levels increase, the resistance of water layer forming between the electrodes reduces; the conduction pathway between the electrodes becomes more dominant. The reduction of the resistance of water layer on the test PCB is reflected in the drop of impedance at $f = 0.01$ Hz with every step of increase in RH. In this case, the impedance at low frequency is comparable with the low voltage DC resistance measurement.

Similar effect is indicated in the graphs of leakage current (b. and c. in Figure 10.3), where the increase of RH is followed by increase of measured current levels. It can be seen, at low humidity levels the flux residues are characterized by leakage currents as low as nA, and the

current increase with increase of RH. For some fluxes the current exceeds mA, which is attributed to the narrowing of the gap between the electrodes due to corrosion and dendrite formation.

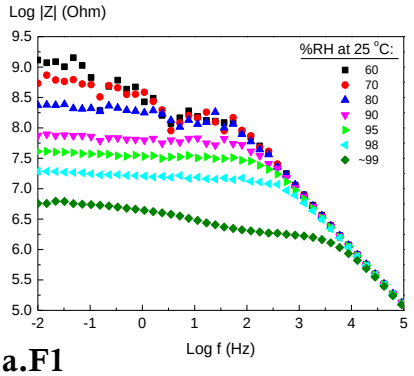

a.F1

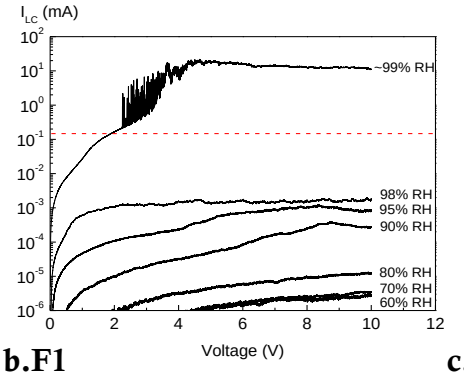

b.F1

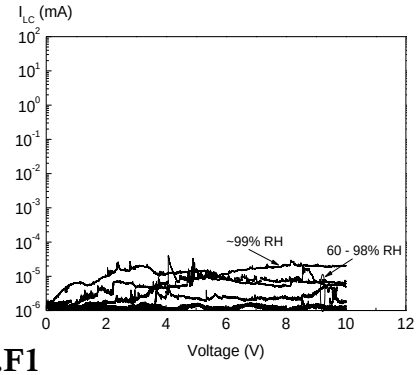

c.F1

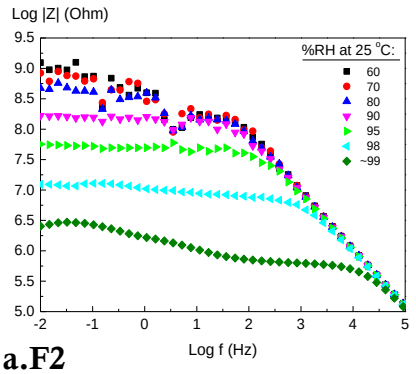

a.F2

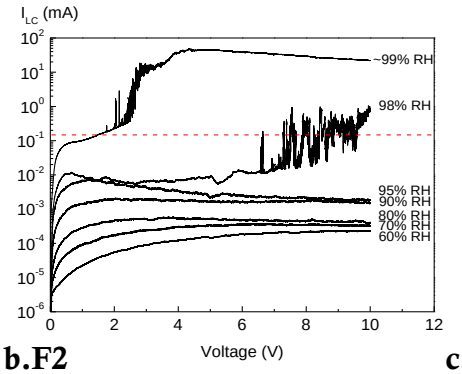

b.F2

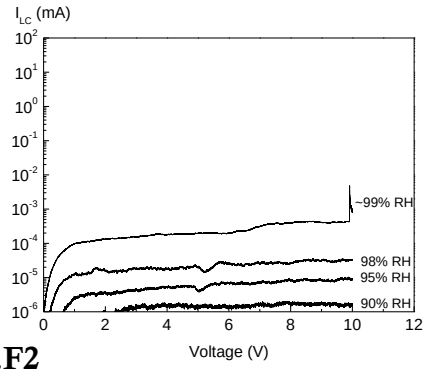

c.F2

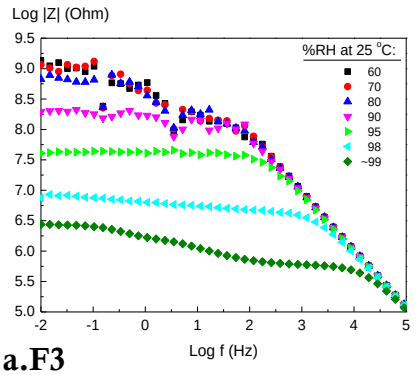

a.F3

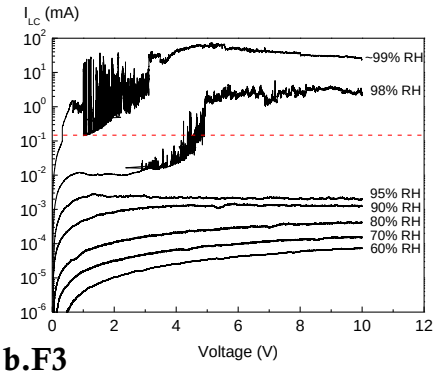

b.F3

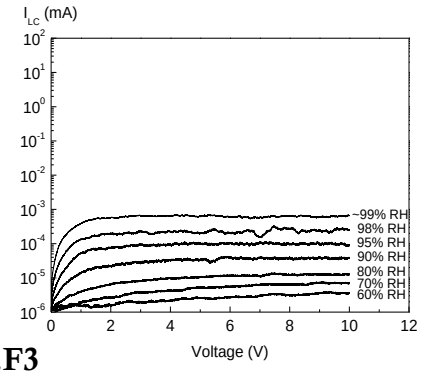

c.F3

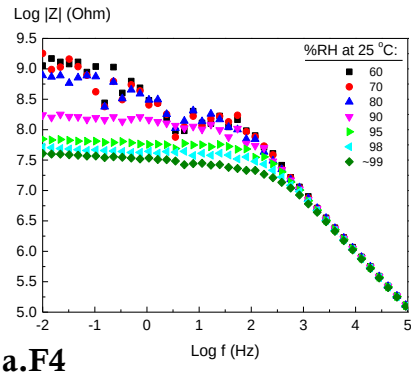

a.F4

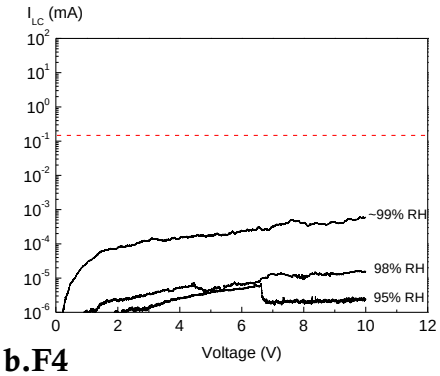

b.F4

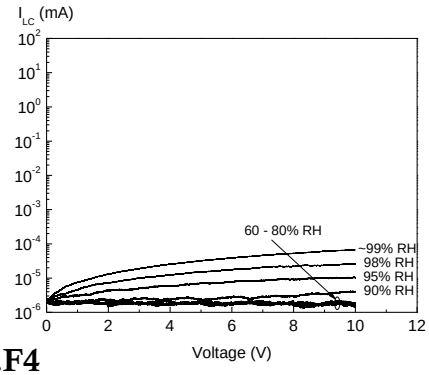

c.F4

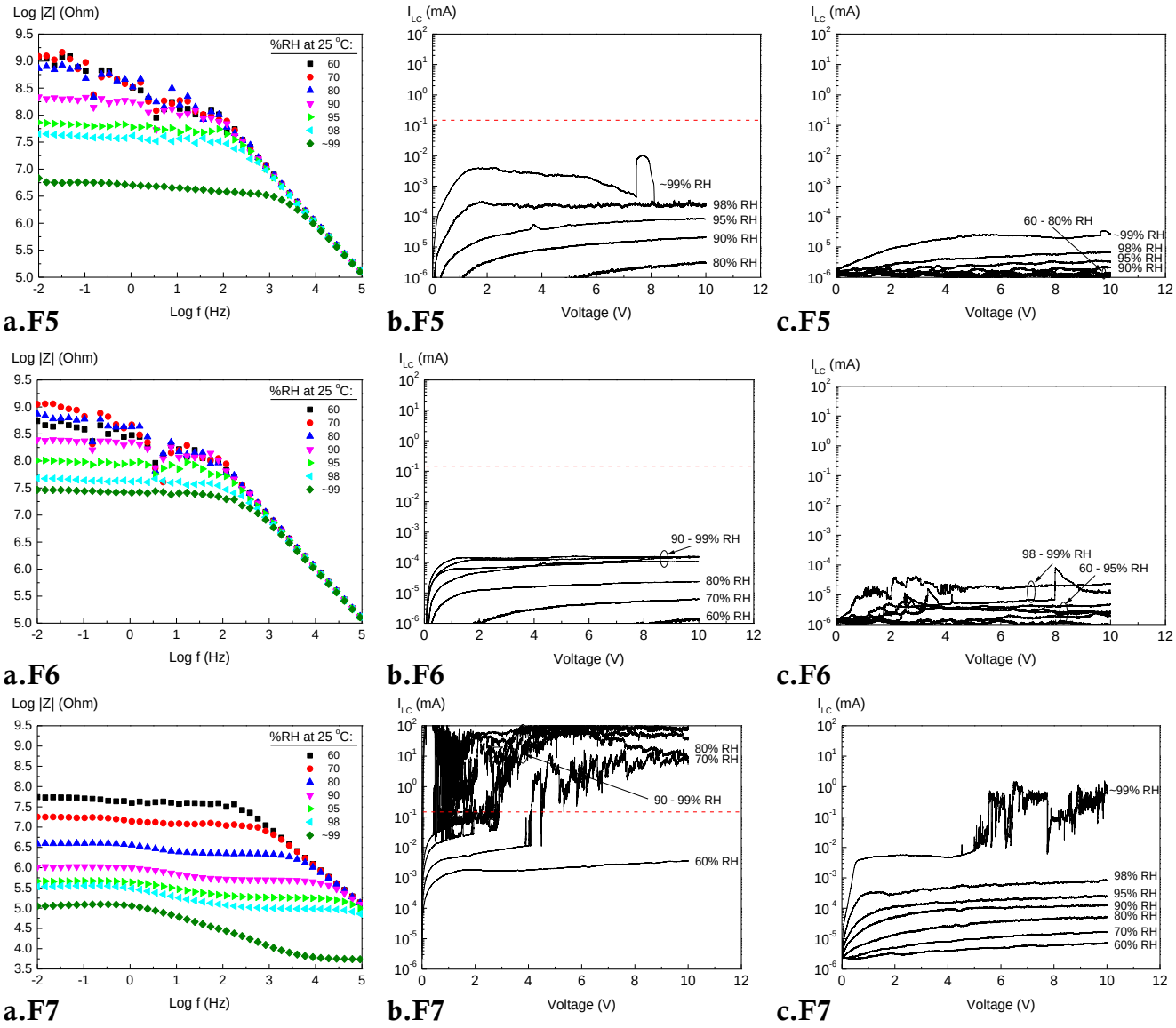

Figure 10.3: Results from climatic testing of solder flux: a. impedance spectra (Log|Z| (Ohm) vs Log f (Hz)); b. leakage current without heating of test board (I (mA) vs E (V)), and c. leakage current after heating of test board at 220-245 °C for 45 seconds (I (mA) vs E (V))

The current level of 0.1476 mA indicated in Figure 10.3 b is equivalent to 100 MOhm per square for SIR pattern with 1476 squares at 10 V DC. This limit is referred as SIR failure in IPC J-STD-004 [35] and IPC-TM-650 [23].

Figure 10.3 b. shows that the succinic and glutaric acid containing fluxes F1, F2, F3, and F7 caused an increase of currents above the failure limit at humidity levels of ~99, 98, 98, and 70 % respectively. For adipic and palmitic acids containing fluxes F4-F5 and F6 the failure level of 0.1476 mA has not been reached.

Exposure to 220-245 °C for 45 seconds caused partial decomposition and evaporation of the WOAs and as a result it drastically reduced the leakage currents (Figure 10.3 c). There were no SIR failures observed for solder fluxes F1, F2 and F3, whereas solder flux F7 showed an increase of current above 0.01476 mA, indicating SIR failure at ~99 % RH.

Figure 7.3 summarized the results from leakage current and AC impedance measurements shown in Figure 10.3. The SIR was calculated from the leakage current reading at 10 V DC, while for impedance, an average of two data points at 839 Hz and 1242 Hz is provided. The impedance at lower frequencies would more effectively represent resistivity of water layer under DC voltage; however, the impedance at $f \approx 1$ kHz excludes polarization effect and diffusion control charge transfer related resistance, typical for DC measurements. The impedance at $f \approx 1$ kHz reflects major change of surface resistance, which in this case is an indication of deliquescence of contaminant. Some cases $f = 1$ kHz frequency was also used for surface conductivity measurements and determination of deliquescence RH of salt mixtures [26].

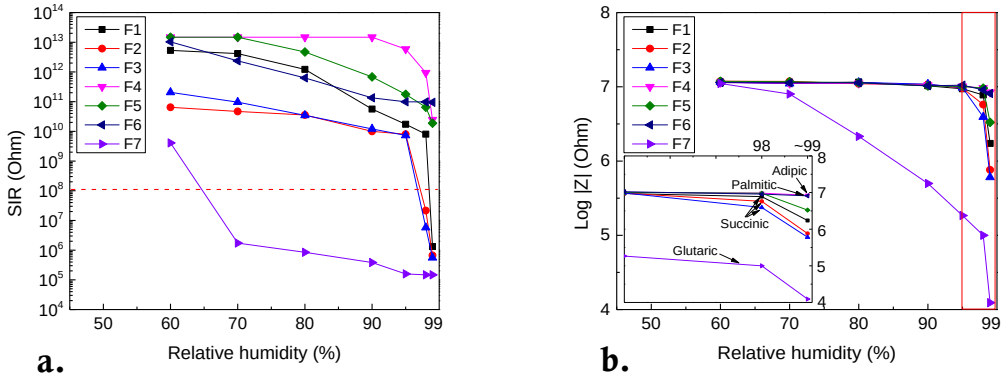

Figure 10.4: Summary of a. SIR from leakage current measurements at 10 V DC, and b. impedance reading at $f \approx 1$ kHz

As shown in Figure 7.3, the impedance follows the trend observed from leakage current measurements, represented as SIR in the graph. The solder flux which exhibited electrochemical migration and caused dendrite formation (F1, F2, F3 and F7) showed a sudden increase of leakage current equivalent to the reduction of SIR below 100 MΩ, also showed a reduction of impedance at $f \approx 1$ kHz. For the glutaric acid, a significant decrease of impedance was observed in the RH range of 70 % - 80%, succinic acid showed a decrease above 98 % RH, whereas the impedance reading for adipic and palmitic acids remained unchanged at a values of ~10 M Ohm. When comparing two measurements, it must be noted that the impedance and leakage current measurements were performed with different test boards; the SIR (Ohms/square) (Figure 7.3 a.) is calculated from leakage current measurements, while impedance (Figure 7.3 b.) is confined to the geometry of the electrodes.

SURFACE MORPHOLOGY OF SIR AFTER CORROSION

The optical micrographs of SIR patterns after climatic testing are provided in Figure 10.5. The pictures indicate the difference in the corrosiveness of the flux residue depending on the type of WOAs in the flux.

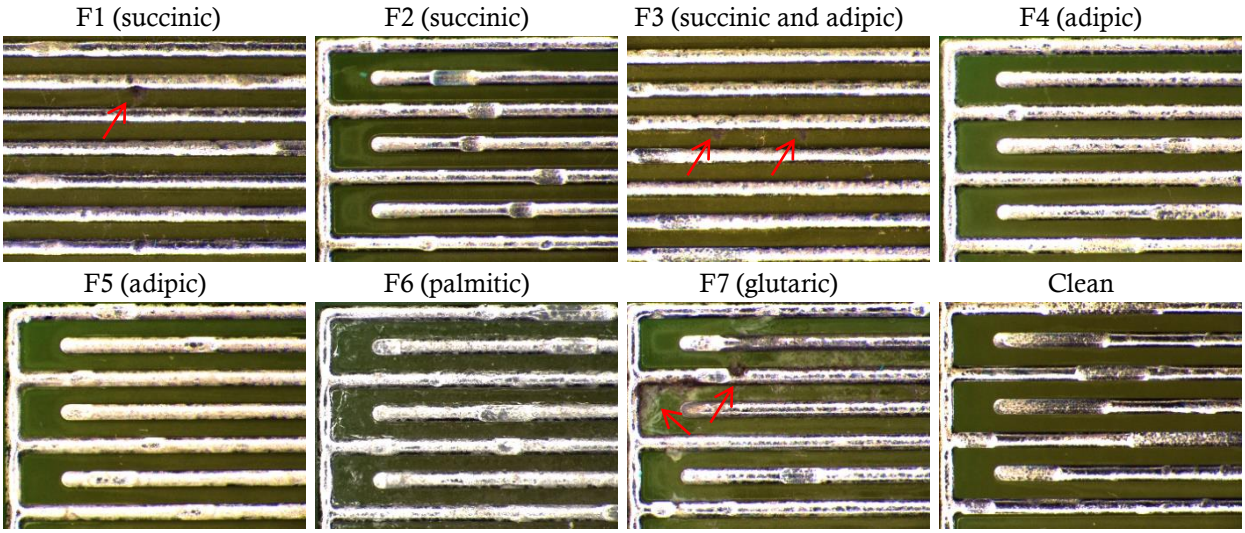

Figure 10.5: Optical micrographs of SIR pattern after climatic testing (test boards did not experience heating prior to humidity exposure)

No dendrites were formed on the SIR patterns precontaminated with adipic acid containing fluxes F4 and F5 (Figure 10.5). The relatively clean appearance (without bulky white residue) is attributed to low solid content of these flux systems. It is in high contrast with palmitic acid containing flux F6, leaving most residues.

The tin dendrites formed at 98 and ~99 %RH on the SIR patterns precontaminated with succinic acid containing fluxes F1 and F3 are indicated by arrows in Figure 10.5. These SIR patterns had moderate level of solid flux residue and few sites where tin dendrites were formed. For solder flux F7, a severe corrosion of SIR pattern was observed, although initially appeared with moderate amount of flux residue (white residue).

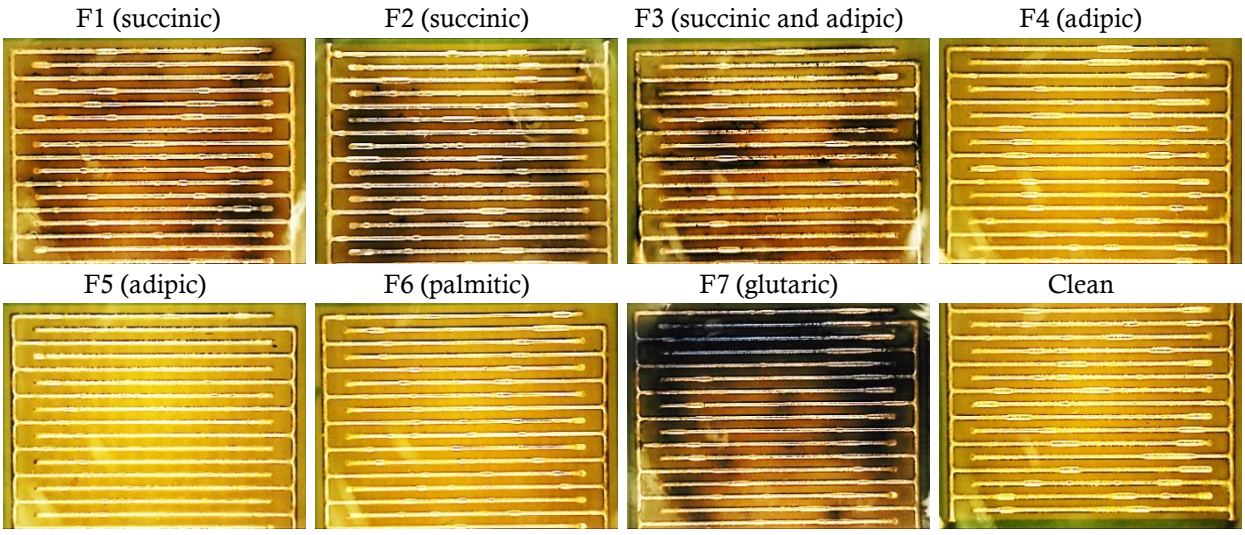

Figure 10.6: Optical micrographs of SIR patterns after climatic testing (corrosion of tin is indicated by blue coloration, while clear yellow colour indicates no corrosion of the SIR pattern)

Additional information on the degree of corrosion of SIR pattern is provided by the gel containing tin indicator, as shown in Figure 10.6. The areas with dark blue colour on the SIR pattern indicate locations where dissolution of tin during humidity exposure under bias voltage occurred, while

the clear yellow colour is attributed to no corrosion of tin from the electrodes. Comparing with the picture shown in Figure 10.6, it is noticeable that solder fluxes F1, F2, F3 and F7 caused high corrosion of SIR pattern, but fluxes F4, F5 and F6 did not. Among the fluxes, F7 appeared most corrosive with tin indicator, and it was in agreement with optical micrographs in Figure 10.5 and test results from impedance and leakage current measurements in Figure 10.3.

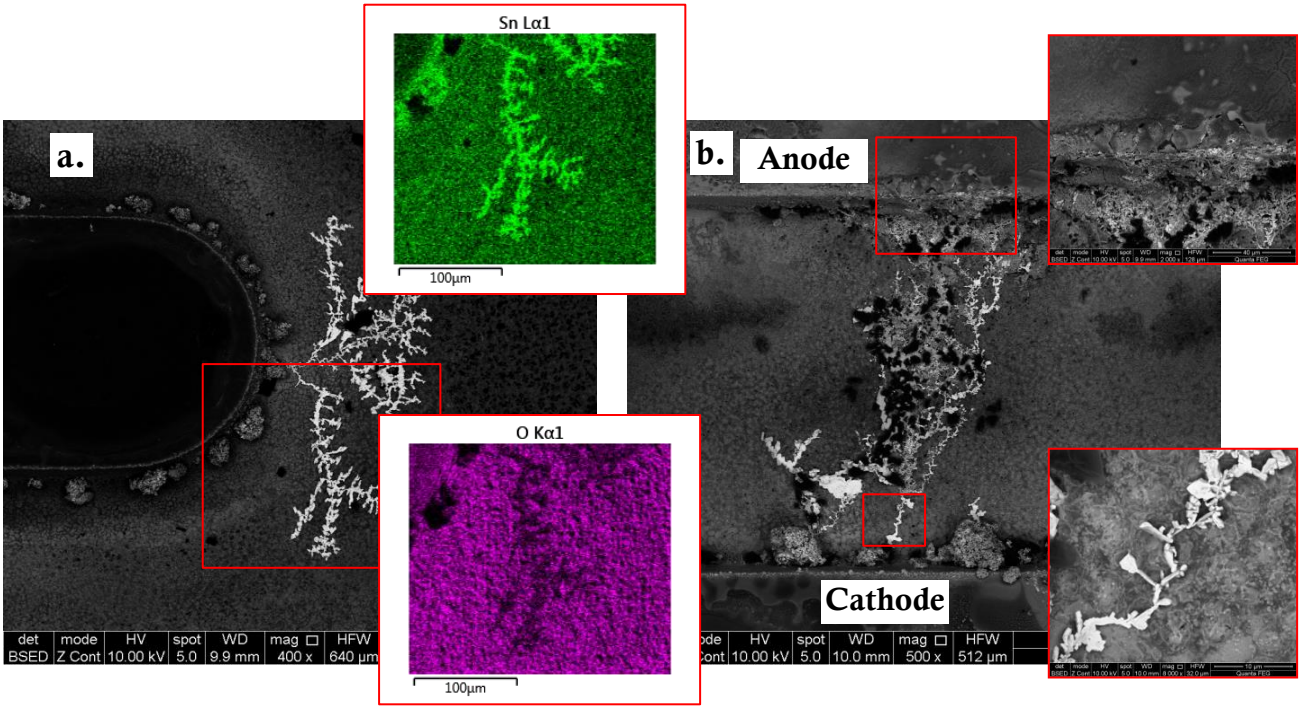

Figure 10.7: SEM image of dendrite on the SIR pattern (flux F7 heated at 220-245 °C for 45s): a. initiation and growth of tin dendrite, and magnified view of EDS map obtained on the tin dendrite, b. bridging of cathode and anode by dendrites and corrosion product

The microstructure of typical tin dendrite forming on the SIR pattern during climatic testing is shown in Figure 10.7. The dissolution of tin is taking place at the positively biased electrode-anode, while the reduction of metal ions and precipitation occurs at the cathode. As it is seen from EDS map in Figure 10.7 a., the micro structure of tin dendrite consists mainly of tin, thus the dendrite is conductive and able to conduct current at the level of mA. The short circuiting due to dendrite bridging of oppositely biased electrodes is clearly seen in the leakage currents curves as an abrupt increase of current by more than an order of magnitude.

IV. DISCUSSION

The leakage current and impedance measurements as a function of RH showed that solder flux systems are characterized by different threshold RH, above which a sudden increase in leakage current by 2-4 orders of magnitude, and a pronounced reduction of impedance is observed (Figure 10.3 and Figure 7.3). For succinic acid containing fluxes F1, F2 and F3 the threshold RH was observed at 98 and ~99 % RH; for glutaric acid containing flux F7 at 70 % RH, while for adipic and palmitic acid containing fluxes F4, F5 and F6 no significant increase of leakage current was

observed under test conditions. The observation is attributed to the hygroscopic property of WOA(s) in the flux. The deliquescence RH for adipic and succinic acids are respectively ≥99 % and ~98 %, while the deliquescence RH for glutaric acid is in the range from 75 to 89 % [36]–[39].

Further, the nature of the impedance spectra changes, it shows two time constants when RH exceeds critical value for particular WOA in the flux. The observed behaviour indicates that the reactions at the electrodes are taking place within the water layer formed on the surface of the test board. Palmitic acid, which is a fatty acid, is insoluble in water and is not characterized by deliquescence RH. As a result, the solder flux containing palmitic acid (F6) causes low-level leakage currents, compared to that of other WOAs, especially when comparing the results at high humidity. The results from QCM measurement on the flux residue F6 are indicating higher increase of mass compared to low solubility adipic acid fluxes F4 and F5, and it suggests that the solid content of the flux (acid + film-former), which is more than 3 times higher for the F6 influenced higher adsorption of the water. It has to be noted that the fixed volume of the flux and not the weight of the residue was fixed for the comparison of the flux systems in this work. The solder flux F1 contains halides, however no considerable changes in the SIR and impedance measurements compared to halide free succinic acid fluxes F2 and F3 were observed. This might be due to the fact that the amount of halides in the flux is lesser compared to the amount of WOA activator.

Overall, glutaric acid containing flux F7 with a moderate solid content, highest acid number, and lowest critical RH, showed highest leakage currents and caused electrochemical migration at low humidity levels. The observed corrosiveness of glutaric acid containing flux is in agreement with the observations in literature [19], [20], and suggests that the residue of this system is most critical to be present on the PCBAs. In addition to the high corrosiveness of the glutaric acid in the flux F7, which is mainly related to its solubility in water, this flux system was also volatile organic compound (VOC) free. Water as a solvent influences the spreading of the residue during evaporation, resulting in more localized residues, thereby could result in higher leakage current. The lower SIR values for VOC free flux is also reported in the literature [2]. Succinic acid containing fluxes F1, F2 and F3 appeared to give moderate leakage current levels at intermediate humidity, however exhibited electrochemical migration at high humidity. The ability of succinic acid to be dissolved in the humidity range of 98-99% makes it more critical than adipic or palmitic acid, as activator in the flux. The behaviour of palmitic acid containing flux (F6) was similar to that of adipic (F5). Both fluxes created comparable levels of leakage current, and no dendrites were observed within the time of test exposure, although palmitic acid containing flux (F6) had the highest solid residue on the boards.

The *ex situ* corrosion testing of SIR pattern using gel containing tin ion indicator showed clear difference of the corrosiveness of flux system dependent on the type of activator in the flux, similarly as observed from leakage current measurements. The highest level of corrosion was observed on the SIR pattern precontaminated with glutaric acid containing flux F7 (Figure 10.6), and was followed by succinic acid fluxes F1, F2, and F4. No trace of tin corrosion was identified on SIR patterns precontaminated with adipic and palmitic acid fluxes F4-F5 and F6.

The leakage current measured on the test boards exposed to soldering temperature (Figure 10.3 c) showed the importance of soldering temperature on the decomposition and volatilization of no-clean flux. A clear reduction in leakage currents was observed for all the flux systems,

correspondingly no electrochemical migration was observed for the fluxes F1, F2 and F3, while for the flux F7, which was the most aggressive, the electrochemical migration was observed only at ~99% RH. However, the difference in leakage currents observed for adipic and palmitic acid fluxes before and after heating of the residue was lower compared to succinic or glutaric acid. The observation indicates possible saturation of water layer forming on the surface, and the importance of solubility of WOAs saturating thin water layers. Variation in solubility of the activator component in water layer is an important aspect as a sparingly soluble acid need thicker water layer to dissolve considerable amount of residue compared to the highly soluble acid for which a thin layer of water can take up appreciable amounts. For comparison, solubility for adipic, succinic, and glutaric acids at room temperature is receptivity 15, 83.5, and 1400 g/1000 g H_2O [40].

In addition to the decomposition and volatilisation of the flux during soldering process, a high amount of the flux will react with the metal oxides on the PCB during soldering, and the new species characterized by different hygroscopic property and aggressiveness for corrosion may be formed [21]. In the current study, the SIR measurements were performed at room temperature, however it is important to note, that the ranking for aggressiveness for corrosion of the flux residue based on the type of WOA may be affected by temperature as accelerating factor during climatic testing.

The SIR testing as a function of RH enables ranking of the flux systems based on their response to various RH levels. Following ranking based on the corrosiveness and hygroscopicity of the WOA tested at 25 °C was determined for the fluxes in this work: glutaric > succinic > adipic > palmitic. Selection of flux systems with low solubility and high deliquescence RH activators would improve the SIR and reduce the probability for electrochemical migration under humid conditions.

V. CONCLUSIONS

1. Flux residues are characterized by different hygroscopic nature which is dependent on the activator in the flux. The results from quartz crystal microbalance test showed the adsorption of water by the flux residue is primarily dependent on the type of activator in the flux, while the film-former may influence the coverage of the activator, thereby influencing water adsorption by the activator.
2. The results from leakage current and impedance measurement obtained as a function of RH were in close correlation; both indicated the deliquescence RH of particular WOAs in the flux systems. The reduction in impedance at low frequencies attributed to the resistance of water layer forming on the surface with flux residue was more pronounced. Leak current measurement showed an abrupt increase in leakage current by 2-4 orders of magnitude (representing a reduction of SIR below 100 MΩ) and electrochemical migration was observed.
3. The temperature to which flux residues are exposed during soldering is to great extent influencing amounts of flux residues remaining on the PCBAs. A significant reduction of leakage current and electrochemical migration was observed for all the flux systems after exposure to 220-245 °C for 45 seconds.

4. The test with tin ion indicator on the SIR pattern revealed high corrosiveness of glutaric acid containing flux F7 followed by the succinic acid fluxes F1, F2, and F3, under high humidity condition used in this work. No trace of tin corrosion was identified on SIR patterns precontaminated with adipic and palmitic acid fluxes F4-F5 and F6. The results from corrosiveness determination with tin ion indicator reflected the observations from the SIR testing.

VI. ACKNOWLEDGMENTS

The research reported here was conducted as part of the CELCORR/CreCon consortium (www.celcorr.com) and the authors would like to acknowledge the funding and help received from the consortium partners.

VII. REFERENCES

[1] J. E. Sohn, U. Ray, V. Heideman, B. Schubert, J. E. Anderson, K. M. Adams, and G. Becka, "How clean is clean: effect of no-clean flux residues and environmental testing conditions on surface insulation resistance," in *Proceedings of Surface Mount International*, 1994.

[2] D. X. Xu, D. Bin Wang, and Y. P. Lei, "Study of VOC-Free, No-Clean Flux for Lead-Free Soldering in Electronic Packaging," *Adv. Mater. Res.*, vol. 154–155, pp. 1012–1018, 2010.

[3] S. Zhan, M. H. Azarian, and M. Pecht, "Reliability of Printed Circuit Boards Processed Using No-Clean Flux Technology in Temperature – Humidity – Bias Conditions," *IEEE Trans. Device Mater. Reliab.*, vol. 8, no. 2, pp. 426–434, 2008.

[4] S. Canumalla, K. Ludwig, R. Pedigo, and T. Fitzgerald, "A study on ranking of commercial fluxes for electrochemical migration (ECM) propensity for Cu, Sn and Ag surface finishes," in *56th Electronic Components & Technology Conference*, 2006, pp. 625–632.

[5] D. Minzari, M. S. Jellesen, P. Møller, and R. Ambat, "On the electrochemical migration mechanism of tin in electronics," *Corros. Sci.*, vol. 53, no. 10, pp. 3366–3379, Oct. 2011.

[6] V. Verdingovas, M. S. Jellesen, and R. Ambat, "Influence of sodium chloride and weak organic acids (flux residues) on electrochemical migration of tin on surface mount chip components," *Corros. Eng. Sci. Technol.*, vol. 48, no. 6, pp. 426–435, Sep. 2013.

[7] P.-E. Tegehall and B. D. Dunn, "Influence of flux residues and conformal coatings on the surface resistance properties of spacecraft circuit boards," *ESA J.*, vol. 16, no. 3, pp. 255–273, 1992.

[8] C. Hunt, A. Mensah, A. Buxton, and R. Holman, "Determining conformal coating protection," *Solder. Surf. Mt. Technol.*, vol. 18, pp. 38–47, 2006.

[9] H. Conseil, M. Stendahl Jellesen, and R. Ambat, "Contamination profile on typical printed circuit board assemblies vs soldering process," *Solder. Surf. Mt. Technol.*, vol. 26, no. 4, pp. 194–202, Aug. 2014.

[10] U. Rathinavelu, M. S. Jellesen, P. Moller, and R. Ambat, "Effect of No-Clean Flux Residues on the Performance of Acrylic Conformal Coating in Aggressive Environments," *IEEE Trans. Components, Packag. Manuf. Technol.*, vol. 2, no. 4, pp. 719–728, 2012.

[11] K. Seeling and T. O'Neill, "Conformal Coating over No-Clean Flux," *SMT Surf. Mt. Technol. Mag.*, vol. 29, no. 4, pp. 52–58, 2014.

[12] R. Rörgren, P. Tegehall, and P. Carlsson, "Reliability of BGA Packages in an Automotive Environment," *J. Surf. Mt. Technol.*, vol. 11, no. 2, pp. 35–44, 1998.

[13] D. Pauls, "Residues in printed wiring boards and assemblies," *Circuit World*, vol. 27, no. 1, pp. 32–41, 2000.

[14] R. Michalkiewicz, "Addressing flux corrosion and reliability concerns early," *SMT Surf. Mt. Technol. Mag.*, vol. 28, no. 1, pp. 20–29, 2014.

[15] M. S. Jellesen, D. Minzari, U. Rathinavelu, P. Møller, and R. Ambat, "Corrosion failure due to flux residues in an electronic add-on device," *Eng. Fail. Anal.*, vol. 17, no. 6, pp. 1263–1272, Sep. 2010.

[16] D. Geiger and D. Shangguan, "Investigation of the effect of solder flux residues on RF signal integrity using real circuits," *Solder. Surf. Mt. Technol.*, vol. 17, no. 4, pp. 27–32, 2005.

[17] L. J. Turbini, B. A. Smith, J. Brokaw, J. Williams, and J. Gamalski, "The Effect of Solder Paste Residues on RF Signal Integrity," *J. Electron. Mater.*, vol. 29, no. 10, pp. 1164–1169, 2000.

[18] M. Duffy, L. Floyd, P. Mccloskey, C. Ó. Mathúna, K. Tellefsen, M. Liberatore, and A. Sreeram, "RF Characterisation of No-clean Solder Flux Residues," *Proc. SPIE - Int. Soc. Opt. Eng.*, vol. 4587, pp. 138–143, 2001.
[19] J. E. Sohn and U. Ray, "Weak Organic Acids and Surface Insulation Resistance," *Circuit World*, vol. 21, no. 4, pp. 22–26, 1994.
[20] Y. Zhou, L. J. Turbini, D. Ramjattan, B. Christian, and M. Pritzker, "Characterizing Corrosion Effects of Weak Organic Acids Using a Modified Bono Test," *J. Electron. Mater.*, vol. 42, no. 12, pp. 3609–3619, Aug. 2013.
[21] B. A. Smith and L. J. Turbini, "Characterizing the weak organic acids used in low solids fluxes," *J. Electron. Mater.*, vol. 28, no. 11, pp. 1299–1306, Nov. 1999.
[22] V. Verdingovas, M. S. Jellesen, and R. Ambat, "Solder Flux Residues and Humidity-Related Failures in Electronics: Relative Effects of Weak Organic Acids Used in No-Clean Flux Systems," *J. Electron. Mater.*, vol. 44, no. 4, pp. 1116–1127, 2015.
[23] "IPC-TM-650 Test Methods Manual, 2.6.3.3 Surface Insulation Resistance, Fluxes," Northbrook, IL, 2004.
[24] "IPC-TM-650 Test Methods Manual, 2.6.14.1 Electrochemical Migration Resistance Test," Northbrook, IL, 2009.
[25] L. Ferrero, G. Rovelli, L. D' Angelo, G. Sangiorgi, M. G. Perrone, M. Moscatelli, M. Casati, V. Rozzoni, and E. Bolzacchini, "Determination of aerosol deliquescence and crystallization relative humidity for energy saving in free-cooled data centers," *Int. J. Environ. Sci. Technol.*, 2014.
[26] L. Yang, R. T. Pabalan, and M. R. Juckett, "Deliquescence relative humidity measurements using an electrical conductivity method," *J. Solution Chem.*, vol. 35, no. 4, pp. 583–604, 2006.
[27] "IPC-9201 Surface Insulation Resistance Handbook," Northbrook, IL, 1996.
[28] K. S. Hansen, M. S. Jellesen, P. Moller, P. J. S. Westermann, and R. Ambat, "Effect of Solder Flux Residues on Corrosion of Electronics," in *Annual reliability and maintainability symposium*, 2009, pp. 503–509.
[29] C.-Y. Huang, M.-S. Li, C.-L. Ku, H.-C. Hsieh, and K.-C. Li, "Chemical characterization of failures and process materials for microelectronics assembly," *Microelectron. Int.*, vol. 26, no. 3, pp. 41–48, 2009.
[30] Y. B. Kar, N. A. Talik, F. C. Seng, L. H. Yang, R. Vithyacharan, and T. C. Yong, "Flux residue cleaning process optimization effect on flip chip ball grid array reliability," in *IEEE 14th Electronics Packaging Technology Conference*, 2012, vol. 855, pp. 608–613.
[31] R. M. Silverstein, F. X. Webster, and D. J. Kiemle, *Spectrometric identification of organic compounds*, 7th ed. John Wiley & Sons, 2005.
[32] S. Choknud, O. Saisa-ard, and K. J. Haller, "Preparation and Characterization of Carboxylic Acid Adducts of Gabapentin," *Eng. J.*, vol. 16, no. 3, pp. 29–36, 2012.
[33] D. Minzari, M. S. Jellesen, R. Ambat, P. Møller, and P. S. Westermann, "Process, kit and composition for detecting residues and contaminants in an object with three-dimensional geometry," WO 2011/048001 A12011.
[34] G. Sauerbrey, "The Use of Quartz Oscillators for Weighing Thin Layers and for Microweighing," *Z. Phys.*, vol. 155, pp. 206–222, 1959.
[35] "IPC J-STD-004B Requirements for Soldering Fluxes," Bannockburn, IL, 2008.
[36] C. Peng, M. N. Chan, and C. K. Chan, "The hygroscopic properties of dicarboxylic and multifunctional acids: measurements and UNIFAC predictions.," *Environ. Sci. Technol.*, vol. 35, no. 22, pp. 4495–501, Nov. 2001.
[37] P. Saxena and L. M. Hildemann, "Water absorption by organics: survey of laboratory evidence and evaluation of UNIFAC for estimating water activity," *Environ. Sci. Technol.*, vol. 31, no. 11, pp. 3318–3324, Nov. 1997.
[38] K. M. Adams, J. E. Anderson, and Y. B. Graves, "lonograph Sensitivity to Chemical Residues from 'No Clean' Soldering Fluxes: Comparison of Solvent Extract Conductivity and Surface Conductivity," *Circuit World*, vol. 20, no. 2, pp. 41–44, 1994.
[39] C. Cruz and S. Pandis, "Deliquescence and hygroscopic growth of mixed inorganic-organic atmospheric aerosol," *Environ. Sci. Technol.*, vol. 34, no. 20, pp. 4313–4319, 2000.
[40] W. M. Haynes and D. R. Lide, *CRC Handbook of chemistry and physics*, 94th Editi. CRC Press, 2013, p. 2668.

11. INFLUENCE OF SODIUM CHLORIDE AND WEAK ORGANIC ACIDS (FLUX RESIDUES) ON ELECTROCHEMICAL MIGRATION OF TIN ON SURFACE MOUNT CHIP COMPONENTS

Vadimas Verdingovas, Morten Stendahl Jellesen, and Rajan Ambat

Abstract—The electrolytic properties of sodium chloride and no-clean solder flux residue, and their effects on electrochemical migration and dendrite growth on surface mount chip capacitors were investigated. The leakage current dependency on concentration of contaminants was measured by a solution conductivity method and compared with current measurements using DC voltage. The effect of electrolyte concentration and potential bias on the probability of electrochemical migration was investigated using a water droplet method on chip capacitors. The results from leakage current and conductivity measurement showed a difference which is caused by polarization effects, and demonstrated existing issues when indexing contamination levels on printed circuit board assemblies using a standardized solvent extract method. The experimental results showed that dendrite growth was dependent on the type and amount of contamination. The probability of migration becomes less dependent on the amount of contamination for sodium chloride at high concentrations. However, for organic acids from flux residues the migration probability shows an abrupt decrease with increasing concentration, which is attributed to a pH change in the condensed electrolyte phase.

Keywords—Solder flux residue weak organic acids, Tin corrosion, Electrochemical migration, Electronics

I. INTRODUCTION

The corrosion of various metallic parts on printed circuit board assemblies (PCBA) is an increasing problem in recent years. A number of inherent factors such as: the use of multimaterial combinations, closer spacing due to demand for miniaturization, contamination issues, and widespread use of electronic devices under outdoor conditions is contributing to the dramatic increase in reliability issues [1]–[4]. Owning to technological advances, electronic devices have become more sensitive towards climatic conditions synergistically with levels of ionic contamination present on the surface of PCBAs today. Trace amounts of ionic contamination are able to acts as corrosion enhancing factors by: assisting water adsorption to the surface by their hygroscopic nature and increasing the surface electrolyte conductivity by dissolution of ionic contamination within the adsorbed water layer. Both of these factors increase the risk of leakage currents that subsequently lead to corrosion and premature failures.

A major source of ionic contamination on the PCBA surface is from the manufacturing processes. This includes bare printed circuit board (PCB) manufacturing processes involving the use of various plating, etching, and cleaning solutions, and most importantly the use of no-clean

V. Verdingovas, M. S. Jellesen, and R. Ambat, "Influence of sodium chloride and weak organic acids (flux residues) on electrochemical migration of tin on surface mount chip components," *Corros. Eng. Sci. Technol.*, vol. 48, no. 6, pp. 426–435, Sep. 2013.

flux systems for soldering process during the PCB assembling stage. One of the commonly used flux systems consists of weak organic acids (irrespective of wave or reflow soldered) as activators. Consequently, organic acid residues remain on PCBA surfaces [5], [6] and can dissolve into the water layer, resulting from humidity exposure, thereby causing leakage current and corrosion issues, especially electrochemical migration (ECM) under certain conditions [4], [7]–[10].

The cleanliness levels of a PCBA after the manufacturing are generally assessed through solution conductivity measurements called solvent extract conductivity or resistivity of solvent extract testing using the IPC-TM-650 tests methods manual no. 2.3.25. This test method relies on assessment of the level of ionic contamination through conductivity measurement of solution extracted from PCB or PCBA immersion [11]. As the level of ionic contamination increases, the resistivity of extracted solution decreases. The level of contamination on a PCBA surface is commonly expressed in terms of NaCl equivalent as described in the IPC J-STD-001 standard. The critical level of total contamination is then defined as 1.56 $\mu g \cdot cm^{-2}$ NaCl equivalent irrespective of the type of ionic contamination. However, the effect of various ionic residues on the leakage current and electronic corrosion mechanisms is different, which is not differentiated by the above method of cleanliness assessment. Therefore, inorganic residues such as chlorides will contribute more to the conductivity and also more aggressive to corrosion of metals/alloys in general compared to partially ionised weak organic acids resulting from organic acid based solder flux systems. The effect of weak organic acids on electronic corrosion mechanisms such as ECM is likely to be different from chloride, while it can also adsorb onto the metal surface resulting in different surface chemistry [10]. Literature shows a number of investigations on the effect of flux residues on the leak current and corrosion on the PCBAs as a function of humidity levels, temperature, flux concentrations, and flux types [6], [8], [12]–[14]. However, none of these investigations have correlated the behaviour of flux residue with NaCl at equivalent concentrations, which is the standard method for comparing different species with respect to surface contamination levels.

Therefore, the focus of this investigation is to compare the behaviour of a known organic acid based wave solder flux system with equivalent levels of NaCl with respect to electrolytic properties and corrosion behaviour, including ECM. The aim is to demonstrate the difference between the effect of flux residues and NaCl in causing leakage currents and, therefore to show that both types of residues need to be treated differently with respect to allowable levels of contamination. The results of this investigation are also useful to show the difference between weak organic acid type fluxes, and halide fluxes (as some of the flux systems have chlorides) and their effects on PCBA surface at levels defined by the IPC J-STD-001 standard.

II. MATERIALS AND METHODS

COMPONENTS USED FOR EXPERIMENTS

All the tests for determining probability of electrochemical migration were conducted using a chip capacitor as the substrate. The component used was a surface mount multilayer ceramic capacitor (Yageo, Phycomp) with 0805 housing size, 10 nF capacitance, and 50 V voltage rating. The electrode terminals of the capacitor were made of pure tin [15]; the average distance between the terminals was 1 mm. All the parameters were tested on 18 replicate chip capacitors.

ELECTROLYTES USED AS CONTAMINATION

Two electrolytes (equivalent to different contamination) were used in this study namely: NaCl, which is also used to define the equivalent contamination levels on a PCBA as described before; and no-clean organic acid based wave solder flux, and thus typical of residue found on PCBA surfaces. The acid number of the flux is 15.8 mgKOH (+/-2.5%). The volatile organic compound content of the flux is 92 wt.%, water content is 5 wt.%, and the solid content is 2.2 wt.%. The flux contains synthetic resin as the film former. Both electrolyte solutions were prepared using water purified with Synergy UV system from Millipore Corp, and the base level resistivity of the water was the range between 2 MΩ·cm and 2.5 MΩ·cm as measured before the electrolyte preparation.

The concentrations of the electrolytes are presented in Table 11.1. Amounts of NaCl and flux residues in solutions were selected to represent concentrations below and above the IPC standard value of 1.56 μg·cm^{-2}. The volume of electrolyte and therefore the amount of contaminants was confined to the surface area of the components with the relationship of 1 mm^3 / 1 mm^2 providing the units of μg·cm^{-2}.

Table 11.1: Electrolyte concentrations and amounts (shown in brackets as μg·cm^{-2}) following relationship of 1 mm^3/1 mm^2

	Concentration and amount of contamination, g·dm^{-3} (μg·cm^{-2})					
NaCl	0.00156 (0.156)	0.00858 (0.858)	0.0156 (1.56)	0.039 (3.9)	0.0858 (8.58)	0.156 (15.6)
Flux residues	0.00625 (0.625)	0.0375 (3.75)	0.125 (12.5)	0.920 (92)	1.68 (168)	3.42 (342)

The electrolyte containing flux residues was prepared by pouring a desired amount of flux into a petri dish, allowing for the solvent to evaporate for 24 h at room temperature, and dissolving the remaining residues into the purified water. The concentrations given in Table 11.1 represent the residual solids content, which is comprised from water insoluble resin, and organic activators which contribute to ionic conductivity in the electrolytes. The main organic acid used in this flux system as an activator is adipic, as was determined by ion chromatography.

LEAKAGE CURRENT MEASUREMENTS USING PLATINUM ELECTRODES

The level of leakage current that can be sustained in various electrolyte solutions was measured using a pair of closely spaced platinum electrodes immersed into a droplet of the electrolyte solution on a clean polystyrene substrate. The diameter, length of each electrode, and the distance between them are respectively 0.5 mm, 2.5 mm and 3 mm. All measurements were carried out at 5 V DC and by placing 100 mm^3 droplets of the desired solution under the electrodes. Current passing through the solution was then measured for 2 minutes and the steady state value of the leakage current was noted. The leakage current measurements were performed using a "BioLogic VSP" multichannel potentiostat having three independent potentiostat units with 0-20 V compliance voltage and 1 nA resolution.

CONDUCTIVITY MEASUREMENT OF ELECTROLYTE

In order to differentiate between the leakage currents from applied DC voltage, and standard conductivity measurements using AC voltage (IPC-TM-650 2.3.25), the conductivity of the

electrolyte solutions were also measured using a conductivity meter with 4-electrode conductivity cell (cell constant k = 0.521 cm^{-1}) from Radiometer Analytical, "CDM210".

SINGLE COMPONENT ELECTROCHEMICAL MIGRATION TESTS

Electrochemical migration tests at single component level were conducted using a special in-house built "single component electrochemical migration" set-up described elsewhere [16]. Figure 11.1 shows a picture of the setup where three components can be loaded simultaneously for experiments (Figure 11.1 (b) shows magnified view of the component with droplet connecting both electrodes of the component). The set-up consists of a sample holder having two small adjustable probes, which act as connectors to each end of the surface mount component under test. Therefore, a single test component is fixed between the metal which being spring-loaded onto the sample to ensure good electrical contact.

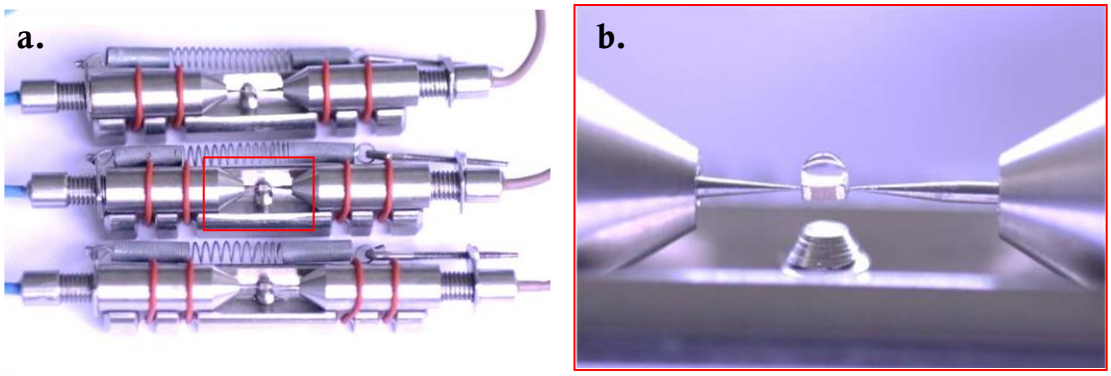

Figure 11.1: View of single component electrochemical migration set-up: a. set-up with mounted three components for testing, and b. magnified view of chip capacitor with droplet of solution for testing

Once within the set-up, a microdroplet of the desired electrolyte is placed on top of the components using a micropipette. The volume of droplet was confined to the area of the component providing a fixed level of contamination in terms of $\mu g \cdot cm^{-2}$ (using solutions shown in Table 11.1). A relationship of 1 mm^3 of solution over 1 mm^2 area enabled an equivalent between $g \cdot dm^{-3}$ and $\mu g \cdot cm^{-2}$ with a ratio of 1:100. The test component used in this work was a size 0805 multilayer ceramic capacitor (surface area 2.5 mm^2), and accordingly 2.5 mm^3 of solution was applied on top of it.

The effect of potential bias of potential bias on the tendency for electrochemical migration was examined in the DC voltage range 1 V – 25 V using an in-house built multi-channel multiplexer unit described elsewhere [17]. The leakage current, and any short circuits currents as a result of dendrite growth were measured with a 1 µA resolution ammeter connected in the circuit via a two switch system. The sampling rate for the leakage current reading was set to 1 s. The experiments were carried out under ambient conditions: temperature 23.5 °C – 24.5°C, relative humidity 30 % - 40 %.

III. RESULTS

COMPARISON OF ELECTROLYTIC PROPERTIES OF CONTAMINANTS

Leakage current and solution conductivity dependence on the concentration at room temperature was measured experimentally for various sodium chloride and flux residue levels with quantities equivalent to IPC standard level 1.56 µg·cm^{-2}. The results are shown in Figure 11.2. The conductivity values for both NaCl and flux residue are of similar magnitude at lower concentration levels. However, the conductivity of NaCl follows a linear dependence with concentration while the organic acid flux residue showed a curved response that flattens off above a concentration indicating a maximum current limit compared to NaCl contamination. The measured base leakage current for pure water at 5 V DC was in the range between 1.25 µA and 1.6 µA.

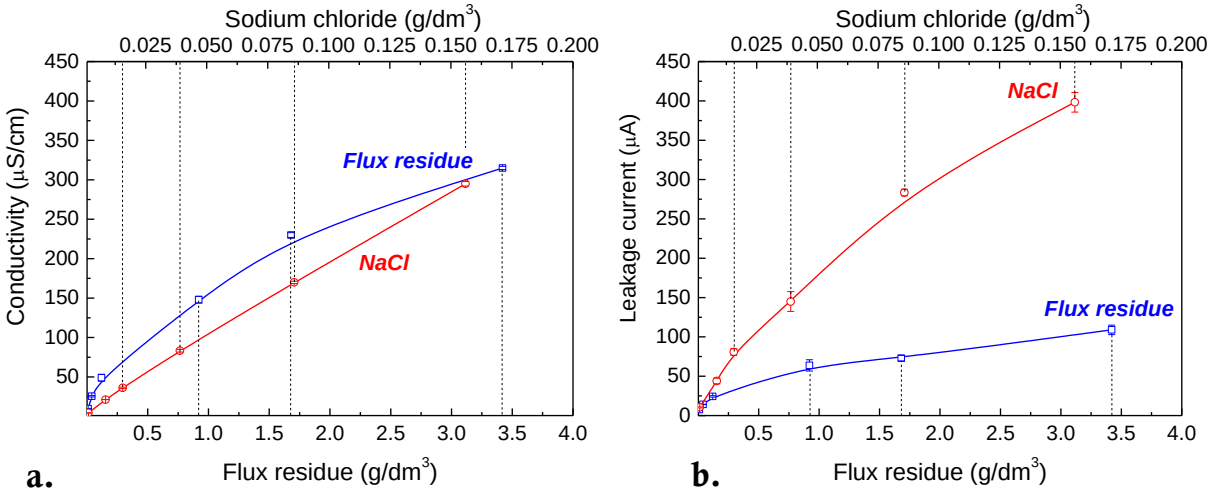

Figure 11.2: Solution conductivity and leakage current for NaCl and flux residue solution: a. solution conductivity and b. leakage current

The conductivity dependence of NaCl on concentration can be understood because of the fact that NaCl is a strong electrolyte and completely dissociates into Na^+ and Cl^- ions following Kohlrausch's law [18]:

$$\Lambda_m = \Lambda_0 - \kappa\sqrt{c} \quad (1)$$

where Λ_0 is termed the molar conductivity at infinite dilution. According to Kohlrausch's law, the molar conductivity plotted against the square root of concentration gives a linear relationship between conductivity and concentration in the range of concentrations below the level where interionic interactions has to be taken into account [18]. This is in agreement with present result for NaCl. However, in the case of the organic acid flux residue, the dissociation of ions is partial, and the conductivity dependence on concentration is non-linear (Figure 11.2 (a)). The dissociation constant and solution conductivity dependence on the concentration for weak electrolyte can be calculated from Ostwald's dilution law:

$$K_a = \frac{\Lambda_m^2}{(\Lambda_0 - \Lambda_m)\Lambda_0} c \quad (2)$$

The dissociation rate here is described as the ratio of the concentrations of the dissociated ions and the un-dissociated molecules. The negative of the logarithm of the acid dissociation constant

(pK_a) for weak organic acids common in the flux residues are presented in Table 11.2. The logarithm of dissociation constant of adipic acid is 4.43 and 5.41 for first and second dissociation respectively (Table 11.2). The larger the value of pK_a, the smaller is the extent of dissociation and the lower the conductivity.

Table 11.2: pK_a values for various weak organic acids usually used in no-clean fluxes at 25 °C

	Adipic acid	**Glutaric acid**	**Malic acid**	**Succinic acid**
Step 1	4.43	4.31	3.40	4.16
Step 2	5.41	5.41	5.11	5.61

The increase in concentration shifts the dissociation equilibrium in the direction of non-dissociated acid resulting in hindering of conductivity with increase in flux residue concentration. It causes the main difference in solution conductivity dependence on concentration for NaCl and WOAs in the flux residue. When comparing the leakage current at higher concentrations, the difference between NaCl and flux residue is further widened. This also can be attributed to polarisation effects on the surface of electrodes, whereas the conductivity measurements with AC voltage exclude the polarisation factor.

It is important to remember that the cleanliness predictability of PCBAs and its effect on corrosion reliability is measured using an AC method avoiding electrode polarisation (IPC-TM-650 method 2.3.25) method, while the surface insulation resistance uses a DC method that would result in electrode polarisation (IPC-TM-650 methods 2.6.3.3 and 2.6.3.7). The results reported above clearly demonstrate that the contamination level calculated in terms of NaCl equivalent from conductivity measurements need not necessarily match with the actual leakage current on PCBA surfaces, which can be purely a DC effect. Therefore, electrode polarization becomes a dominating factor. Further, defining the cleanliness level in terms of NaCl equivalent indirectly assumes that all the ionic contamination types contribute to the leakage current at similar levels, but this is seldom true, instead it depends more on the nature of the ionic residue (such as strong or weak ionic residue, and its effects on metal dissolution).

The discrepancy between conductivity and leakage current measurement is further illustrated in Figure 11.3, where the leakage current measured using the platinum electrode is compared with the leakage current calculated from the conductivity using Ohms law. Figure 11.3 shows higher current values calculated from the conductivity measurement for both electrolytes, however as expected the difference is much higher for flux residue. The main organic acid content in the present system is adipic acid, however the results are generally applicable to all organic acid based flux systems. Therefore, weak organic acids in solution usually adsorb on to the electrode surface, which can influence both the dissolution during corrosion of positively biased electrodes on a PCBA, and also influence the metal deposition during electrochemical migration [19], [20].

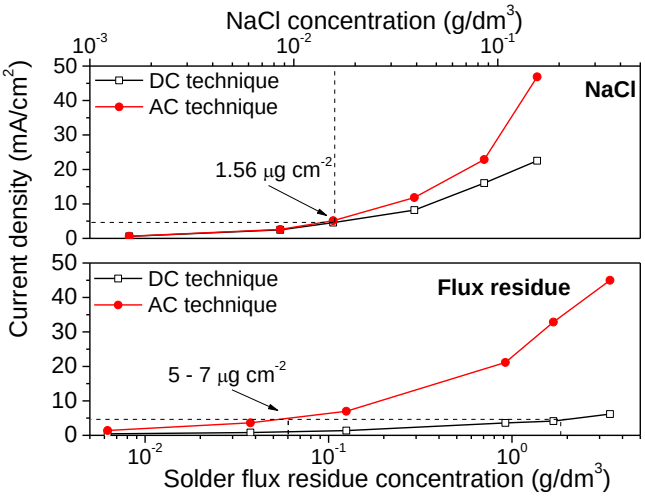

Figure 11.3: Current density dependence on concentration of NaCl and solder flux residues (equivalent between g·dm^{-3} and µg·cm^{-2} is selected with a ratio of 1:100 as is followed in the ECM test on single components)

Extrapolation of the leakage current for NaCl at a contamination level of 1.56 µg·cm^{-2} to that of the flux residue shows that about 3-5 times more flux residue is needed to create similar levels of leakage current as for NaCl. This is valid when comparing the leakage currents calculated using conductivity measurements; however, if the leakage current is directly measured using DC method the difference between the two electrolytes is higher and it requires nearly 100 µg·cm^{-2} of flux residue in order to get the same current density as for 1.56 µg·cm^{-2} NaCl. Therefore, the corrosion reliability of PCBAs is a DC effect for which the type of contamination is an important factor. Here we show that at very low levels of NaCl contamination can cause much higher leakage currents (Faraday current) than the equivalent levels of flux residue. Therefore, the correlation of contamination levels based on NaCl equivalent is not necessarily correct when the major contamination on a PCBA is organic acid based flux residue. In other words the magnitude of the leakage current on the board depends on the type of contamination.

Figure 11.4 shows the influence of temperature on conductivity of solutions with NaCl and organic acid flux residue. The temperature dependency of conductivity for solutions is related to the changes in properties of water and changes in dissociation rate of the electrolytes [18], [21]. The results show that the temperature dependence of conductivity, and therefore the expected leakage current, on PCBAs is determined by the type of contamination. The variation of temperature on the PCBA during use can reduce the reliability significantly if high humidity levels are present. It requires less contamination to cause the same reduction of surface insulation resistance as the temperature increases. As a result, increases the propensity of the leak currents, corrosion and premature failures in the circuits.

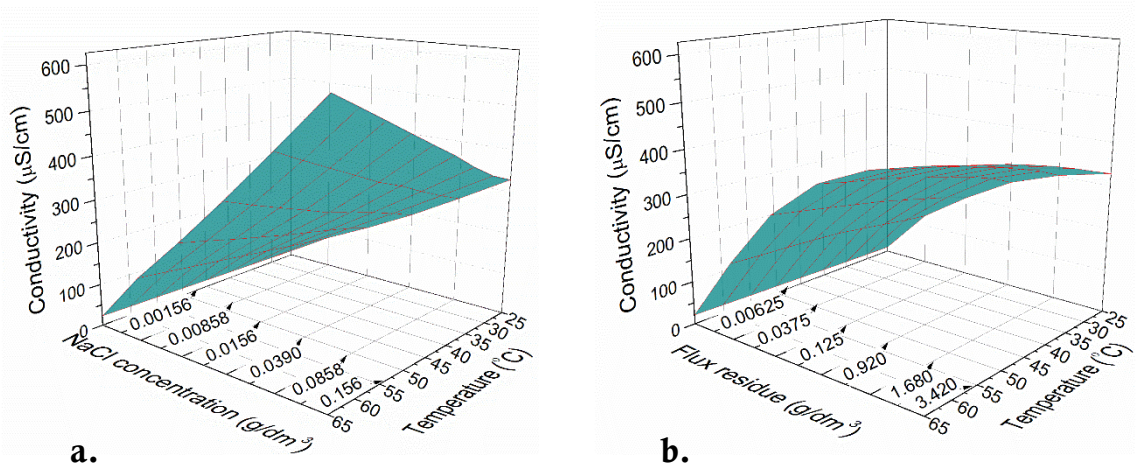

Figure 11.4: Conductivity dependence on temperature and concentration for: a. NaCl and b. solder flux residue

EFFECT OF SODIUM CHLORIDE AND FLUX RESIDUE ON ELECTROCHEMICAL MIGRATION

The influence of contamination levels on electrochemical migration was investigated using a droplet test method by placing microdroplet of solution (equivalent to concentration in $\mu g \cdot cm^{-2}$) on the single multilayer ceramic capacitor as described above. The leakage current between the terminals of the chip capacitor was measured at an applied 5 V DC voltage. A typical potentiostatic current-time curve from the experiment is shown in Figure 11.5. The base line current is representative of the current leaking though the solution between the terminals of the capacitor, while the peaks correspond to ECM, intermittent dendrite shorting, and breakdown of dendrites.

The current-time curves similar to the one shown in Figure 11.5 from various experiments were analysed for three parameters namely: (i) the number of components that showed ECM out of 18 components tested, (ii) the time to first appearance of dendrites, and (iii) the average level of current leaking through the dendrites after the electric short circuit.

Figure 7.5 shows the probability of ECM (i.e. the number of capacitors that showed migration out of 18 experiments in each category expressed as a percentage), and average dendrite current for NaCl and flux residue as a function of concentration. The average time to failure values corresponding to each set are shown on the bars.

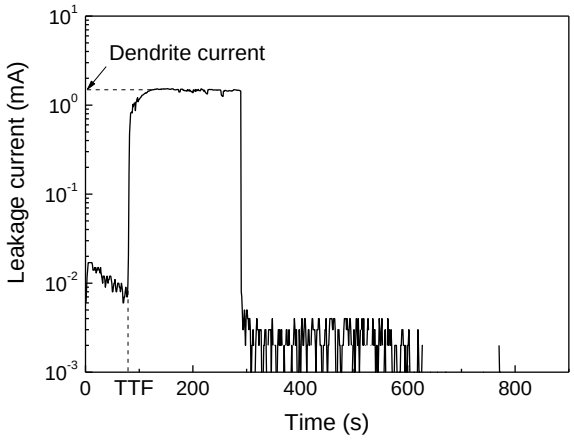

Figure 11.5: Typical potentiostatic current-time graph from ECM testing on 0805 multilayer ceramic capacitor

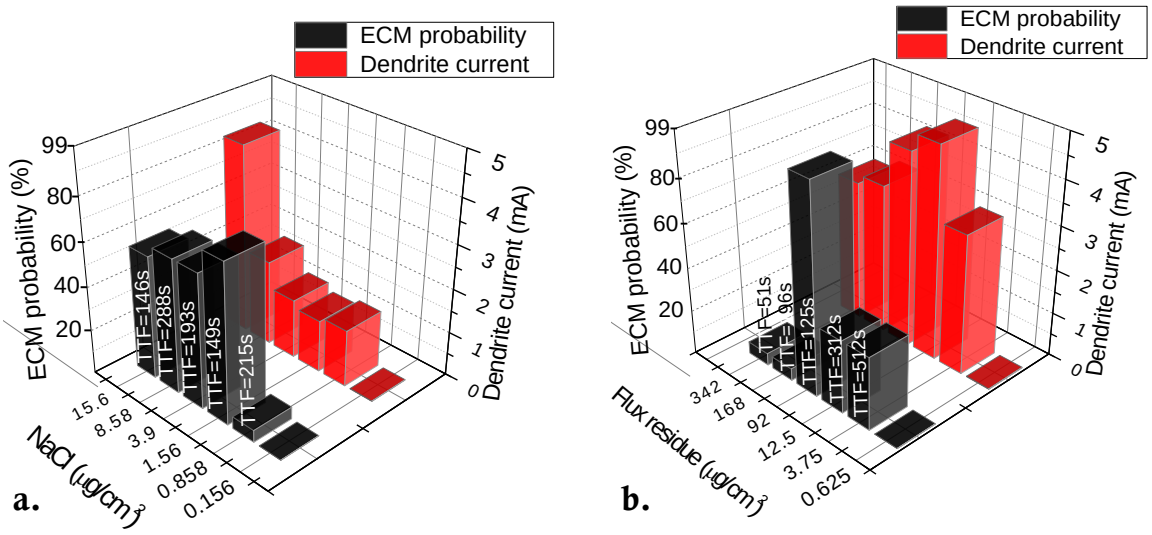

Figure 11.6: ECM probability and dendrite current as function of concentration: a. NaCl and b. flux residue

Figure 11.7 shows the morphology of the dendrite after the migration test for NaCl and the flux residue as a function of concentration. For NaCl, the probability of migration increases rapidly above a concentration of 0.858 µg·cm^{-2}. Below this level, the migration probability is low mainly due to the low dissolution rate of tin. Typical surface morphology of a component (Figure 11.7) shows very little corrosion products with white appearance. However, as the concentration of chloride increases, dendrites start appearing, and at very high concentration levels a mixture of dendrite and white precipitated species can be seen. At high chloride levels the probability of migration also slightly reduces due to the large amounts of dissolved tin ions in the solution which leads to heavy precipitation reducing the migration rate as reported in literature [15], [22]. The precipitated species can be hydroxides of tin namely $Sn(OH)_4$ and/or -$Sn(OH)_2$, although intermediate hydroxyl chloride species are also possible [23].

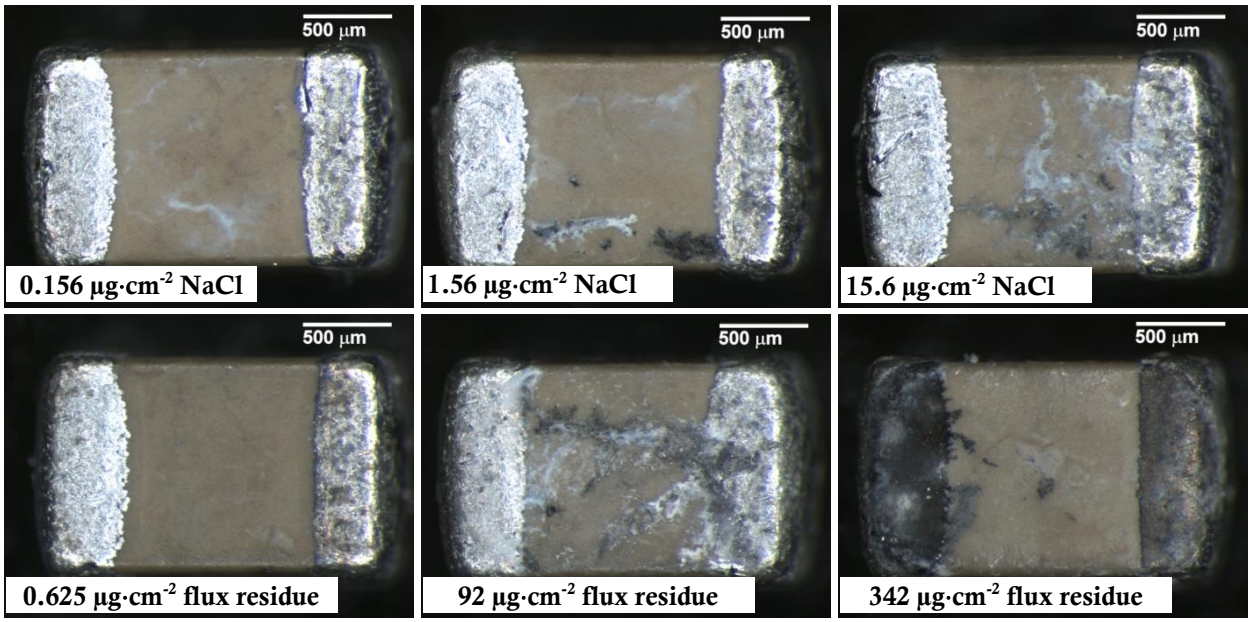

Figure 11.7: Size 0805 capacitors after ECM testing at 5 V DC (NaCl and solder flux residue concentrations are listed in images (anode: right terminal, cathode: left terminal))

Optical micrographs of representative tested components with flux residue (Figure 11.7) shows that the level of corrosion is negligible at lower concentrations, however at 92 µg·cm^{-2}, surface of the component shows a clear dendrite mixed with some hydroxides. The probability of ECM and dendrite growth was highest at this concentration (Figure 11.6). However, further increase in concentration caused only a low probability for migration, where the component showed few dendrite initiation points spread all over the cathode electrode surface and edges, resulting in a black appearance of the surface (Figure 11.7). Also heavy corrosion on the anode resulted in dissolution of the whole tin upper layer revealing Ni and Cu layer beneath.

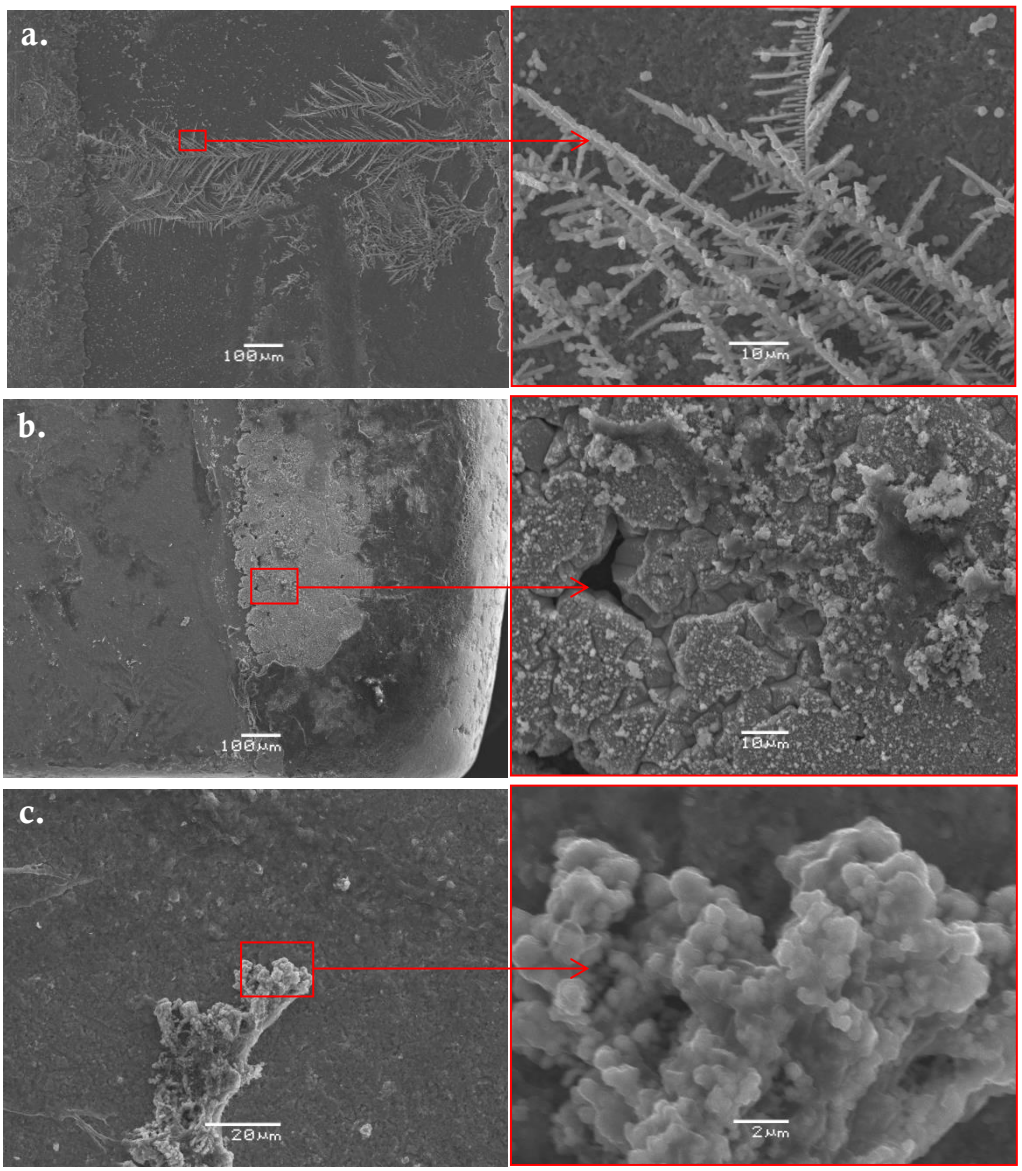

Figure 11.8: Typical SEM images of capacitor after ECM testing: a. tin dendrite on 0805 capacitor with flux residue level of 92 µg·cm^{-2}, b. corrosion of anode terminal, and c. deposition of corrosion product (black deposits) at nearby cathode terminal (b) and (c) are for 342 µg·cm^{-2} of flux residue

Optical microscope images at the highest concentrations of flux residue revealed heavy corrosion of anode terminal but no dendrites or precipitation of tin hydroxides as it was observed for NaCl. This appearance indicates that the pH level of solution was more acidic and thereby the

precipitation of tin hydroxides was thermodynamically unfavourable. The appearance of the capacitors shows that all the metal dissolved on the anode migrated towards cathode and deposited there as an oxide or hydroxide, however the dissolution, migration and precipitation of copper ions is also likely. It is known that the precipitation of tin as an oxide can create a passive film (e.g. cassiterite SnO_2),[24], which stability increases with dehydration of tin hydroxides [25]. This is further illustrated by the SEM picture shown in Figure 8. The appearance of black deposits near the cathode is shown in Figure 11.8 c., while Figure 11.8 b. shows heavy corrosion of the anodic terminal. The EDS analysis of composition of black deposits (Figure 11.8 c) showed high content of tin (65 wt.%) and oxygen (30 wt.%), and small amount of copper (5 wt.%).

The appearance of dendrite formation at flux residue concentrations between 3.75 $\mu g \cdot cm^{-2}$ and 92 $\mu g \cdot cm^{-2}$ is similar to the appearance of dendrites observed with NaCl. Optical microscope images revealed the dendrites of dark grey colour bridging the terminals and the white deposits – tin hydroxides (Figure 11.7).

The presence of copper indicates that the terminal is severely corroded. The electroplated layer of tin was heavily dissolved and the underlying layer of copper, which is the termination of multilayer ceramic capacitor [26], was exposed to electrolyte solution and thereby corroded. The EDS analysis of the corrosion products on the anode terminal indicated mainly tin (85 wt.%), however some amount of copper (20 wt.%) and small amounts of chromium (less than 5 wt.%) were identified. Both elements are known to be used as termination materials for multilayer chip capacitors [27]. They were identified on the very edges of the anode terminal, where the dissolution rate of metal is expected to be the highest.

The results revealed that the remaining solder flux on the components can accelerate ECM considerably if present at certain concentrations. The presence of no-clean solder flux residues at concentrations around 92 $\mu g \cdot cm^{-2}$ increases the migration probability on size 0805 ceramic capacitor to greater than 80 % under water droplet conditions. However, the probability of migration is reduced at both low and high concentrations of flux residues. At low concentration the behaviour is assumed to be due to the low dissolution of metal ions, while at high concentration the effect is due to over production of metal ions thereby precipitation of tin hydroxide dominates. The SEM/EDS analysis of the capacitors with high contamination revealed heavy deterioration of anode terminal and corrosion products on the cathode terminal indicating severely corrosive conditions that are, however, unfavourable for ECM.

In connection with the IPC standard of defining contamination level as NaCl equivalent, the results once again stress the point that the effect on ECM very much depend on the type of contamination (especially the difference between strong and weak electrolytes). The quantities of equivalent levels of flux residue defined by the conductivity measurements is not the critical limit at which the highest levels of migration could be found, but the concentration is more moved towards the corresponding equivalent concentration derived from the leakage current. The information provided here is based on the single organic acid flux system used in this investigation, but the reasoning behind the hypothesis is based on the general difference between strong and weak electrolytes, and difference of reactivity of chloride and carboxylic acid ions to corrosion, which in general could be applied to all flux systems based on weak organic acids.

EFFECT OF ELECTRIC FIELD ON ELECTROCHEMICAL MIGRATION

The effect of electric field in the range between 1 mV·μm^{-1} and 25 mV·μm^{-1} on the probability of electrochemical migration and dendrite formation was investigated at 1.56 μg·cm^{-2} and 15.6 μg·cm^{-2} concentrations of NaCl and on uncontaminated components, Figure 11.9. It is seen that the probability of migration initially increases with voltage until intermediate potential levels are reached after which further increase in potential shows a decrease in probability for migration. The electric field at which maximum probability of migration occurs is a function of NaCl concentration, however, it was found to be around 10 mV·μm^{-1} and 15 mV·μm^{-1}, which respectively was achieved under 10 V DC and 15 V DC voltage. Also the probability of migration in general was low at lower potential bias values such as 1 V - 2.5 V above which the probability increased drastically in solutions containing NaCl, while the probability of migration in the pure water remained low irrespective of the potential bias.

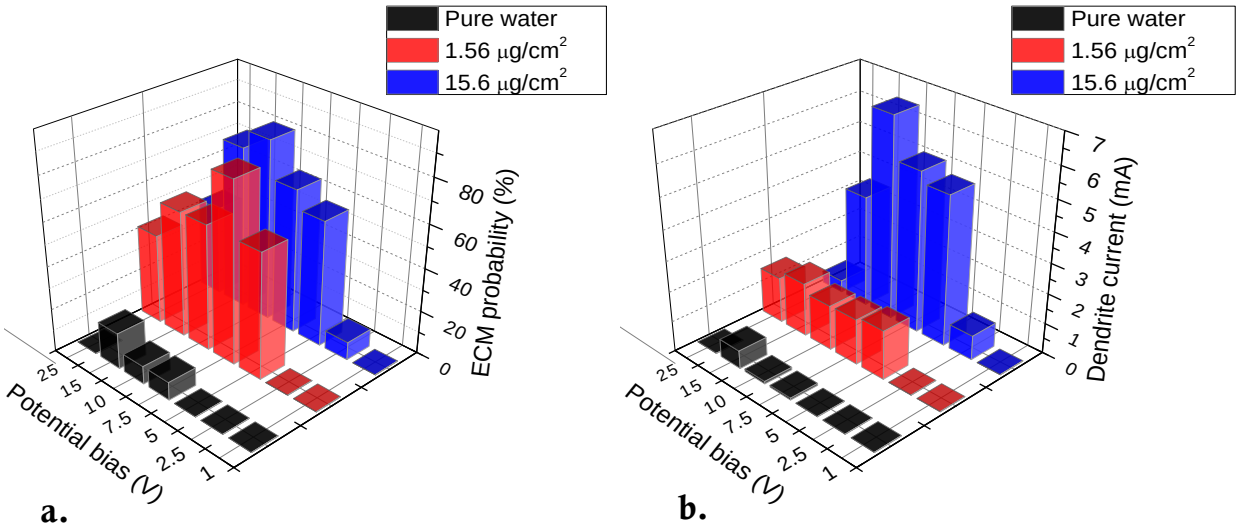

Figure 11.9: Effect of potential bias on: a. probability of ECM and b. dendrite current

In general the probability of migration showed a bell curve with an increasing trend initially followed by a decreasing trend above the maximum – similar to the trend found for increase in concentrations of contaminants. However, Figure 11.9 a. shows, the effect of contamination is more pronounced especially from pure water to 1.56 μg·cm^{-2} NaCl solution. The dendrite current also shows a similar behaviour except that a large increase occurs at a contamination level of 15.6 μg·cm^{-2} indicating the formation of thick dendrites unlike in other cases. It shows that increased contamination level increases the dissolution rate of the metal and consequently forms thicker and more branched dendrites containing more metal and hydroxide precipitation. As a result, the high amount of metal in the dendrites increases the current leaking through. However, as the potential increases, the probability of migration decreases, which also correlates with a decrease in the dendrite current. This is due to the fact that rate of dissolution of tin increases with increase in potential bias similar to increase in contamination. This leads to precipitation of the hydroxide species, while the heavy gas evolution at the anode and cathode also inhibit the formation of dendrite. Minzari et al. [15], [16] have reported similar phenomenon with increase in potential bias or contamination level.

Typical optical micrographs from the potential bias experiments are shown in Figure 11.10. A lack of observed dendrites on the components shown in Figure 11.10 does not mean that there is no migration at the corresponding potential level, instead the micrographs shown in Figure 11.10 shows some of the typical features observed in general at various potential levels. Micrograph for 1 V potential bias shows no dendrites, only a precipitated layer at the middle of the component indicating the transition between the acidic to alkaline side during the experiments where tin hydroxide is precipitated at the intermediate pH areas. The diffusion of the dissolved metal ions is mainly dependent on the effective electrical field strength [28]. It can be assumed that the electric field strength was insufficient enough for tin hydroxides to reach cathode terminal of the capacitor. It has also been reported that the threshold electric field under which the ECM will not occur is below 1 $mV \cdot \mu m^{-1}$ [4].

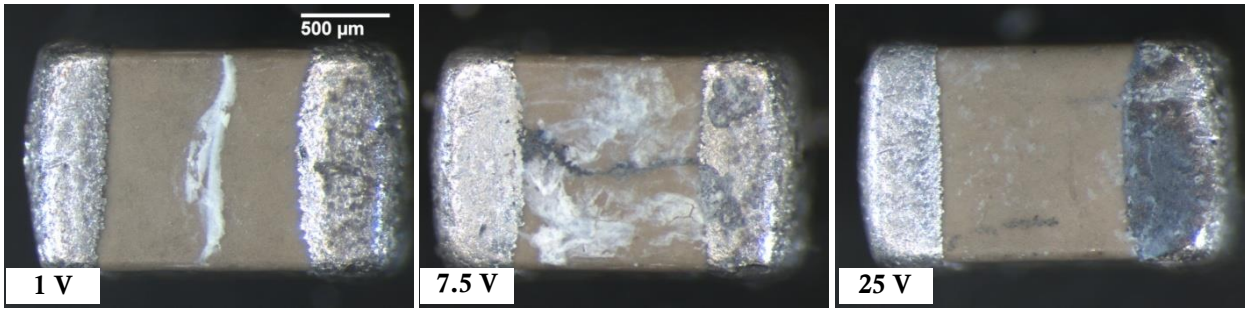

Figure 11.10: Appearance of chip capacitors after ECM testing at 1.56 $\mu g \cdot cm^{-2}$ of NaCl (applied voltages are listed on the images (anode: right terminal, cathode: left terminal))

An increase in electric field widens the precipitation of tin hydroxide, and also promotes the formation of dendrites (Figure 11.10 b). The increase in anode terminal corrosion and hydroxide precipitation is observed with increase of applied voltage in the range between 5–10 V. At very high voltages (Figure 11.10 c.), the anode terminal severely corrodes, but some fragile dendrite formation together with precipitation of hydroxide can be observed. Although the heavily corroded anode is indicating high rate of tin dissolution, the precipitation of hydroxide is overtaking the dendrite formation. This can be attributed to the insufficient alkaline conditions near the cathode to sustain the hexahydroxostannate ions $(Sn(OH)_6)^{2-}$, which are then reduced at the cathode to form dendrites. As the potential bias increases due to the dissolution of large amounts of tin ions, the alkaline boundary for the formation of $(Sn(OH)_6)^{2-}$ becomes unsustainable as reported by Minzari et al. [15]. It is known that tin can be oxidized to state +2 or +4 and form stannic compounds or be passivated if the appropriate conditions are established [25]. If the stannous or stannic ions are formed, they will be rapidly hydrolysed as various tin hydroxides through intermediate species, where $Sn(OH)_4$ is dominant [15], [25], [29]. The tin hydroxides will move towards the cathode and will experience the pH change from acidic at the anode to alkaline at the cathode [15]. The pH change to neutral area would tend to precipitate the hydroxides and this would initially reduce the migration unless the hydroxides are converted to ionic species that can be driven further towards cathode. The tin hydroxides close to cathode will experience alkaline environment and this will enable the formation of $(Sn(OH)_6)^{2-}$. The latter will be reduced and the tin ions will be deposited at the cathode [15].

PROBABILITY ANALYSIS OF ELECTROCHEMICAL MIGRATION RESULTS

The level and the type of ionic contamination are affecting the probability of electrochemical migration events and also the time to initiation. Figure 11.11 shows the cumulative per cent of migration versus time graphs for NaCl and solder flux residues.

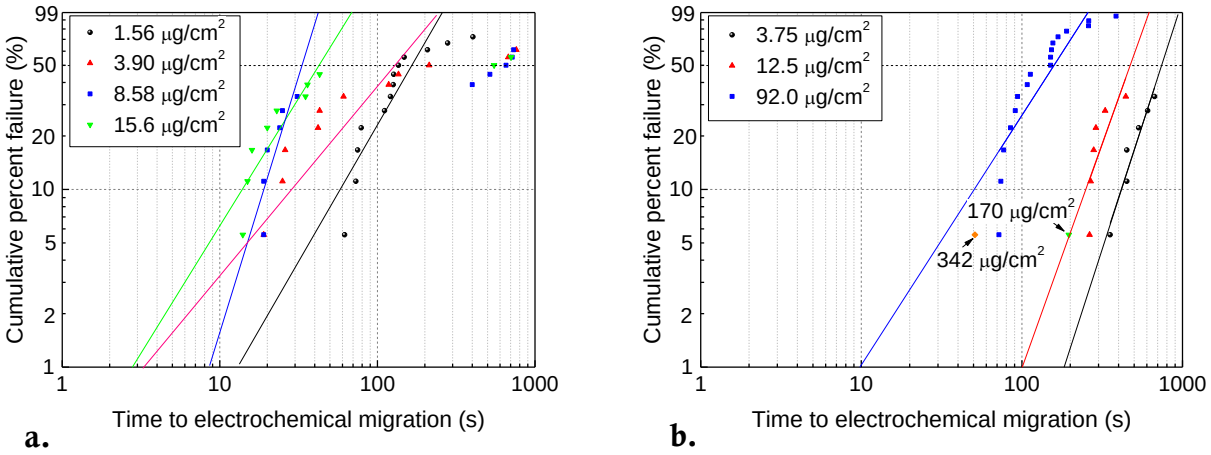

Figure 11.11: Cumulative failure dependence on time calculated from results of ECM: a. NaCl and b. solder flux residues

The increasing concentration in general shortens the time to a migration event (Fig. 11). This can be seen from a comparison of the time needed for 50 % of capacitors to show ECM as well as from the time to the first failure. In the case of NaCl, increase of concentration from 1.56 to 15.6 $\mu g \cdot cm^{-2}$ reduces the time to first failure accordingly: 62 s, 25 s, 19 s and 14 s. The presence of flux residues reduces the time to first ECM from 354 s to 72 s with increase of concentration from 3.75 to 92 $\mu g \cdot cm^{-2}$.

Overall, a decrease in time to failure and to some extent an increase in cumulative per cent failure with increasing level of contamination can be observed. However, there is a certain contamination limit below which the migration event probability is very low. This empirically ascertained limit for NaCl lies in the range 0.858 – 1.56 $\mu g\ cm^{-2}$, whereas for no-clean solder flux residues investigated in this work, the limit is broader where it starts with 3.75 $\mu g \cdot cm^{-2}$ with significantly low probability until it peaks around 92 $\mu g \cdot cm^{-2}$. The main difference between these two contaminants is the ECM behaviour at high concentrations, where for the flux residues it reduces drastically and no dendrites are formed, however in case of NaCl the 20 – 40 % probability for migration remains.

IV. CONCLUSIONS

1. Results show that the solvent extract test used for indexing contamination on PCBs needs to be carefully interpreted as it does not represents the actual leakage current on the board due to expected polarisation effects under DC bias. Current values obtained from solution conductivity measurement are higher compared to leakage currents measured through the solution using DC bias.
2. The level of organic acid flux residue equivalent to the IPC standard level of 1.56 $\mu g \cdot cm^{-2}$ NaCl depends on whether the measurement is based on conductivity or leakage current

through the solution. Quantitatively the equivalent conductivity is about 3–5 times higher than 1.56 $\mu g \cdot cm^{-2}$, while for leakage current equivalent it is approximately 50 times higher than for NaCl. The difference is due to electrode polarization effects during leakage current measurements.

3. The electrochemical migration probability distributions for NaCl and flux residue electrolytes have peak values corresponding to 72 % and 94 % showing migration. For NaCl, the migration probability tends to decrease with increase in concentration above the peak value; however, some level of migration probability remains. For solder flux residues an abrupt decrease of migration probability was observed above the peak value.
4. The influence of electric field on migration probability shows a similar type of dependency as for concentration (Gaussian character distribution). The peak values of migration probability at 1.56 and 15.6 $\mu g \cdot cm^{-2}$ of NaCl were observed at electric fields of 7.5 $mV \cdot \mu m^{-1}$ and 10 $mV \cdot \mu m^{-1}$. The dendrite current shows a tendency to increase with increasing concentration of NaCl.

V. ACKNOWLEDGMENTS

Current research has been conducted as part of the CELCORR/CreCon consortium (www.celcorr.com) and authors would like to acknowledge the funding and help from consortium partners.

VI. REFERENCES

[1] J. Henriksen, R. Hienonen, T. Imrell, C. Leygraf, and L. Sjögren, *Corrosion of electronics (A handbook based on experiences from nordic research project)*. Swedish Corrosion Institute, 1991, p. 86.
[2] R. Hienonen and R. Lahtinen, "Corrosion and climatic effects in electronics," *Vtt Publ.*, 2007.
[3] H. Schweigart, "Humidity and pollution effects on electronic equipment," *CEEES Publ.*, 2001.
[4] C. Schimpf, K. Feldmann, C. Matzner, and A. Steinke, "Failure of electronic devices due to condensation," *Microsyst. Technol.*, vol. 15, no. 1, pp. 123–127, Jun. 2009.
[5] Peter Biocca, "Flux chemistries and thermal profiling considerations in SMT assembly," in *National Electronic Packaging and Production Conference-Proceedings of the Technical Program (West and East)*, 1999, vol. 2, pp. 971–977.
[6] K. S. Hansen, M. S. Jellesen, P. Moller, P. J. S. Westermann, and R. Ambat, "Effect of Solder Flux Residues on Corrosion of Electronics," in *Annual reliability and maintainability symposium*, 2009, pp. 503–509.
[7] M. S. Jellesen, D. Minzari, U. Rathinavelu, P. Møller, and R. Ambat, "Corrosion failure due to flux residues in an electronic add-on device," *Eng. Fail. Anal.*, vol. 17, no. 6, pp. 1263–1272, Sep. 2010.
[8] S. Zhan, M. H. Azarian, and M. Pecht, "Reliability of Printed Circuit Boards Processed Using No-Clean Flux Technology in Temperature – Humidity – Bias Conditions," *IEEE Trans. Device Mater. Reliab.*, vol. 8, no. 2, pp. 426–434, 2008.
[9] C. Dominkovics and G. Harsányi, "Effects of Flux Residues on Surface Insulation Resistance and Electrochemical Migration," in *International Spring Seminar of Electronics Technology*, 2006, pp. 158–162.
[10] P.-E. Tegehall, "Impact of Humidity and Contamination on Surface Insulation Resistance and Electrochemical Migration," in *The ELFNET Book on Failure Mechanisms, Testing Methods, and Quality Issues of Lead-Free Solder Interconnects*, Springer, 2011, pp. 227–253.
[11] K. H. Lee, R. Jukna, J. Altpeter, and K. Doss, "Comparison of ROSE, C3/IC, and SIR as an effective cleanliness verification test for post soldered PCBA," *Solder. Surf. Mt. Technol.*, vol. 23, no. 2, pp. 85–90, 2011.
[12] J. E. Sohn and U. Ray, "Weak Organic Acids and Surface Insulation Resistance," *Circuit World*, vol. 21, no. 4, pp. 22–26, 1994.

[13] C. Hunt and L. Zou, "The impact of temperature and humidity conditions on surface insulation resistance values for various fluxes," *Solder. Surf. Mt. Technol.*, vol. 11, no. 1, pp. 36–43, 1999.
[14] K. G. Schmitt-Thomas and C. Schmidt, "The Influence of Flux Residues on the Quality of Electronic Assemblies," *Solder. Surf. Mt. Technol.*, vol. 3, no. 18, pp. 4–7, 1994.
[15] D. Minzari, M. S. Jellesen, P. Møller, and R. Ambat, "On the electrochemical migration mechanism of tin in electronics," *Corros. Sci.*, vol. 53, no. 10, pp. 3366–3379, Oct. 2011.
[16] D. Minzari, F. B. Grumsen, M. S. Jellesen, P. Møller, and R. Ambat, "Electrochemical migration of tin in electronics and microstructure of the dendrites," *Corros. Sci.*, vol. 53, no. 5, pp. 1659–1669, May 2011.
[17] D. Minzari, "Doctoral Thesis, 'Investigation of Electronic Corrosion Mechanisms,'" Technical University of Denmark, 2010.
[18] W. V. Carl H. Hamann, Andrew Hamnett, *Electrochemistry*, 2nd ed. Wiley-VCH, 2007.
[19] L. M. Vračar and D. M. Dražić, "Adsorption and corrosion inhibitive properties of some organic molecules on iron electrode in sulfuric acid," *Corros. Sci.*, vol. 44, no. 8, pp. 1669–1680, 2002.
[20] P. Kern and D. Landolt, "Adsorption of organic corrosion inhibitors on iron in the active and passive state. A replacement reaction between inhibitor and water studied with the rotating quartz crystal microbalance," *Electrochim. Acta*, vol. 47, no. 4, pp. 589–598, Nov. 2002.
[21] L. T. Vlaev, S. D. Genieva, and M. P. Tavlieva, "Concentration Dependence of the Activation Energy of Conductivity in Aqueous Sodium Selenite and Potassium Tellurite," *J. Struct. Chem.*, vol. 44, no. 6, pp. 995–1000, 2003.
[22] D. Minzari, M. S. Jellesen, P. Møller, P. Wahlberg, and R. Ambat, "Electrochemical Migration on Electronic Chip Resistors in Chloride Environments," *IEEE Trans. Device Mater. Reliab.*, vol. 9, no. 3, pp. 392–402, 2009.
[23] M. Drogowska, L. Brossard, and H. Menard, "Influence of temperature on the electro-dissolution of tin in NaCl aqueous solution at pH4," *J. Appl. Electrochem.*, vol. 20, no. 1, pp. 150–156, Jan. 1990.
[24] H. H. Hassan and K. Fahmy, "Pitting Corrosion of Tin by Acetate Anion in Acidic Media," *Int. J. Electrochem. Sci.*, vol. 3, pp. 29 – 43, 2008.
[25] S. S. Abdel Rehim, S. M. Sayyah, and M. M. El Deeb, "Corrosion of tin in citric acid solution and the effect of some inorganic anions," *Mater. Chem. Phys.*, vol. 80, no. 3, pp. 696–703, Jun. 2003.
[26] T. Williams, *The circuit designer's companion*, Second. (EDN Series for Design Engineers), 2005, p. 341.
[27] Y. Lee, W. Lu, and F. Shieu, "Investigation of thin film end-termination on multilayer ceramic capacitors with base-metal-electrode," *Ceram. Int.*, vol. 35, no. 2, pp. 869–874, Mar. 2009.
[28] S. J. Krumbein, "Metallic electromigration phenomena," *IEEE Trans. Components, Hybrids, Manuf. Technol.*, vol. 11, no. 1, pp. 5–15, Mar. 1988.
[29] S. Lee, M. Jung, H. Lee, and Y. Joo, "Effect of Initial Anodic Dissolution Current on the Electrochemical Migration Phenomenon of Sn Solder," in *Electronic Components and Technology Conference*, 2009, pp. 1737–1740.

12. EFFECT OF PULSED VOLTAGE ON ELECTROCHEMICAL MIGRATION OF TIN IN ELECTRONICS

Vadimas Verdingovas, Morten Stendahl Jellesen, and Rajan Ambat

Abstract—The effect of pulsed voltage on electrochemical migration of tin was studied on size 0805 surface mount capacitors. The study was performed under water droplet condition using 0.0156 $g \cdot L^{-1}$ and 0.156 $g \cdot L^{-1}$ concentrations of NaCl. The amplitude and the offset of rectangular shape pulse were fixed respectively at 10 V and 5 V, while the duty cycle and the pulse width were varied in the range of ms. The results showed that varying of pulse width at fixed duty cycle has a minor effect under investigated conditions, whereas increasing duty cycle significantly reduces the time to short due to dendrite formation and increases the charge transferred between the electrodes over time. With increase of duty cycle, increases the anodic dissolution of tin, which was visualized using a tin ion indicator applied on the components prior to applying the voltage. The anodic dissolution of tin significantly influences the dendritic growth, although a tendency for more hydroxide precipitation was observed for lower duty cycles. The precipitation of tin hydroxides was identified as influencing factor for the reduction of charge transfer under pulsed voltage with low duty cycles, therefore resulting in the suppression of dendrite growth.

Keywords—Electrochemical migration, Dendrite growth, Pulse voltage, Surface mount, Leakage

I. INTRODUCTION

Electrochemical migration (ECM) is a corrosion failure mechanism which causes threat for reliability of electronics operating under humid conditions, or when condensation on the printed circuit boards is likely to occur. Due to the formation of thin continuous water layer connecting oppositely biased electrodes on the printed circuit board and the electric field acting through the medium, the dissolved metal ions from the anode will migrate towards the negatively biased electrode. At the negative electrode, the metal ions will get reduced, which results in the growth of metallic dendrites. As the metallic dendrites growing from the cathode reaches the anode, they cause short-circuiting, and depending on the morphology of the dendrites and level of leakage current, the device will exhibit intermittent or permanent failures.

The rate at which dendrites can be formed is first dependent on the intrinsic property of metal/solder alloy especially the solubility of metal hydroxides [1], [2], and a number of investigations were performed to rank common metallic alloys on the printed circuit board assembly (PCBA) [2]–[4]. However, the process of ECM can be also influenced by the ionic contamination dissolved in the water layer [5]–[7], pH level, bias voltage [3], [8], and the distance between the electrodes [9], [10]. The conductivity of the water layer adsorbed on a PCBA is determined by the ionic contamination present on the surface as it affects the ion transport between the anode and cathode. The electric field between the electrodes is the driving force for metal ions dissolution, transport, and consequent reduction at the cathode. Potential bias at the electrodes can also dissociate water molecules thereby changing the local pH at the electrodes [5].

V. Verdingovas, M. S. Jellesen, and R. Ambat, "Effect of pulsed voltage on electrochemical migration of tin in electronics," *J. Mater. Sci. Mater. Electron.*, vol 26, no. 10, pp. 7997-8007, 2015.

The concentration of metal ions and the pH of the electrolyte determine the stability of metal, ions, and hydroxides/oxides in the solution [5]. The anodic dissolution of tin plays a significant role in ECM kinetics [11], however a certain pH and bias conditions within the water layer has to be established in order for the metal ions to be transported and reduced at the cathode [5].

The effect of electrochemical factors influencing the ECM has been investigated in a number of studies. The tests are typically performed under water droplet condition [2]–[7], thin electrolyte layers [12], [13], or at elevated humidity/temperature conditions [14]–[17]. The test specimens usually used are the surface insulation resistance (SIR) patterns and surface mount components [5]–[7]. Most of the studies focuses on ECM under DC voltage, however, AC or pulsed voltage are also common voltage signals in the electronics, yet relatively low attention has been drawn onto ECM under these conditions.

Climatic testing at 40°C/93%RH of SIR patterns with a Cu finish, precontaminated with solder flux, and biased with 5V AC at 50 Hz [18], indicated insufficient time on each AC cycle to bridge the conductive tracks by the dendrites. The dissolution and precipitation was observed on all the biased tracks and it was concluded that the bias condition was unfavourable for the dendrite formation. Another study of silver migration conducted under similar climatic conditions [19] indicated effect of AC frequency on ECM. The formation of deposits similar to initiation of dendrite growth was detected at 60 Hz, however it was not observable with an increase of frequency to 400 Hz. Investigation of ECM under water droplet condition at 10 V AC in the frequency range of 10 Hz – 480 Hz [20] showed that bridging of the electrodes occurs due to corrosion products forming on each electrode finally closing the gap between the electrodes [21]. The observation is in contrast with dendrite formation mechanism, where the metallic deposits are forming on the cathode and growing towards anode under DC voltage. The deposit formation under AC voltage resulted in significant increase in time to failure with increase of frequency [20].

It is also known that the pulsed voltage can affect the dendritic growth in Li-metal batteries, which has some similarities to the present case. The surface morphology of negative electrode in the battery has been found to have a significant role in the formation of lithium dendrites [22]. However, the dendrite growth can be suppressed by using pulsed charging [23]–[25]. The safety of the battery can also be improved by periodic interruption of steady charging current with short and high-current discharge pulses [26]. In general, a hindering effect on dendrite formation with increase of time ratio t_{OFF} / t_{ON}, and for decreasing time t_{ON} can be deduced from the findings. The findings are connected to the compromise between the timescales for cation diffusion and reduction at the negative electrode [23].

The effect of pulsed voltage on the ECM on the printed circuit boards has been seldom reported and the suppression effect based on the ON/OFF situation is not yet clear. A study conducted under thin electrolyte layer using unipolar square wave showed a decrease of tin dendrite growth and precipitate formation with decrease of duty cycle t_{ON} /(t_{ON} + t_{OFF}) [27], thereby indicating the advantage of longer t_{OFF} cycles for prolongation of time to failure (TTF). The aim of the current study is to investigate the effect of pulsed voltage on the suppression of tin dendrites formation under water droplet conditions. Following parameters are of interest in this study: TTF, current passing through the dendrites at the event of bridging the electrodes, and the total charge transfer between the terminals of the component as a function of time. The influencing parameters are compared in relation to the tin dissolution under investigated pulse conditions. The investigation is conducted on size 0805 multilayer ceramic chip capacitors.

II. MATERIALS AND METHODS

SURFACE MOUNT COMPONENTS

The study was performed on size 0805 multilayer ceramic chip capacitors (470 pF, 200 V, X7R). The capacitors were reflow soldered on the test PCBA, the detailed description of which can be found elsewhere [17]. The average distance between the terminals of chip capacitors is 0.91 ± 0.05 mm (a slight variation between the distances at the centre and at the edges). The terminals are made of pure tin, as it was confirmed by SEM EDS. For statistical analysis, 10 components were used for each set of pulsed voltage parameters and NaCl concentration.

ELECTROLYTE SOLUTION

Two concentrations of NaCl electrolyte solutions were used for testing: 0.156 $g \cdot L^{-1}$ and 0.0156 $g \cdot L^{-1}$. The electrolytes were prepared using Millipore water with resistivity of 18.2 MOhm·cm at 25 °C. The droplet of desired electrolyte solution was applied on the surface mount capacitor with a micropipette. The volume of the droplet was confined to the surface area of the component e.g. 2.4 µL of solution was applied on size 0805 component with approximate surface area of 2.4 mm^2. The resulting approximate contamination levels were 15.6 $\mu g \cdot cm^{-2}$ and 1.56 $\mu g \cdot cm^{-2}$ of NaCl. The tests were performed at ambient conditions where the temperature was 24 ± 1 °C and humidity was 55 ± 5 % RH.

PULSED VOLTAGE AND CURRENT MEASUREMENT

The voltage applied on the surface mount capacitor for testing was generated with single channel arbitrary/function generator "Tektronix AFG 3021B". The current between the terminals of the capacitor was measured with "Bio-logic VSP" electrochemical workstation. A rectangular shape pulse with varying duty cycle, while fixed amplitude and offset of 10 V and 5 V respectively was applied on the components. The summary of the voltage parameters is given in Table 12.1.

Table 12.1: Settings of the pulsed voltage

Experiment with fixed duty cycle				**Experiment with varying duty cycle**			
Period, ms	**t_{ON}, ms**	**t_{OFF}, ms**	**D**	**Period, ms**	**t_{ON}, ms**	**t_{OFF}, ms**	**D**
10	5	5	0.5	-	-	-	1
100	50	50	0.5	250	200	50	0.8
200	100	100	0.5	300	200	100	0.67
400	200	200	0.5	300	100	200	0.33
2000	1000	1000	0.5	250	50	200	0.2

The duty cycle D in Table 12.1 is corresponding to the ratio of time on t_{ON} as a fraction of cycle time T and is given by eq. (1):

$$D = \frac{t_{ON}}{t_{ON}+t_{OFF}} = \frac{t_{ON}}{T} \quad (1)$$

IN SITU OBSERVATION OF TIN DISSOLUTION AND LOCAL PH CHANGE

A universal pH indicator (indicator range: pH 3-10, Sigma-Aldrich) and a tin ion indicator (Sigma-Aldrich) was used respectively for visualization of pH change and tin ion dissolution on the components under different pulsed voltage conditions. The preparation of the gel and

indicator was as following: i) agar gel (type A7921, Sigma-Aldrich) was added into the Millipore water with conductivity of 18.2 MOhm·cm at 25 °C at concentration of 1 $g \cdot L^{-1}$, ii) the solution of water and agar was stirred at temperature of 90°C, and iii) the change of colour of the liquid to transparent indicates complete dissolution of agar powder, and the desired indicator is added while solution is stirred. The pH formation and tin ion dissolution was visualized by placing a droplet of solution containing desired indicator on the top surface of the component, then applying voltage with characteristics of interest. The *in situ* images of the pH change and tin ion dissolution throughout experiment were taken using a "AD7013MZT Dino-Lite" digital microscope.

III. RESULTS

Figure 12.1. shows characteristic curves for the current measurement under pulsed voltage (b and c) and respective *in situ* micrographs (a) showing dendrite growing and braking off. The initiation of tin dendrite growth at the cathode is shown in the images 1-2, and it is followed by a marginal increase in current. Whereas a major increase in current is observed when the terminals of capacitor are bridged by the dendrite, as shown in the image 3. In this case, the current increase of more than 20 % for more than 100 ms is accepted as time to failure (TTF), and this parameter is used for analysis of the results. Further, the level of current passing through a dendrite once it bridges the electrodes (dendrite current) is analyzed. For this measure, ~75% of the highest current observed throughout the measurement is reported. The base current determined by the ionic conductivity of the electrolyte can also be read from the curve in Figure 12.1 b.

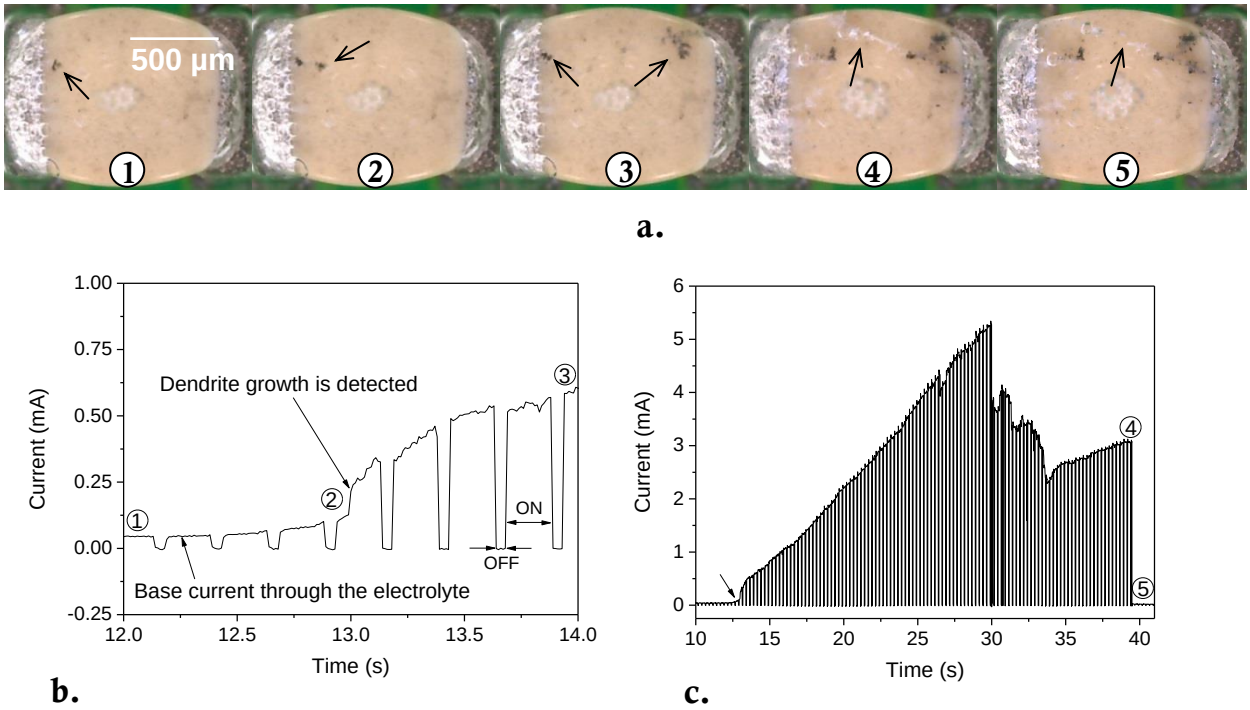

Figure 12.1: Current measurement on size 0805 capacitor with pulsed voltage (t_{ON} = 200 ms, t_{OFF} = 50 ms), at 1.56 $\mu g \cdot cm^{-2}$ of NaCl: a. *in situ* micrographs (time is accordingly indicated in the graphs), b. expanded view of the graph showing details of the pulse and increase in current detected due to dendrite growth, TTF in this example is 13 sec, c. overall view of current vs. time curve

Overall view of current vs. time curve in Figure 12.1 c. indicates typical variation in the current through the dendrite(s). The example shows possible reduction in the current to the base level (number 5 in Figure 12.1 c.), indicating dendrite burn off (arrow in image 5). The time integral of current provides the quantity of charge transferred throughout the duration of experiment. The charge transferred indicates the extent of dendritic growth under applied bias condition, and it was used as part of the analysis of the results.

EFFECT OF DUTY CYCLE ON TTF

Figure 12.2 summarize the effect of duty cycle on the time when first dendrite growth was detected (denoted as TTF) during test on surface mount capacitor tested at two concentrations of NaCl. The results of TTF are presented as Weibull percentiles of the capacitors which exhibited dendrite growth. The number of experimental points in the graphs represents the number of components which exhibited dendritic shorts out of 10 components tested (e.g. for 1.56 μg·cm^{-2} of NaCl: 10 out of 10 for DC voltage, and 7 out of 10 for 50/250 pulse condition).

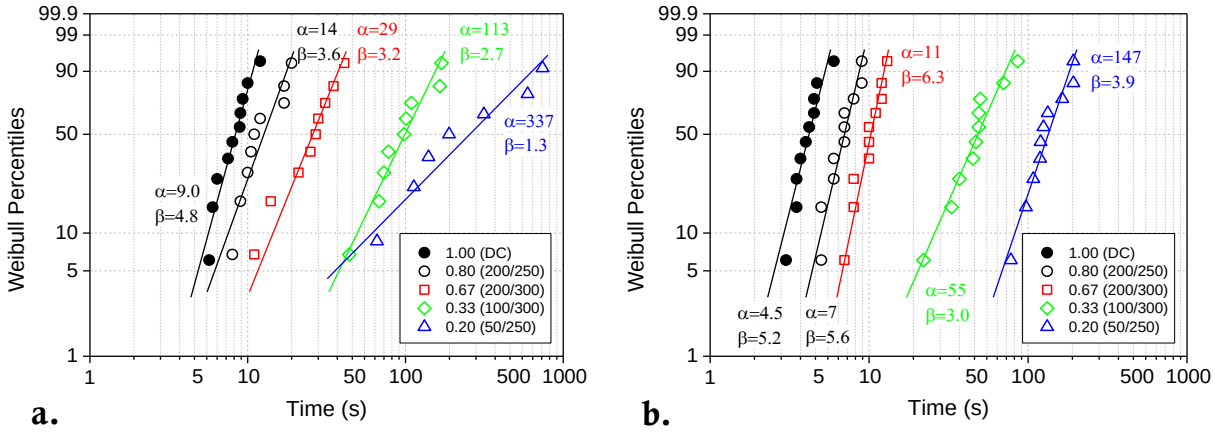

Figure 12.2: Weibull percentiles of time to dendrite detection for varying duty cycle and two concentrations of NaCl: a. 1.56 μg·cm^{-2}of NaCl, b. 15.6 μg·cm^{-2}. (in brackets (t_{ON}/T))

Increased duty cycle reduces the time to dendrite formation, as it is reflected by the scale parameter α indicated in the graphs. The parameter α, also known as characteristic life, is equal to the time when 63.2 % of samples have failed. In the case of β > 1, characteristic life is approximately equal to mean-time-to-failure [28]. The shape parameter β indicates whether the failure rate is increasing (β > 1), constant (β = 1) or decreasing (β < 1). In all the cases observed in this work, the shape (or the slope) parameter β was higher than 1, indicating increasing rate of TTF. At low concentration of NaCl as shown in Figure 12.2 a, a steady reduction of β with reduction of duty cycle was observed. This indicates a suppression effect of decreasing duty cycle on dendrite formation as it reduced the rate of the dendrite formation (number of capacitors exhibiting dendrite formation per time interval). However, with increase of NaCl concentration (graph in Figure 12.2 b) instead of a steady decrease of β with decrease of duty cycle, a slightly higher β parameters were observed for the pulse characteristics with duty cycle D = 0.8 and 0.67 compared to that of duty cycle D = 0.33 and 0.2.

EFFECT OF PULSE WIDTH ON TTF

Figure 12.3 summarizes the effect of pulse width for the constant duty cycle (D = 0.5) on the ECM on size 0805 capacitor measured at two concentrations of NaCl. The results show a negligible effect of the variation of the pulse width in the range from 50 ms to 1000 ms on the time to dendrite formation. For the concentration of 1.56 µg·cm^{-2} of NaCl, the scale parameter α varied between 30 s and 56 s, while in the case of 15.6 µg·cm^{-2} of NaCl α varied between 12 and 16. On average a slightly higher shape parameter β was observed for 15.6 µg·cm^{-2} of NaCl reflecting slightly higher rate of failure for this level of contamination. However, more scattered TTF was observed at 5/10 pulsed voltage at 1.56 µg·cm^{-2} of NaCl (Figure 12.3 a.). A significantly higher TTF was observed for three of the components under t_{ON} = 5 ms and t_{OFF} = 5 ms condition.

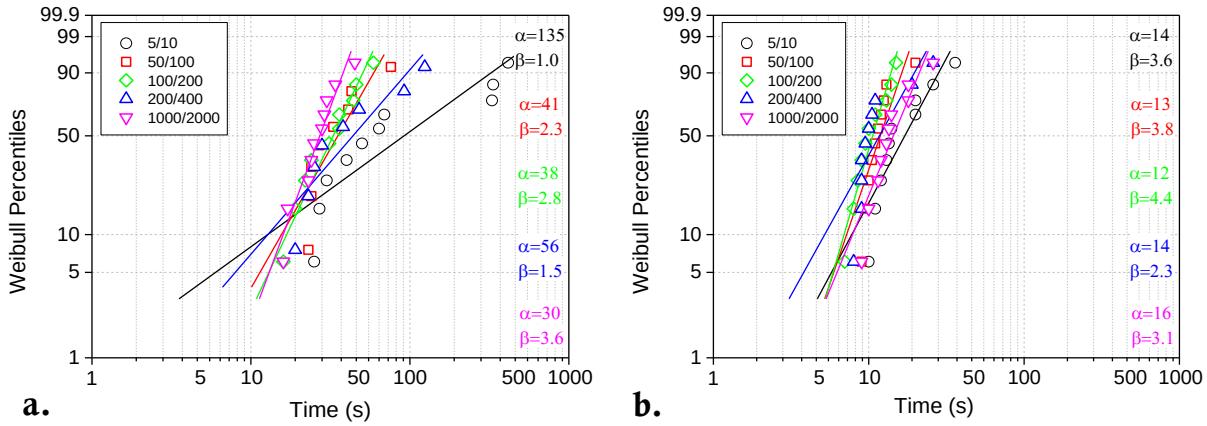

Figure 12.3: Weibull percentiles of time to dendrite detection for fixed duty cycle and two concentrations of NaCl: a. 1.56 µg·cm^{-2}of NaCl, b. 15.6 µg·cm^{-2}

EFFECT OF PULSED VOLTAGE ON DENDRITE CURRENT

The morphology of dendrites e.g. thickness and the density of the branches determines the current they can conduct. The average of the dendrite currents observed on the chip components which showed dendrite formation under different pulse characteristics is shown in Figure 12.4. A trend of increase in dendrite current with increase of duty cycle can be observed for the 15.6 µg·cm^{-2} of NaCl. For the 1.56 µg·cm^{-2} of NaCl, the dendrite current varies between 2 mA and 5 mA on average, while with increase of NaCl concentration, the current increases from 4 mA to 17.5 mA. At 15.6 µg·cm^{-2} of NaCl, the magnitude of dendrite current under 200/250 pulse condition was comparable to the dendrite current measured

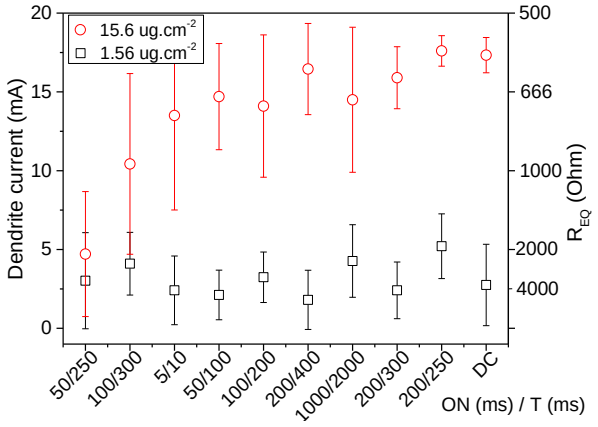

Figure 12.4: Average dendrite current and equivalent resistance measured on size 0805 capacitor at two concentrations of NaCl (standard deviation is indicated in the graph)

with applied DC voltage. The equivalent resistance for higher concentration of NaCl is in the range of hundreds of Ohms and it increases to the kOhm level for the lower concentration of NaCl.

CHARGE VS TIME UNDER PULSED VOLTAGE

The charge transferred between the electrodes of the component is an indicative measure of the dendrite thickness and the rate of dendrite formation/"breaking off" due to high current. Figure 12.5 indicates the average charge transferred between the terminals of the capacitor with time measured with different pulse width and period for two concentrations of NaCl. As it is seen, increase of duty cycle increases the total charge transferred and decreases the time until a sharp increase of charge was measured (arrows in the main graphs in Figure 12.5). The sharp increase in charge transferred between the electrodes is a characteristic of short circuiting due to dendrites bridging the electrodes, thus it is comparable to the first TTF in the Weibull graphs in Figure 12.2 and Figure 12.3.

The graphs for multiple pulse width with the fixed duty cycle (D = 0.5) are presented in the upper right corner of Figure 12.5. Curves indicate a sharp increase of charge transferred at 23-25s and at 8-10s for 1.56 μg·cm^{-2} and 15.6 μg·cm^{-2} of NaCl respectively. The time intervals are again comparable to the results observed in Weibull graphs. For the lower concentration, 5/10 settings appeared to cause highest charge, while no clear trend of the effect of pulse period was possible to identify for the 50/100, 100/200, 200/400, and 1000/2000 pulses. Whereas, in the case of 15.6 μg·cm^{-2} of NaCl (graph in insect in Figure 12.5 b) a slight decrease of charge with increase of pulse period could be noticed. A significantly higher (more than 2 times for the readings at 240 seconds) charge was measured at 5/10 pulse settings and the observation complies with the observation at 1.56 μg·cm^{-2} of NaCl.

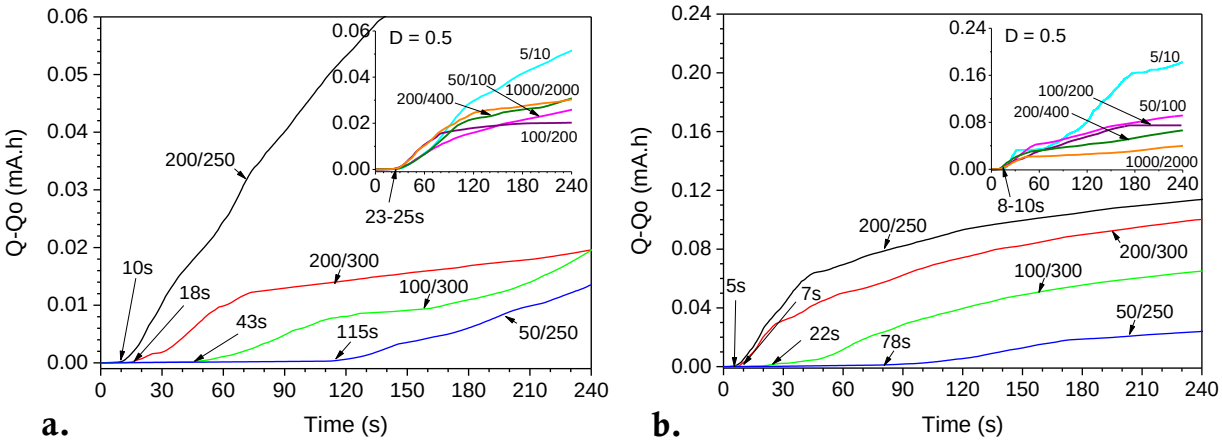

Figure 12.5: Average charge transferred between the terminals of component vs time obtained under various pulse conditions for two concentrations of NaCl: a. 1.56 μg·cm^{-2}, and b. 15.6 μg·cm^{-2}

The results in Figure 12.5 are directly indicating prolongation of the time to migration and lowering of the charge transferred between the electrodes with the reduction of duty cycle. Based on the knowledge about ECM, this observation can be expected, and it is related to the increase of the OFF time. However, in order to emphasize the effect of pulsed voltage conditions rather

than prolongation of the OFF time on the charge transferred, the curves in Figure 12.6 were normalized with respect to the ON time, as indicated on the X-axis (Figure 12.6). The curves are compared in regard to the time when the potential bias was applied to the components e.g. in order to compare the charge transferred after 30 seconds of ON cycle, it would require 150, 150, 300, and 600 cycles with the settings of 200/250, 200/300, 100/300 and 50/250 respectively. This will result in comparison of the components after test times of 37.5, 45, 90, and 150 seconds respectively. The time relationship between the cycles was used to construct the graphs in Figure 12.6. For reference, the charge measured under DC voltage is also included in the graphs.

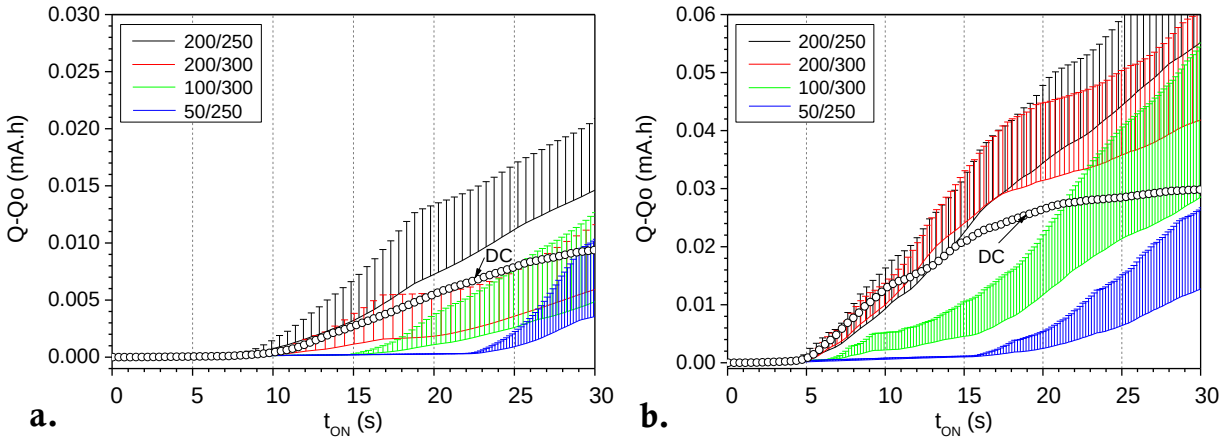

Figure 12.6: Relative comparison of charge transferred throughout ON cycle for various pulsed voltage characteristics: a. 1.56 μg·cm^{-2}, and b. 15.6 μg·cm^{-2} of NaCl. For easier readability of the graphs only the positive part of standard deviation is shown in the graph

From the normalized curves in Figure 12.6, it can be seen that the time to ECM with duty cycles 0.8 and 0.67 (200/250 and 200/300) is very similar compared to the DC voltage. The observation was valid for both concentrations of NaCl. It is important to note, the charge transferred with the pulsed voltage with high duty cycle e.g. 0.8 and 0.67 for 15.6 μg·cm^{-2} of NaCl, also 0.8 for 1.56 μg·cm^{-2} of NaCl, appeared to be higher compared to the DC voltage. On the other hand, the prolongation of the TTF and lower charge was evident from the normalized graphs in Figure 12.6 for the pulses with the duty cycles of 0.33 and 0.2 (100/300, 50/250). This observation indicates suppression effect of current pulse conditions on the dendrite formation.

OPTICAL OBSERVATIONS

During ON cycle, the voltage applied on the component is significantly higher than the potential for dissociation of water molecules resulting in evolution of hydrogen and oxygen gas, and accordingly changes in local pH at the electrodes. The detailed mechanism of pH change during ECM is beyond the scope of this paper and can it be found elsewhere [5]. However, the representative *in situ* local pH change at the electrodes for constant 10 V DC condition as a function of time is shown in Figure 12.7 along with *in situ* visualization of Sn dissolution from the electrode using the indicator method. Figure 7 shows the increase of local concentration of tin ions from anode towards cathode with increase in test time. Corresponding pH change shows the buildup of alkaline conditions at the cathode and acidic conditions at the anode.

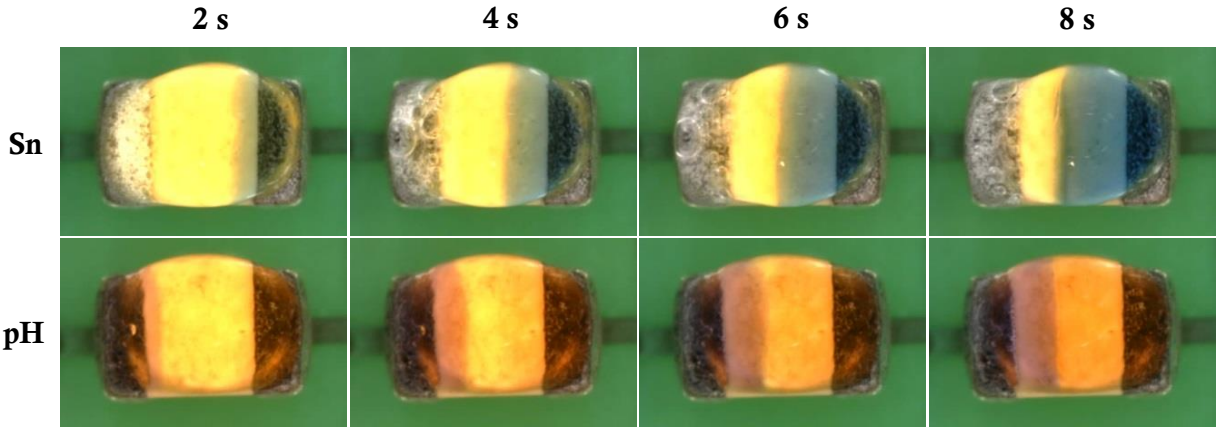

Figure 12.7: Dissolution of tin and local pH change observed on the component biased with 10 V DC (anode is on the right side)

Figure 12.8 shows the tin ions buildup as a function of duty cycle. The images clearly indicate the difference in the amount of tin ions being dissolved as well as the distance at which the ions migrated from the anode towards the cathode. The movement of ions from anode to cathode is a function of the electric field established between the electrodes during ON cycle plus the concentration gradient driven shift during the OFF cycle. The blue coloration on the components reflects the timing of the ON cycle, as it is clearly seen in Figure 12.8 d. A close comparison of the pictures shows that the spreading of tin ions increases with decrease in duty cycle.

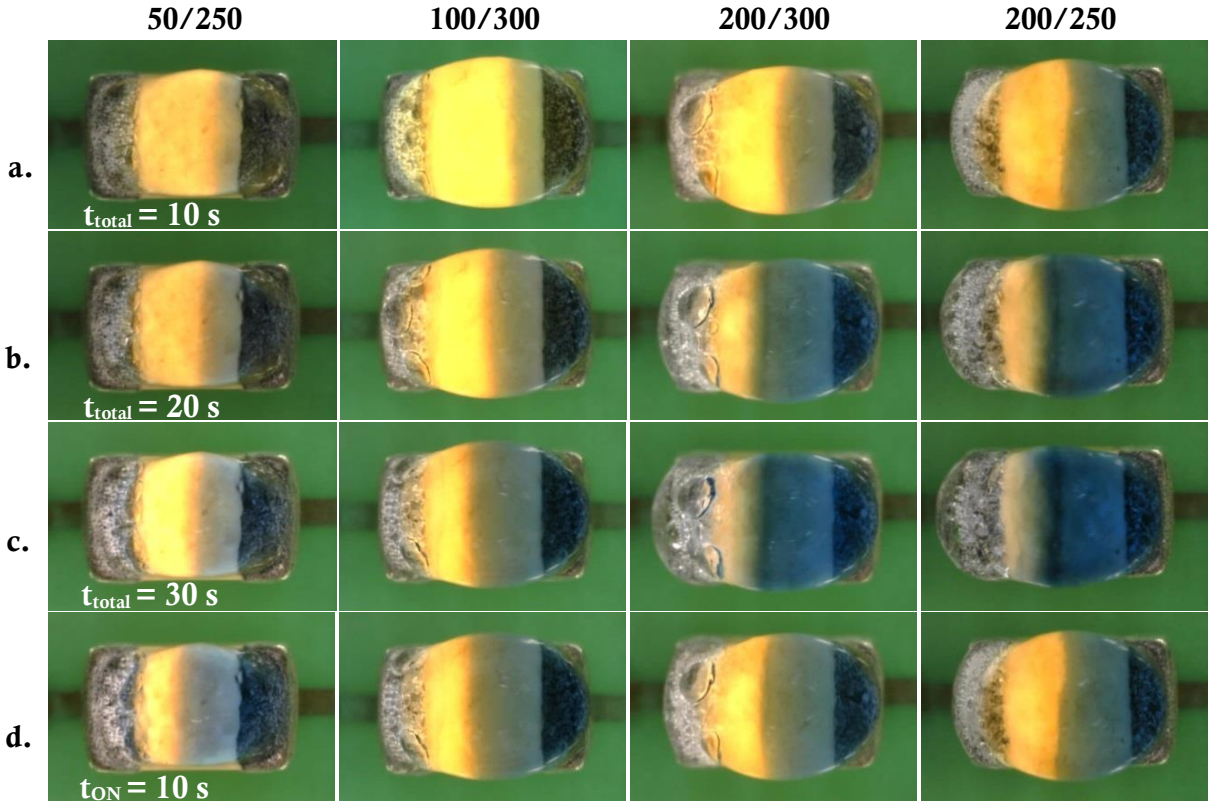

Figure 12.8: Dissolution of tin as a function of pulsed voltage (anode on the right, cathode on the left). Anodic dissolution of tin after different time intervals: a. 10 s, b. 20 s and c. 30 s; d. anodic dissolution of tin after equivalent ON time of 10 s

The comparison of the components after 150 seconds of testing time with pulsed voltage is provided in Figure 12.9 a. (first row). The t_{ON} indicated in the pictures directly represents the amount of dissolved tin as it was visualized in Figure 12.8 a, b, and c. and it is increasing with the duty cycle. Similarly with increase of duty cycle increases the average charge transferred between the electrodes from 0.0035 mA·h to 0.0626 mA·h (indicated as $Q\text{-}Q_0$ in the micrographs). Optical micrographs in Figure 12.9 a show increase of corrosion of anode electrode and the amount of precipitates and dendrites on the surface of the components with increase of duty cycle. For the pulse condition (50/250), the precipitation of tin hydroxides (white precipitates) was more favourable.

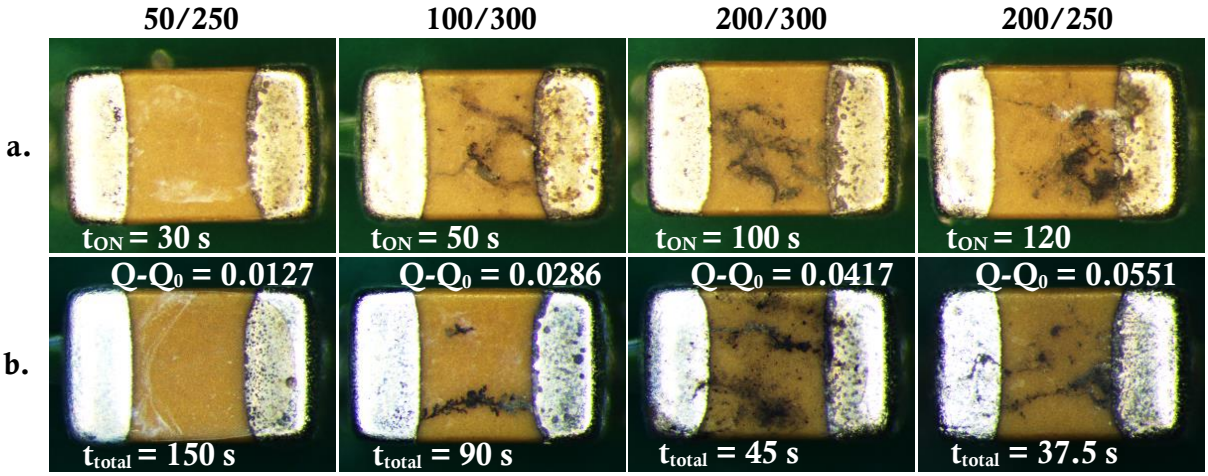

Figure 12.9: Optical appearance of ECM on the components after evaporation of electrolyte: a. effect of ON time (comparison after 150 s of test time) at 1.56 μg·cm^{-2} of NaCl, and b. effect of pulsed voltage (comparison after 30 s of ON time) at 15.6 μg·cm^{-2} of NaCl. (Q-Qo in the micrographs indicates average charge transferred, as readings from Figure 12.5)

The appearance of the components after equivalent time of ON cycle is shown in Figure 12.9 b. (second row). The comparable level of tin ions was dissolved in this case, referring to Figure 12.8 d; however, it resulted in a different morphology, and ratio of tin dendrites and precipitates. For high duty cycles (0.8 and 0.67) an extensive amount of metallic tin deposits were observed spread over a large area of the component, which appear in black in the micrographs in Figure 12.9 b. With the reduction of duty cycle to 0.33, the formation of tin dendrites was more localized, and the precipitation of tin hydroxides (appear in white colour in the image) became more evident. For the duty cycle of 0.2, the precipitation of tin hydroxide without dendrites was seen in the representative optical micrographs. For the charge over time ($Q\text{-}Q_0$), a slight increase with increase of duty cycle was observed.

The effect of the duty cycle on the formation of tin dendrites is emphasized in Figure 12.10. The images provide a comparison between the components with equivalent periods of test time (150 s), thus different ON time; and equivalent ON time (120 s), thus different time intervals when pulsed voltage was applied on the components.

From the comparison of the components after equivalent test time with two duty cycles (first two micrographs in Figure 12.10) shows no tin dendrites, however some amount of tin hydroxide precipitates can be seen for the low duty cycle. However, the component with high duty cycle shows high amount of metallic tin precipitates (dendrites). Comparing low and high duty cycle

after equivalent ON time (first and third micrographs in Figure 12.10), significantly more precipitation of tin hydroxide is observed for the low duty cycle

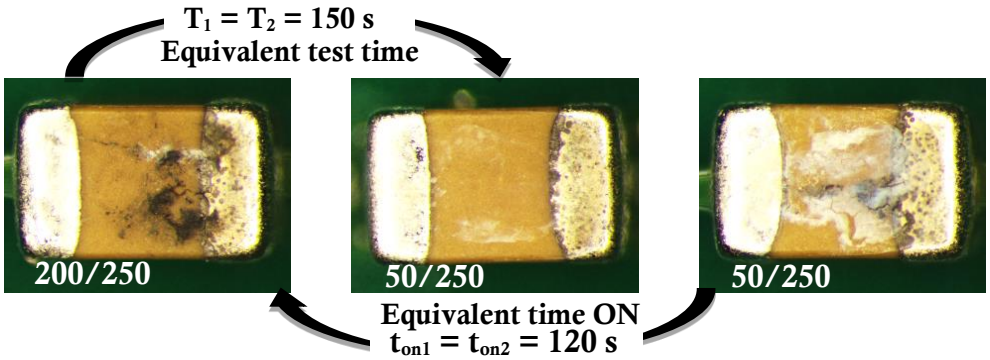

Figure 12.10: Comparison of the morphology of tin dendrites/precipitates in respect with equivalent test time of 150 s, and equivalent time of ON cycle (120 s) under pulsed voltage with duty cycles of 0.2 and 0.8

IV. DISCUSSION

Testing of ECM under pulsed voltage conditions showed the significance of anodic dissolution of tin and time of migration to the cathode for the dendrite growth. The dissolution of tin occurs during ON cycle, therefore the concentration of tin ions in the solution increases with the ON time. The increase of tin ions concentration with the duty cycle was effectively visualized by the gel containing tin ion indicator in Figure 12.7 and Figure 12.8. Increasing tin dissolution rate (increase of duty cycle), reduces the TTF, as indicated in Weibull graphs in Figure 12.2. The effect of dissolution rate on the TTF can be also emphasized by the comparison of TTF observed for two concentrations of NaCl in Figure 12.2. The amount of dissolved metal ions increases with the concentration of NaCl thereby resulting in reduction of TTF. The observations correspond well with the findings reported in literature as follows. From the comparison of potentiodynamic polarization and time to failure vs. potential obtained under DC voltage, it was reported that the dissolution of metal is the rate determining step in ECM mechanism [11]. Further, correlation between the TTF and the initial anodic dissolution rate was observed during potentiodynamic polarization in sodium chloride and sodium sulfate electrolytes [29]. Electrochemical migration of tin under thin layers of sodium chloride electrolytes [12] indicated a reduction of TTF with increase of NaCl concentration from 10^{-4} M to $5 \cdot 10^{-3}$ M. The concentrations of NaCl used in the current work falls within the range of concentrations used in the above investigations. A reduction in TTF with increase of DC bias voltage and NaCl concentration under water droplet condition was also reported in the literature [7].

The mean TTF obtained for a number of pulse widths having fixed duty cycle fell within a narrow time interval (parameter α indicated in Figure 12.3). The charge conducted over time (Figure 12.5) was comparable under these cases except for a slight deviation for the pulse condition of 5/10. In the current vs. time curves for the pulses with t_{OFF} of 5 ms and shorter, the steps of ON and OFF time were no longer observable, thereby indicating the transition from pulsed to DC voltage conditions on the components. Therefore conditions with t_{OFF} 5 ms or shorter increased the charge transfer.

The dendrite current at the event of short circuiting the electrodes by dendrites was ~2-4 times higher for the higher concentration of NaCl and it varied between 4 mA and 17.5 mA in Figure 12.4. The equivalent resistance corresponding to such dendrites current is 2.5 kOhm and 571 Ohm respectively. For comparison, the resistance of the dendrites formed for Sn-Pb and lead free solder alloys under distilled water varies in the range of kOhms [3]. Similar resistance values were reported in the study of ECM on electronic chip resistors in chloride environments [6]. An increase of dendrite current with increase of duty cycle observed for 15.6 $\mu g \cdot cm^{-2}$ of NaCl indicated that the longer ON cycles is more dynamically favourable condition for dendrite growth and suggests different morphology of dendrites formed under pulsed voltage.

The reduction of TTF with low duty cycle is primarily attributed to the reduced anodic tin dissolution; however the reduction of β parameter in the Weibull graphs and reduction of charge transfer over time indicated an additional suppression effect of low duty cycle (0.2 and 0.33) on the dendrite formation. Significantly lower charge calculated for low duty cycles in Figure 12.5 and Figure 12.6 indicated reduction in the formation rate of tin dendrites, although a comparable amount of tin ions were dissolved in time (comparison with equivalent t_{ON}). With the duty cycle of 0.2, the precipitation of tin hydroxides rather than dendrite growth was preferred (Figure 12.9 and Figure 12.10). However, for the duty cycles of 200/250 and 200/300, the bulky metallic tin deposits spread over a large area of the capacitors indicating high rate of the "breaking off" and redeposition of the dendrites thereby resulting in high charge conduction with time.

Summarizing the discussion above, during ON cycles of pulsed voltage three important processes determining dendrite growth rate are in place: i) anodic dissolution of tin, ii) transport of metal ions through the electrolyte, and iii) reduction at the cathode. The rate of anodic dissolution is determined by the duty cycle, thus it significantly influence the TTF. Transport of metal ions under water droplet condition is primarily influenced by the electric field, whereas for ECM under humid conditions, the thickness of water layer between the conductors becomes the determining factor for the ion transport. An additional factor affecting the TTF is hidden in iii), which is the so called efficiency of electrodeposition (in this case the efficiency of dendrite formation) i.e. the ratio between the tin ions reduced at the cathode and the tin ions "lost" within the electrolyte solution due to the formation of tin hydroxides. Results show that the efficiency factor depends on the pulse voltage conditions. The comparison of dissolved tin ions after equivalent ON times for various duty cycles indicated similar amount of ions in the solution, however an additional suppression effect was observed from the charge transfer results (Figure 12.6). The significantly larger amounts of tin hydroxides for the duty cycle of 0.2 (50/250) in Figure 12.9 and Figure 12.10 indicated the condition least favourable for ECM among the pulse conditions tested in this work. An important aspect in connection with this observation is the localized change in pH. With increase in OFF cycle time, localized pH variation equalizes thereby affecting the zone where tin hydroxide formation is favourable [5], and this will result in precipitation of tin hydroxide reducing the possibility of dendrite formation. Increase of tin hydroxide precipitation can also be influenced by the OFF cycle itself as the driving force for migration and reduction at the cathode is interrupted. This variation in tin hydroxide precipitation with the duty cycle is an important observation as it relates to the commonly reported correlation between the solubility of metal ion hydroxides in water with the TTF [1]–[4]. The TTF increases with decrease of metal ion hydroxide solubility, which is also related to the tendency for metal hydroxide precipitation. For reference, the solubility of common metal hydroxides expressed as

–log K is provided [4]: Sn^{2+} (27), Pb^{2+} (20), Cu^{2+} (20), Cu^{+} (15) and Ag^{+} (8). The Sn^{2+} hydroxides are least soluble in water and suggest the possibility of highest amount of hydroxide precipitation. The observations suggest that the pulsed voltage may have a different effect on the ECM for various metals and needs to be further investigated.

V. CONCLUSIONS

1. Increase of duty cycle reduces the time to dendrite formation and to an extent the rate of dendrite formation. The result is primarily attributed to the concentration of tin ions being dissolved from the positively biased electrode as visualized by a tin ion indicator.
2. The increase of dendrite current with increase of duty cycle was evident for higher concentration of NaCl, however for lower concentration the dendrite current was less affected by the variation of duty cycle.
3. The reduction of time to dendrite formation and the increase of dendrite current were observed with increasing NaCl concentration from 1.56 $\mu g \cdot cm^{-2}$ to 15.6 $\mu g \cdot cm^{-2}$.
4. The comparable amount of tin ions was dissolved from the anode after equivalent ON times for various duty cycles; however the formation of tin dendrites was less efficient with duty cycles of 0.2 (t_{ON} = 50 ms, t_{OFF} = 200 ms) and 0.33 (t_{ON} = 100 ms, t_{OFF} = 200 ms). It resulted in a slight increase of TTF and reduction of charge transferred between the electrodes. The significantly larger amounts of tin hydroxides observed at a duty cycle of 0.2 indicated that this condition is least favourable for ECM.

VI. ACKNOWLEDGMENTS

The research reported here was conducted as part of the CELCORR/CreCon consortium (www.celcorr.com) and the authors would like to acknowledge the funding and help received from the consortium partners. Shruti Borgaonkar (Technical University of Denmark), Daniel Minzari (IPU), and Lutz Müller (Robert Bosch GmbH) are acknowledged for their contributions to the preparation of the manuscript.

VII. REFERENCES

[1] J. J. Steppan, J. A. Roth, and L. C. Hall, "A review of corrosion failure mechanisms during accelerated tests Electrolytic metal migration," *J. Electrochem. Soc.*, vol. 134, no. 1, pp. 175–190, 1987.

[2] G. Harsányi and G. Inzelt, "Comparing migratory resistive short formation abilities of conductor systems applied in advanced interconnection systems," *Microelectron. Reliab.*, vol. 41, no. 2, pp. 229–237, Feb. 2001.

[3] D. Q. Yu, W. Jillek, and E. Schmitt, "Electrochemical migration of Sn-Pb and lead free solder alloys under distilled water," *J. Mater. Sci. Mater. Electron.*, vol. 17, no. 3, pp. 219–227, Mar. 2006.

[4] B. Medgyes, B. Illés, and G. Harsányi, "Electrochemical migration behaviour of Cu, Sn, Ag and Sn63/Pb37," *J. Mater. Sci. Mater. Electron.*, vol. 23, no. 2, pp. 551–556, Jun. 2011.

[5] D. Minzari, M. S. Jellesen, P. Møller, and R. Ambat, "On the electrochemical migration mechanism of tin in electronics," *Corros. Sci.*, vol. 53, no. 10, pp. 3366–3379, Oct. 2011.

[6] D. Minzari, M. S. Jellesen, P. Møller, P. Wahlberg, and R. Ambat, "Electrochemical Migration on Electronic Chip Resistors in Chloride Environments," *IEEE Trans. Device Mater. Reliab.*, vol. 9, no. 3, pp. 392–402, 2009.

[7] V. Verdingovas, M. S. Jellesen, and R. Ambat, "Influence of sodium chloride and weak organic acids (flux residues) on electrochemical migration of tin on surface mount chip components," *Corros. Eng. Sci. Technol.*, vol. 48, no. 6, pp. 426–435, Sep. 2013.

[8] S.-B. Lee, M.-S. Jung, H.-Y. Lee, T. Kang, and Y.-C. Joo, "Effect of bias voltage on the electrochemical

migration behaviors of Sn and Pb," *IEEE Trans. Device Mater. Reliab.*, vol. 9, no. 3, pp. 483–488, 2009.

[9] B. Noh, J. Yoon, W. Hong, and S. Jung, "Evaluation of electrochemical migration on flexible printed circuit boards with different surface finishes," *J. Electron. Mater.*, vol. 38, no. 6, pp. 902–907, 2009.

[10] B. Noh, J. Lee, and S. Jung, "Effect of surface finish material on printed circuit board for electrochemical migration," *Microelectron. Reliab.*, vol. 48, pp. 652–656, 2008.

[11] M.-S. Jung, S.-B. Lee, H.-Y. Lee, C.-S. Ryu, Y.-G. Ko, H.-W. Park, and Y.-C. Joo, "Improvement of Electrochemical Migration Resistance by Cu/Sn Intermetallic Compound Barrier on Cu in Printed Circuit Board," *IEEE Trans. Device Mater. Reliab.*, vol. 14, no. 1, pp. 382–389, Mar. 2014.

[12] X. Zhong, G. Zhang, Y. Qiu, Z. Chen, W. Zou, and X. Guo, "In situ study the dependence of electrochemical migration of tin on chloride," *Electrochem. commun.*, vol. 27, pp. 63–68, Feb. 2013.

[13] X. Zhong, G. Zhang, Y. Qiu, Z. Chen, and X. Guo, "Electrochemical migration of tin in thin electrolyte layer containing chloride ions," *Corros. Sci.*, vol. 74, pp. 71–82, Sep. 2013.

[14] C. Xie, X. Tang, J. Chen, B. Song, J. Jin, and H. Zhang, "Reliability Analysis and Accelerated Statistical Model of CNC PCB for Electrochemical Migration," *IEEE Trans. Device Mater. Reliab.*, vol. 14, no. 1, pp. 90–98, Mar. 2014.

[15] X. He, M. Azarian, and M. Pecht, "Evaluation of Electrochemical Migration on Printed Circuit Boards with Lead-Free and Tin-Lead Solder," *J. Electron. Mater.*, vol. 40, no. 9, pp. 1921–1936, Jun. 2011.

[16] S. Zhan, M. H. Azarian, and M. Pecht, "Reliability of Printed Circuit Boards Processed Using No-Clean Flux Technology in Temperature – Humidity – Bias Conditions," *IEEE Trans. Device Mater. Reliab.*, vol. 8, no. 2, pp. 426–434, 2008.

[17] V. Verdingovas, M. S. Jellesen, and R. Ambat, "Impact of NaCl Contamination and Climatic Conditions on the Reliability of Printed Circuit Board Assemblies," *IEEE Trans. Device Mater. Reliab.*, vol. 14, no. 1, pp. 42–51, 2014.

[18] L. C. Zou and C. Hunt, "Characterization of the Conduction Mechanisms in Adsorbed Electrolyte Layers on Electronic Boards Using AC Impedance," *J. Electrochem. Soc.*, vol. 156, no. 1, pp. C8–C15, 2009.

[19] S. W. Chaikin, J. J. Janney, F. M. Church, and C. W. McClelland, "Silver Migration and Printed Wiring," *Ind. Eng. Chem.*, vol. 51, no. 3, pp. 299–304, Mar. 1959.

[20] J. Kim, M. Park, D. Nam, and H. Kwon, "Electrochemical Migration Behavior of a Fine-Pitch IC Substrate by Alternating Current," *J. Nanosci. Nanotechnol.*, vol. 14, no. 11, pp. 8258–8263, Nov. 2014.

[21] O. Short, "Silver Migration in Electric Circuits," *Tele-Tech Electron. Ind.*, no. February, pp. 64-65-113, 1956.

[22] K. J. Harry, D. T. Hallinan, D. Y. Parkinson, A. a MacDowell, and N. P. Balsara, "Detection of subsurface structures underneath dendrites formed on cycled lithium metal electrodes," *Nat. Mater.*, vol. 13, no. 1, pp. 69–73, Jan. 2014.

[23] M. Z. Mayers, J. W. Kaminski, and T. F. Miller, "Suppression of Dendrite Formation via Pulse Charging in Rechargeable Lithium Metal Batteries," *J. Phys. Chem. C*, vol. 116, no. 50, pp. 26214–26221, Dec. 2012.

[24] A. Aryanfar, D. Brooks, B. V. Merinov, W. A. Goddard, A. J. Colussi, and M. R. Hoffmann, "Dynamics of Lithium Dendrite Growth and Inhibition: Pulse Charging Experiments and Monte Carlo Calculations," *J. Phys. Chem. Lett.*, vol. 5, no. 10, pp. 1721–1726, 2014.

[25] H. Yang, E. O. Fey, B. D. Trimm, N. Dimitrov, and M. S. Whittingham, "Effects of Pulse Plating on lithium electrodeposition, morphology and cycling efficiency," *J. Power Sources*, vol. 272, pp. 900–908, Dec. 2014.

[26] B. Tsenter and M. Golod, "Safe and efficient charging algorithm for lithium batteries," *J. Power Sources*, vol. 65, no. 1–2, pp. 284–285, Mar. 1997.

[27] X. Zhong, X. Guo, Y. Qiu, Z. Chen, and G. Zhang, "In Situ Study the Electrochemical Migration of Tin under Unipolar Square Wave Electric Field," *J. Electrochem. Soc.*, vol. 160, no. 11, pp. 495–500, 2013.

[28] R. B. Abernethy, *The New Weibull Handbook*, 5th ed. 536 Oyster Road, North Palm Beach, FL.: Dr. Robert B.Abernethy, 2006.

[29] S. Lee, M. Jung, H. Lee, and Y. Joo, "Effect of Initial Anodic Dissolution Current on the Electrochemical Migration Phenomenon of Sn Solder," in *Electronic Components and Technology Conference*, 2009, pp. 1737–1740.

13. EFFECT OF IODINE ON THE CORROSION OF AU-AL WIRE BONDS

Vadimas Verdingovas, Lutz Müller, Morten Stendahl Jellesen, Flemming Bjerg Grumsen, Rajan Ambat

Abstract—Corrosion study was performed on Au-Al wire bonds, thin layers of sputter deposited Au and Al, and Au-Al intermetallic nuggets. The test environment was iodine-vapour in air (1 $mg \cdot L^{-1}$) at 85 °C with varying relative humidity, and 500 $mg \cdot L^{-1}$ of KI in water. GDOES, XRD, SEM EDS, wire bond shear, and electrochemical testing were used to characterize the samples. Failures of Au-Al wire bonds were found to be primarily attributed to the corrosion of Al via formation of Al iodides and consequent formation of Al oxides and/or hydroxides. Most susceptible to corrosion are Al metallization and Al rich intermetallic phases.

Highlights

- Formation of Au-Al intermetallics during heat treatment are investigated *in situ* by XRD
- Increase of RH in iodine containing environment accelerates the corrosion of Au-Al
- Corrosion resistance of Au-Al decreases with increase of Al in the intermetallic phase
- Failures are primarily attributed to corrosion of Al at the bond interface and in the intermetallic phases
- Chemical reactions describing corrosion mechanism are suggested

Keywords—A. Aluminium; A. Electronic materials; A. Intermetallics; B. Polarization B. X-ray diffraction; C. Interfaces; C. Oxidation

I. INTRODUCTION

The combination of Au and Al is sensitive to corrosion, but it is commonly used as interconnections in microelectronics. The corrosion of Al in contact with Au is driven by high difference in the electrochemical potential with respect to Au. However, when Au-Al wire bonds are exposed to halogen containing environments, the degradation of wire bond is dependent on the Au-Al intermetallics formed at the interface during the bonding or during life in service [1]. There are five Au-Al intermetallic phases (IMPs): Au_4Al, Au_8Al_3, Au_2Al, AuAl, and $AuAl_2$ [2], which can also be formed in Au-Al interconnections. In literature, the intermetallic phase Au_8Al_3 can be designated as Au_5Al_2, however, correct stoichiometry is reported to be Au_8Al_3 [2]–[5].

Failures associated with the formation of Au-Al intermetallics or corrosion at the wire bonds can be related to reduction of mechanical strength of the bond, and/or the increase of electrical resistance. It has been shown that the Kirkendall voids can be formed during prolonged thermal exposure at the bond interface and between the intermetallic phases due to different interdiffusion rates of Au and Al [6], [7]. The formation of voids caused by volumetric shrinkage due to phase transformation across and lateral to the ball band, also shown with theoretical calculations [8], is considered as the common failure mechanism of Au-Al wire bonds.

V. Verdingovas, L. Müller, M. S. Jellesen, F. B. Grumsen, and R. Ambat, "Effect of iodine on the corrosion of Au-Al wire bonds," *Corros Sci.*, vol. 97, pp. 161-171, 2015.

The quality of wire bonds is usually assessed by destructive tests e.g. bond pull test or ball-bond shear test. Several failure modes can occur during testing namely ball lift, ball shear, bond pad lifting, cratering, wire shear, metallization failure etc. The corrosion resistance of wire bonds is tested by combining thermal stress with a corrosive environment such as gas or types of ionic contamination. However, halides are a common part of the corrosive atmosphere usually encountered by the wire bonds.

The degradation of wire bond strength due to halides is a well-known problem in microelectronics. Halogens are known to corrode Al metallization in the integrated circuits [9]. However, they can also corrode Au-Al wire bonds, thereby reducing the strength of the bonds or eventually causing ball lifts. The commonly reported corrosion issues related to halogens are attributed to chlorine [10]–[12], bromine [10]–[14], or fluorine [15]. The source of halogens in microelectronic devices is typically the polymeric mould-compounds used for the encapsulation of the integrated circuits or the halide surface contaminations on the dies prior to moulding. Degassing from relatively stable halogenated compound tetrabromobisphenol-A, which is used as flame retardant in mould-compounds [16] and laminated printed circuit boards [17] also reported to corrode Au-Al wire bonds [10], [18].

Another important aspect is the effect of iodine, however there is little attention drawn to the corrosion of wire bonds in iodine containing environments. Iodine-containing compounds are widely used as stabilizers against thermo-oxidative decay in polyamides and polyphthalamides (high performance polyamides) which are common housing materials. Polyamides can be stabilised against thermo-oxidative degradation with various stabilizers e.g., phenolic antioxidant, aromatic amine and copper, either in the form of elementary copper, or in a form of copper (I) iodide in combination with potassium iodide or potassium bromide [19]. One of the first applications of iodides as stabilizer in polyamides was reported in 1955 [20]. Iodine as thermo-oxidative decomposition product of the stabilizers of polyamides and root cause of wire bond failure was reported [21], besides there is only limited number of cases addressing iodine as possible a root cause of wire bond failure [22], [23].

The aim of this work is to understand the effect of iodine on the corrosion of bare or gel-potted Au-Al wire bonds with respect to the effect of intermetallic formation. Three types of samples were used for the investigations namely: i) Au-Al wire bonds, ii) heat treated multilayers of sputter deposited Au and Al, and iii) Au_4Al, Au_8Al_3 and Au_2Al intermetallic nuggets prepared by remelting Au and Al under argon atmosphere. The nuggets of intermetallics enabled to study corrosion of IMPs separately, while the heat treated multilayers were used to simulate wire bond connections, IMPs formation, and resulting corrosion problems. Investigations include direct samples exposure to iodine gas at 1 $mg \cdot L^{-1}$ in air at 85 °C with varying RH, and electrochemical corrosion testing in iodide containing solution. Formation of intermetallic phases as a function of temperature was investigated using X-ray diffraction. Corrosion morphology of the surfaces was analysed using optical and scanning electron microscopy.

II. MATERIALS AND METHODS

SPUTTER DEPOSITED AU AND AL ON A SI WAFER

Three sets of sputter deposited Au and Al layers on Si wafers were prepared namely: i) thin layer of gold (119 nm), ii) thin layer of aluminium (1 μm), and iii) multilayer of gold and aluminium (1.1 μm of gold on top of 1 μm of aluminium). Purity of the Au was ~99.99% and Al layer contained 0.5% Cu. The multilayer coating was heat treated at 175 °C for 1 h and 4 h in order to form the intermetallic phases. The heat treatment was performed in the oven under air atmosphere. The selected temperature of 175 °C is a typical temperature for moulding and curing processes in the manufacturing of the electronic packages [1]. Prior to the heat treatment and testing, the samples were diced into 3.5 mm × 3.5 mm using a standard wafer saw cooled by DI-water.

NUGGETS OF AU-AL INTERMETALLICS

The nuggets of Au-Al intermetallics namely Au_4Al, Au_8Al_3, and Au_2Al were prepared for investigating the corrosion of intermetallic phases (IMPs) that are possible between gold and aluminium. The preparation was carried out by melting the alloying elements (Au and Al) in required ratio under argon shielding gas in a water-cooled copper mould in an electric arc furnace. This was followed by remelting (about 10 times) for better homogeneity and completion of the intermetallic formation. Following this the nuggets of Au_2Al and Au_4Al were homogenized at 500 °C for 2 weeks and Au_8Al_3 for 8 weeks.

Prior evaluation of the nuggets by SEM EDS showed that the Au_4Al intermetallic nugget is a homogeneous sample comprised of single phase Au_4Al, however, minor percentage of additional phases were identified in the nuggets of Au_2Al and Au_8Al_3. The X-ray diffraction analysis showed that the phase Au_2Al contains slight amounts of AuAl phase, while minor amounts of Au_2Al were found in Au_8Al_3.

AU-AL WIRE BONDS

Silicon dies with Au-Al wire bonds were used to evaluate the severity of environments in terms of corrosion and shear strength degradation of the bonds. The diameter of Au wire thermo-sonically bonded to the AlCu0.5 bond pad metallization was 32 μm, and the diameter of the ball formed was (100 ± 10) μm.

X-RAY DIFFRACTION

X-ray diffraction (XRD) was carried out on a "Bruker D8" equipped with a parallel beam (Göbel mirror) and a secondary side divergence assembly in 1D, and a MRI temperature controlled dome stage. The X-ray diffraction was used to identify IMPs formed in the Au-Al multilayers during heat treatment for 1 h and 4 h. The complete range of IMPs in comparison with the references available in the international centre for diffraction data "ICDD" database was obtained from *in situ* XRD measurements as a function of temperature and time. The measurements were performed under normal atmospheric conditions in the temperature range from 120 °C to 300 °C with the step of 5 °C. The thermocouple for temperature control was mounted between the Si

wafer with Au-Al multilayer and the aluminium spacing plate, which was placed on top of a platinum-rhodium heating band in order to avoid contamination of the heating band from the Si wafer. The XRD scans were performed once the measured temperature between the heating band and the bottom of the Si wafer reached the set temperature. The duration of each XRD scan was 29 min 07s.

WIRE BOND SHEAR TEST

"Dage series 4000" multi-function bond tester with the ball shear cartridge BS250 (maximum shear force of 250 g) was used for shear test. Instrument has a flat chisel shape shearing tool (062-006) with a shearing edge dimensions slightly higher than the diameter of the gold ball. The shear height and shear speed was accordingly set to 4 μm and 56 $\mu m \cdot s^{-1}$.

GLOW DISCHARGE OPTICAL EMISSION SPECTROSCOPY (GDOES)

"Horiba Jobin Yvon GD-Profiler 2" was used for the investigation of Au-Al intermetallic phase formation on Au-Al multilayers heat treated at 175 °C. The depth profiling was done by plasma sputtering at a pressure of 450 Pa and a power of 25 W. The intensity of the signal of Au and Al elements as a function of sputtering time followed by the creator depth measurements with the profilometer (for depth calibration) was used to observe the formation of Au-Al intermetallics as a function of heating time.

LIQUID PHASE TESTING IN KI SOLUTION

Potentiodynamic polarization and zero resistance ammetry measurements were performed with a "Gamry PCI4/300" potentiostat. The measurements were performed in the standard electrochemical cell with 400 mL of 500 $mg \cdot L^{-1}$ of KI in water. The conductivity of electrolyte solution was (442 ± 3) $\mu S \cdot cm^{-1}$ at (24 ± 1) °C. The reference electrode used was Ag/AgCl.

The zero resistance ammetry measurements were performed between three intermetallic nuggets of Au-Al, which were repolished before each measurement, and Au-Al multilayers heat treated at 175 °C. During ZRA measurements, the current between the two test specimens in KI electrolyte solution is passively (without applying voltage) measured and it represents the galvanic current. Also the potentials versus reference electrode are monitored. The galvanic current between two test specimens was obtained during 8 hours of continuous current measurement with the acquisition rate of 30 s. The distance between anode and cathode was (5 ± 0.5) cm. The electrodes were facing to each other. The surface area of the electrodes for galvanic couples was equal (7.068 ± 0.06) mm^2. Masking of the surface area was done by PVC tape with punched holes with approximate diameter of 3 mm.

Potentiodynamic polarization measurements were performed at a scan rate of 1 $mV \cdot s^{-1}$ in the range from -400 mV to 800 mV vs. open-circuit potential (OCP) which was measured for 10 min prior to the polarization scans to stabilize the samples. The conditions were chosen to mimic the conditions in the crevice of Au-Al ball bond due to exposure to iodine under humid conditions.

GAS PHASE TESTING IN IODINE CONTAINING ENVIRONMENT

Test environment with iodine gas was created in a 330 mL "Duran" glass bottles closed with "SCHOTT 180 °C" proof caps with PTFE coated silicone rubber seals. Analytical grade iodine (Aldrich 99,99%) was placed in a small glass vial, which was placed in the centre of the bottle. The experiments were performed at a constant temperature of 85 °C, while the relative humidity (RH) was controlled by the volume of deionized water added into the bottles (e.g. 57 µL of deionized water would create approx. 50 %RH at 85 °C in a 330 mL bottle). These conditions were chosen to mimic the conditions of Au-Al ball bonds during practical applications due to the iodine generated by oxidation of iodide stabilized polyamide under humid conditions.

SURFACE MORPHOLOGY ANALYSIS

Surface morphology analysis of samples prior and after corrosion testing was carried out using optical microscope "Axioskop 2 MAT" from "Carl Zeiss", imaging done in differential interference contrast (DIC) mode, and scanning electron microscope "FEI Quanta 200 ESEM FEG". An "Olympus GX41" metallurgical microscope was used for analysis of cross-section of the corroded Au-Al multilayers.

III. RESULTS

FORMATION OF AU-AL INTERMETALLICS AT 175 °C

The glow discharge optical emission spectroscopy results of depth profiling of Au-Al layers in Figure 13.1 indicate the progress of interdiffusion (leading to IMP formation) as the samples were exposed to 175 °C for 1 h and 4 h. The composition profiles show the shift in Au-Al interface due to interdiffusion during heat treatment.

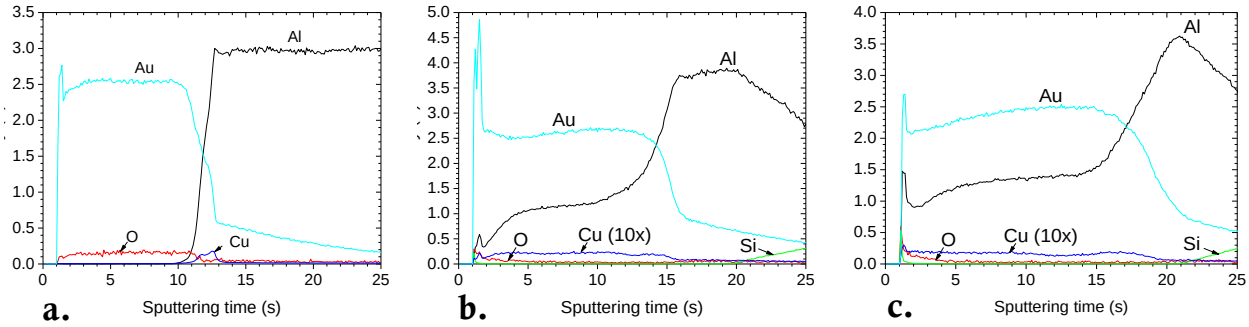

Figure 13.1: GDOES composition profiles of Au-Al multilayer during heat treatment at 175°C: a. 0 h, b. 1 h and c. 4 h

The surface morphology of the Au-Al layers using optical and SEM before and after heat treatment is shown in Figure 13.2. The grains of Au formed during sputter deposition process can be clearly seen in SEM images (Figure 13.2 a.2, b.2), while with heat treatment, the interdiffusion of Au and Al changes the morphology of the surface (Figure 13.2. c.2, b.3). Overview of the samples in optical micrographs indicate that for the Au-Al layer heat treated for 1 h, most of the surface was still covered by a layer of Au, but with some sites where Al has reached the surface. After 4 h of heating, the pure Au on the surface was no longer present. The observation from optical micrographs is well supported by GDOES composition profiles in Figure 13.1.

The results from XRD measurement showing a full range of intermetallic phase formation in the Au-Al layer within the temperature interval of 120 °C – 300 °C are presented in Figure 13.3. a. The IMP formation is temperature and time dependent as indicated on the Y-axis. High intensity of Au peak resembles single crystal Au reflection which is due to the surface texture, whereas the reflections from Au-Al intermetallic phases forming deeper into the bulk appear with lower intensity. The colour scale representing the count number in the graph was adjusted accordingly to include both. The offset of the peaks due to thermal expansion of IMPs is taken into account when aligning the scans at increasing temperatures. The representative peaks of different intermetallic phases are indicated in Figure 13.3. The powder diffraction file (PDF) numbers of identified intermetallic phases can be found in Table 13.1. The identification of Au_4Al, Au_8Al_3, AuAl, and $AuAl_2$ was possible using powder diffraction database from "ICDD", while the Au_2Al phase was identified by comparison with the XRD pattern from intermetallic nugget with known composition.

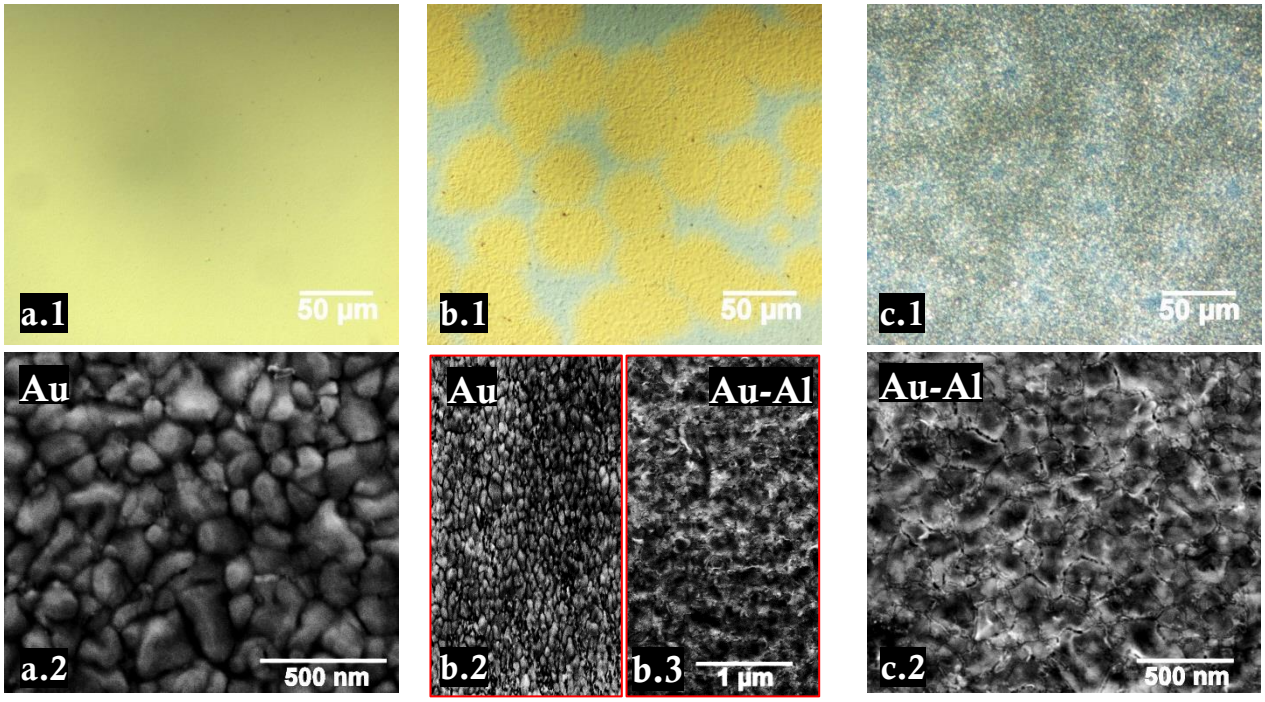

Figure 13.2: Optical and SEM micrographs showing the appearance of Au-Al multilayer after heat treatment at 175 °C: a. 0 h, b. 1 h and c. 4 h

Among the intermetallics during *in situ* heat treatment in Figure 13.3 a, Au_8Al_3 appears first and it is the predominant IMP formed, while at higher temperatures or after a longer time Au_4Al and Au_2Al forms. With diffusion of Al into the original Au layer, the penetration depth of X-rays increases, thus the peaks related to $AuAl_2$ intermetallic phase appears later (at higher temperature and longer time) than the peaks from Au_4Al and Au_2Al. With increase in temperature and time of heating, interdiffusion of Au and Al reaches an equilibrium condition at which the AuAl phase is formed.

Figure 13.3 b. shows single XRD scans on the samples heat treated for 1 h and 4 h at 175 °C as used in the present work for corrosion studies (Figure 13.1 - Figure 13.2), in comparison with the scans obtained at 170 °C and 190 °C during *in situ* IMP formation, which are indicated by

dashed lines in Figure 13.3 a. The sample heat treated for 1 h contains Au, Au_4Al, and Au_8Al_3, while sample heat treated for 4 h contains $AuAl_2$, Au_2Al and Au_8Al_3.

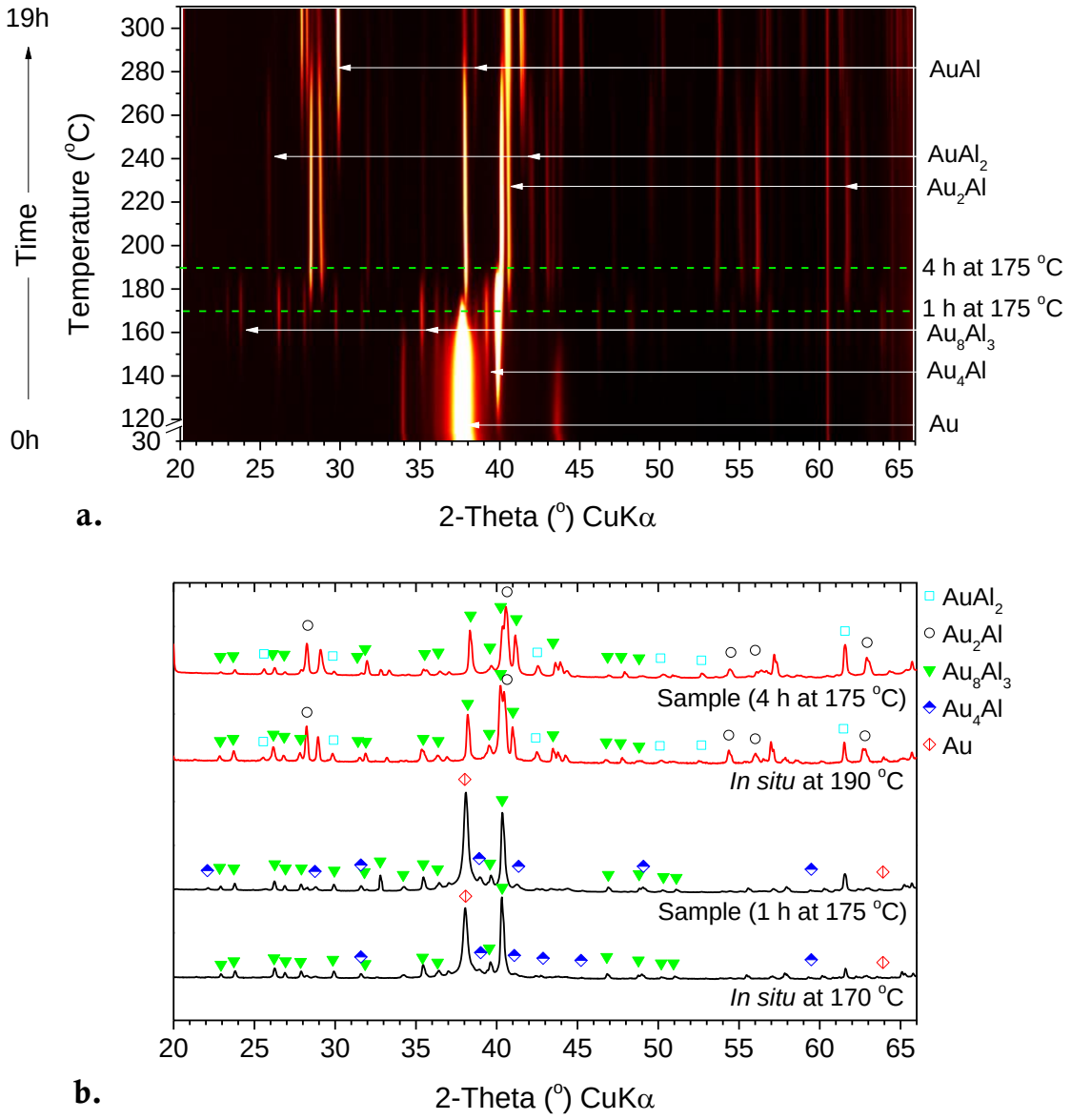

Figure 13.3: XRD results obtained on Au-Al multilayer: a. *in situ* formation of IMPs as a function of time and temperature and b. IMPs formed during heat treatment of multilayer for 1 h and 4 h (provided in comparison with spectra obtained during *in situ* IMP formation as indicated by dashed line in Figure 13.3 a.)

Table 13.1: Au-Al intermetallic phases identified from the XRD measurements in Figure 13.3

Intermetallic phase	**Powder diffraction file number for the references in ICDD database**
Au	04-0784
Au_4Al	29-0036
Au_8Al_3	48-1341
Au_2Al	26-1005
AuAl	50-1021
$AuAl_2$	17-0877

CORROSION OF AU-AL INTERMETALLICS

POTENTIODYNAMIC POLARISATION AND ZERO RESISTANCE AMMETRY MEASUREMENTS

The results of zero resistance ammetry (ZRA) measurements between the nuggets of Au-Al intermetallics coupled with thin sputtered layers of Al and Au obtained in 500 mg·L^{-1} KI solution are summarized in Figure 13.4. Results provide the minimum, the maximum, and the average current density values, which were obtained during 8 hours of continuous current measurement with the acquisition rate of 30 s. The average electrochemical potential of the coupled test specimens is provided as galvanic potential in the graph.

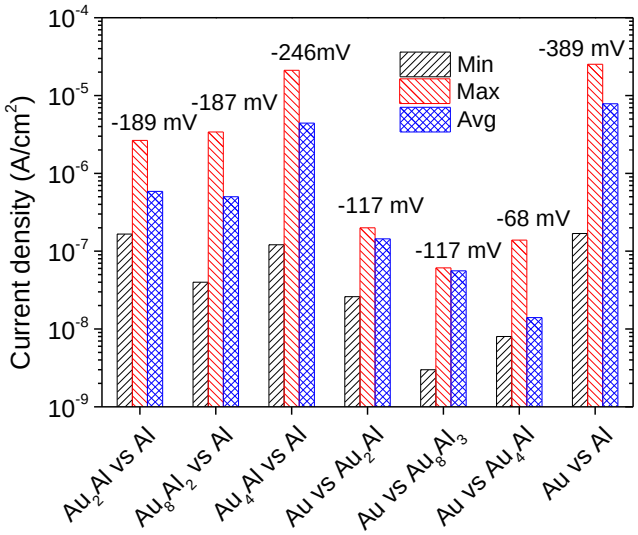

Figure 13.4: Results of ZRA measurements (cathode vs. anode coupling), galvanic potential vs. Ag/AgCl in mV is indicated above the bars

For Al layer coupled as an anode with three intermetallic nuggets, the corrosion rate (current density) was increasing with increasing content of Au in the intermetallic compound coupled as cathode. Conversely, when an intermetallic nugget was coupled as an anode with the Au, the corrosion rate was decreasing with increasing amount of Au in the intermetallic. The highest corrosion rate was observed between Al and Au. Overall, the galvanic current was following the galvanic potential difference between the electrodes which is indicated in Figure 13.4

The potentiodynamic polarization measurements shown in Figure 13.5 indicate the difference in the electrochemical activity of intermetallic phases. A slight decrease in current density in the passive region, and an increase in breakdown potential during anodic polarization was observed with increase of Au content in Au-Al IMP. Whereas the cathodic current density for Au-Al intermetallics was comparable, and only for the sample heat treated for 4 h showed slight decrease in cathodic current. Overall, the potentiodynamic polarization measurements showed that with decrease of Au content in the IMP reduces the electrochemical potential and to some extent increases the corrosion rate. Summary of corrosion potential (E_{corr}) and corrosion current density (I_{corr}) obtained from the polarization curves can be seen in Table 13.2. The corrosion potential of Au-Al layers heated for 1 h and 4 h lies respectively above and below the

potential values observed for three intermetallics nuggets: Au_2Al, Au_8Al_3, and Au_4Al. The current density for 4 h sample is also higher than that of the sample heated for 1 h at 175 °C. The Al sample showed lowest (more negative) corrosion potential, and it did not show any passivation. Therefore, a significant increase in current density during anodic polarisation was observed.

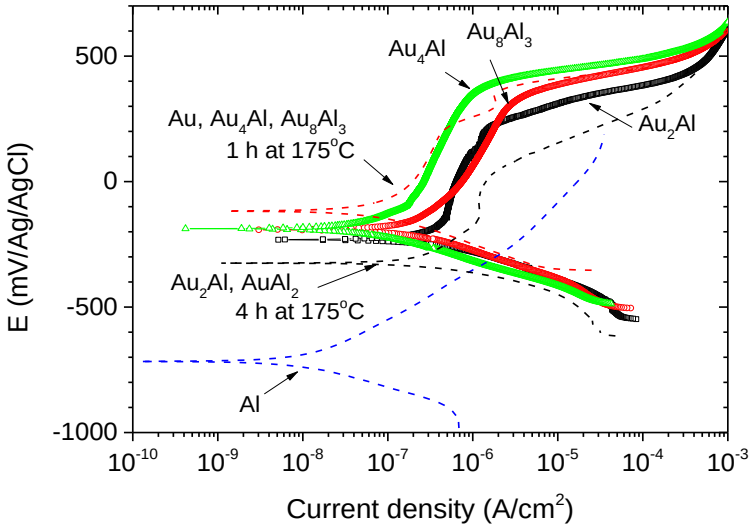

Figure 13.5: Potentiodynamic polarization in 500 mg·L^{-1} KI solution for intermetallic nuggets: Au_2Al. Au_8Al_3, Au_4Al (solid line+symbol), and sputter deposited Au and Al layers heat treated for 1 h and 4 h (dash line)

Table 13.2: Corrosion potential (E_{corr}) and corrosion current density (I_{corr}) obtained from potentiodynamic polarization curves in Figure 13.5

Sample	**E_{corr} (mV vs Ag/AgCl)**	**I_{corr} (A·cm^{-2})**
Al	-727 ± 13	(1.78E ± 1.03) × 10^{-8}
Au_2Al, $AuAl_2$ (4 h at 175 °C)	-331 ± 12	(3.41E ± 0.44) × 10^{-7}
Au_2Al	-239 ± 17	(3.15E ± 0.49) × 10^{-7}
Au_8Al_3	-187 ± 8	(2.49E ± 0.30) × 10^{-7}
Au_4Al	-189 ± 4	(1.15E ± 0.09) × 10^{-7}
Au, Au_4Al, Au_8Al_3 (1 h at 175 °C)	-96 ± 19	(1.01E ± 0.12) × 10^{-7}

EFFECT OF EXPOSURE TO I_2 AND HUMIDITY

A significant difference in the corrosion resistance of Au and Al under combined effect of iodine and RH was observed as shown in optical micrographs in Figure 13.6 and Figure 13.7. The micrographs were taken after 24 h exposure to 1 mg·L^{-1} of iodine at (15, 50, and 85) % RH at 85 °C. For Au sample in Figure 13.6 a, no corrosion was seen at 15 % RH and 50 % RH, while the tarnishing of the surface was observed at 85 % RH. The SEM micrograph in Figure 13.6 a.3-2 indicated corrosion of Au layer and exposure of underlying Si substrate. For thin layer of Al, an increase of oxidation with an increase of RH was observed. The scaling of the Al oxide is shown in Figure 13.6 b.3-2.

The multilayers of Au-Al heated for 1 h and 4 h, showed significant corrosion even at lowest humidity levels (15% RH/85 °C) (Figure 13.7). The corrosion of non-heated Au-Al layers starts at the dicing streets where both layers of Au and Al are exposed to iodine and water vapour. Further, some localized corrosion indicated by arrows in Figure 13.7 was observed.

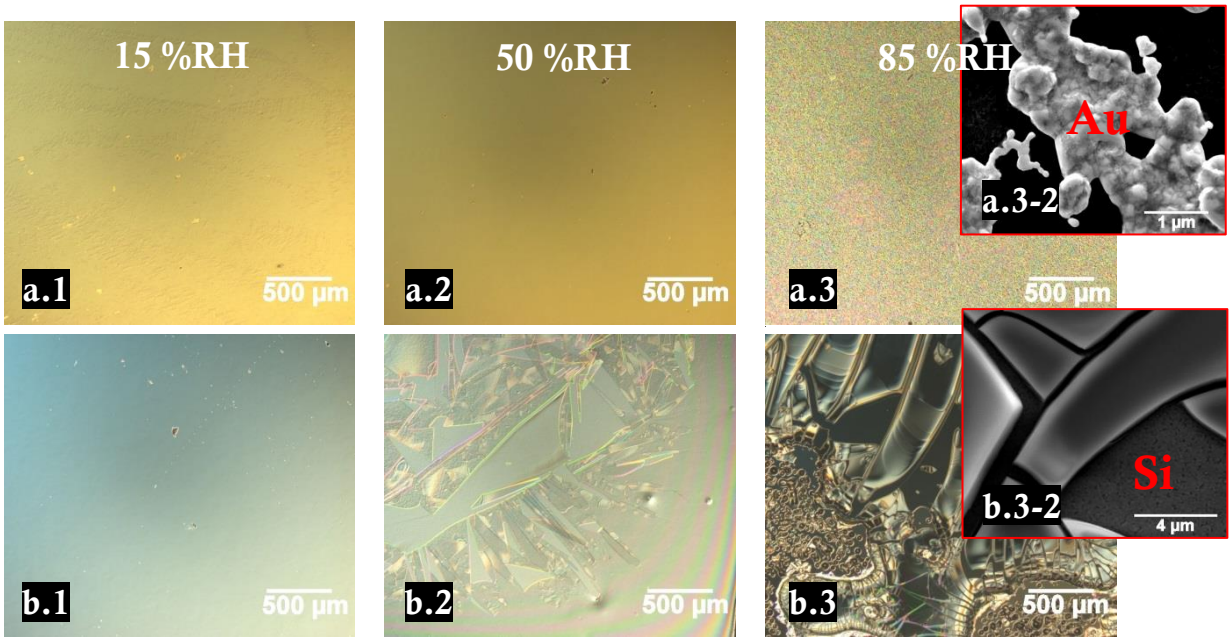

Figure 13.6: Corrosion of Au layer (a) and Al layer (b) after 24 h exposure to 1 mg·L^{-1} of iodine at 85 °C and three levels of relative humidity: 1. 15 %RH, 2. 50 %RH, 3. 85 %RH

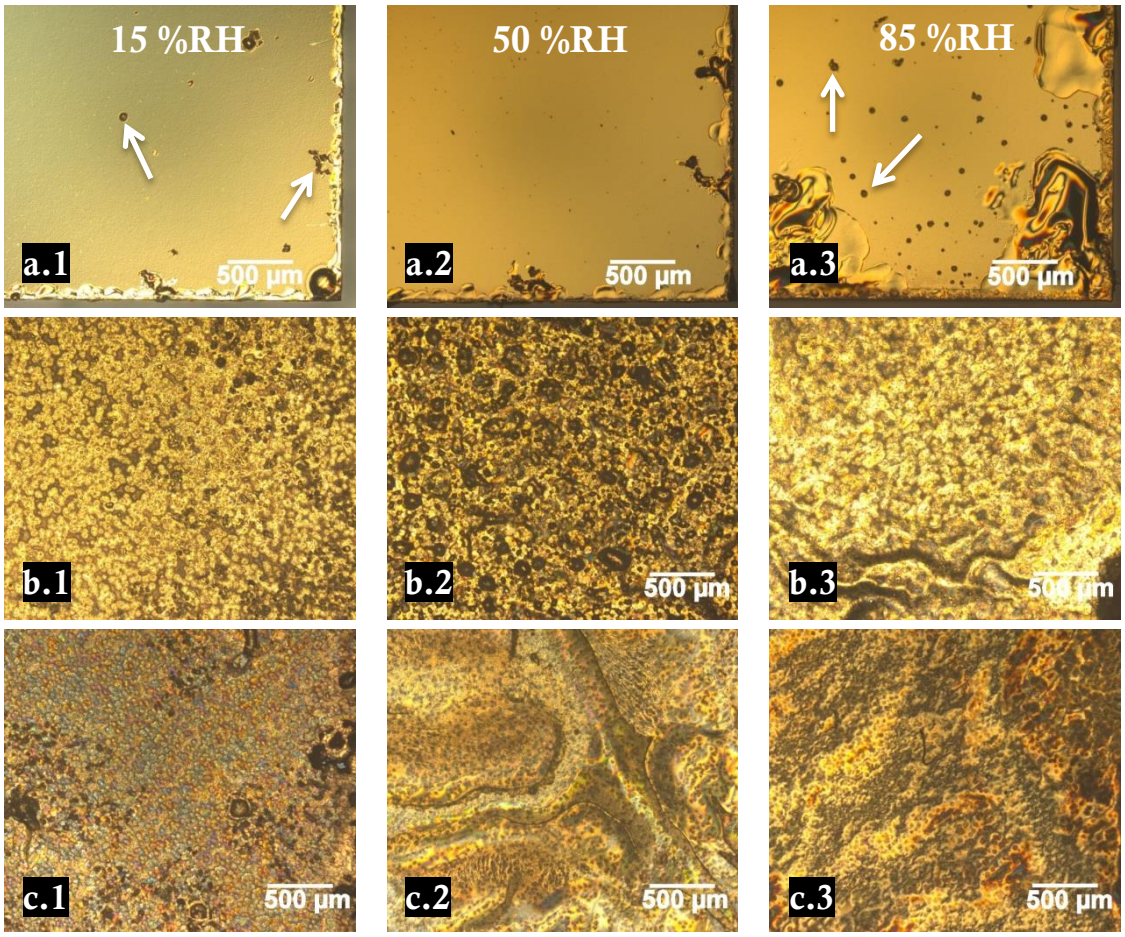

Figure 13.7: Corrosion of Au-Al multilayer heat treated at 175 °C: a. 0 h, b. 1 h, and c. 4 h after 24 h exposure to 1 mg·L^{-1} of iodine at 85°C and three levels of relative humidity: 1. 15 %RH, 2. 50 %RH, 3. 85 %RH

The corrosion of underlying Al layer was also observed in the cross sections of Au-Al multilayers in Figure 13.8. The two layers of Au and Al start to separate, and it can be seen that the preferential area for corrosion attack is at the interface between the two layers (Figure 13.8. a.1). The corrosion of heated samples (Figure 13.8. a.2 and a.3) appears similar, both showing preferential corrosion of Al, separation between Au-Al multilayers thus formation voids. For reference, the cross section of a sample heated for 4 h, but not exposed to iodine is provided in Figure 13.8. b.3.

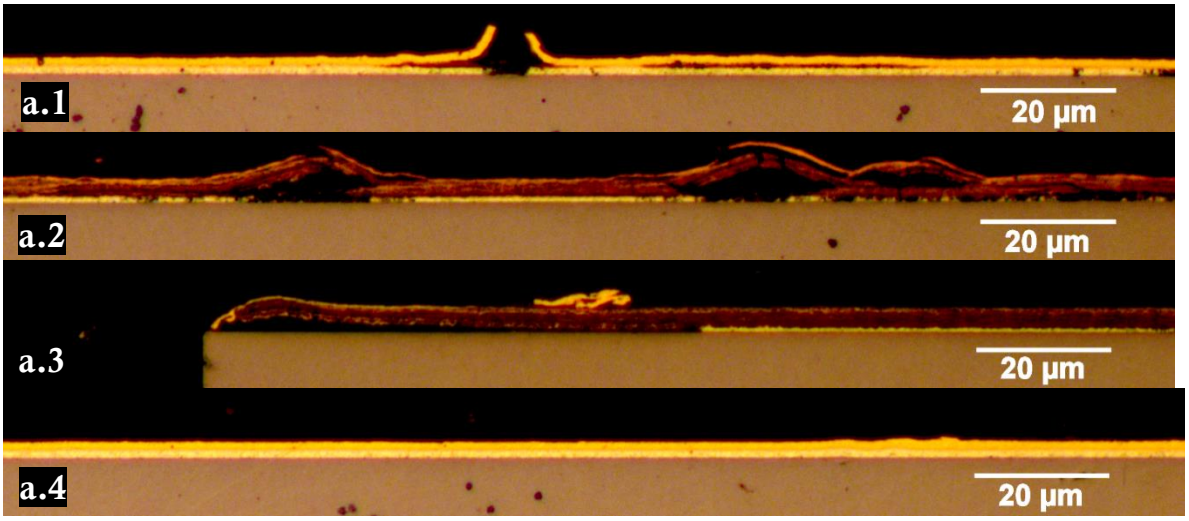

Figure 13.8: Cross section of Au-Al multilayers: after 24 h exposure to 1 mg·L^{-1} of iodine at 85°C/85%RH: a.1 non-heated, a. 2 heat treated for 1 h a.3 heat treated for 4 h; b.3 reference sample (non-heat treated and unexposed to iodine)

The SEM EDS analysis of the surface of the corroded Au-Al multilayer is shown in Figure 13.9. In connection with the surface roughness seen in Figure 13.7, the presence f Al rich areas (bumps) containing high amounts of oxygen combined with iodine was identified in the EDS map of elemental composition.

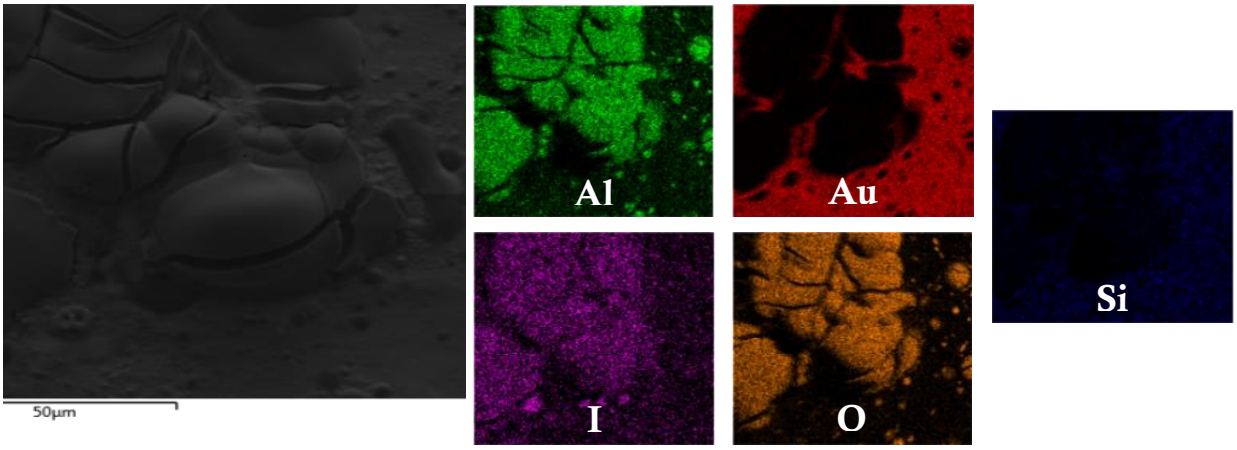

Figure 13.9: Corrosion of Au-Al multilayer heat treated for 1 h, after 24 h exposure to 1 mg·L^{-1} of iodine at 85°C/85%RH

CORROSION OF AU-AL WIRE BOND CONNECTIONS

SHEAR STRENGTH DEGRADATION OF WIRE BONDS

Figure 13.10 a. shows the reduction of the shear strength of bare Au-Al wire bond connections on Si dies after immersion in 500 mg·L^{-1} KI solution as a function of time. The shear strength of wire bonds was reduced by approx. 9 % after 24 h immersion and by approx. 18 % after 48 h immersion, compared to the control samples. No ball lift occurred after 48 h, while after 168 h immersion 21 out of 32 balls were lifted from the bond pad. The remaining wire bonds showed significant corrosion indicated by reduced shear force strength.

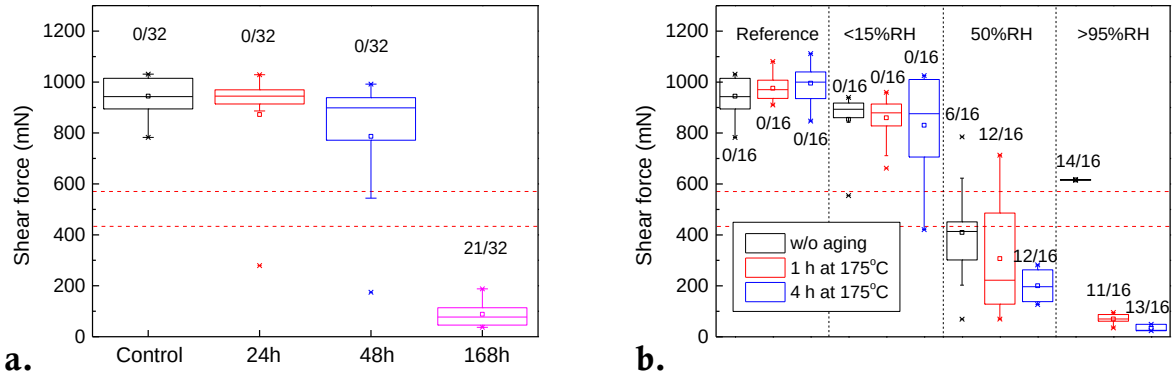

Figure 13.10: Shear force degradation of wire bonds: a. immersion in 500 mg·L^{-1} KI solution as a function of time and b. exposure to I_2 at 1 mg·L^{-1} as a function of RH at 25 °C (number of lifted off bonds is indicated in the graph i.e. 0 out of 32)

Figure 13.10 b. shows the test results for Au-Al wire bonds after 24 h exposure to 1 mg·L^{-1} of iodine and three humidity conditions at 85 °C. Prior to exposure to the corrosive environments, the samples were heat treated at 175 °C for 1 h and 4 h as it was done for multilayers of Au and Al. Increased corrosion attack indicated by the reduced shear force was observed for all exposure conditions; however, a slight increase of the shear force was observed for the unexposed (reference) samples after heat treatment. The samples dried at 85 °C for 12 h (in the graph denoted as <15 % RH) and exposed to 1 mg·L^{-1} of iodine indicated a slight reduction in the shear force from approx. 970 mN to 850 mN. However, a drastic reduction in the wire bond shear strength was observed with increase of RH to the level of 50 % and higher. Similarly, the number of bond lifts was increasing with increase of RH, with 0 at lowest RH, and approximately 12 out 16 at highest RH level. However, the shear force of the remaining wire bonds after exposure to high humidity and iodine was below 100 mN. As provided in the standard wire bond shear test method EIA/JESD22-B116 [24], the minimum recommended individual and sample average ball bond shear values should be accordingly 434 mN and 571 mN for 101 µm Au ball diameter. Whereas according to the test method ASTM F 1269 [25], approximately 550 mN is referred as 50 % of strength of the Au-Al wire bond (32 µm Au wire bonded to Al with 100 µm ball).

MORPHOLOGY OF CORRODED WIRE BONDS

Severe corrosion of Al bond pads after 24 h exposure to 1 mg·L^{-1} of iodine at 85 % RH was observed (Figure 13.11). The lifted off Au balls revealed oxidation of Al bond pad, which was

comparable to the cracking of Al oxide on sputter deposited Al exposed to the same test conditions (Figure 13.6). A layer of Al was also observed on the wire ball shown in SEM image in Figure 13.11 b.

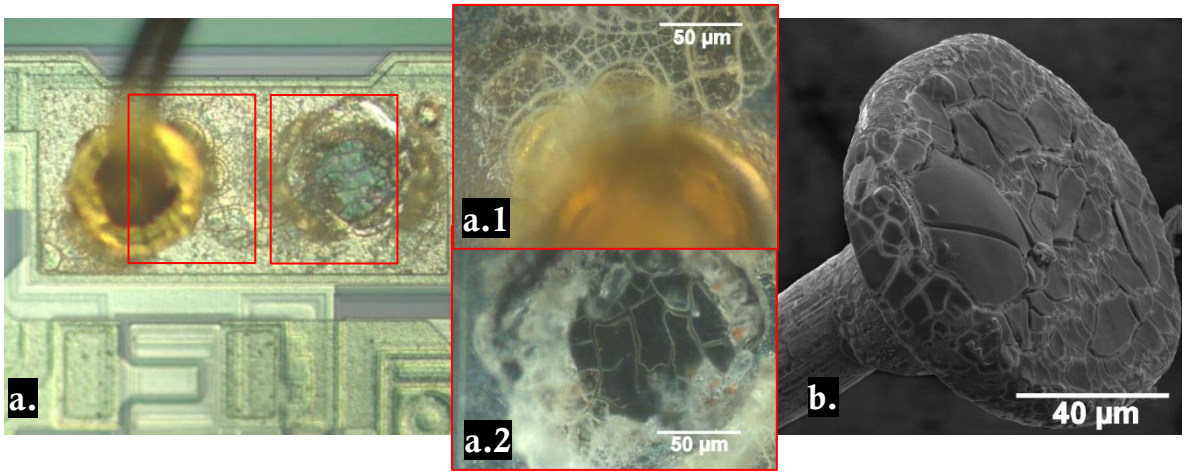

Figure 13.11: Micrographs of corrosion on Si dies after 24 h exposure to 1 mg·L^{-1} of iodine at 85°C/85%RH: a. severe oxidation of the bond pad (a.1 and a.2 is close-up view), and b. lifted off wire bond (EDS map of the bond is provided in Figure 13.13)

The SEM EDS mapping of the bond pads after ball lift off is shown in Figure 13.12. Aluminium oxide and traces of iodine were identified at the foot print of lifted ball in Figure 13.12. At the periphery of the bond, aluminium oxide is present. Whereas at the centre of the bond the aluminium was lifted off with the bond, and underlying Si was exposed.

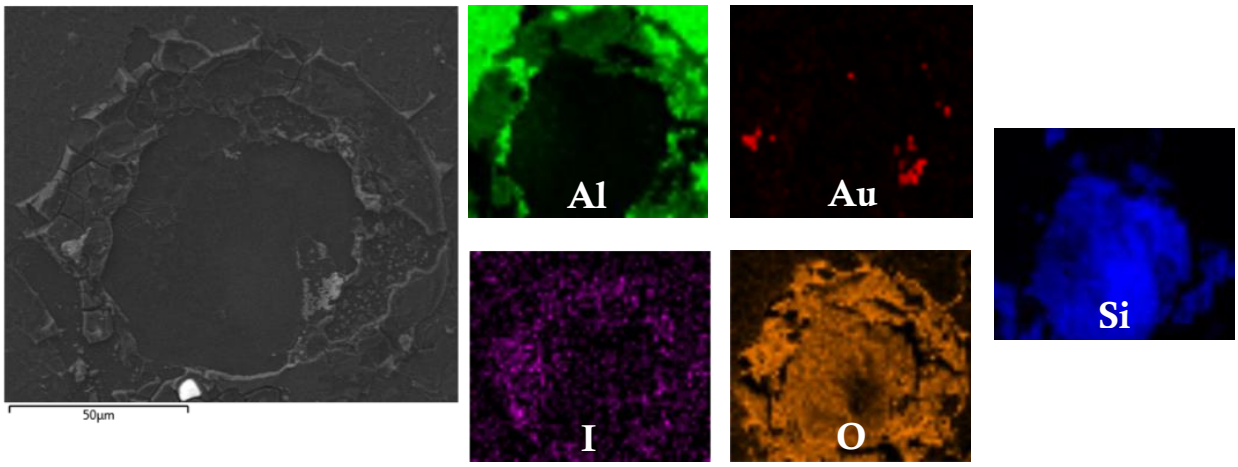

Figure 13.12: SEM EDS mapping of the bond pad after ball lift off (after 24 h exposure to 1 mg·L^{-1} of iodine at 85°C/85%RH)

SEM EDS analysis of lifted wire bond in Figure 13.13 (magnified view of Figure 13.11 b.) indicated presence of a layer composed of a mixture of Al, oxygen, and minor amounts of Au and iodine. The close-up view of the wire bond indicated that the cracking layer visible in the SEM image is Al oxide, while beneath Au is present.

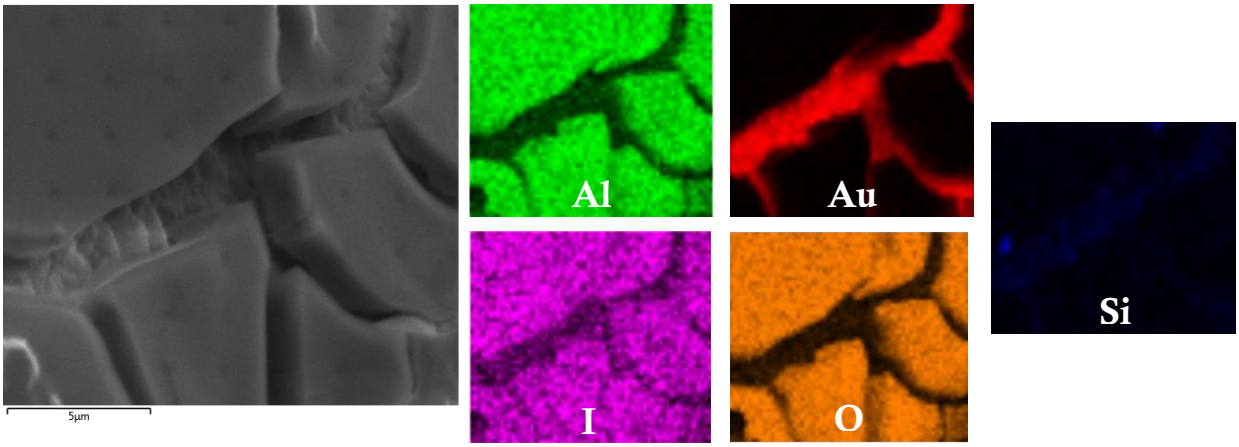

Figure 13.13: SEM EDS mapping of the wire bond after ball lift off (after 24 h exposure to 1 mg·L^{-1}of iodine at 85°C/85%RH)

IV. DISCUSSION

CORROSION OF AU-AL INTERMETALLICS

A reduction of corrosion resistance of the Au-Al layer with increase of heat treatment time is attributed to the interdiffusion of Au and Al and formation of Al rich intermetallic phases. Following observations are in agreement with this, namely: (i) the GDOES results in Figure 13.1 shows composition change indicating the interdiffusion of two layers, and (ii) the optical and SEM micrographs in Figure 13.2 showed change in surface morphology with time of heating, indicating formation of intermetallics. The columnar morphology at the top surface of the coating in Figure 13.2 b.3 and c.3 might be due to the fact that the interdiffusion of Au and Al is preferentially occurring through the column/grain boundaries. The formation of intermetallic phases with temperature and time of heating followed with the use of *in situ* XRD measurements in Figure 13.3, indicated that after heat treatment for 1 h, the original Au close to the surface is still present, while deeper into the bulk the Au_4Al and Au_8Al_3 intermetallic phases are being formed, with Au_8Al_3 as the predominant phase. In case of 4 h heat treatment, the Au from the upper layer is consumed; the interdiffusion of Au and Al transforms the intermetallic phases Au_4Al and Au_8Al_3 into IMPs with higher amount of Al namely: Au_2Al and $AuAl_2$. Formation of intermetallics in the present work is in agreement with the phase diagram [2], and with studies reported on the IMP formation during Au-Al bonding and aging process [5]–[7].

The results from corrosion testing of Au-Al intermetallics formed within the Au-Al multilayer in gaseous iodine at 1 mg·L^{-1} with varying RH and aqueous 500 mg·L^{-1} KI solution shows clear effect of increased aluminium concentration in the intermetallics. Corrosion rate of the various intermetallics increased with increasing amount of Al in the IMPs. Investigations using the aqueous KI solution shows shift in the corrosion potential towards active side (negative side) with increase in content of Al in the IMP, which is in agreement with the corrosion rate measurements. The average current density between Al and Au-Al intermetallics increased from 0.6 to 4.4 µA·cm^{-2} with increase of Au from Au_2Al to Au_4Al and up to 7.8 µA·cm^{-2} between Al and Au. The highest galvanic current was measured between Au coupled with the Al, which is typical for Au-Al couples due to large difference in the electrochemical potential.

Corrosion testing of Au-Al layer in gaseous iodine at 1 $mg \cdot L^{-1}$ and varying RH indicated decrease of corrosion resistance of Au-Al intermetallics with increasing Al in the IMPs (Figure 13.6-8). Aluminium itself has low resistance to iodine and oxidizes fast (Figure 13.6). For a thin layer of Au, the corrosion appears as tarnishing of the surface (Figure 13.6), similarly as it was reported in iodine containing solution [26]; however, corrosion initiates at higher humidity levels. Increase of humidity acts as accelerating factor in corrosion of Au, Al and Au-Al in iodine environment.

Overall, the results show that with increased time of exposure to high temperatures the gold from the surface is consumed for the intermetallic phase formation, thus resulting in reduction of corrosion resistance as corrosion rate of Au-Al intermetallic increases with increasing amount of Al in the intermetallic. The results allow one to assume that the corrosion would initiate at the interface between Au ball and Al metallization of the bond pad, as it was observed as preferential area for corrosion initiation from the cross section of the corroded Au-Al layer in Figure 13.8, and from the highest corrosion rate of Al in aqueous iodide solution.

CORROSION OF AU-AL WIRE BONDS

Significant reduction of wire bond shear strength was observed for the wire bonds exposed to 1 $mg \cdot L^{-1}$ of iodine at 50 %RH and >95 %RH, compared to that of dried samples (<15 %RH) and reference samples (Figure 13.10 b.). A slight increase of the shear force for the reference samples heated at 175 °C can be attributed to the formation of intermetallics, as the Au-Al intermetallic phases have higher strength than Au or Al, but at the same time they are more brittle [1], [8]. The heat treatment of wire bonds also had an effect on corrosion, which in turn resulted in the reduction of wire bond shear strength. In comparison with the microstructural effects explained above, the increased corrosion of the bonds might be attributed to the interdiffusion and IMP formation. With increase in the time of heating, IMP zone size increases while the composition will become rich in Al. Both increase in size of the IMP zone and increased Al content makes it more corrosive and brittle leading to reduced shear force for bond failure.

The SEM EDS analysis of the failed wire bonds in gaseous iodine environment showed that most of the ball lifts occurred from the layer of the Al metallization. The severe oxidation of the bond pads in Figure 13.12 and presence of Al oxide/hydroxide and iodine on the lifted off wire bond in Figure 13.13 indicated that the corrosion is preferentially taking place at the interface between the Au ball and Al metallization. Further, the presence of iodine on the corroded Al metallization in Figure 13.12 confirm this fact that the crack propagated through the interface exposing the crack wall to iodine as it propagates. Higher amounts of iodine are concentrated at the periphery of the ball bond, where less Au rich phases are known to be formed [18].

Literature suggests the formation of weak lamellar microstructure as the main mechanism of wire bond degradation in halide containing environments [11], [15], [27], [28]. However, the void formation as a result of Al removal from the IMP in the form of volatile halides is also proposed as a mechanism for wire bond failure, observed during aging in the heating oven at temperatures (125 – 180) °C [11]. A study reported on the effect of bromine and chlorine on the degradation of Au-Al wire bonds, suggested that the failure of the bond is caused by halogen-aluminium corrosion reactions between Au and Au-Al intermetallics, particularly Au_4Al and Au_5Al_2 (Au_8Al_3) [29]. The fracture within or between intermetallic compounds was furthermore reported

as a cause of failure of Au-Al wire bonds due to aging of the bonds [4]. The decoupling of Au bond from the transformed intermetallic phases due to formation of Al_2O_3 between the Au ball and the remaining intermetallics structure has been reported as the failure mechanism induced by the bromine from the flame retardants [18]. The wire bond detaching mechanism related to the bromine effect is similar to the mechanism observed in current work, however, in current study the oxidation of Al was significantly accelerated by the RH. As such Au-Al-bonds are often coated with silicone potting gel, which will reduce the available humidity and hence shift the mechanism to the dry mechanism until the humidity reaches the interface. Therefore, some level of improvement in life time can be achieved by potting; however, the time interval for safe use is determined by the water permeation properties of the gel and humidity level in the user atmosphere.

A general comparison of the results in this paper clearly shows corrosion susceptibility of Au-Al wire bond connections exposed to iodine containing environments. Results show the importance of the formation of intermetallics during the wire bonding process in introducing failures by a combination of mechanical stress and corrosion at the wire bond-metallization interface. Further, humidity is an important factor in increasing the aggressiveness of iodine through mechanism of the formation of iodine containing species.

CORROSION MECHANISM OF AU-AL IN IODINE ENVIRONMENTS

Based on the observation of the corrosion of the Au-Al multilayer and directly on the Au-Al wire bonds exposed to iodine containing environments, the following mechanism for the corrosion of Au-Al interconnections is proposed. The feasibility of suggested reactions was verified based on the Gibbs free energy calculation using a HSC Chemistry 7.1™ [30].

First step in the process assumed to be the reaction of iodine with water and oxygen forming hypoiodous acid and hydrogen iodide:

$$I_2 + H_2O \rightarrow HIO + HI(g) \quad (1)$$

The produced hydrogen iodide reacts with the aluminium thereby forming aluminium iodides AlI_3 [21] which can also be present in dimeric form Al_2I_6, according to eq. 2.

$$6HI(g) + 2Al \rightarrow 2AlI_3[-\text{or } Al_2I_6] + 3H_2(g) \quad (2)$$

The aluminium iodides in excess of oxygen forms alumina and iodine according to eq. 3, or they can hydrolyse in presence of water to form Al hydroxide and hydrogen iodide (eq. 4) [21]. Formation of Al oxide and hydroxide is an important process in degradation of wire bonds, and it is the main reason for the ball lifts occurring from the Al bond pads. Whereas recycling of iodine allows starting over the sequence of reactions and corrosion process continues until Al is accessible.

$$4AlI_3[-\text{or } 2Al_2I_6] + 3O_2 \rightarrow 2Al_2O_3 + 6I_2 \quad (3)$$

$$AlI_3\left[-\text{or } \tfrac{1}{2}Al_2I_6\right] + 3H_2O \rightarrow Al(OH)_3 + 3HI(g) \quad (4)$$

Alternatively, Al can be oxidized via eq. 5, where hypoiodous acid (eq. 1.b) can attack Al forming alumina and hydrogen iodide, which further can react with Al according to eq. 2.

$$3HIO + 2Al \rightarrow Al_2O_3 + 3HI(g) \quad (5)$$

Overall, the role of oxygen and water is essential in the above mechanism, which involves the formation of hydrogen iodine and hypoiodous acid in the presence of water, while both oxygen and water are reactive with aluminium iodides thereby resulting in Al_2O_3 (eq. 3) or $Al(OH)_3$ (eq.

4). The favourability of the reactions towards the formation of alumina or aluminium hydroxide is dependent on the humidity level in the user environment.

Under dry condition (without water or even oxygen), direct reaction of iodine with aluminium is thermodynamically feasible (eq. 6), however, the recycling of iodide will not take place without oxygen.

$$2Al + 3I_2 \rightarrow 2AlI_3 \quad (6)$$

Although Au has the highest corrosion resistance compared to Au-Al intermetallics, it can also corrode, but will react slower. Practically, an aqueous solution of iodine and potassium-iodide is used to etch gold [31][32], thus iodine can directly react with the gold according to eq. 7:

$$2Au + I_2 \rightarrow 2AuI \quad (7)$$

The corrosion of Au observed on sputter deposited samples in (Figure 13.6 a.) could be also caused by gold reaction with the hydrogen iodide according to eq. 8; however, the reaction becomes thermodynamically unfavourable with increase of temperature above 50 °C:

$$2Au + 2HI(g) \rightarrow 2AuI + H_2(g) \quad (8)$$

In case if gold iodide is formed (eq. 7 and 8), it rapidly reacts with water and oxygen thereby causing redeposition of the Au, as it was observed on Si wafer in Figure 13.6 a.3 according to eq. 9:

$$4AuI + 2H_2O + O_2(g) \rightarrow 4Au + 4HIO \quad (9)$$

Gold-iodide also reacts with residual Al and thereby redeposit according to eq. 10:

$$3AuI + Al \rightarrow AlI_3 + 3Au \quad (10)$$

Overall the mechanism suggested above can be compared with the corrosion mechanisms of aluminium under chloride conditions [33] and some of the suggested mechanisms in relation with iodine [21]. The suggested steps in the mechanisms are the adsorption of halogen on the oxide, incorporation into the bulk of oxide, movement towards the oxide metal interface through oxide films, and at the last formation of blister and rupture of the oxide film [33]. However, in the present case majority of the corrosion is taking place due to IMPs with significant amount of gold. High noble electrochemical potential of gold could oxidize aluminium; however, the present result did not show any significant effect due to the presence of gold in repassivating aluminium under iodine conditions.

V. CONCLUSIONS

1. Electrochemical testing of Au-Al intermetallics in 500 $mg \cdot L^{-1}$ of KI in water showed a reduction of the corrosion potential and an increase of the corrosion current density with increase of Al content. The highest galvanic current was measured between Au and Al, and reduced with decrease of Au in intermetallic coupled with Al and with decrease of Al in intermetallic coupled with the Au.
2. The corrosion susceptibility of Au-Al multilayer increased with time of heat treatment. The observation is attributed to formation of intermetallic phases with lower content of Au. Thin layer of Au acts as a barrier for corrosion; however, it is affected by the interdiffusion of Au and Al during aging. A preferential corrosion of Al and at the interface between Au-Al intermetallics was observed.
3. Humidity accelerates corrosion significantly, which reflected in the reduction of shear strength of the wire bonds and from the extent of corrosion of Au-Al multilayer. A slight

decrease of the wire bond shear strength was observed on the heat treated wire bonds after exposure tests. The observation is related to increase of intermetallic zone and formation of Al reach intermetallic phases at the periphery of the bond, and thereby increase of area for preferential corrosion of Al from the intermetallic phases.

4. Failures of Au-Al wire bonds in iodine environment are mainly attributed to the corrosion of Al via formation of Al iodides and consequent formation of Al oxides and/or hydroxides. Al metallization and Al rich intermetallic phases are most susceptible to corrosion.

VI. ACKNOWLEDGMENTS

This work was supported by Robert Bosch GmbH and CELCORR/CreCon consortium (www.celcorr.com). Acknowledgments are also to Prof. Dr. H. Dosch, and J. Major from Max-Planck-Institut für Metallforschung, Stuttgart, for preparation Au-Al intermetallics nuggets for Robert Bosch GmbH, and Mr. B. Klein from Robert Bosch GmbH, Automotive electronics, for the preparation of sputter deposited Au-Al samples. Dr. Michael Leineweber from Robert Bosch GmbH is acknowledged for helpful discussions during writing of the paper.

VII. REFERENCES

[1] G. Harman, *Wire bonding in microelectronics*, 3rd ed. McGraw Hill Professional, 2010, p. 426.

[2] H. Okamoto, "Al-Au (Aluminum-Gold)," *J. Phase Equilibria Diffus.*, vol. 26, no. 4, pp. 391–393, Aug. 2005.

[3] K.-J. Range and H. Büchler, "High pressure synthesis and crystal structure of Al3Au8," *J. Less-Common Met.*, vol. 154, no. 2, pp. 251–260, 1989.

[4] V. Koeninger, H. H. Uchida, and E. Fromm, "Degradation of gold-aluminum ball bonds by aging and contamination," *IEEE Trans. components, Packag. Manuf. Technol. Part A*, vol. 18, no. 4, pp. 835–841, 1995.

[5] H. S. Liu, J. Wang, Y. Du, and Z. P. Jin, "Thermodynamic description of the Au–Al system," *Zeitschrift für Met.*, vol. 95, no. 1, pp. 45–49, Jan. 2004.

[6] N. Noolu, N. Murdeshwar, K. Ely, J. C. Lippold, and W. A. Baeslack III, "Partial diffusion reactions and the associated volume changes in thermally exposed Au-Al ball bonds," *Metall. Mater. Trans. A Phys. Metall. Mater. Sci.*, vol. 35A, no. 3, pp. 1273–1280, 2004.

[7] N. Noolu, N. Murdeshwar, K. Ely, J. C. Lippold, and W. A. Baeslack III, "Phase transformations in thermally exposed Au-Al ball bonds," *J. Electron. Mater.*, vol. 33, no. 4, pp. 340–352, 2004.

[8] N. J. Noolu, N. M. Murdeshwar, K. J. Ely, J. C. Lippold, and W. a. Baeslack, "Degradation and failure mechanisms in thermally exposed Au–Al ball bonds," *J. Mater. Res.*, vol. 19, no. 5, pp. 1374–1386, 2004.

[9] W. M. Paulson and R. P. Lorigan, "The Effect of Impurities on the Corrosion of Aluminum Metallization," in *Reliability Physics Symposium*, 1976, pp. 42–47.

[10] M. Khan, H. Fatemi, J. Romero, and E. Delenia, "Effect of high thermal stability mold material on the gold-aluminum bond reliability in epoxy encapsulated VLSI devices," in *Reliability Physics Symposium*, 1988, pp. 40–49.

[11] R. Gale, "Epoxy degradation induced Au-Al intermetallic void formation in plastic encapsulated MOS memories," *Reliab. Phys. Symp.*, pp. 37–47, 1984.

[12] R. Lum and L. Feinstein, "Investigation of the Molecular Processes Controlling Corrosion Failure Mechanisms in Plastic Encapsulated Semiconductor Devices," *Microelectron. Reliab.*, vol. 21, no. 1, pp. 15–31, 1981.

[13] S. S. Ahmad, R. C. Blish, T. J. Corbett, J. I. King, and C. G. Shirley, "Effect of Bromine in Molding Compounds on Gold - Aluminum Bonds," *IEEE Trans. Components, Hybrids, Manuf. Technol.*, vol. 9, no. 4, pp. 379–385, 1986.

[14] Y. Jianhai, B. Shengxiang, M. Lili, and L. Dechun, "Failure analysis of halide of epoxy molding compound used for electronic packing," in *2009 International Conference on Electronic Packaging Technology and High Density Packaging*, 2009, pp. 759–762.

[15] R. Ritchie and D. Andrews, "CF4/O2 Plasma Accelerated Aluminum Metallization Corrosion in Plastic Encapsulated ICs in the Presence of Contaminated Die Attach Epoxies," in *Reliability Physics Symposium*, 1981, pp. 88–92.
[16] H. F. M. M. Khan, "Gold-aluminum bond failure induced by halogenated additives in epoxy molding compounds," in *1986 International Symposium on Microelectronics*, 1986, pp. 420–427.
[17] G. Grause, M. Furusawa, A. Okuwaki, and T. Yoshioka, "Pyrolysis of tetrabromobisphenol-A containing paper laminated printed circuit boards.," *Chemosphere*, vol. 71, no. 5, pp. 872–8, Mar. 2008.
[18] K. N. Ritz, W. T. Stacy, and E. K. Broadbent, "The Microstructure of Ball Bond Corrosion Failures," in *Reliability Physics Symposium*, 1987, pp. 28–33.
[19] H. Qin, N. Sun, and R. J. Palmer, "Heat stabilized palyamide moulding," US 2010/0120985 A1.
[20] S. G. Stoeff, "Heat stabilization of polyamides," US2705227 A.
[21] M. Leineweber and L. Müller, "Iodide based polyamide stabilisers as potential risk for corrosion in electronics," *Corros. Eng. Sci. Technol.*, vol. 48, no. 6, pp. 445–451, 2013.
[22] R. Klengel, S. Bennemann, J. Schischka, C. Grosse, and M. Petzold, "Advanced failure analysis methods and microstructural investigations of wire bond contacts for current microelectronic system integration," in *2009 European Microelectronics and Packaging Conference*, 2009.
[23] R. Klengel, S. Klengel, T. Stephan, and M. Petzold, "Novel investigation of influencing factors for corrosive interface degradation in wire bond contacts," in *2013 European Microelectronics Packaging Conference (EMPC)*, 2013.
[24] "EIA/JEDEC STANDARD EIA/JESD22-B116, Wire Bond Shear Test Method." 1998.
[25] "ASTM F1269-89 Test Methods for Destructive Shear Testing of Ball Bonds," 2001.
[26] N. Takasusuki, Y. Ida, Y. Hirose, M. Ochi, and K. Endo, "In vitro corrosion of dental Au-based casting alloys in polyvinylpyrrolidone-iodine solution," *Dent. Mater. J.*, vol. 32, no. 3, pp. 390–397, 2013.
[27] R. Thomas, V. Winchell, K. James, and T. Scharr, "Plastic outgassing induced wire bond failure," in *27th Electronic Components Conference*, 1977, pp. 182–187.
[28] H. Ji, M. Li, J. Kim, D. Kim, and C. Wang, "Nano features of Al/Au ultrasonic bond interface observed by high resolution transmission electron microscopy," *Mater. Charact.*, vol. 59, no. 10, pp. 1419–1424, 2008.
[29] M.-H. Lue, C.-T. Huang, S.-T. Huang, and K.-C. Hsieh, "Bromine- and Chlorine-Induced Degradation of Gold-Aluminum Bonds," *J. Electron. Mater.*, vol. 33, no. 10, pp. 1111–1117, 2004.
[30] "HSC Chemistry 7.1." Outotec (Finland) Oy Information Center.
[31] A. Davis and T. Tran, "Gold dissolution in iodide electrolytes," *Hydrometallurgy*, vol. 26, pp. 163–177, 1991.
[32] J. M. Köhler, *Ätzverfahren für die Mikrotechnik*. Wiley-VCH, 1998, p. 398.
[33] P. M. Natishan and W. E. O'Grady, "Chloride Ion Interactions with Oxide-Covered Aluminum Leading to Pitting Corrosion: A Review," *J. Electrochem. Soc.*, vol. 161, no. 9, pp. C421–C432, Jun. 2014.

14. COLORIMETRIC VISUALIZATION OF TIN CORROSION: A METHOD FOR EARLY STAGE CORROSION DETECTION ON PRINTED CIRCUIT BOARDS

Vadimas Verdingovas, Morten Stendahl Jellesen, and Rajan Ambat

Abstract— A majority of printed circuit board surfaces are covered with tin, therefore tin corrosion under humid conditions and movement of tin ions under the influence of an electric field plays an important role in the corrosion failure development. Tracking tin corrosion products spread on the printed circuit board assembly (PCBA) provides a basis for the mechanistic understanding of PCBA corrosion failures and leak current tracks which eventually can lead to electrochemical migration. This paper presents a method for identification of such failures at the early stage of corrosion by using a colorimetric tin ion indicator applied as a gel. The examples provided in this paper include visualization of corrosion caused by weak organic acids found in solder fluxes, corrosion profiling on the PCBAs after climatic device level testing, and failure analysis of field returns.

Highlights

- A new method for tin corrosion profiling on the PCBA surface is presented
- High sensitivity of the method enables detection of tin corrosion at its early stage
- Color change enables easy detection of corrosion initiation sites during visual inspection
- Examples provided include device level testing and corrosion failure analysis of field returns

Keywords—Tin corrosion, Leakage current, Electrochemical migration, Surface insulation resistance, Reliability, Testing, Humidity

I. INTRODUCTION

The reliability of electronics can be compromised by the presence of contamination on the printed circuit board assembly (PCBA) and humidity exposure during its service life [1]. Corrosion of PCBA involves local humidity build-up and formation of water layer containing ionic residues connecting metallic parts on multiple components and metallic tracks. The driving force for corrosion is usually the applied potential bias. Unlike conventional corrosion of a single surface, water layer formation and electrochemical corrosion process on the PCBA cause an interaction between components by the movement of corrosion products across the board to nearby points due to the electric field acting through the water layer. In terms of functionality of the PCBA, this represents leak current which subsequently leads to electrochemical migration failures. Tracing such leak current tracks and movement of corrosion products by visual examination is difficult due to the lower levels of corrosion products and masking effects.

Climatic testing of electronics is a part of product optimization and verification process. The climatic testing can be performed either on the actual device by exposing electronics to severe

V. Verdingovas, M. S. Jellesen, and R. Ambat, "Colorimetric visualization of tin corrosion: A method for early stage corrosion detection on printed circuit boards," draft to be submitted to *Microelectron. Reliab.*, 2015.

conditions expected in a user environment, or using standardized test boards under well-defined climatic profile. The IPC-TM-650 manual describes various standardized test methods for improving the reliability of electronics. For example, the corrosive effects of soldering fluxes can be assessed by methods such as surface insulation resistance (SIR) (method 2.6.3.3) [2], electrochemical migration (method 2.6.14.1) [3], corrosion (method 2.6.15) [4], and copper mirror test (method 2.3.32) [5]. During life in service and device level testing, the intermittent failures and faults are common under humid and condensing conditions; however, the detection of such failures is more difficult once the surface of the PCBA dries and the functionality of the device partly recovers. Mostly such failures in the field are reported as 'no-fault-found'[6], [7].

The majority of the PCBA surface is covered by tin (Sn) or tin-based alloys such as boards with hot air solder leveled (HASL) surface finish, and use of tin-based alloys for soldering and as a surface finish for contacts. In the case of tin corrosion in presence of high humidity, the precipitation of tin hydroxides can be seen; however, the appearance of tin hydroxides is similar to that of flux residues introduced by soldering processes. Therefore, identifying precipitation of tin corrosion products on the PCBA surface is an important part of understanding the susceptibility of a PCBA design to corrosion as a result of exposed climate conditions.

The aim of this paper is to demonstrate a method for tracing tin corrosion even at tiny levels on the PCBA surface. The method consists of the use of a colorimetric tin ion indicator in the form of a gel and application of the gel on the PCBA for corrosion inspection. The paper illustrates examples of gel application on standardized test boards and on device PCBAs. The detection of tin corrosion in its early stage reveals regions of PCBA most susceptible to failures due to humidity exposure. If combined with accelerated testing, such information would provide useful input for design modifications or taking remedial measures.

II. MATERIALS AND METHODS

CLIMATIC EXPOSURE TESTS

An "Espec PL-3KPH" climatic chamber with the specified accuracy of ±0.3 °C / ±2.5 %RH was used for climatic exposure tests. Climatic testing was carried out on the test boards with well-defined amounts of ionic residues, and on device PCBAs with contamination levels naturally present from the manufacturing processes. After climatic testing, all the boards were tested for the occurrence of tin corrosion using a gel with tin ion indicator. The temperature/humidity conditions used for specific testing are provided in the corresponding sections of results and discussion.

PCBAS USED FOR ANALYSIS

TEST PCBA

Visualization of tin corrosion using tin ion indicator in a gel was performed on the standardized test boards with known surface mount components and SIR comb pattern, and on the actual device PCBAs. The test board contains chip capacitors and chip resistors connected in parallel in rows of 10 components, and two SIR patterns. The surface finish of the SIR pattern was HASL with SN100C solder alloy. The dimensions of SIR pattern were 13 x 25 mm, while the width of conducting lines and the distance between them were 0.3 mm. The geometry related nominal

square count of the SIR pattern was 1476. A detailed description of the test board can be found elsewhere [8].

DEVICE PCBAS

A set of results was obtained on actual device PCBAs. The detailed information about the device type, application or electrical functionality is not provided here; however, all the devices which were tested are designed to operate under high humidity conditions typically seen in outdoor applications. The PCBAs are without a conformal coating or potting, thus the climatic reliability of devices greatly relies on the design of electronic enclosures. However, in this paper, the main focus was on the corrosion reliability of PCBA itself, thus the actual testing was performed without electronic enclosures.

PRECONTAMINATION OF THE PCBAS

For the investigations carried out on the test PCBAs, the precontamination of surface mount components and SIR comb patterns was done by dispensing a defined volume of weak organic acids (WOAs) dissolved at 10 g/L in isopropyl alcohol solution. The WOAs namely adipic, succinic, glutaric, DL-malic, and palmitic, were used for investigation, and the selected acids are representing the contamination from WOA based soldering fluxes. For the application of the WOAs, the ratio between surface area and volume was fixed, so that the resulting contamination of WOAs on the surface was 100 µg/cm2. For a set of experiments performed on a device PCBA, the precontamination with succinic acid was done by spraying the solution over the entire surface of the PCBA. Thereby, overall contamination level of (100 ± 30) µg/cm2 was achieved.

THERMAL IMAGING OF THE PCBAS

The thermal imaging camera "Trotec IC080LV" was used for imaging thermal profile of the PCBAs in operation mode. The colder areas on the PCBAs by default are identified as potential areas for local humidity effects and corrosion. Therefore, the thermal profiles are also taken into consideration when analyzing corrosion profiles after climatic testing.

VISUALISATION OF TIN CORROSION USING TIN ION INDICATOR GEL

Visualization of tin corrosion on the PCBAs was done by using a gel with colorimetric tin ion indicator. The methodology of the test is similar to the method used for detection of production residues on PCBA surface described in the patent WO 2011/048001 A1 [9], although the composition of the gel is modified. The preparation of the gel with indicator was done as follows: i) agar gel (type A7921, Sigma-Aldrich) was added into Millipore water with a conductivity of 18.2 MOhm·cm at 25 °C at concentration of 10 g/L, ii) the water containing agar gel was heated to a temperature above 80 °C for homogeneity of the solution, and iii) catechol violet as tin ion indicator was added into solution, while the solution was being stirred. The prepared gel solution was applied by spraying onto the entire printed circuit board, or by applying locally on the areas of interest by using a pipette. The presence of tin in its oxidation state +2 and +4 due to corrosion was visualized by color change of the gel from light yellow to blue/violet as a result of forming chelate complexes with tin ions. The detailed description of the complexation reactions and the properties of colored tin chelates can be found in the following reference [10]. For consistency of

the results, the inspection of the boards and the corresponding photographs were taken within 5-7 minutes after application of the gel. The use of tin ion indicator in a gel has been previously reported in the following applications: i) ranking of solder flux systems based on corrosion extent on the SIR patterns after climatic exposure [11], and ii) visualization of tin dissolution from the terminals of surface mount chip capacitors under pulsed voltage conditions [12]. Whereas this current work discusses the use of tin ion indicator gel in detail and the focus is placed on analyzing corrosion on actual device PCBAs after accelerated humidity testing and PCBAs failed in service.

III. RESULTS AND DISCUSSION

VISUALISATION OF CORROSION ON THE TEST BOARDS

COMPARISON BETWEEN CORROSION AND LEAKAGE CURRENT MEASUREMENTS

Effect of contamination, such as solder flux residues, on the electrical performance of electronics, is usually assessed by the SIR testing using standardized test patterns. In this case, the criterion for failure is the drop of SIR below 108 Ohms or the visual observation of corrosion and dendrites due to electrochemical migration [2], [3]. Visual inspection of test patterns after climatic testing does not always give unambiguous results. Sometimes, the corrosion traces on the tested boards are difficult to identify due to the mix up of white color produced both by the flux residues present from the soldering process and tin hydroxides. The morphology of flux residues is known to change throughout climatic exposure tests [13], especially at the elevated temperatures [14]; however, that does not necessarily have a negative effect on corrosion. While the presence of tin hydroxides is a clear indication of tin corrosion and it typically correlates with an increase in leakage currents, as shown in the following example.

The micrographs in Figure 14.1 a. show the SIR patterns with weak organic acids namely: DL-malic, glutaric, succinic, adipic and palmitic, after exposure to elevated humidity under bias condition. Throughout the testing, the leakage current was measured as a function of applied voltage between 0 V and 10 V for varying RH from 60 % RH to 98 % RH at 25 °C. The detailed description of the test method can be found elsewhere [15].

After climatic exposure, the visual inspection of SIR patterns with succinic, adipic and palmitic acids revealed no dendrites and only white residues spread between conductor lines, as seen in Figure 14.1 a. A white trace connecting two opposite conductors was seen on succinic acid contaminated SIR pattern (indicated by red arrow in the micrograph). Corrosion and formation of tin dendrites were seen on SIR patterns contaminated with DL-malic and glutaric acids. The growth of tin dendrites for those samples was also easily identifiable from leakage current spikes observed during SIR measurements. As an example in Figure 14.2 a, the leakage current curves for the glutaric acid are provided. Whereas, Figure 14.2 b. shows an overview of total charge transferred between the electrodes throughout the measurements and serves the purpose to summarize the results obtained for all the tested WOAs. The arrows in Figure 14.2 b. indicate the time corresponding to the first observation of conductor gap bridging by dendrite or corrosion products.

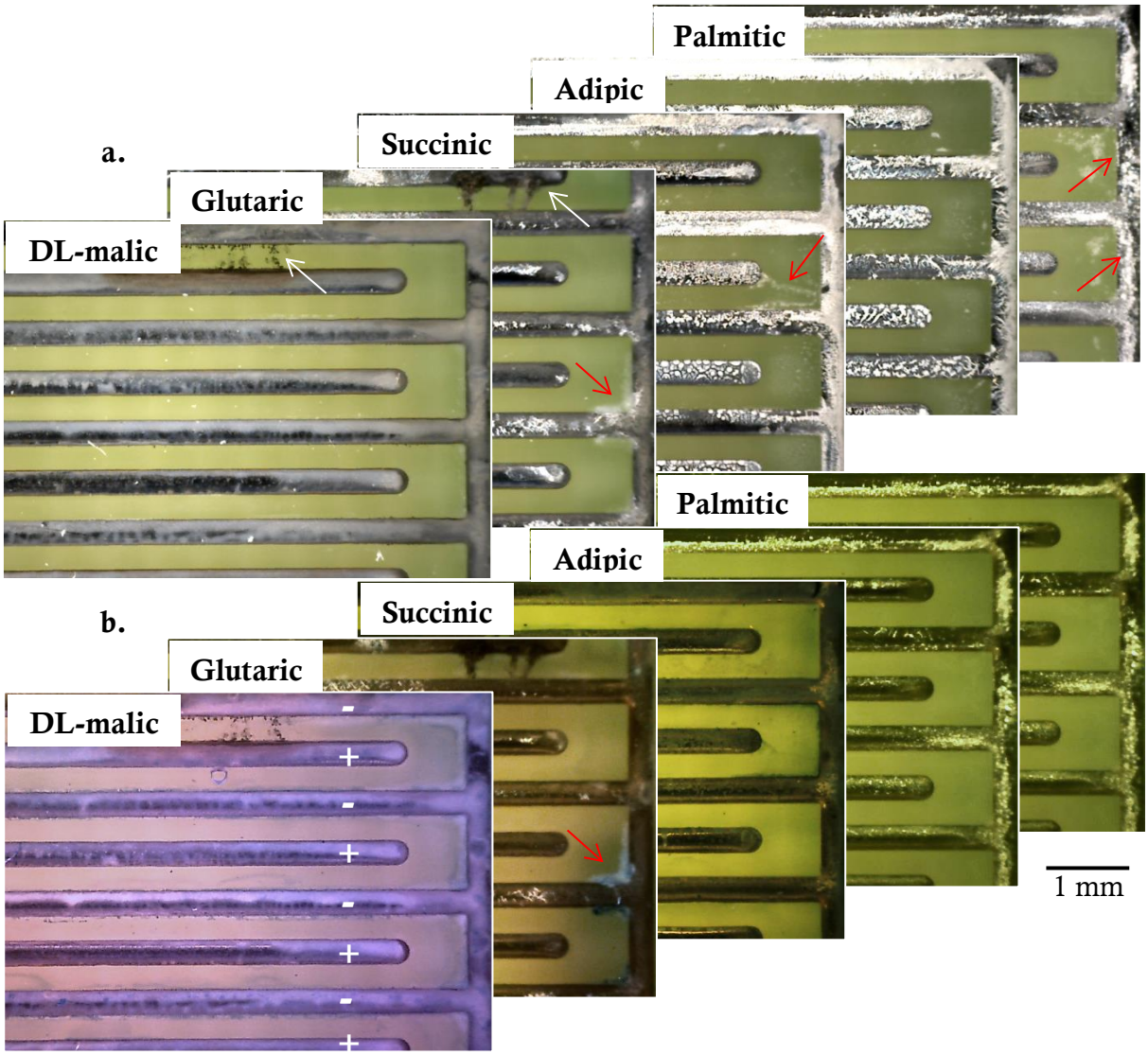

Figure 14.1: Optical micrographs of SIR patterns contaminated with different WOAs: a. after humidity testing and b. followed by applying tin ion indicator gel (white arrows indicate tin dendrites, red arrows indicate locations with white residues)

The summary graph in Figure 14.2 b. indicates that DL-malic acid was the most corrosive under humid conditions as it showed the highest charge transfer starting from the lowest RH levels. A high charge was also conducted on the SIR pattern contaminated with glutaric acid, especially, at the event of short-circuiting due to corrosion and dendrite formation (Figure 14.2 b). For glutaric acid, the formation of tin dendrites was more localized and resulted in the formation of thicker, more conductive dendrites as indicated by the white arrow in Figure 14.1 a. Whereas, for DL-malic acid, there were several sites where dendrite formation has initiated, while the formed dendrites were thinner (Figure 14.1 a). Although these initial observations do not allow explanation of the significant increase in charge transfer for DL-malic, the reason for high charge transfer can be attributed to the high ionic conductivity of the formed water film and the high corrosion attack as visualized by blue coloration after application of tin ion indicator gel (Figure 14.1 b). The overall blue coloration of SIR pattern contaminated with DL-malic acid suggests that the dissolution of tin has taken place over a large surface area of electrodes. The traces of corrosion

product containing tin ions/hydroxides became clearly visible, especially, nearby cathode electrodes, indicated by '-' in the micrographs.

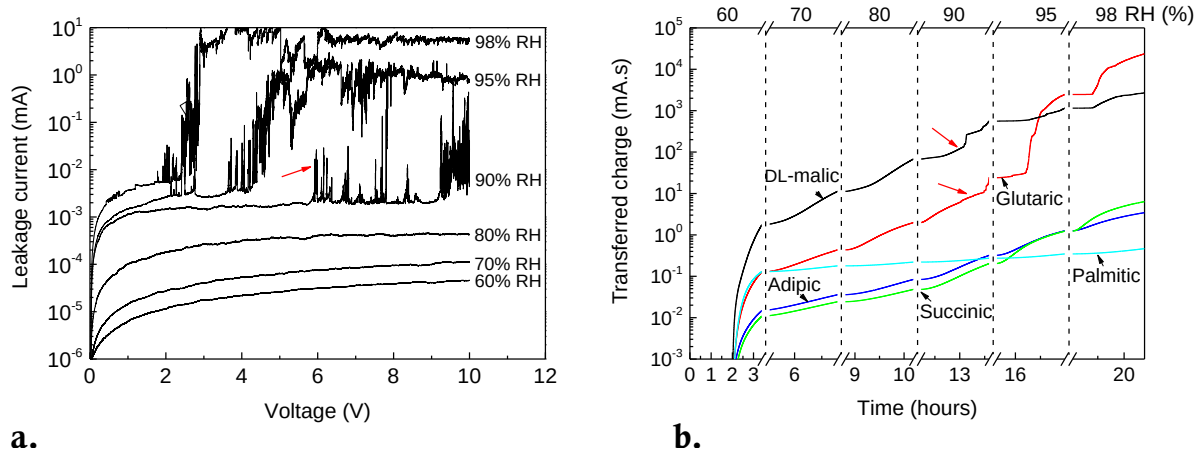

Figure 14.2: Leakage current response of WOAs on SIR pattern under humid conditions: a. typical leakage current curves for glutaric acid and b. overview of results from leakage current measurements presented as charge transferred between the electrodes of SIR pattern (arrows in the graphs indicate events of short circuiting due to corrosion and dendrite formation)

In Figure 14.2 b., adipic and succinic acids showed a steady and comparable increase of charge as a function of RH until 95%, however at 98% RH, the succinic acid showed a slightly higher increase compared to adicpic acid. The low water soluble palmitic acid showed the least increase in charge transfer. The adipic and palmitic acid did not show any corrosion and that was in good agreement with leakage current measurements. The white deposits observed on the SIR pattern, as indicated by red arrows for adipic and palmitic acids in Figure 14.1a, were originated from WOA contamination, and not as a result of the tin dissolution. For succinic acid, only slight blue appearance near the electrodes was observed. Overall, the results in Figure 14.1 show that the level of tin corrosion can be visualized using tin ion indicator and results are in agreement with the corrosivity of WOAs reported in other studies [15], [16].

The effect of various WOAs on the corrosion of tin is further demonstrated on the surface mount components. The tin dissolution and movement of tin ions and corrosion products are mapped ex-situ after 24 h exposure to 98 % RH at 25 °C and at 5 V DC in Figure 14.3. It is important to note that in total 10 components were tested for each WOA, however, only 1 representative component is shown here.

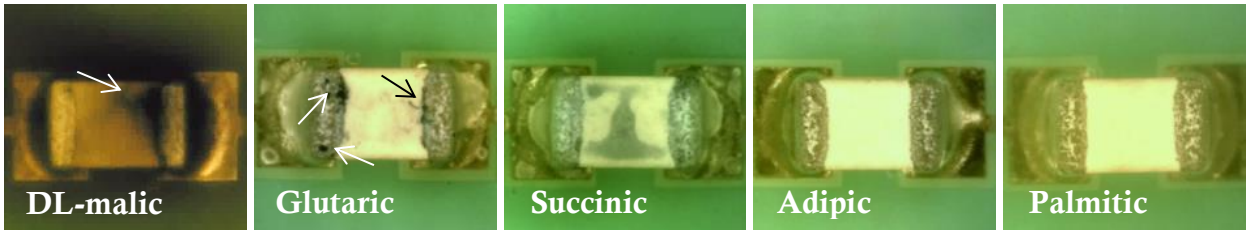

Figure 14.3: Corrosion of tin on surface mount chip capacitors precontaminated with different WOAs at 100 μg·cm^{-2} visualized using tin indicator gel (arrows indicate the areas where tin corrosion products were identified)

The corrosion and dendrite formation was observed on some of the components contaminated with DL-malic, glutaric, and succinic acids. The blue spots seen on the anode electrode of the component contaminated with glutaric acid indicated by white arrows show the pitting of the

electrode, that can be influenced by the formation of tin oxide during soldering [17], [18]. The gel with tin ion indicator showed no corrosion on size 0805 the chip capacitors precontaminated with adipic and palmitic acids, and that also supports the results observed on the SIR pattern in Figure 14.1 and Figure 14.2. In contrast to the results found for succinic acid on the SIR patterns (short time exposure at elevated RH up to 98 %RH), the dendrites were formed on some of the surface mount components tested at 98 %RH for 24 h. The micrograph representing succinig acid in (Figure 14.3) shows that application of tin ion indicator gel revealed the pattern of tin corrosion product on the component that otherwise was not visible. The corrosion of tin observed on the surface mount component contaminated with succinic acid indicate that the 98 %RH is the critical RH for the formation of conductive water layer (also previously seen as a slight increase in charge transfer in Figure 14.2 b.). The observation is related to the deliquescence RH for succinic acid [15], [19]–[21], that consequently results in corrosion of tin electrodes under bias voltage. The time interval of 24 h for testing was sufficient to cause corrosion that is indicated by blue coloration in the micrographs in Figure 14.3. Overall, these examples show the possibility of visualization of tin corrosion using tin ion indicator in a gel, and it can be used to map the extent of corrosion on the surface mount components. A clear correlation between the effects of various WOAs on the SIR and the corrosion on the surface mount capacitors was observed.

CORROSION UNDER SURFACE MOUNT COMPONENTS

Corrosion of tin under surface mount components is possible due to water layer formation together with trapped flux residues usually from reflow process. Electrical failures under humid conditions are sometimes due to corrosion hidden under the components. The identification of corrosion is difficult in this case due to the tiny levels of corrosion product as well as the difficulty in observing the area beneath of the components. Figure 14.4 shows corrosion under a surface mount component visualized ex-situ by using tin ion indicator gel. Tin corrosion products formed due to corrosion under the component can be clearly seen with trails of products moving out of the component area.

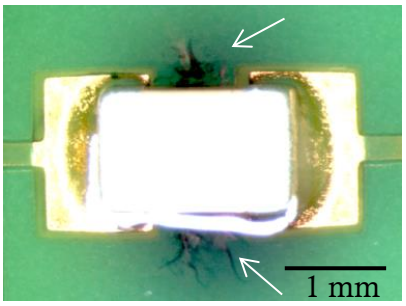

Figure 14.4: Corrosion under a surface mount component traced using tin ion indicator gel, as indicated by arrows

ACCELERATED DEVICE LEVEL TESTING

EX SITU CORROSION MAPPING AFTER DEVICE LEVEL TESTING

The temperature profile of the PCBA is important in consideration of local humidity effects and consequent corrosion issues. Figure 14.5 shows a variation of temperature on the surface of a device PCBA in operation mode. The temperature difference of approximately 20 °C between the right-hand side and the-left hand side of the PCBA can be seen, and the components with high heat dissipation can be identified. If the PCBA is exposed to high humidity as in accelerated humidity test for devices, the cold part of the PCBA will experience higher RH levels locally.

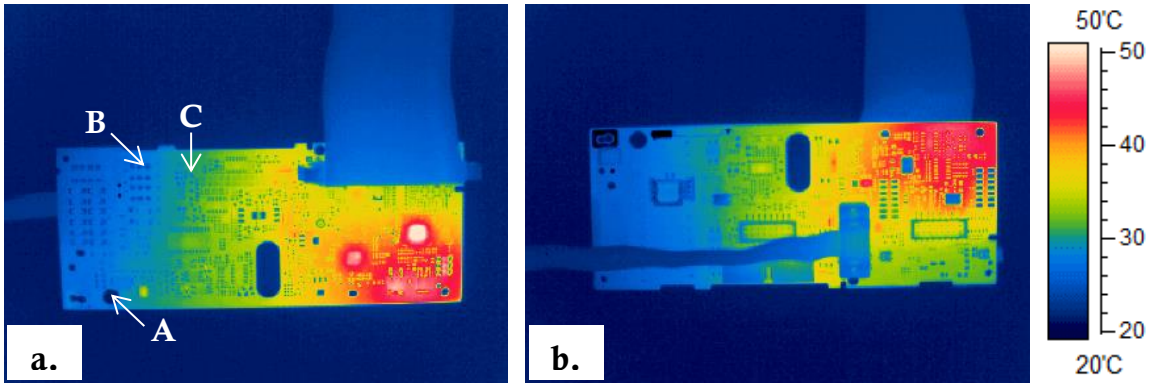

Figure 14.5: Temperature profile of a typical PCBA: a. top side, and b. bottom side. (A, B and C indicate locations where corrosion of contaminated PCBA was observed, related images are shown in Figure 14.7)

The RH locally on the PCBA, contamination, and bias voltage will influence the corrosion. For the identification of the corrosion prone areas on the 'as produced' PCBA in Figure 14.5, it was tested under high humidity and cycling temperature conditions (97% RH and cycling temperature between 25 °C and 40°C with the step duration of 2 hours, for 20 cycles). The selected test conditions are based on the cycle defined in the IEC 60068-2-30 standard, however, the original cycle was modified in order to prolong transient water condensation conditions occurring at the step of temperature increase. After climatic testing, the PCBA was subjected to ex-situ tin ion indicator gel test. Figure 14.6 shows the PCBA before and after humidity test showing the regions where the corrosion has initiated during testing. As shown in Figure 14.6 b., cold areas of the PCBA showed a higher level of corrosion compared to hot areas. The dissolution of tin has taken place on the positively biased terminals of surface mount component in Figure 14.6 b. 4.

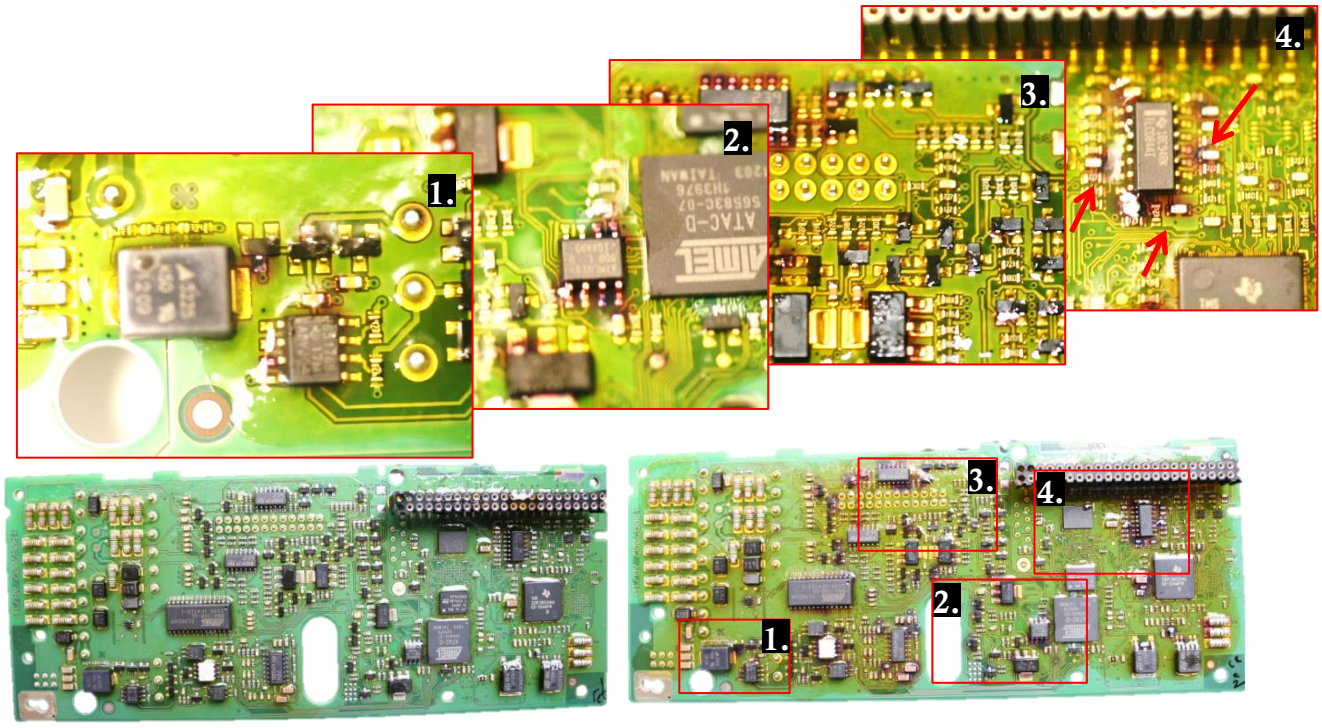

Figure 14.6: Corrosion on the PCBA after climatic testing traced using tin indicator gel test: a. no bias is applied, and b. the device is biased

The effect of temperature differential on the corrosion is further demonstrated by accelerated corrosion testing of deliberately precontaminated PCBA. For that purpose, the new PCBA of the same device, but contaminated with (100 ± 30) µg/cm^2 of succinic acid was exposed to 98 %RH at 25 °C for 24 h. Thereafter, the PCBA was inspected for corrosion. Figure 14.7 shows extensive corrosion of surface mount components, the tin corrosion products appeared as a mixture with the reduced metal ions (in the form of a dendrite) which appears in black. The corresponding locations of the components are indicated by arrows in the infrared image in Figure 14.5 a.

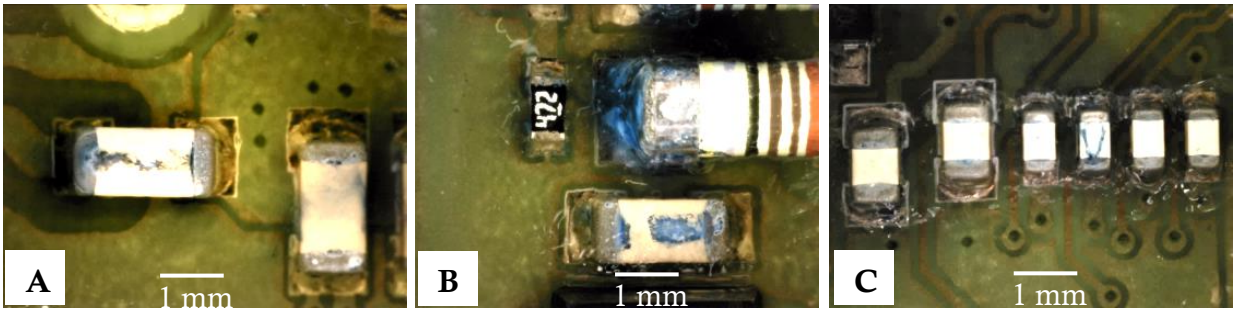

Figure 14.7: Corrosion of PCBA after accelerated humidity testing at 98 %RH for 24 hours with and cycling temperature conditions. PCBA was deliberately precontaminated with succinic acid at approximate concentration (100 ± 30) µg·cm^{-2} (the respective locations of A, B and C can be identified in Figure 14.5 a.)

The identification of contamination type and amount enables prediction of certain SIR values in relation to the humidity level in the environment. However, on the actual PCBA, the levels of RH locally on the surface vary and are dependent on a number of factors e.g. temperature variation on the PCBA, On/Off cycles, heat transfer and humidity build-up inside an electronic enclosure [22]–[24]. Further, the bias voltage on the PCBA influences the electrochemical processes and it is a driving force for the ion transfer. A synergetic effect of humidity, bias voltage and contamination requires thorough analysis for the prediction of corrosion prone areas at the PCBA level. As a result, it is very difficult to predict where corrosion will happen on the PCBA surface. However, if the conditions for corrosion to take place on the PCBA are met, the tin will be dissolved into the water layer. The dissolved tin ions will be transferred towards cathode due to electric field acting though the water layer and some of the tin ions would form tin hydroxides. This can be considered as the first step of corrosion, that at the later stage would likely result in formation of tin dendrites, which can be considered as failure mode that has a high impact on reliability compared to the leakage current increase typically observed at initial steps of corrosion. The method presented here is addressing the on-set of corrosion, as gel is optimized to react with tin ions and tin hydroxides, the presence of which is more difficult to detect, compared to the appearance of tin dendrites. The method enables detection of corrosion at its initial steps and in turn enables to pin point the corrosion prone areas on the PCBA surface, thereby it is an easy way to understand the effect of synergistic factors on the corrosion directly from board to board.

LOCAL EFFECTS OF BIAS VOLTAGE AND HUMIDITY

When analysing the PCBA layout for critical areas and components likely to corrode under high humidity conditions, the areas with high voltage and dissipating low heat naturally can be expected to be more susceptible to corrosion. The profile of no-clean flux residues is another obvious factor to bear in mind, as higher levels of ionic residues on the PCBA surface can

jeopardize the climatic reliability of entire PCBA; however, the effect of contamination was already discussed in the previous section. The following example instead addresses the effect of bias voltage and local humidity/temperature. Figure 14.8 shows a bias voltage map of the PCBA, and following temperature distribution when the device is in operation mode. Some of the components on the PCBA were selectively wave soldered using succinic acid based flux system. The climatic reliability of the PCBA was evaluated by 168 h of climatic testing at 40°C and 93% RH.

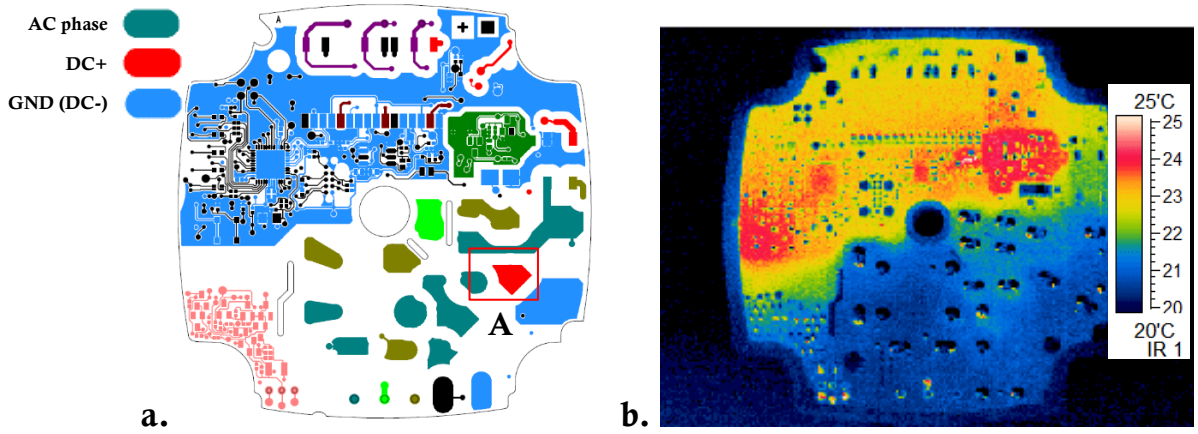

Figure 14.8: a. Bias voltage map and b. temperature profile of PCBA when the bias voltage is applied (A indicates the area with high risk of corrosion, as further analyzed in Figure 14.9)

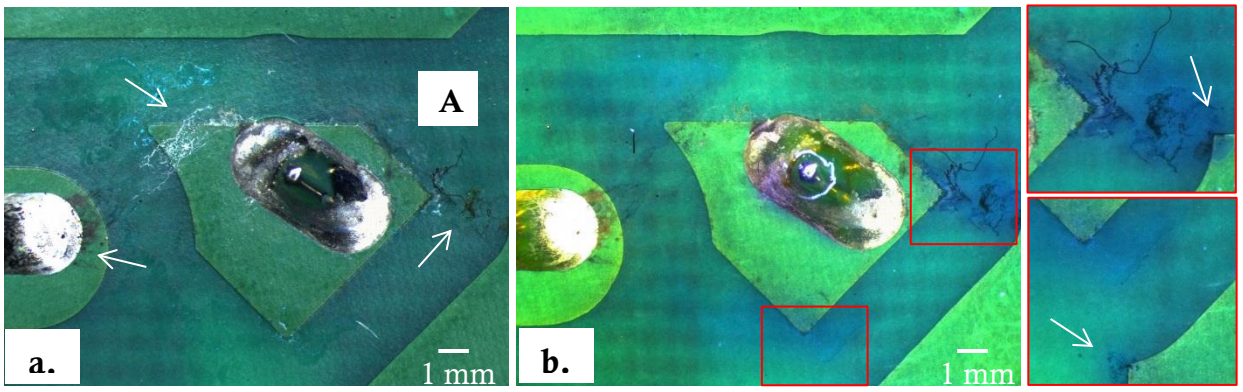

Figure 14.9: a. Corrosion between different bias points on the PCBA (DC+ and ground, and DC+ and AC phase; this area can be identified on bias voltage map in Figure 14.8), b. visualization of tin corrosion using tin ion indicator gel, with the magnified view of corrosion sites

The micrographs in Figure 14.9 show corrosion in wave soldered area in between the solder joints with different bias voltages. The micrograph taken prior to application of tin ion indicator gel shows a white trace connecting 'DC+' solder joint and the 'AC phase', which appears with metallic dendrites, as black deposits seen nearby 'AC phase' solder joint. The metallic dendrites observable on the PCBA surface are likely to be metallic tin, typically surrounded by an oxide layer which is attributed to unstable growth conditions during the electrochemical migration [25]. However, due to the thin layer of the solder mask near the underlying copper edges and high bias voltage during testing, it is likely that the corrosion products will also contain some amount of

copper. The appearance of green color precipitates nearby 'DC+' solder joint, is similar to copper oxide/hydroxides [26], [27]. Similar bridging can be identified in the gap between 'DC+' and 'ground'.

After application of tin ion indicator gel on the PCBA, the light blue clouds nearby the edges of solder mask covering the copper layer of 'DC+' became visible and indicates spreading of corrosion products, which were confined by a thin water film, the formation of which is greatly dependent on the spreading of flux residues and the electric field between the conductors. The blue coloration at the edges of the 'ground' electrode, as shown in the insert of Figure 14.9 b, indicates the sites for tin and possibly copper reduction with hydroxide/oxide precipitation nearby. The reduction of metal ions at the edge of copper layer covered with the solder mask is another indication of defects or porosities in solder mask. In that case the actual distance for the conducting path connecting the conductors has been significantly reduced. The image obtained after application of tin ion indicator gel in this example, helps to identify the sites of tin dissolution, and reduction, as well as spreading of corrosion products. The latter is useful to define leakage current conduction paths, and for leakage current sensitive devices to reconstruct circuitry failure.

CORROSION FAILURE ANALYSIS OF FIELD RETURNS

EFFECT OF HUMIDITY CONTROL INSIDE ELECTRONIC ENCLOSURE

Figure 14.10 a. shows corrosion on power electronics PCBA. The failure was induced by exposure of the device to severe humidity conditions in service life. The build-up of water vapour inside electronic enclosure caused an increase of water layer thickness on the PCBA, and under AC voltage the dissolution of tin from the solder joints of through-hole components occurred. The corrosion seen from the visual observations of the PCBA was verified by application of tin ion indicator gel. Usually, the white cloud seen under these conditions need not be tin products, but can also be due to flux residue after humidity exposure. Figure 14.10 b. shows a visualization of the area after tin ion indicator gel test confirming the tin corrosion product movement over the surface.

After a modification of the device enclosure, the humidity build-up inside and the corrosion risks were minimized. Figure 14.10 c. shows the PCBA from improved design after similar humidity exposure followed by tin ion indicator gel test. White colored wave soldered residue can be seen, however, application of tin ion indicator gel did not show any indication of tin corrosion. The example provided here illustrates that the tin ion indicator gel can be used as a complementary technique for profiling corrosion on the PCBA to verify electronic enclosure design towards humidity ingress and build-up under harsh climatic conditions.

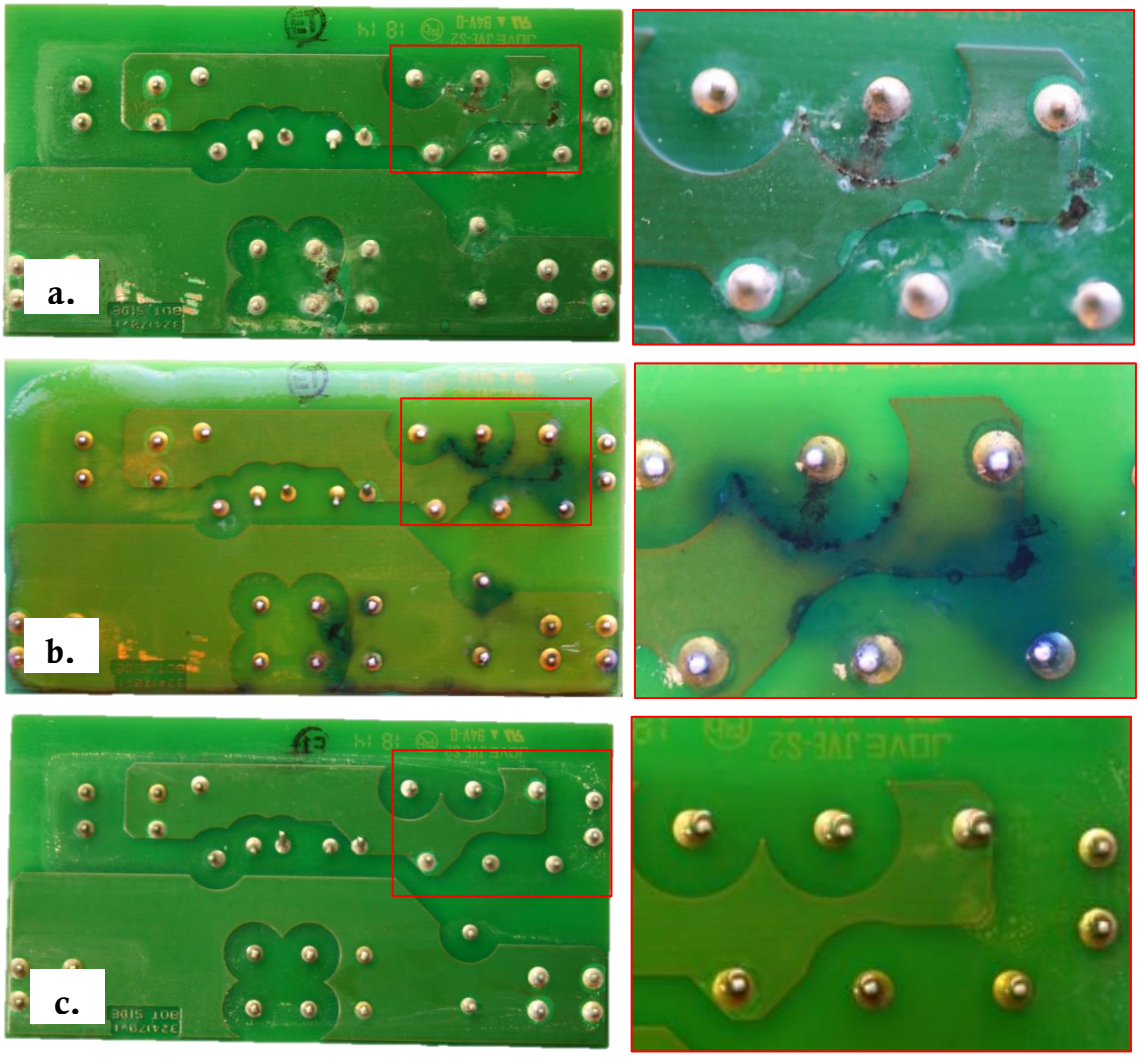

Figure 14.10: High AC voltage induced corrosion on the PCBA: a. original appearance of the PCBA, b. appearance after application of tin indicator, and c. PCBA with modified enclosure (white residues were seen after climatic testing, though no corrosion was identified)

HUMIDITY INGRESS DUE TO CORROSION OF DIE CAST ALUMINIUM ENCLOSURE

The pictures in Figure 14.11 show an example of the PCBA corrosion failure induced by lost integrity of electronic enclosure due to corrosion of die cast aluminum. This unit is from the automotive application, where it is exposed to harsh environmental conditions, and contamination of enclosure exterior with deicing salts is also likely. Due to a high content of copper and iron in die cast aluminium, the galvanic corrosion propagated along the rubber gasket, thereby reducing tightness of electronic enclosure for water entry (Figure 14.11 b). This is expected to result in humidity build-up inside the electronic enclosure, and failure of the control unit.

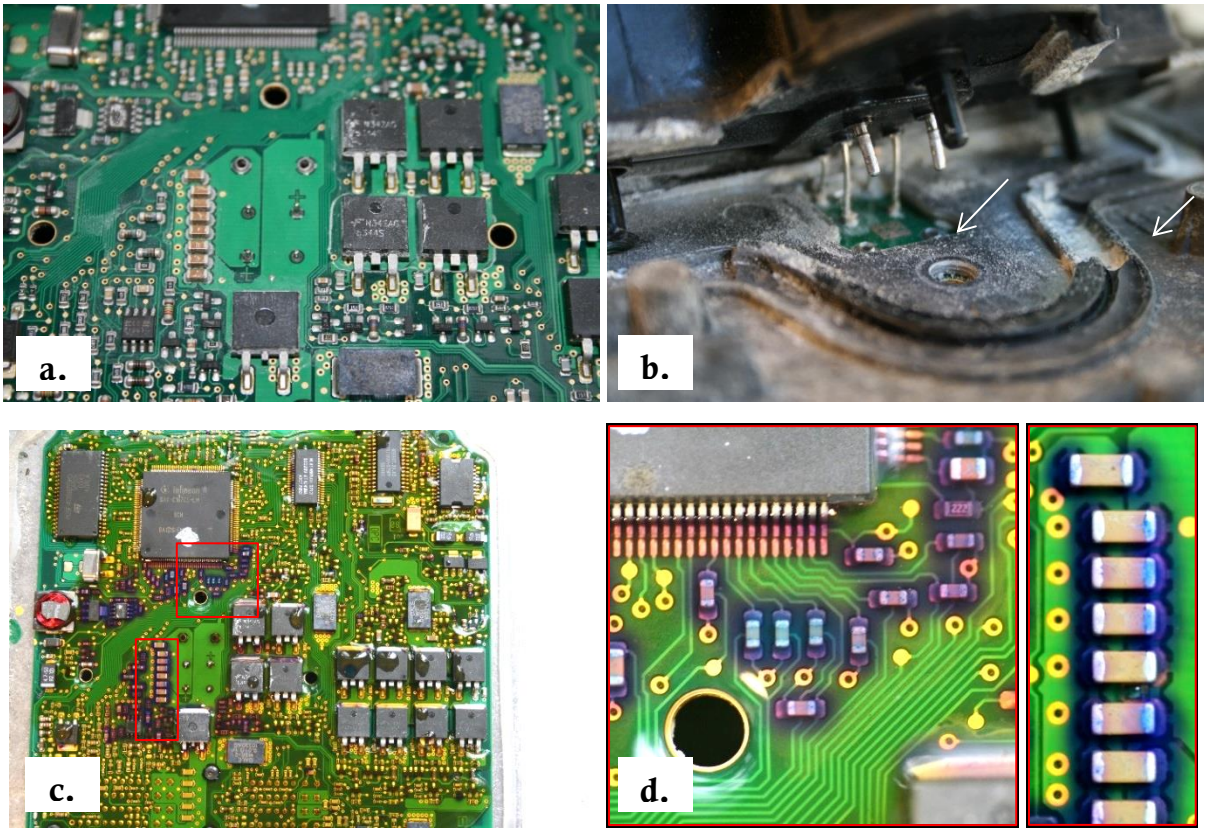

Figure 14.11 a. Visual inspection of the failed PCBA (top side) b. failed gasket and corrosion of aluminium enclosure served as entry point for humidity (bottom side), c. corrosion profile of the failed PCBA (top side), and d. close-up view of some of the components showing corrosion

Visual observation of the failed PCBA (Figure 14.11 a.) indicated traces of white deposits all over the surface, however, no specific area, nor component could be identified as the potential site of the failure. However, the test method using the gel has revealed that the corroded components are just around the entry points where gasket has failed (Figure 14.11 b. and c.). In this case, the pattern of corroded components is a clear indication of which components experienced high humidity, or more likely the condensation.

This example shows, that corrosion profiling of the failed PCBA can help to understand failure development mechanism. Often such failures occur due to the build-up of high humidity inside an electronic enclosure, thus tracing back the corrosion pattern can reveal humidity distribution and a 'weak points' of a device.

IV. SUMMARY

A new method for mapping tin corrosion on the PCBA was developed using a colorimetric tin ion indicator in a gel, which can be applied directly on the PCBA for visual inspection. Corrosion profiling using this method allows visualization of tiny levels of corrosion, which otherwise are hidden and therefore provide a feasible method for early detection of corrosion on the PCBA during accelerated testing or corrosion failure analysis. Mapping using tin ion indicator provide further information on the leak current paths as it traces the movement of tin ions on the surface of the PCBA. The method can also be used for tracing corrosion under surface mount

components, which otherwise is hard to detect. When combined with climatic testing, this method provides means to profile corrosion of various PCBAs and visualizes the synergistic results of local humidity effects, contamination, bias voltage and device design. The information can be used for design changes or remedial measures. Further, this method can be used for corrosion failure analysis of field returns.

V. ACKNOWLEDGMENTS

The research reported here was conducted as part of the CELCORR/CreCon consortium (www.celcorr.com) and authors would like to acknowledge the funding and help received from the consortium partners.

VI. REFERENCES

[1] R. Ambat, "Climatic Reliability of Electronic Devices and Components," *SMT Surf. Mt. Technol. Mag.*, vol. 29, no. 4, pp. 12–28, 2014.
[2] "IPC-TM-650 Test Methods Manual, 2.6.3.3 Surface Insulation Resistance, Fluxes," Northbrook, IL, 2004.
[3] "IPC-TM-650 Test Methods Manual, 2.6.14.1 Electrochemical Migration Resistance Test," Northbrook, IL, 2009.
[4] "IPC-TM-650 Test Methods Manual, 2.6.15 Corrosion, Flux," Northbrook, IL.
[5] "IPC-TM-650 Test Methods Manual, 2.3.32 Flux Induced Corrosion (Copper Mirror Method)," Northbrook, IL, 2006.
[6] D. A. Thomas, K. Avers, and M. Pecht, "The 'trouble not identified' phenomenon in automotive electronics," *Microelectron. Reliab.*, vol. 42, no. 4–5, pp. 641–651, 2002.
[7] M. Pecht, "Physics-of-failure-based prognostics for electronic products," *Trans. Inst. Meas. Control*, vol. 31, no. 3–4, pp. 309–322, Jun. 2009.
[8] V. Verdingovas, M. S. Jellesen, and R. Ambat, "Impact of NaCl Contamination and Climatic Conditions on the Reliability of Printed Circuit Board Assemblies," *IEEE Trans. Device Mater. Reliab.*, vol. 14, no. 1, pp. 42–51, 2014.
[9] D. Minzari, M. S. Jellesen, R. Ambat, P. Møller, and P. S. Westermann, "Process, kit and composition for detecting residues and contaminants in an object with three-dimensional geometry," WO 2011/048001 A1, 2011.
[10] K. L. Cheng, K. Ueno, and T. Imamura, *CRC Handbook of Organic Analytical reagents*. 1982.
[11] V. Verdingovas, M. S. Jellesen, and R. Ambat, "Relative effect of solder flux chemistry on the humidity related failures in electronics," *Solder. Surf. Mt. Technol.*, vol. 27, no. 4, pp. 146–156, 2015.
[12] V. Verdingovas, M. S. Jellesen, and R. Ambat, "Effect of pulsed voltage on electrochemical migration of tin in electronics," *J. Mater. Sci. Mater. Electron.*, vol. 26, no. 10, pp. 7997–8007, 2015.
[13] M. S. Jellesen, M. Dutta, V. Verdingovas, and R. Ambat, "Detection of acid release from reflow solder flux residues using localized test methods," in *Eurocorr 2012*, 2012, pp. 1–10.
[14] "IPC-CH-65B Guidelines for Cleaning of Printed Boards and Assemblies." 2011.
[15] V. Verdingovas, M. S. Jellesen, and R. Ambat, "Solder Flux Residues and Humidity-Related Failures in Electronics: Relative Effects of Weak Organic Acids Used in No-Clean Flux Systems," *J. Electron. Mater.*, vol. 44, no. 4, pp. 1116–1127, 2015.
[16] Y. Zhou, L. J. Turbini, D. Ramjattan, B. Christian, and M. Pritzker, "Characterizing Corrosion Effects of Weak Organic Acids Using a Modified Bono Test," *J. Electron. Mater.*, vol. 42, no. 12, pp. 3609–3619, Aug. 2013.
[17] J. M. Song, Y. C. Chang-Chien, B. C. Huang, W. T. Chen, C. R. Shie, and C. Y. Hsu, "Spectroscopic investigation of oxidized solder surfaces," *Corros. Sci.*, vol. 53, no. 6, pp. 2283–2288, 2011.
[18] P. T. Lee, W. Z. Hsieh, T. C. Yeh, H. K. Wang, and C. E. Ho, "Comparative study between Au/Pd/Cu and Au/Pd(P)/Cu films in soldering applications," *Surf. Coatings Technol.*, vol. 303, pp. 103–111, 2016.
[19] K. M. Adams, J. E. Anderson, and Y. B. Graves, "Ionograph Sensitivity to Chemical Residues from 'No Clean' Soldering Fluxes: Comparison of Solvent Extract Conductivity and Surface Conductivity," *Circuit World*, vol. 20, no. 2, pp. 41–44, 1994.
[20] C. Peng, M. N. Chan, and C. K. Chan, "The hygroscopic properties of dicarboxylic and multifunctional

acids: measurements and UNIFAC predictions.," *Environ. Sci. Technol.*, vol. 35, no. 22, pp. 4495–501, Nov. 2001.

[21] P. Saxena and L. M. Hildemann, "Water absorption by organics: survey of laboratory evidence and evaluation of UNIFAC for estimating water activity," *Environ. Sci. Technol.*, vol. 31, no. 11, pp. 3318–3324, Nov. 1997.

[22] B. Medgyes, B. Illes, and G. Harsanyi, "Effect of water condensation on electrochemical migration in case of FR4 and polyimide substrates," *J. Mater. Sci. Mater. Electron.*, vol. 24, no. 7, pp. 2315–2321, 2013.

[23] J. B. Jacobsen, J. P. Krog, A. H. Holm, L. Rimestad, and A. Riis, "Climate-Protective Packaging: Using basic physics to solve climatic challenges for electronics in demanding applications," *IEEE Ind. Electron. Mag.*, vol. 8, no. 3, pp. 51–59, 2014.

[24] H. Conseil, V. C. Gudla, M. S. Jellesen, and R. Ambat, "Humidity Build-Up in a Typical Electronic Enclosure Exposed to Cycling Conditions and Effect on Corrosion Reliability," *IEEE Trans. Components Packag. Technol.*, vol. 6, no. 9, pp. 1379–1388, 2016.

[25] D. Minzari, F. B. Grumsen, M. S. Jellesen, P. Møller, and R. Ambat, "Electrochemical migration of tin in electronics and microstructure of the dendrites," *Corros. Sci.*, vol. 53, no. 5, pp. 1659–1669, May 2011.

[26] H. Huang, Z. Pan, X. Guo, and Y. Qiu, "Effects of direct current electric field on corrosion behaviour of copper, Cl^- ion migration behaviour and dendrites growth under thin electrolyte layer," *Trans. Nonferrous Met. Soc. China*, vol. 24, no. 1, pp. 285–291, 2014.

[27] B. Medgyes, X. Zhong, and G. Harsanyi, "The effect of chloride ion concentration on electrochemical migration of copper," *J. Mater. Sci. Mater. Electron.*, vol. 26, no. 4, pp. 2010–2015, 2015.

15. ANALYSIS OF SURFACE INSULATION RESISTANCE RELATED FAILURES IN ELECTRONICS BY CIRCUIT SIMULATION

Vadimas Verdingovas, Morten Stendahl Jellesen, Salil Joshy, and Rajan Ambat

Abstract— *Purpose* – At first, to show that the humidity levels for SIR failures are dependent on the type of activators used in no-clean flux systems, and secondly, to demonstrate the possibility of simulating effects of humidity and contamination on the printed circuit board components and sensitive parts if typical SIR data connected to the particular climatic condition is available. This is shown on representative components and typical circuits. *Design/methodology/approach* - A range of surface insulation resistance values obtained on SIR patterns with 1476 squares was used as an input data for circuit analysis. The SIR data was compared to the surface resistance values observable on the real device PCBA. Surface insulation resistance (SIR) issues at the component and circuit level were analysed based on the parasitic circuit effects owing to the formation of water layer as an electrical conduction medium. *Practical implications* – The methodology of analysis of the circuits using a range of empirical leakage resistance values combined with the knowledge of the humidity and contamination profile of the electronics can be used for the robust design of a device, which is also important for electronic products relying on low current consumption for long battery lifetime. *Findings* – This paper provides a summary of the effects of various weak organic acids (WOAs) contamination representing the active components in no-clean solder flux residue, and demonstrates the effect of humidity and contamination on the possible malfunctions and errors in electronic circuits. Effect of contamination and humidity is expressed as drift from the nominal resistance values of the resistors, self-discharge of the capacitors, and the errors in the circuits due to parasitic leakage currents (reduction of SIR). *Originality/value* – Examples provide a basic link between a combined effect of humidity and contamination and the performance of electronic circuits. The methodology shown provides the possibility of addressing the climatic reliability of electronic device at the early stage of device design using typical SIR data representing the possible climate exposure.

Keywords—Surface resistance, Circuit testing, Failure analysis, Circuit analysis, Surface contamination, Corrosion, Reliability, Leakage current, No-Clean flux

I. INTRODUCTION

The climatic conditions (temperature and humidity) have a direct impact on the functioning, lifetime, and overall reliability of an electronic device. The increase of relative humidity (RH) is known to increase the corrosion rates of metals [1]–[4]. Similarly, high humidity increases leakage currents on the surface of the printed circuit boards, which is commonly referred to as reduction of surface insulation resistance (SIR). The threshold RH for the SIR failures in the circuitry is greatly affected by the type and amount of ionic contamination present on the printed circuit board assemblies (PCBAs).

V. Verdingovas, M. S. Jellesen, S. Joshy, and R. Ambat, "Analysis of surface insulation resistance related failures in electronics by circuit simulation," draft to be submitted to *Circuit World*, 2015.

Solder flux residues can be addressed as the major source of ionic contamination on the manufactured PCBAs, and their corrosiveness is determined by the activator type in the flux [5]–[8]. The flux residues have been reported as a root cause of different issues on the PCBAs, which are mainly related to the SIR or leakage currents [9]–[13], and short-circuiting due to electrochemical migration [14]–[16] leading to electrical malfunctions.

The electronics manufacturers aim is to minimize the amount of flux residues [17]–[19]; however, maintaining contamination below the allowed levels on the printed circuit boards is not easy [20]. A reference value of 1.56 μg $\cdot cm^{-2}$ (NaCl eq.) stated in the IPC J-STD-001 (Requirements for Soldered Electrical and Electronic Assemblies) is often used as a limit for the maximum ionic contamination on the printed circuit board. However, the actual safe level of contamination for a specific PCBA will depend on the sensitivity of electronic circuits to the reduction of SIR, which is a function of RH (device exposure conditions), and the physical properties of the contaminants i.e. adsorption, absorption, and solubility in water, ionic conductivity, and dependency of temperature.

The reduction of SIR on the printed circuit boards has a direct impact on the functioning of electronic circuits [12], [21], [22]. In general, the effect due to humidity and contamination can be looked at as the formation of a local conduction layer on the PCBA surface in parallel to the insulation resistance between electrical connections, which in turn will influence the operating parameters of the circuit components. The tolerances of the components which are specified by the manufacturers are usually taken into account when analysing the performance of the circuits; however, it is seldom that the effect of contamination after assembly process and humidity in user environment is taken into consideration during the design of electronic circuits.

The examples for analysing the sensitivity of electronic circuits, defined as the ability of a particular part of the circuit to respond to certain changes in the circuit, can be found in the literature [23], [24]. Similar to analysing the sensitivity of the circuits for component tolerances and other factors, humidity effects can be analysed using a range of empirical data related to the measured electrical properties of the water layer formed under various conditions. Such analysis will allow the circuit designer to determine the potential humidity related issues on a printed circuit board at initial design stages or analyse the failures due to a particular part of the circuit or a set of components. The set of data for analysis in this case should be the experimentally determined electrical properties of the water layer formed on the PCBA surface measured under various humidity, contamination, and bias conditions.

The aim of this paper is to demonstrate the possibility of simulating effects of humidity on the printed circuit board components and sensitive parts of the assemblies using selected representative components and typical circuits. The analysis is carried out based on the assumption that the condition when water layer forms on the surface of the PCBA connecting between biased points can be simulated by assuming a parallel resistor represented by the electrical properties of the water layer. The electrical properties of the water layer depend on the humidity level, hygroscopicity of contamination, and dissociation of ionic residues in water, while the overall charge transferred between the electrodes will also be influenced by the corrosion reactions at the electrodes. Therefore, empirical data on leakage current and impedance change due to the formation of water layer under various humidity conditions and contamination levels are used for the analysis. The contamination types analysed in this paper include weak organic acids (WOAs) commonly found in soldering fluxes, namely: adipic, succinic, glutaric, DL-malic, and

palmitic. The circuits analysed are the drift in resistance values of chip resistors, discharging of surface mount capacitors, and components associated with a differential amplifier based circuit.

II. MATERIALS AND METHODS

TEST BOARD USED FOR CHARACTERISATION OF CONTAMINATION AND HUMIDITY

The test boards with SIR pattern was made on FR-4 laminate (according to IPC-4101/21) with the thickness of 1.6 mm. The SIR pattern had 1476 squares and HASL surface finish (SN100C solder alloy). The surface area of the comb pattern was 325 mm^2 (13 mm × 25 mm), the width of conducting lines and the distance between them was 0.3 mm. The detailed description of the test board layout can be found elsewhere [25].

PREPARATION OF THE TEST BOARDS

The test boards were cleaned with a 1:1 mixture of isopropyl alcohol and deionized water, and then rinsed in deionized water with a resistivity of 18.2 MOhm·cm at 25 °C. Thereafter the SIR patterns were precontaminated with WOAs, namely adipic, succinic, glutaric, DL-malic, and palmitic acid. The solution of analytical grade WOAs dissolved in isopropyl alcohol at the concentration of 10 $g \cdot L^{-1}$ was applied on the SIR pattern using a micropipette. The volume of WOA solution dispensed on the SIR patterns resulted in the following amounts of WOA on the surface: 25, 50, 75, and 100 $\mu g \cdot cm^{-2}$.

CLIMATIC CONDITIONS FOR SIR MEASUREMENTS

The SIR measurements were performed in an "Espec PL-3KPH" climatic chamber, the tolerances of which are ±0.3 °C / ±2.5 %RH. The relative humidity during testing was elevated from 60 % to ~ 99 %, while the temperature was maintained constant at 25 °C. The SIR measurements were performed accordingly at 60, 70, 80, 90, 95, 98, and ~ 99 %RH. The equilibration time before each step of RH increase in the climatic chamber was 2 h.

SIR MEASUREMENTS

The measurements were performed using a "BioLogic VSP" multichannel workstation. The leads of the workstation were connected in a two-electrode cell configuration. The current was measured as a function of the applied potential, which was scanned from 0 V to 10 V at 2 $mV \cdot s^{-1}$ sweep rate, for varying relative humidity.

SIMULATION AND ANALYSIS OF HUMIDITY EFFECTS USING EMPIRICAL DATA

The effect of humidity and contamination on the PCBA components like chip resistors and capacitors of various nominal values was analyzed by assuming a parasitic component with variable resistance representing the formation of the water layer on the surface with ionic residues.

"OrCAD PSpice" was used to simulate the effect of humidity related SIR reduction on the output error of the differential amplifier circuit. The SIR was simulated with a parametric sweep of the resistor in parallel to the affected component and in the range from 1 kOhm to 10 MOhm corresponding to the SIR change due to various humidity and contamination levels.

III. RESULTS AND DISCUSSION

CONTAMINATION, HUMIDITY, AND SURFACE INSULATION RESISTANCE

Figure 15.1 a.-e summarizes the effect of type and concentration of WOA on the surface insulation resistance values presented as an overall resistance (R) and as surface insulation resistance expressed in Ohms per square (SIR) for different RH levels. An example of the leakage current measurement from which the data for Figure 15.1 a.-e was obtained is shown in Figure 15.1 f. The horizontal dashed line in the graphs indicates commonly accepted pass/fail criteria of 100 MOhm for SIR testing.

Generalizing all acids, the SIR reduces with increase in concentration of the WOAs. A significant reduction in SIR at particular humidity level indicates narrowing of the spacing between the electrode due to corrosion and electrochemical migration (points indicated by red circles in the graphs). The vertical dashed lines in the graphs designate the deliquescence RH for respective acids reported in a number of studies [26]–[31], which correlate with the events when a significant reduction in SIR was observed. Palmitic acid is practically insoluble in water, therefore it is not characterized by a deliquescence RH.

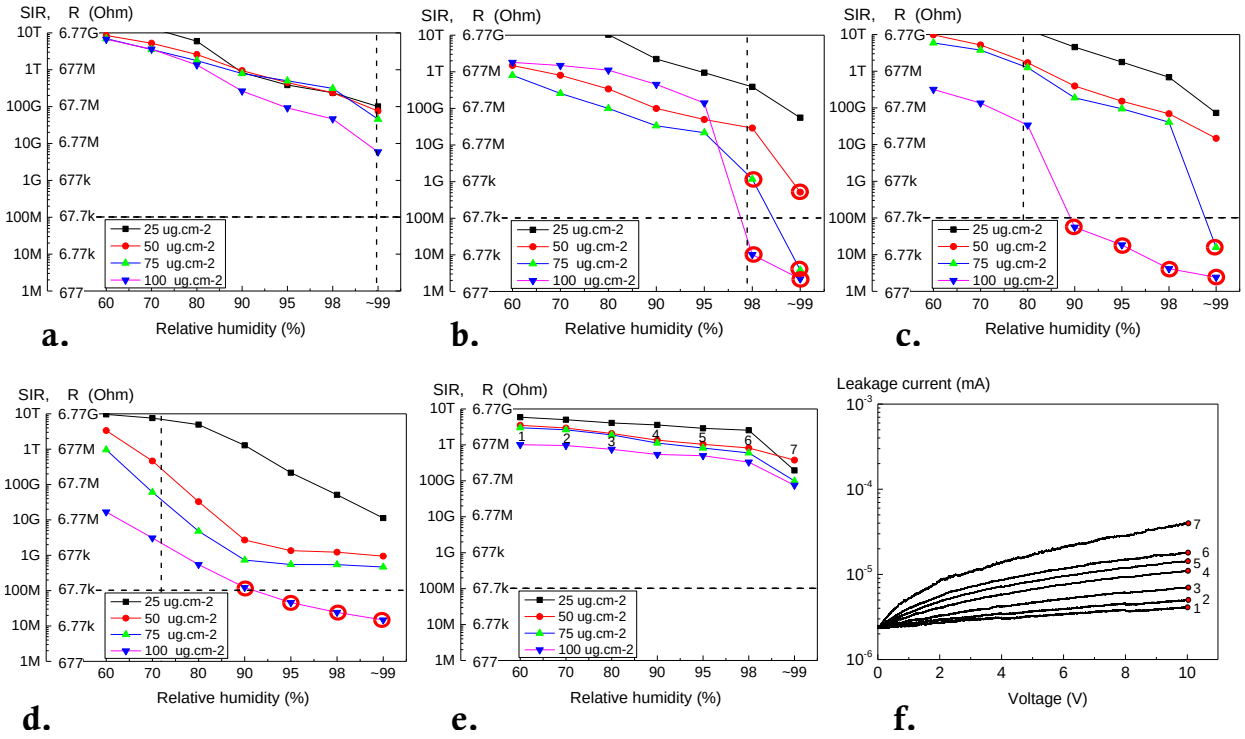

Figure 15.1: SIR (further is also named as leakage resistance) as a function of RH for 5 WOAs: a. adipic, b. succinic, c. glutaric, d. DL-malic and e. palmitic acid, and f. an example of in-situ-leakage current measurements data obtained at different humidity levels for palmitic acid at 50 μg·cm^{-2} (red marks shows the values extracted from the curves for constructing graphs in Figure 15.1 a.-e)

Above the deliquescence RH of the acids, the decrease of SIR is more pronounced as seen in Figure 15.1 (a)-(e). A significant reduction of SIR occurs due to an increase of water adsorption and absorption by the WOAs. At the deliquescence RH of WOAs, the uptake of water continues

until complete dissolution and some degree of solution dilution have reached [32]. This results in an increase of water layer thickness and amount of ions in the solution, which contributes to the increase of surface conductivity. The water layer thickness on the surface is influenced by the solubility of the contaminant, while ionic conductivity is dependent on the dissociation rate and the ion mobility in the electrolyte. The results from SIR measurements suggest that for the acids investigated in this work, the solubility in water has a major contribution to the surface conductivity. The highly soluble acids showed the highest reduction in the SIR value, and the threshold RH for significant reduction of SIR correlated with the deliquescence RH of contaminants.

TYPICAL LEVELS OF FLUX CONTAMINATION FOUND ON THE PCBA AFTER THE MANUFACTURING PROCESS

Analysis of a large number of PCBAs directly from the manufacturing line showed that the average amount of flux residue left on the PCBA depends on the soldering process [33]. Among various soldering processes, reflow soldering showed minimum residue, with the level below 1 $\mu g \cdot cm^{-2}$, while the maximum levels of 17.3 $\mu g \cdot cm^{-2}$ (average 6.2) and 44.1 $\mu g \cdot cm^{-2}$ (average 11.4) of WOAs in the flux residue were identified respectively for the wave soldering and selective wave soldering processes [33]. It is important to note that in contrast to wave soldering, reflow process leaves more benign flux residues (due to higher effect of filmformer); however, the exposure to elevated temperature and humidity is likely to enhance release of active WOAs [34].

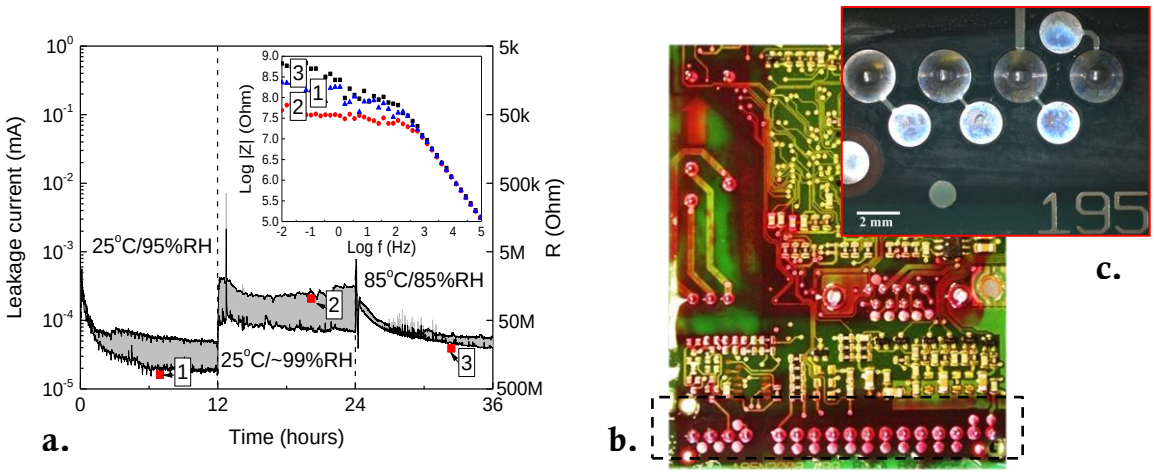

Figure 15.2: Leakage current (DC), and impedance (AC) measurements performed directly on the device PCBA, and b. Flux residue profile revealed by residues RAT test method (the area where electrical measurements were performed is indicated in by dasher line), c. Magnified view of selective wave solder flux residue nearby solder joints of connectors

For further analysis, the SIR reduction due to flux residues was measured on the PCBA from the actual device. As per the visual inspection of the PCBA, extensive contamination from the selective wave soldering fluxes was seen (Figure 15.2 (b)). The mapping of acidic residues on the PCBA using the Residues RAT (reliability assessment test) method [35] clearly showed the template of soldering pallet, revealing areas selectively exposed to the wave soldering (Figure 15.2 (b)). The red coloration on the PCBA in Figure 15.2 (b) represents the residue of active component

in the flux, the adipic acid in this case. The quantitative analysis of the flux residues using ion chromatography showed that the amount of acid is in the range from 15 to 30 $\mu g \cdot cm^{-2}$.

Further, the electrical properties of flux residues on the PCBA under humid conditions were analysed using DC leakage measurements and impedance spectroscopy. The measurements were performed on highly contaminated solder joints of digital/analog input and output connectors of the device. The part with soldered connectors was cut off from the entire PCBA in order to perform the measurements (indicated by dashed line in Figure 15.2 (b)). The electrical measurements were performed uninterruptedly under three climatic conditions, namely: 25 °C/95% RH, 25 °C/~99% RH, and 85 °C/85% RH, and on the neighbouring joints simultaneously. The results in Figure 15.2 (a) are provided as a range of leakage currents from two measurements obtained with 5 V DC. The impedance spectra shown as an insert in Figure 15.2 (a) were obtained in the frequency range from 0.01 Hz to 100 kHz with 50 mV sine amplitude. The leakage current measurements at 5 V DC indicated current levels in the range between 0.02 μA and 0.25 μA, and that would respectively translate into a resistance of 250 MOhm and 20 MOhm. Comparing the impedance at f = 0.01 Hz, the values with a minor deviation falls within the range of resistance calculated from the DC measurement. The red points indicated in the graph represent the resistance values from the impedance measurements at f = 0.01 Hz, while the numbers connected to each red point indicate different temperature/humidity conditions.

COMPARISON OF SIR MEASUREMENTS ON TEST PATTERN AND DEVICES PCBA

The resistance measured directly on device PCBA in Figure 15.2 (a) was in the range from 20 to 250 MOhm. When comparing this result to the SIR testing in Figure 15.1 (a), it can be seen that both measurements are in the same order of magnitude i.e. 67.7 MOhm on SIR pattern in Figure 15.1 (a), versus 20 to 250 MOhm on device PCBA in Figure 15.2 (a). It is important to note, that even though the SIR pattern has significantly higher surface area compared to that of provided by electrode geometry on device PCBA, both measurements are comparable. This also implies that using the resistance expressed in Ohms per square as an input data for circuit analysis would result in resistance values significantly higher compared to that of seen on device PCBA under similar conditions. On the other hand, it is not surprising, as similar behaviour was also reported earlier, when the measurements of leakage current on the same SIR pattern were compared to the leakage currents measured on surface mount capacitors and resistors contaminated at equivalent concentrations of NaCl [25].

This suggests that the SIR data provided in Figure 15.1 would relatively well represent the effect of RH and contamination conditions on actual device PCBAs. However, for more accurate prediction of climate and humidity effects, a more precise correlation of the results from test SIR results to actual SIR on the board would be required. The data used for circuit analysis in this work was the overall resistance values obtained from the test SIR pattern as it represents a similar magnitude of SIR changes found during measurement on actual PCBA surface with flux contamination. This can be assumed as the worst-case scenario; however, using these relative effects demonstrates the circuit analysis simulation as well the usefulness of the method.

ANALYSING EFFECT OF SIR ON THE PERFORMANCE OF SINGLE COMPONENTS AND ELECTRONIC CIRCUITS

The variation of SIR due to humidity and contamination (Figure 15.1) provide information for analysis of the performance of certain components on the PCBA due to an impact of similar contamination and humidity conditions. If we assume that the water layer forming on the PCBA dissolves ionic contamination on the surface thereby reducing the surface insulation resistance, then circuits and components that require high surface insulation resistance, in general, will be more susceptible to performance degradation due to water layer formation. The equivalent circuits representing the water layer formation on the component leading to a current leakage or reduction in surface resistance can be represented as shown in Figure 15.3 (a) and (b) for resistors and capacitors respectively. As an example, Figure 15.3 (c) shows the consequence of the water layer formation on a chip capacitor leading to high leakage current and formation of dendrite due to electrochemical migration. High amounts of tin hydroxide precipitation and tin dendrites below the surface mount component as well as on the top of the component indicate the pathways for leakage current, which can be assumed in the suggested models in Figure 15.3 (a) and (b).

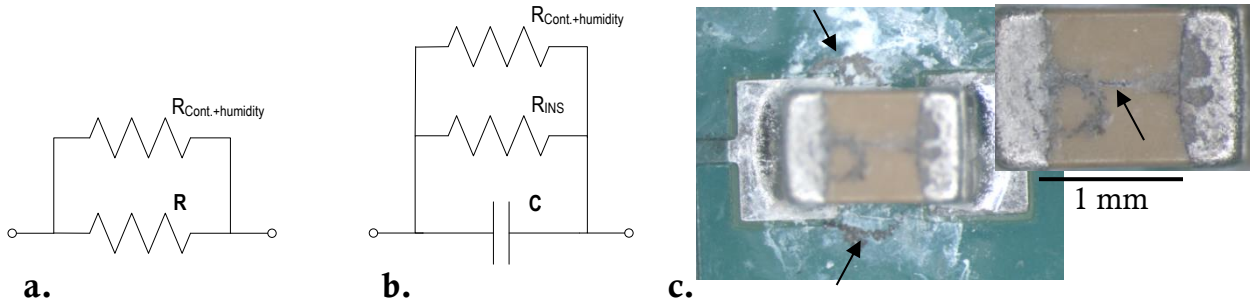

Figure 15.3: Equivalent circuits representing leakage currents due to contamination and humidity for a. resistor and b. capacitor (R is a nominal resistance of the resistor including associated tolerance, $R_{Cont+Humidity}$ represents SIR between the pads/terminals of component, and R_{INS} is an insulation resistance of ceramic used in the capacitor) and c. an example of severe corrosion below and dendrite formation on top of a surface mount capacitor

DRIFT FROM NOMINAL RESISTANCE DUE TO HUMIDITY AND CONTAMINATION

The sensitivity of a particular component towards the reduction of SIR is primarily dependent on the degree of insulation resistance intended for a specific application i.e. the higher the intended SIR, the more sensitive the component is towards humidity exposure. This effect can be seen as the drift from the nominal resistance value, which is due to the SIR drop across the terminals of the surface mount resistors on the PCBA as shown in eq. 1:

$$\text{Drift} = \frac{R - R_{\text{SIR}}}{R} \cdot 100\ \% \qquad (1)$$

where R is the nominal resistance of the component, while R_{SIR} is the resistance resulting from the water layer and the nominal resistance in parallel:

$$R_{SIR} = \frac{R \cdot R_{Cont+Humidity}}{R + R_{Cont+Humidity}} \qquad (2)$$

This example shows the effect of a water layer forming on the surface of a chip component such as a resistor, and between the solder pads, where a presence of reflow flux residues is more likely.

This effect can be analysed as a range of resistance drift from intended SIR or nominal resistance of a component for varying RH levels (Figure 15.4). The graphs in Figure 15.4 were constructed using the experimentally obtained SIR values for succinic and DL-malic acids at contamination level of 50 µg·cm^{-2} in Figure 15.1. Figure 15.4 contains the results for only two acids and it serves to show the method of analysing rather than discussing in detail the effect of all the acids. However, similar graphs can be constructed using empirical data for other WOAs and contamination levels in Figure 15.1.

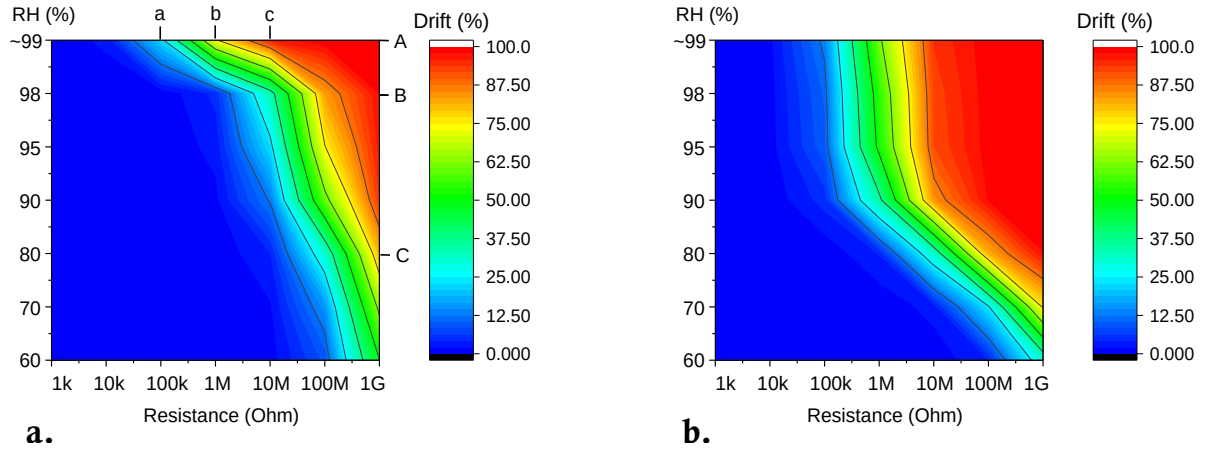

Figure 15.4: Calculated drift in resistance from the nominal value for the WOAs at 50 µg·cm^{-2}: a. succinic acid (cross-sections of the profile corresponding to the marking a, b, c, A, B, and C are provided in Figure 15.5), and b. DL-malic acid

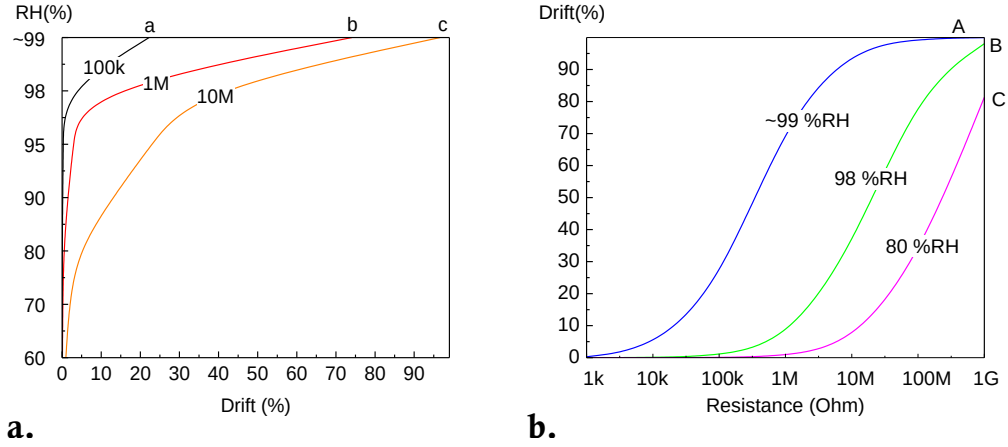

Figure 15.5: a. Profile cross-sections from Figure 15.4: RH vs resistance drift for 100k, 1M and 10M, and b. Resistance drift as a function of nominal resistances for ~ 99, 98, and 80 %RH.

From the comparison of SIR results for DL-malic and succinic acids in Figure 15.1, DL-malic acid cause significant reduction of SIR starting at lower RH levels, whereas for succinic acid significant reduction in SIR occurs only at RH levels above the 98 %RH when deliquescence of the acid occurs. Similarly, the relatively high reduction in SIR for succinic acid at the last step of RH ramp is also reflected in the shift of sensitive region (upper right corner in Figure 15.4 values and lower resistance values would similarly occur for increasing the amount and hygroscopicity of WOA contamination, as expected from Figure 15.1 and respectively shown by the example for DL-malic acid in Figure 15.4 (b). The drift dependency on the RH and for different resistance values in Figure 15.4 (a) is more emphasized in the cross-section profiles in Figure 15.5. The

curves in Figure 15.5 show an increase of sensitivity for the drift with an increase of nominal resistances of the components, and for varying RH levels.

Generalizing the results in Figure 15.4 and profile cross-sections in Figure 15.5 it can be seen that the higher is the nominal value of the resistor, the more sensitive it is to the humidity and contamination. Further, the contamination type is an important factor as the more hygroscopic WOA cause higher drift due to the low SIR associated with high conductivity and thickness of water layer, and the resulting corrosion. Among the WOAs used for no-clean flux, WOAs such as DL-malic and glutaric acid reported being more aggressive for humidity related effects due to their high solubility in the water layer, and ability to form strong electrolyte causing high leakage currents [5], [26]. The effect can be directly linked to the use of different types of no-clean flux systems with various WOAs used in the present work as the flux systems with more active acids also reported causing similar effects [8].

In general, the amount of active WOA flux residue left from the soldering process is important in determining the drift level of resistors located in a sensitive circuit. Figure 15.4 shows that a significant difference in drift levels could be observed by changing the flux chemistry. The use of flux systems containing WOAs with deliquescence at higher RH levels would shift the safe operation conditions towards higher RH levels thereby improving climatic robustness of electronic device. Therefore, the use of low active no-clean flux types together with optimizing cleanliness during soldering could significantly improve the reliability of the PCBAs. Further, the simulation results also show the importance of designs using low value resistors compared to high values as the effect due to parallel resistor formation corresponding to climatic conditions will be insignificant.

INFLUENCE ON THE DISCHARGE RATE OF A CAPACITOR

When a capacitor is connected to a voltage source, a reduction of SIR would lower the voltage across the capacitor compared to the input voltage. Effectively it will cause a continuous drainage of power from the voltage source. An example is the humidity related leakage on capacitors used in Lithium-ion battery management systems (BMS) in various applications i.e. automotive, consumer electronics etc.

The effect of SIR reduction can be analysed in terms of self-discharge rate of a capacitor. The self-discharge rate is first dependent on the insulation property of the dielectric used in the capacitor, which varies with temperature and voltage. Although, the degradation of the capacitance due to exposure to harsh climate condition and the effect of the salt fog/humidity/temperature on the breakdown voltage and equivalent series resistance has been shown [36], [37], the contamination and humidity will affect the discharging of the capacitor regardless of selection of dielectric with superior insulation property. The rate of self-discharge with decreasing capacitor voltage can be described by eq. 3:

$$U(t) = U_0 \cdot e^{-t/\tau} \tag{3}$$

where the self-discharge constant is:

$$\tau = R_{\text{ins}} \cdot C \tag{4}$$

Assuming the equivalent circuit shown in Figure 15.3 b, the contamination and humidity clearly will have an effect on the discharge constant of the capacitor as shown by eq. 5:

$$\tau = \left(\frac{R_{\text{ins}} \cdot R_{Cont+Humidity}}{R_{\text{ins}} + R_{Cont+Humidity}}\right) \cdot C \qquad (5)$$

Figure 15.6 shows the voltage dependence on time of the 10 nF capacitor, charged at 5 V, and discharging due to the current leakage as a function of RH. For comparison, the effect is demonstrated for two WOAs namely less active adipic acid and highly active DL-malic seen in no-clean flux systems. The experimental SIR data used for the analysis corresponds to 50 µg·cm^{-2} flux residue on the PCBA surface as described before. The component used for analysis is assumed to be a class 1 chip capacitor with R_{ins} of 10 GOhm, while the resistance values from Figure 15.1 used as the experimental data for $R_{Cont+Humidity}$.

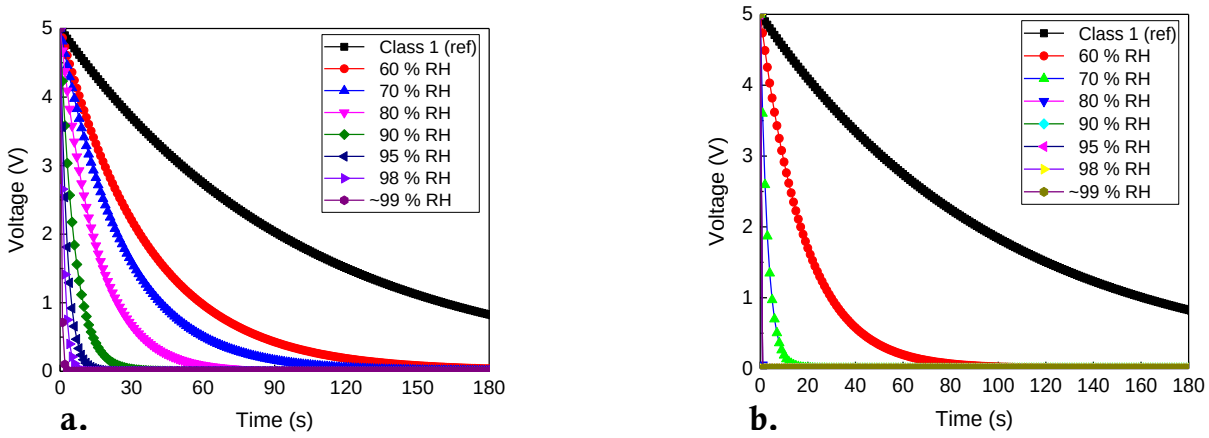

Figure 15.6: Simulation of the effect of RH on the discharging of the capacitor with a contamination level of WOA at 50 µg·cm^{-2}: a. adipic and b. DL-malic acid

The graphs in Figure 15.6 clearly show that the RH and contamination above a level significantly influence the discharging time of the capacitor. As the RH approaches saturation for the low solubility adipic acid, the discharging time reduces drastically. For DL-malic as contaminant, the discharging takes place within a fraction of a second at RH as low as 80 %RH. For the relative comparison of different contamination on the discharging, similar map as shown in Figure 15.4 can be constructed. For relative comparison, the time (τ) (eq. 5) when the voltage on the capacitor drops to 37% of its initial voltage can be used.

Similar to the simulation results presented for the resistors, Figure 15.6 shows that the chemistry of no-clean flux, the amount of residue, and humidity level have a significant influence on the discharging rate of the capacitor used under sensitive conditions on the PCBA layout. For the applications where the self-discharge rate of a capacitor is important, a selection of the capacitors with high insulation resistance of the dielectric is a common practice. However, as it was shown in this example, despite the selected capacitor type, the discharge-rate will be also affected by the humidity and contamination. In this case, the leakage current paths will rather be on the surface of chip components or on the PCBA between the solder pads, where the increase of water layer will contribute to the current leakage. This suggests importance of humidity control, and production process cleanliness for the designs where a low self-discharge rate is required.

EFFECT OF HUMIDITY ON THE OPERATION OF DIFFERENTIAL AMPLIFIER CIRCUIT

Figure 15.7 shows an example of an op-amp based differential amplifier, which is commonly used as part of detection/sensing circuit. The input to the differential amplifier is the voltage difference between the resistors, mounted in the Wheatstone's bridge circuit. The resistors in the Wheatstone's bridge may act as the strain gauges i.e. R3 and R6 are mounted such that when one strain gauge experiences tension, the other will experience compression. The resistors R2 and R7 in the circuit are dummy strain gauges, with fixed value of resistance.

A typical example of such measurement circuit could be in micro temperature and pressure sensors. As the sensing devices are likely to be exposed to harsh climate conditions, there is a high likelihood for high humidity or water condensation on the surface of the printed circuit board where the sensor is located. This will provide leakage current paths between the terminals of surface mount components. The presence of any flux residue on the PCBA surface could enhance the problem as it increases the conductivity of the water layer [8], [26] forming under humid conditions as described earlier.

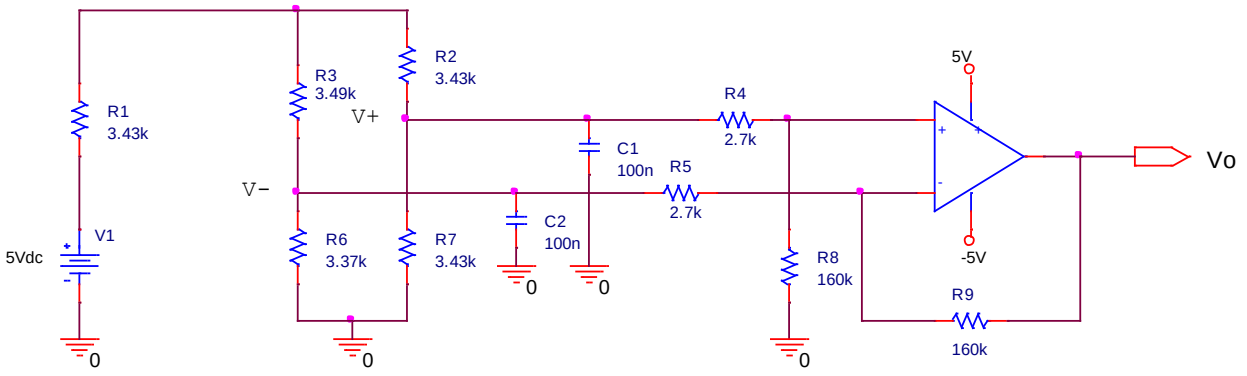

Figure 15.7: Diagram of differential amplifier based measurement circuit

The capacitors C1 and C2 are usually placed very close to the strain gauge and act as a filter for un-wanted noise from the sensor. The exposure of the sensor to the outdoor environment, or due to cooling effects, will increase the relative humidity on the nearby placed filter capacitors. The effect of increased water layer thickness, or in the extreme case of condensation, would effectively increase the leakage current across the capacitors or in other words decrease their leakage resistance similar to that shown in Figure 15.4.

A similar reduction of leakage resistance is also possible for other components in the differential amplifier circuit. The water layer formation can be simulated as a leakage resistance in parallel to the component of interest using the data from Figure 15.1 as described above. The effective resistance can be significantly lower than the nominal resistance value of the resistors when the leakage resistance is comparable to or lower than the resistor value, as it was shown in Figure 15.4. The deviation of the amplifier output voltage due to leakage resistance added to the various components in the circuit is shown in Figure 15.8. The X-axis in Figure 15.8 represents the range of parallel resistance values attributed to the humidity and contamination effect as in Figure 15.1 The graphs represent the variation of the output voltage as a function of the leakage

resistance simulated in parallel to the components indicated in the circuit diagram Figure 15.7. The red curve represents the deviation of the voltage expressed as percentage error.

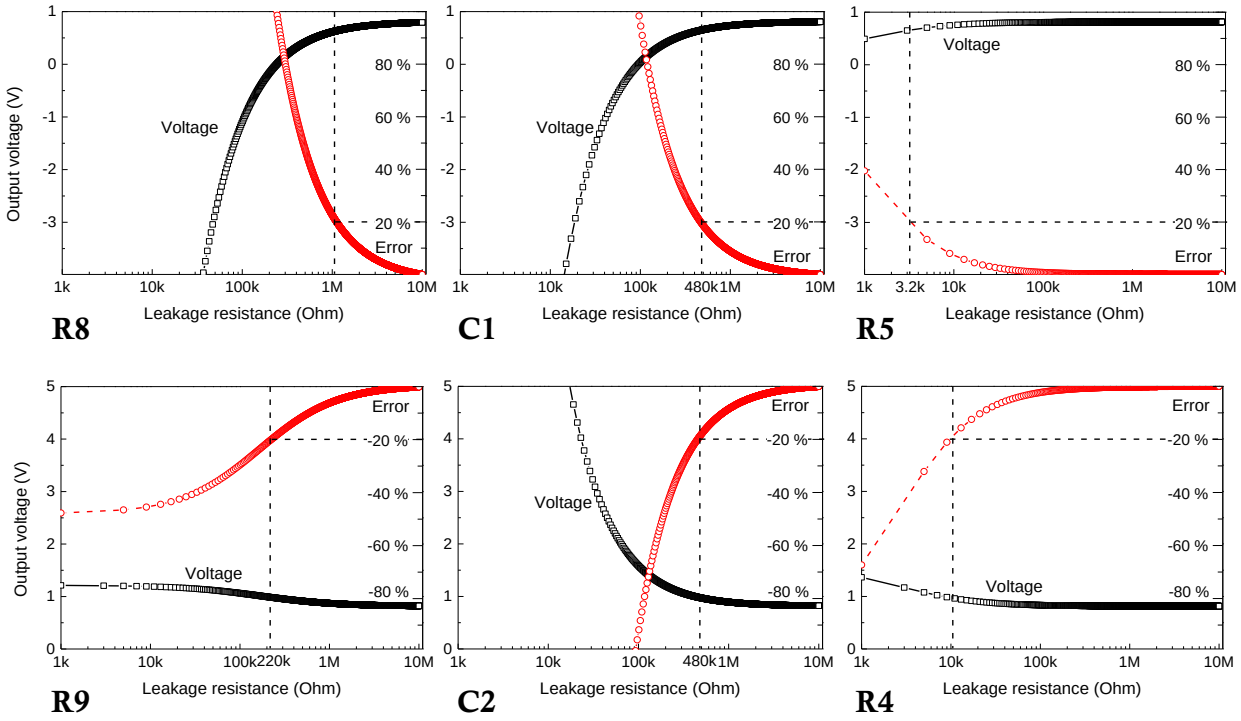

Figure 15.8: Effect of leakage resistance (attributed to the humidity and contamination) on the output voltage, and related percentage error of differential amplifier expressed as $(V_0-V_x)/V_0$). The notations of the graphs correspond to the components in the circuit diagram in Figure 15.7

The leakage resistance values, for which the error of ±20 % in the measurements was observed, are indicated in the graphs by the dashed line. The most critical component in the circuit is the resistor R8, with the threshold value of ~1 MOhm, followed by the filter capacitors C1 and C2 with ~480 kOhm, and resistor R9 with ~220 kOhm. The leakage across the resistors R4 and R5 with relatively low resistance values is least critical and may cause a 20 % deviation in the circuit only in case of severe condensation and corrosion leading to the dendrite formation. In the case of short-circuiting due to dendrites formation, the drop of leakage resistance to the level of several kOhms can be expected [16], [38].

From the analysis of the effect of leakage currents for various components in the circuit, the following actions could be considered for the improvement of the circuit design, making the device more robust towards humidity and contamination effects. The remedies shown below are more of an indication to show the possibility of design changes wherever applicable for reducing the sensitivity towards humidity.

Remedies for Resistor R8:

i) One solution would be to remove the most sensitive resistor R8 altogether. This would add a constant offset voltage to the output of the amplifier. This offset voltage could be subtracted in software after analog-to-digital conversion. Avoiding use of the component in this part of the circuit would significantly improve the climatic reliability of the measurement circuit.

ii) Second option could be the implementation of most sensitive resistor R8 as a series combination of several resistors. That would improve its sensitivity towards drift from nominal resistance value, illustrated as following: splitting the 160 kOhm resistance into two series resistors of 82 kOhm, would require the leakage resistance to drop to 434 kOhm assuming that both components are affected by the humidity effects. This is already a significant improvement compared to the 1 MOhm leakage resistance causing the same effect for the use of single component. Further, the use of two components reduces the chance for both of them to be significantly affected by the humidity simultaneously. If water layer forms on only one of the 82 kOhm resistors, the leakage resistance of 176 kOhm on the other component would be required for the 20 % error in the output voltage.

Remedies for capacitors C1 and C2:

Relocation of these components further away from the sensor, where condensation is less likely to occur can be a solution to the problem. However, this would be a compromise, since the capacitors are preferably placed near the entry point of the sensor signal to the PCB. Alternatively, the robustness of the circuit towards humidity and contamination effects can be further improved by applying local conformal coating or potting.

OVERALL SUMMARY OF CIRCUIT SIMULATION FOR HUMIDITY EFFECTS

The aim of the examples shown in this paper was to bring attention to the effect of humidity and contamination on the possible malfunctions and errors in electronic circuits. The empirical data used in this work provides a relative comparison of the effects and serves to show possible effects rather than to predict exact deviation of the parameters. For the analysis of the circuits, a worst-case scenario was assumed, and the overall resistance values measured on the SIR pattern were used.

The examples of potential performance issues of single components and as part of the differential amplifier circuit are linked to the reduction of SIR resulting from the humidity and contamination. The resistance values used in the examples were obtained on the standardized SIR test pattern, with a high number of squares. The use of resistance per square values would result in misleading analysis, as it was observed from the comparison to the resistance values observable directly on the device PCBA with the geometry of electrodes close to 1 square. The actual surface resistance values on the PCBA exposed to low RH conditions i.e. (60-80) %RH, or below the deliquescence RH, were lower by ~2-3 orders of magnitude than that of SIR value in Ohms per square measured on the SIR patterns i.e. 10^9 Ohm instead of 10^{12} Ohm. Although 10^9 Ohm is relatively high resistance, it would seldom cause any noticeable performance issues in most of the electronic circuits. However, as seen from Figure 15.1, the SIR reduces with increase of RH and the amount of ionic contamination. The increased RH and contamination level will enhance the effect, which will be more pronounced with a significant reduction of SIR when RH level exceeds the deliquescence RH of the contaminant.

The flux chemistry plays a big role in defining the leakage current values depending on the type of activator used. The knowledge of these parameters itself provides a safe way to find viable boundaries for electronics with regard to humidity and contamination. As shown in Figure 15.1 humidity level reaching to the deliquescence point of contamination increases the probability for short-circuiting due to corrosion and dendrite formation. The SIR in this case drops to the range

of MOhm (the actual resistance locally drops to the range of kOhm). This is also the resistance typically observed in the event of short-circuiting due to dendrite formation [16], [38].

IV. CONCLUSIONS

1. SIR testing of WOAs with varying concentrations and as a function of RH showed that the humidity levels for SIR failures are dependent on the type and amount of contamination on the surface. The solubility and deliquescence RH of the WOAs commonly found on the PCBAs significantly influences the conductivity of water layer forming on a surface, which determines the magnitude of SIR reduction, and the extent of subsequent corrosion issues.
2. The examples shown demonstrate possible parameter shifts of single components i.e. drift from the nominal resistance values of the resistors and self-discharge of the capacitors, and the errors in the circuits due to parasitic leakage currents (reduction of SIR) linked to the effects of ionic contamination and high humidity. The methodology of analysis of the circuits using a range of empirical leakage resistance values combined with the knowledge of the humidity and contamination profile of the electronics can be used for robust design of the device, which is also important for electronic products relying on low current consumption for long battery lifetime.
3. The difference between the SIR values obtained on the pattern with a high number of squares and the resistance practically seen on the device PCBAs indicates a non-linear dependency for the out scaling of the result based on the resistance square concept. A high number of squares provide good sensitivity for the measurements, and similarly, the relative changes of surface resistance on the PCBA can be analysed. However, for the use of SIR data for more accurate analysis the correlation between two measures is needed. This also suggests the need for SIR patterns with modified geometry, more closely representing the actual structures on the PCBAs, or performing the tests on the actual components.

V. ACKNOWLEDGMENTS

The research reported here was conducted as part of the CELCORR/CreCon consortium (www.celcorr.com) and authors would like to acknowledge the funding and help received from the consortium partners.

VI. REFERENCES

[1] C. Leygraf, "Atmospheric Corrosion," in *Corrosion Mechanisms in Theory and Practice*, P. Marcus, Ed. CRC Press, 2002, pp. 669–704.

[2] G. S. Frankel and J. W. Braithwaite, "Corrosion of Microelectronic and Magnetic Data-Storage Devices," in *Corrosion Mechanisms in Theory and Practice*, P. Marcus, Ed. CRC Press, 2002, pp. 825–861.

[3] J. F. Dante and R. G. Kelly, "The evolution of the adsorbed solution layer during atmospheric corrosion and its effects on the corrosion rate of copper," *J. Electrochem. Soc.*, vol. 140, no. 7, pp. 1890–1897, 1993.

[4] G. F. Cerofolini and C. Rovere, "The role of water vapor in the corrosion of microelectronic circuits," *Thin Solid Films*, vol. 47, no. 2, pp. 83–94, 1977.

[5] J. E. Sohn and U. Ray, "Weak Organic Acids and Surface Insulation Resistance," *Circuit World*, vol. 21, no. 4, pp. 22–26, 1994.

[6] B. A. Smith and L. J. Turbini, "Characterizing the weak organic acids used in low solids fluxes," *J. Electron. Mater.*, vol. 28, no. 11, pp. 1299–1306, Nov. 1999.

[7] Y. Zhou, L. J. Turbini, D. Ramjattan, B. Christian, and M. Pritzker, "Characterizing Corrosion Effects of Weak Organic Acids Using a Modified Bono Test," *J. Electron. Mater.*, vol. 42, no. 12, pp. 3609–3619, Aug. 2013.

[8] V. Verdingovas, M. S. Jellesen, and R. Ambat, "Relative effect of solder flux chemistry on the humidity related failures in electronics," *Solder. Surf. Mt. Technol.*, 2015.

[9] J. E. Sohn, U. Ray, V. Heideman, B. Schubert, J. E. Anderson, K. M. Adams, and G. Becka, "How clean is clean: effect of no-clean flux residues and environmental testing conditions on surface insulation resistance," in *Proceedings of Surface Mount International*, 1994.

[10] D. X. Xu, D. Bin Wang, and Y. P. Lei, "Study of VOC-Free, No-Clean Flux for Lead-Free Soldering in Electronic Packaging," *Adv. Mater. Res.*, no. 154–155, pp. 1012–1018, 2010.

[11] S. Zhan, M. H. Azarian, and M. Pecht, "Reliability of Printed Circuit Boards Processed Using No-Clean Flux Technology in Temperature – Humidity – Bias Conditions," *IEEE Trans. Device Mater. Reliab.*, vol. 8, no. 2, pp. 426–434, 2008.

[12] D. Geiger and D. Shangguan, "Investigation of the effect of solder flux residues on RF signal integrity using real circuits," *Solder. Surf. Mt. Technol.*, vol. 17, no. 4, pp. 27–32, 2005.

[13] M. Duffy, L. Floyd, P. Mccloskey, C. Ó. Mathúna, K. Tellefsen, M. Liberatore, and A. Sreeram, "RF Characterisation of No-clean Solder Flux Residues," in *Proceedings of SPIE - the International Society for Optical Engineering*, 2001, pp. 138–143.

[14] S. Canumalla, K. Ludwig, R. Pedigo, and T. Fitzgerald, "A study on ranking of commercial fluxes for electrochemical migration (ECM) propensity for Cu, Sn and Ag surface finishes," in *56th Electronic Components & Technology Conference*, 2006, pp. 625–632.

[15] D. Minzari, M. S. Jellesen, P. Møller, and R. Ambat, "On the electrochemical migration mechanism of tin in electronics," *Corros. Sci.*, vol. 53, no. 10, pp. 3366–3379, Oct. 2011.

[16] V. Verdingovas, M. S. Jellesen, and R. Ambat, "Influence of sodium chloride and weak organic acids (flux residues) on electrochemical migration of tin on surface mount chip components," *Corros. Eng. Sci. Technol.*, vol. 48, no. 6, pp. 426–435, Sep. 2013.

[17] B. Kanegsberg and E. Kanegsberg, *Handbook for Critical Cleaning. Applications, processes, and controls*, 2nd ed. CRC Press, 2011.

[18] "IPC-CH-65B Guidelines for Cleaning of Printe Boards and Assemblies," Northbrook, IL, 2011.

[19] W. Harald, "Preventing contamination-caused assembly failure," *Circuits Assem.*, vol. 20, no. 6, pp. 42–43, 2009.

[20] M. Bixenman, J. Chan, and T. C. Loy, "Removal of flux residues from highly dense assemblies," *2012 35th IEEE/CPMT Int. Electron. Manuf. Technol. Conf.*, pp. 1–9, Nov. 2012.

[21] M. S. Jellesen, D. Minzari, U. Rathinavelu, P. Møller, and R. Ambat, "Corrosion failure due to flux residues in an electronic add-on device," *Eng. Fail. Anal.*, vol. 17, no. 6, pp. 1263–1272, Sep. 2010.

[22] C.-Y. Huang, M.-S. Li, C.-L. Ku, H.-C. Hsieh, and K.-C. Li, "Chemical characterization of failures and process materials for microelectronics assembly," *Microelectron. Int.*, vol. 26, no. 3, pp. 41–48, 2009.

[23] M. Fortunato, "Analyzing circuit sensitivity for analogue circuit design," *Embed. Syst. Des.*, vol. 21, no. 4, pp. 1–6, 2008.

[24] E. A. Gonzalez, M. C. G. Leonor, L. U. Ambata, and C. S. Francisco, "Analyzing Sensitivity in Electric Circuits," *IEEE Multidiscip. Eng. Educ. Mag.*, vol. 2, no. 1, pp. 1–3, 2007.

[25] V. Verdingovas, M. S. Jellesen, and R. Ambat, "Impact of NaCl Contamination and Climatic Conditions on the Reliability of Printed Circuit Board Assemblies," *IEEE Trans. Device Mater. Reliab.*, vol. 14, no. 1, pp. 42–51, 2014.

[26] V. Verdingovas, M. S. Jellesen, and R. Ambat, "Solder Flux Residues and Humidity-Related Failures in Electronics: Relative Effects of Weak Organic Acids Used in No-Clean Flux Systems," *J. Electron. Mater.*, vol. 44, no. 4, pp. 1116–1127, 2015.

[27] K. M. Adams, J. E. Anderson, and Y. B. Graves, "lonograph Sensitivity to Chemical Residues from 'No Clean' Soldering Fluxes: Comparison of Solvent Extract Conductivity and Surface Conductivity,"

Circuit World, vol. 20, no. 2, pp. 41–44, 1994.

[28] C. Peng, M. N. Chan, and C. K. Chan, "The hygroscopic properties of dicarboxylic and multifunctional acids: measurements and UNIFAC predictions.," *Environ. Sci. Technol.*, vol. 35, no. 22, pp. 4495–501, Nov. 2001.

[29] P. Saxena and L. M. Hildemann, "Water absorption by organics: survey of laboratory evidence and evaluation of UNIFAC for estimating water activity," *Environ. Sci. Technol.*, vol. 31, no. 11, pp. 3318–3324, Nov. 1997.

[30] C. Cruz and S. Pandis, "Deliquescence and hygroscopic growth of mixed inorganic-organic atmospheric aerosol," *Environ. Sci. Technol.*, vol. 34, no. 20, pp. 4313–4319, 2000.

[31] A. Apelblat, M. Dov, J. Wisniak, and J. Zabicky, "The vapour pressure of water over saturated aqueous solutions of malic, tartaric, and citric acids, at temperatures from 288 K to 323 K," *J. Chem. Thermodyn.*, vol. 27, no. 1, pp. 35–41, Jan. 1995.

[32] L. Van Campen, G. L. Amidon, and G. Zografi, "Moisture sorption kinetics for water-soluble substances. I: Theoretical considerations of heat transport control," *J. Pharm. Sci.*, vol. 72, pp. 1381–1388, 1983.

[33] H. Conseil, M. Stendahl Jellesen, and R. Ambat, "Contamination profile on typical printed circuit board assemblies vs soldering process," *Solder. Surf. Mt. Technol.*, vol. 26, no. 4, pp. 194–202, Aug. 2014.

[34] M. S. Jellesen, M. Dutta, V. Verdingovas, and R. Ambat, "Detection of acid release from reflow solder flux residues using localized test methods," in *Eurocorr 2012*, 2012, pp. 1–10.

[35] D. Minzari, M. S. Jellesen, R. Ambat, P. Møller, and P. S. Westermann, "Process, kit and composition for detecting residues and contaminants in an object with three-dimensional geometry," WO 2011/048001 A1, 2011.

[36] D. N. Donahoe, M. Pecht, I. K. Lloyd, and S. Ganesan, "Moisture induced degradation of multilayer ceramic capacitors," *Microelectron. Reliab.*, vol. 46, no. 2–4, pp. 400–408, Feb. 2006.

[37] J. Virkki and P. Raumonen, "Testing the Effects of Seacoast Atmosphere on Tantalum Capacitors," *Act. Passiv. Electron. Components*, vol. 2011, pp. 1–9, 2011.

[38] D. Minzari, M. S. Jellesen, P. Møller, P. Wahlberg, and R. Ambat, "Electrochemical Migration on Electronic Chip Resistors in Chloride Environments," *IEEE Trans. Device Mater. Reliab.*, vol. 9, no. 3, pp. 392–402, 2009.

16. OVERALL DISCUSSION AND CONCLUSIONS

This chapter contains a short discussion combining the investigations presented in the appended papers. The results presented in the papers clearly show the importance of the synergistic effect of contamination and humidity on the climatic reliability of electronics. As shown, the chemistry of the flux and the level of flux residue play a significant role in water layer formation and its effects on corrosion in electronics.

Due to the ionic and hygroscopic nature of the activator component in the flux residue, it can cause multiple effects on a PCBA. Although the activators in many of no-clean flux systems are defined as WOA with minimal aggressiveness, the investigations in this thesis showed the importance of the type of WOA on climatic reliability issues. The low critical relative humidity of a WOA combined with high solubility and ionization can cause a significant increase in the capacity of the water layer for leak currents altering the reliability of PCBAs relative to the use of a flux with more benign WOA. Therefore, the process cleanliness is an important part in achieving corrosion reliability, which includes the selection of proper flux systems and optimizing the amount of use.

As shown, hygroscopic contaminants are characterised by deliquescence RH at which the water adsorption to the surface increases significantly. The adsorption and dissolution of contaminants continue until complete dissolution and, to an extent, dilution occurs. The increase of water layer thickness saturated with highly soluble contaminants will increase the leakage currents and probability of metal ion migration. Therefore, as suggested earlier, the use of no-clean flux systems with WOAs of low solubility and high deliquescence RH would improve the SIR and overall reliability of a PCBA.

When water layer thickness between the adjacent conductors on the PCBA is sufficient for the metal ion transport, the time to short-circuiting due to dendrite formation will depend on the bias voltage applied. The DC voltage is most favourable for electrochemical migration, while dendrite formation under AC bias conditions is least likely. The investigations on the effect of pulsed voltage have shown that by applying pulsed voltage instead of DC voltage, an increase in time to failure can be achieved. Reducing the duty cycle of pulsed voltage increases the time needed to bridge the gap between conductors by tin dendrites. The findings are primarily related to the reduced ion dissolution with reduction of the ON cycle; however, the prolongation of the OFF cycle is also more favourable for tin hydroxide precipitation, thereby resulting in fewer tin ions reduced at the cathode.

Also important in relation to climatic reliability is the possibility to recognize the corrosion hot spots on a PCBA surface. Metallic materials on the PCBA surface dissolve in presence of water layer connecting biased electrodes. The dissolved metallic ions move in the vicinity of the corroded area due to the electric field between adjacent conductors on a PCBA. The movement of metallic ions through the water layer also shows the possible leak current paths, which might lead to electrochemical migration paths if corrosion continues. In this thesis, the prediction of corrosion prone regions on a PCBA surface is attempted based on two approaches namely: (i) profiling tin corrosion on the PCBA surface and its movements under humidity exposure, and (ii) circuit simulation for possible humidity effects by parasitic circuit modelling using empirical data on leak currents under humid conditions. Both attempts showed good results pointing to the possibility of using them as prediction methods at early stages of circuit design or at a PCBA

layout level to understand the susceptibility of a specific design to climate variations. As demonstrated, the methods can also be used for failure analysis to understand the location of even tiny levels of corrosion, which otherwise invisible. The prediction possibility using circuit simulation procedure followed in this thesis is a demonstration, which needs to be improved further using more accurate data and procedures. Nevertheless, using presented approaches, useful design guidelines can be developed.

16.1 OVERALL CONCLUSIONS

1. Overall, the magnitude of leakage current measured on the surface mount components, and the SIR patterns was strongly dependent on the humidity levels, and the presence of ionic contaminants.
2. As tested under water droplet condition, for NaCl, the migration probability tends to decrease with increase in concentration above the peak value; however, some level of migration probability remains. Whereas solder flux residues showed an abrupt decrease of migration probability above the peak value.
3. Formation of tin whiskers and hillocks was observed *in situ* on surface mount capacitors exposed to near condensing conditions. The growth of hillocks and whiskers was more likely on the anode terminal of a capacitor, indicating that corrosion of the anode terminal and depletion of the oxide film increases the probability for whisker growth.
4. The climatic testing of adipic, succinic, glutaric, DL-malic, palmitic acids and no-clean flux systems showed a clear correlation between the hygroscopicity and resistivity of the water layer. An abrupt increase in the leakage current by 2-4 orders of magnitude, followed by electrochemical migration, and similarly, the reduction of impedance of water layer, was observed at RH close to the deliquescence point of the acids. Based on the leakage current and impedance measurements, the following ranking of the acids for their effects on corrosion reliability was observed: palmitic, adipic, succinic, glutaric, and DL-malic.
5. Heating of the test boards with WOAs and no-clean flux residues reduced the leakage currents on the SIR patterns. The heating effect was more pronounced for glutaric and DL-malic acids, which is attributed to the high solubility of the acids, as they can saturate at high concentration in a thin water layer compared to low-solubility acids (adipic, succinic, and palmitic acids).
6. The differences between DC and AC measurements of solution conductivity for determination of the level of ionic contamination equivalent to NaCl were demonstrated. The equivalent values obtained from solution conductivity measurement are higher compared to the values obtained from leakage current measured through the solution using DC bias. The difference is due to the electrode polarisation effects during leakage current measurements.
7. The increase of duty cycle of pulsed voltage under water droplet conditions reduced the time to dendrite formation. The results are primarily attributed to the concentration of tin ions being dissolved from the positively biased electrode, as visualized by a tin ion indicator. The comparison of the TTF and charge transfer between the electrodes after equivalent ON times for various duty cycles indicated further hindering effect of lower duty cycles on electrochemical migration. A slight increase in TTF and reduction of charge transferred between the electrodes is related to the increase in precipitation rate of tin hydroxides.
8. Failures of Au-Al wire bonds in iodine environment are mainly attributed to the corrosion of Al via formation of Al iodides and consequent formation of Al oxides and/or hydroxides. The Al metallization and Al rich intermetallic phases were most susceptible to corrosion. Heat treatment of the Au-Al wire bonds resulted in an increase of intermetallic zone, and thus an increase of corrosion. Humidity was found to be an accelerating factor for corrosion.

The galvanic current between Au and Au-Al intermetallics in aqueous KI solution followed the electrochemical potential difference between the Au, Al and Au-Al intermetallics.

9. A new method for tin corrosion profiling on the PCBAs using a colorimetric tin ion indicator in a gel was developed. Corrosion profiling using this method allows visualization of tiny levels of tin corrosion, which otherwise hidden, therefore provide means for early detection of corrosion on the PCBA during testing or failure analysis. When combined with humidity exposure testing, the corrosion profile on PCBA surface obtained by tin ion indicator gel can be used to verify design changes or remedial measures.
10. Corrosion prediction using circuit simulation is attempted and demonstrated. Empirical data on the reduction of SIR due to water layer formation was used for parasitic circuit analysis of the drift in nominal resistance values of the resistors, discharge of the capacitors, and the variation in the output voltage of a differential amplifier. Similar analysis of the circuits using a range of empirical leakage resistance values combined with the knowledge of the humidity and contamination profile of the electronics can be used for early prediction and design guidelines.

16.2 SUGGESTIONS FOR FUTURE WORK

The climatic testing of the WOAs and flux residues was performed at 25°C, although actual device PCBAs may experience higher temperatures during operation. This suggests similar investigations could be performed at higher temperatures for verification of the relative consistency of the results on water adsorption, leakage currents, and corrosion. A focus could be placed on the properties of acid-metal complexes formed during the soldering processes.

The investigation of pulsed voltage on electrochemical migration and use in the actual application could be explored. Possible applications are in the PCBAs for sensing devices where continuous electrical measurements are not needed.

Corrosion investigation of Au-Al wire bonds in iodine environments showed corrosion of Al at the bond pad and wire interface, and from the Au-Al intermetallics is primarily accountable for the failures in wire bonds. This suggests that replacement of Al by more corrosion resistant metal could improve the reliability of wire bonds. Future investigations can focus on the iodine resistant and ultrasonically bondable combination of materials suitable for wire bond connections in microelectronics.

The usefulness of the tin corrosion profiling method is described in this thesis. However, additional work needs to be done for the approach for corrosion reliability analysis after humidity exposure to be more systematic i.e. data on the contamination type and amount, the temperature of a PCBA, and voltage could be linked to the corrosion profile of a PCBA. Understanding of these factors will provide a way for more reasonable prediction of corrosion prone areas on a PCBA.

Further improvement in reliability prediction includes circuit simulation analysis using more accurate SIR data on components and developing a comprehensive method for analysis of climatic effects with an overall aim of providing the design guidelines for robust electronics.

DTU Mechanical Engineering
Section of Materials and Surface Engineering
Technical University of Denmark

Produktionstorvet, Bld. 425
DK-2800 Kgs. Lyngby
Denmark
Phone (+45) 4525 2205
Fax (+45) 4593 6213
www.mek.dtu.dk
ISBN: 978-87-7475-471-8